University of Leuven

Group Biomedical Sciences

Faculty of Pharmaceutical and Pharmacological Sciences

Drug Delivery and Disposition

Formulation and Process Considerations in Manufacturing Spray-Dried Amorphous Solid Dispersions: A Case Study with Naproxen-Polyvinylpyrrolidone

Amrit Paudel

Jury:

Promoter:	Prof. Dr. G. Van den Mooter
Chair:	Prof. Dr. A. Van Schepdael
Jury members:	Prof. Dr. S. De Smedt
	Prof. Dr. J. Rantanen
	Prof. Dr. J. Van Humbeeck
	Prof. Dr. E. Nies

Leuven, 29.04.2013
Doctoral thesis in Pharmaceutical Sciences

Acknowledgments

It is my pride and honor to be a student of drug delivery and disposition group, KU Leuven, which has prestigious international recognition in pharmaceutical research. It has been an overwhelming experience for me working on the Ph.D. It is certainly wonderful to realize owns metamorphosis from simply understanding the research topic to enormous experience of writing papers and proposals, delivering talks and on the top of all the real learning of staying focused. At every step, there are many people, I am indebted to for their time and ceaseless efforts.

To begin with, I am extremely grateful to my Ph.D. supervisor Prof. Guy Van den Mooter for accepting me as a Ph.D. student at the department. It was a great pleasure working under your mentorship which was always exciting and insightful. Be it in scientific input or on the personal front, your steady support, promptness, patience and encouragement have made my stay very pleasant. Your experience and expertise in approaching research problems helped me a lot to shape myself as an independent researcher. Besides, I appreciate from my heart for your very friendly interactions throughout my Ph.D.

I am very grateful to Prof. Eric Nies, Prof. Jan Van Humbeeck and Prof. Ann Van Schepdael for their insightful advises in my Ph.D. work as the member of my thesis advisory committee (TAC). I appreciate your times for motivating discussions in many occasions and also evaluating my Ph.D. periodically by providing rational comments. Together with my TAC members, I would also like to extend my sincere thanks to my external reviewers Prof Stefaan de Smedt and Prof. Jukka Rantanen for carefully reading my thesis and for providing constructive comments and pleasing feedbacks.

In addition, I am very grateful to many of my colleagues with whom I shared research work, bench, office cube, journal clubs and all fun together at lab, bicycle tour and conferences for years. I am very thankful to Sandrien and Elke for becaming my very intimate friends and instructors during the early days in lab. Furthermore, I feel myself blessed to get all wonderful colleagues at drug delivery and disposition group. The cherishing and intellectual moments I shared with you would be an everlasting asset for my life. Sagnik and Zola: your company was often the platform to reminisce the NIPER nostalgia. Also, I had a lot pleasure working with Masters Students, Yves and Lode. Continuing a tradition, many studies of this thesis would not have been possible without the magical Patrick Rombaut. I am always amazed how he devices others idea into working reality. Also, hearing his three

decades of experience about life and work is like going self to yesteryears. I would like to sincerely acknowledge department of pharmaceutical analysis, M.T.M. and C.O.K., KU Leuven for allowing me to use various analytical instruments during my Ph.D. Special thanks to Danny for his help with TGA.

I also thank D.B.O.F., KU Leuven for providing me the Ph.D. scholarship. It was the fate that has driven me all the way to Leuven. This is the place where I was able to grow scientifically and also met my soulmate. Thank you Leuven for being so dear!

Words fall short to express how much I am indebted to my wife. Sunita: you always stood unconditionally by me throughout my Ph.D. This fruitful journey I could make in my Ph.D. is the blossom of your ceaseless love and support. My parents in-law and brothers in-law: you always replenished my family in Leuven, provided me a cosy home of love thousand miles away from my own home. Sudip and Dipesh: I enjoyed the graphic and IT expertise of you guys! Thank you with all my heart.

Finally, I thank almighty for giving me such a loving and caring family. I would like to thank my mom, dad, brothers and sisters for their infinite support throughout everything. After these many years, I am still not inhabitated without you. The sacrifice you have made for my grandeur is not a matter to describe in words. For my parents especially, whose effort succeeded to make me the man of the destiny: it is just your vows and blessing which stood after my all successful steps.

Amrit

Contents

Abbreviations and Symbols

AFM	:	Atomic Force Microscopy
API	:	Active Pharmaceutical Ingredient
ASD	:	Amorphous Solid Dispersions
ATR	:	Attenuated Total Reflectance
AUC	:	Area Under the Curve
BCKV	:	Brostow, Chiu, Kalogeras, Vassilikou-Dova
BCS	:	Biopharmaceutics Classification System
CK	:	Cauchman-Karasz
COSMO-RS	:	Conductor-like Screening Model for Real Solvents
COX	:	Cyclooxygenase
CRR	:	Cooperatively Rearranging Region
DCM	:	Dichloromethane
DES	:	Dielectric Relaxation Spectroscopy
DLS	:	Dynamic Light Scattering
DoE	:	Design of Experiments
dRHF	:	First Derivative of the Reversing Heat flow signal with respect to the Temperature
DSC	:	Differential Scanning Calorimetry
FH	:	Flory–Huggins
EOC	:	Extent of Crystallization
FT-IR	:	Fourier Transform-Infrared
FWHM	:	Full Width at Half Maximum
GI	:	Gastrointestinal
GL	:	Gaussian−Lorentzian
GT	:	Gordon-Taylor
GVS	:	Gravimetric Vapor Sorption
H-bonding	:	Hydrogen-Bonding
HPLC	:	High Performance Liquid Chromatography
HPMC	:	Hydroxypropyl Methylcellulose
HPMC-AS	:	Hydroxypropyl Methylcellulose-Acetate Succinate
IGC	:	Inverse Gas Chromatography
IR	:	Infrared
IT	:	Inlet Temperature
KT	:	Kamlet–Taft
mDSC	:	Temperature Modulated Differential Scanning Calorimetry
NMP	:	*n*-methylpyrrolidone
NMR	:	Nuclear Magnetic Resonance
NRHB	:	Non-Random Hydrogen-Bonding
NRTL-SAC	:	Non-Random Two Liquid-Segment Activity Coefficient
NSAID	:	Non-Steroidal Anti-Inflammatory Drug
PCAM	:	Painter and Coleman Association Model

PDF	:	Pairwise Distribution Function
PEG	:	Polyethylene Glycol
PFG	:	Pulsed Field Gradient
PLM	:	Polarized Light Microscopy
PVP	:	Poly(Vinylpyrrolidone)
PVPVA	:	Poly(Vinylpyrrolidone-co-Vinyl Acetate)
pXRD	:	Powder X-ray Diffractometry
QbD	:	Quality by Design
RH	:	Relative Humidity
RHF	:	Reversing Heat Flow
SDD	:	Spray Dried Dispersion
SEM	:	Scanning Electron Microscopy
TEM	:	Transmission Electron Microscopy
TGA	:	Thermogravimetric Analyzer
UNIFAC	:	Universal Functional Activity Coefficient
VP	:	N-vinyl pyrrolidone
WTPT	:	Wertheim Thermodynamic Perturbation Theory
XPS	:	X-Ray Photoelectron Spectroscopy
K_B	:	Boltzmann Constant
χ	:	Flory-Huggins Interaction Parameter
τ	:	Structural Relaxation Time
ρ	:	Density
η	:	Viscosity
ε	:	Dielectric Constant
ΔH_f	:	Heat of Fusion
V_{site}	:	Molar Volume of a Lattice Site
VP	:	*n*-vinylpyrrolidone
T_m	:	Melting Temperature
T_g	:	Glass Transition Temperature
R	:	Gas Constant
P_e	:	Peclet number
$\emptyset$	:	Volume Fraction
H	:	Boundary Layer Thickness
γ	:	Activity Coefficient
dw/dt	:	Rate of Dissolution
D	:	Diffusion Coefficient
δ	:	Total Solubility Parameter
C_S	:	Saturation Solubility
C_p	:	Heat Capacity at Constant Pressure
A	:	Surface Area
ΔS_{mix}	:	Entropy of Mixing
ΔH_{mix}	:	Enthalpy of Mixing
ΔG_{mix}	:	Gibbs Free Energy of Mixing

Chapter I: General Introduction

This chapter is partially based on the review:

Paudel, A.; Worku, Z.A.; Meeus, J.; Guns, S. and Van den Mooter, G. (2012). Manufacturing of Solid Dispersions of Poorly Water Soluble Drugs by Spray Drying: Formulation and Process Considerations. *International Journal of Pharmaceutics (In Press)*.

The oral route is the most preferred route for administering medicines due to its convenience and patient acceptability. Following oral ingestion of a solid dosage form, the active pharmaceutical ingredient (API) is released in the gastrointestinal (GI) tract, dissolved in GI medium and transported across the intestinal barrier to the systemic circulation and thereafter the designated site of action. Therefore, appreciable aqueous solubility, intestinal membrane permeability and metabolic stability are the prerequisites for adequate absorption and bioavailability of orally administered drugs. The Biopharmaceutics Classification System (BCS) proposed by Amidon et al., for predicting oral deliverability of APIs, categorizes them in four classes based on their aqueous solubility and intestinal permeability[1]. This includes drugs with high solubility-high permeability (class 1), low solubility-high permeability (class 2), high solubility-low permeability (class 3) and low solubility-low permeability (class 4). The criterion of high solubility for a drug substance is that the highest dose strength is soluble in ≤ 250 ml aqueous media (pH: 1-7.5) while the same for high permeability is that ≥ 90% of the administered dose is transported across GI barrier.

The advancement in high throughput screening, combinatorial chemistry and an improved understanding of structural biology in the last two decades have significantly raised the number of pharmacologically efficacious, selective and thus safer candidates[2]. However, compounds showing promises in cellular assays and animal models may not necessarily make their way through the pharmaceutical product development. This is because of the fact that the concurrently rising structural complexity of these drug candidates has turned into the main factor behind their poor pharmaceutical portfolio (solubility, permeability, stability etc) and hence for the failure of up to 70% of all developmental candidates. More specifically, the low aqueous solubility accounts for the large number of attritions with the majority of early drug candidates belonging to either BCS class 2 or class 4[3]. Thus, a significant part of current academic and industrial research is directed towards developing efficient solubilizing formulation strategies for the candidates in these categories.

Some existing solubilization strategies to address low drug solubility are chemical modifications (prodrug and salt formation), solubilized formulation approaches (cosolvent system, micellar delivery with surfactants, cyclodextrin complexes, lipid based systems etc) and physical modifications (particle size reduction, co-crystals, metastable polymorphs and amorphous solid dispersions)[4]. Among them, the physical modifications are comparatively easier and thus more popular for oral solid dosage form development. The classical Nernst-Brunner equation, which simply correlates the rate of dissolution of a drug substance (dw/dt)

with its saturation solubility (C_s) and surface area (A), describes how the different physical approaches enhance the dissolution rate[5]:

$$\frac{dw}{dt} = \frac{A \times D \times (C_S - C_t)}{h} \quad \text{Equation I. 1}$$

where, D is the diffusion coefficient, C_t is the concentration of drug in the dissolution medium at time t and h is the thickness of the diffusion boundary layer. The use of high energy metastable crystalline or amorphous drug substances primarily increases solubility (C_s) compared to the stable crystal form while particle size reduction to submicron or nano range increases A and decreases h, thus overall contribute to the enhanced dw/dt. Besides, the presence of hydrophilic carrier in nanocrystalline or amorphous solid dispersions also possibly increases the wettability of hydrophobic drugs in aqueous medium.

I.1 Characteristics of the Amorphous State

A pharmaceutical solid can be broadly classified into two forms based on its degree of structural ordering namely, a crystalline form and an amorphous form. The crystalline solid is characterized by the presence of a three dimensional long range order of a repeating unit that is structured through various molecular and supramolecular interactions. In contrast, an amorphous form possesses a definite ordering only at the short range order, typically over a few molecular dimensions, resulting into very different physicochemical properties than those from the crystalline state. Since amorphous materials lack a long range order, the need of overcoming the lattice energy for the solubilization process is waived[6]. Therefore, it exhibits higher solubility compared to that of a crystalline form. The other main differences are the higher enthalpy, entropy, free volume and molecular mobility in comparison to the crystalline state (Figure I.1).

These values progressively decrease while supercooling a melt, the process of cooling a liquid without freezing or crystallization. From a certain temperature, this line suddenly deviates to attain a slower rate of these values on further lowering the temperature. This is called glass transition temperature (T_g), a characteristic feature to the amorphous form. Below T_g, the amorphous form is referred to be in a glassy state wherein the disordered structure is kinetically frozen. The supercooled liquid state of an amorphous material above T_g is also referred to as the rubbery state showing higher thermodynamic values. Therefore, nucleation and crystallization processes are more favorable.

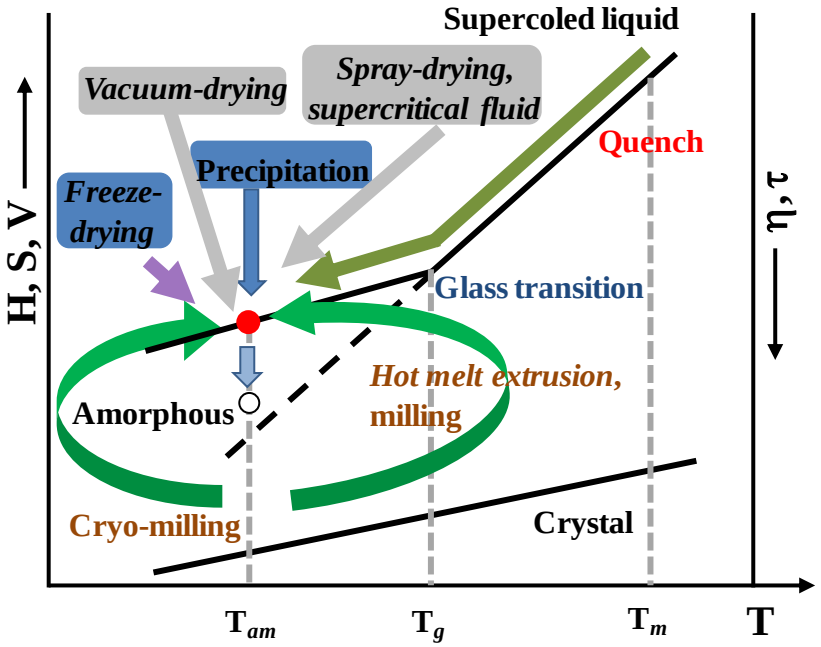

Figure I.1 Schematic diagram of the thermal history of amorphous systems. The italicized methods are industrially applicable. The closed circle is for as prepared systems and open circle for relaxed system. H: enthalpy, S: entropy, V: free volume, η: viscosity, τ: relaxation time, T: Temperature, T_{am}: ambient temperature, T_g: glass transition temperature and T_m: melting temperature[7].

Due to higher degree of disorder, the molecular mobility in amorphous materials originate from vibrational and rotational molecular motions that partially resemble to the liquid state except the latter also constitutes the translational motions. The physical structure of a disordered state can be represented as a collection of smaller units that are capable of undergoing structural rearrangement. These units are known as cooperatively rearranging regions (CRRs) and the rearrangement process is called structural relaxation[8]. The primary relaxation process is slower and global connective molecular motions among CRRs are called alpha (α) process. The α-process follows nonlinear temperature dependence in the supercooled liquid region and linear Arrhenius behavior below T_g. It is considered as the main kinetic factor for crystallization. On the other hand, the faster secondary relaxation process referred to as beta (β)-process originates from localizing molecular motions such as fluctuation of dipole vector or segmental motion and remains dominant below T_g. This sub-T_g process is also reported to be responsible for crystallization below T_g for many systems. Besides β-process, other faster sub-T_g process such as gamma- and/or delta-processes occur in some systems[9]. The structural relaxation time (τ) is taken as the measure of the molecular mobility and a predictor of physicochemical stability of amorphous systems. Nevertheless, the relation between the homogeneity of the relaxation time and the particular amorphous structure is still unclear. In general, the higher energetics and the faster molecular mobility in

the amorphous state drive towards the nucleation and crystallization. Importantly, the augmentation of this process by the exposure of an amorphous API to an elevated moisture and/ or heat during pharmaceutical processing or administration leads to the loss of the claimed solubility advantage[10]. Therefore, an amorphous form of a drug substance alone as such is seldom used.

I.2 Amorphous Solid Dispersions

Amorphous solid dispersions (ASD) is one of the prominent strategies for improving the solubility/dissolution rate limited oral bioavailability of poorly water soluble drugs[6]. Early inventors defined a pharmaceutical solid dispersion as the dispersion of one or more active ingredients in an inert carrier matrix at solid-state prepared by melting and/or solvent methods[11]. The classical solid dispersions were based on the drug-carrier eutectic mixture and crystalline dispersions. The paradigm later shifted towards the dispersion of amorphous API in a hydrophilic matrix formed of an amorphous or semicrystalline carrier. Especially, high T_g amorphous polymers are common carriers for ASD. The polymer stabilizes an amorphous phase by antiplasticization, i.e. the process of increase in the T_g of a mixed phase of ASD significantly above the storage temperature that tend to slow down the molecular mobility of API and hence inhibit or retard the rate of nucleation/crystallization. As given in eq I.2, the T_g of a mixed phase can be predicted by the Gordon-Taylor equation assuming equality of homo- and heteromolecular interactions between drug and polymer and volume additivity[12]:

$$T_{g=} \frac{W_{drug}T_{g(drug)} + KW_{polymer}T_{g(polymer)}}{W_{drug} + KW_{polymer}} \dots\dots\dots\dots\dots\dots\dots \text{Equation I. 2}$$

where, $K \approx \frac{\rho_{drug}\ T_{g(drug)}}{\rho_{polymer}\ T_{g(polymer)}}$ and W and ρ are weight fraction, glass transition temperature and density, respectively. The extended form of this equation is also often used to calculate the plasticized T_g of drug-polymer ASD in presence of moisture or residual solvent (ternary system). Apart from antiplasticization, the specific intermolecular interactions between drug and polymeric carrier such as hydrogen (H)-bonding, ionic complex formation, dipolar interactions etc, decrease the homomolecular (drug-drug) interaction that eventually reduces or prevent the nuclei formation. Depending upon a certain drug-carrier combination, one or both mechanisms may take part in stabilization.

The physical state of a solid dispersion primarily relies on the drug-to-polymer ratio[13]. Up to a certain composition the drug molecules are intimately mixed with the polymer, best at the molecular level, in ASD regardless of the amorphization procedure. This is often referred

to as glass solution. This composition represents the equilibrium or thermodynamic solid solubility of drug in polymer. In practice, most of ASDs are in the non-equilibrium state because of contribution of kinetic and other dynamic factors involved during manufacturing. This means that the excess drug molecules can still be kinetically solubilized in the amorphous state by the polymeric matrices to generate supersaturated ASD by an energy-intensive process. However, this solubilization capacity is maintained only up to a certain composition that represents the kinetic miscibility limit. The drug loading beyond this will result in the amorphous-amorphous/crystalline phase separation. Appreciable solid solubility and miscibility of drug in the selected polymeric matrix is very crucial for the stabilization of the amorphous state of drug in the resulting ASD[14]. The presence of specific interactions such as intermolecular H-bonding between drug and polymer molecules increases the miscibility in the system. Generally, the molecular level miscibility between the drug and polymer in ASD is desirable for higher physical stability. Moreover, interplay between various thermodynamic and kinetic factors in ASD through an ambient or non-ambient (elevated temperature and/ or humidity) storage period determines the physicochemical stability. Similar physicochemical events occurring during *in vitro* dissolution testing or exposure to the GI environment can affect the phase behavior of ASD[15]. Therefore, it is very important that the selection of a suitable carrier for formulating ASD of a poorly soluble drug is based on the comprehensive understanding of the drug-polymer phase behavior.

I.2.1 Prediction of Miscibility and Phase Behavior of Drug-Polymer Solid Dispersions

Extensive pharmaceutical literature is available on the use of Flory–Huggins (FH) solution theory for studying drug-polymer miscibility in solid dispersions[14]. The Gibbs free energy change (ΔG_{mix}) accompanying mixing of a drug and a polymer at constant temperature and pressure can be expressed as:

$$\Delta G_{mix} = \Delta H_{mix} - T\Delta S_{mix} \quad \text{Equation I. 3}$$

where ΔH_{mix} and ΔS_{mix} are, respectively the enthalpy and entropy of mixing drug and polymer at absolute temperature *T*. The FH theory supposes that each segment or a side group of a polymer occupies a site of a lattice. Each lattice site is also occupied by a drug molecule. Then, ΔG_{mix} per mole of lattice sites for a drug-polymer mixture is calculated in terms of mean-field approximation, assuming the random distribution of drug molecules in the polymer matrix using eq I.4.

$$\frac{\Delta G_{mix}}{RT} = \frac{\emptyset_{drug}}{m_{drug}} ln\emptyset_{drug} + \frac{\emptyset_{polymer}}{m_{polymer}} ln\emptyset_{polymer} + \chi_{FH}\emptyset_{drug}\emptyset_{polymer} \quad \text{Equation I. 4}$$

Where R, $\emptyset$, m and χ_{FH} are the gas constant, the volume fraction, the number of lattice sites occupied by a molecule (the ratio of molar volume to the volume of lattice site) and the Flory-Huggins interaction parameter, respectively. On the right hand side, the first two terms represent the combinatorial contribution to the entropy of mixing (computed from the number of ways the chains can randomly pack in a lattice) while the third component corresponds to the enthalpy of mixing term. The non-combinatorial entropic contributions of drug-polymer mixing such as free volume effect or packing effects are also reported[16]. The value of χ_{FH} for a certain drug-polymer system has major impact on ΔG_{mix} and thus on the entire phase behavior. Different direct and indirect methods for the estimation of composition and temperature dependent χ_{FH} for drug-polymer systems of solid dispersions are reported[17]. The classical method to estimate χ_{FH} is by applying the Hildebrand solubility parameter equation (eq I.5):

$$\chi_{FH} = \frac{V_{site}\left(\delta_{polymer} - \delta_{drug}\right)^2}{RT} \quad \text{Equation I. 5}$$

Here, δ is the solubility parameter of a component (the square root of the ratio of cohesion energy density to molar volume) that is often calculated by group contribution methods and V_{site} is volume of a lattice site. This means that the higher the match between δ_{drug} and $\delta_{polymer}$, the closer will be the value of χ_{FH} to zero. The other methodologies to determine χ_{FH} such as by scaling thermodynamic activity of drug in liquid analogues to that in the polymer, by studying the polymer composition dependent depression on drug melting point and by moisture sorption data of a drug-polymer system are detailed in Chapter III. In general, negative values of χ_{FH} indicate the presence of higher adhesive (heteromolecular) interactions, hence favoring molecular mixing. Conversely, a positive value of χ_{FH} indicates the prevailing cohesive (homomolecular) interaction over adhesive for a system which indeed characterizes unfavorable miscibility between the components. However, the threshold value of χ_{FH} for phase separation can be larger than 0 (≥ 0.5). This is because the value of entropy terms in eq I.4 is always negative and minimal up to -0.5.

Once χ_{FH} is determined for a drug-polymer system, ΔG_{mix} isotherms can be plotted for the entire composition at different temperatures. A typical ΔG_{mix} isotherm below critical temperature for a hypothetical binary system with miscibility gap is depicted in Figure I.2. The two positively curved portions surround a negatively curved portion of the curve that is separated by two inflection points (A' and C'). A common tangent can be drawn to pass through two different $\emptyset_{drug}$ points of the ΔG_{mix} curve (point A and C) representing the

coexisiting phases. The homogeneous compositions between the inflection points A' and C' will spontaneously separate upon any concentration fluctuation. The miscible composition at point B tends to phase separate into A and C to attain the total ΔG_{mix} noted by point B'. The first- and second-derivative transformations of the ΔG_{mix}–$Ø_{drug}$ isotherms with respect to $Ø_{drug}$ generate the binodal and spinodal decomposition curves, respectively[18]. The binodal miscibility boundary is derived from the points of common tangent to the ΔG_{mix} curve, where the chemical potentials of the two co-existing phases will be identical. The spinodals represent the metastability limits as indicated by the change in ΔG_{mix} curvature from positive to negative and hence the second derivative of ΔG_{mix} tends to zero. Even a trivial concentration fluctuation within the spinodal region leads to spontaneous phase separation. Overall, this helps in identifying the stable, metastable and unstable region in phase diagram.

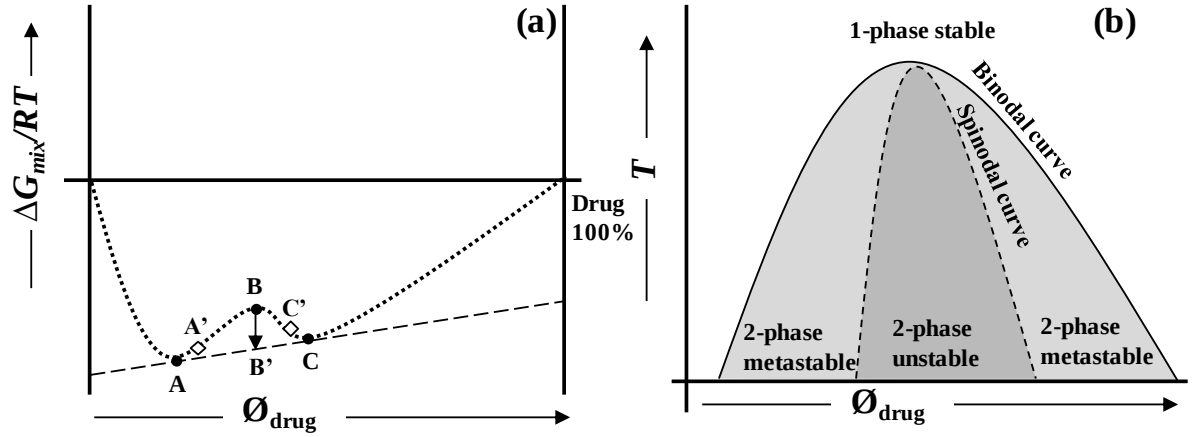

Figure I.2 A Plot of ΔG_{mix}/RT versus volume fraction of drug ($Ø_{drug}$) for a drug-polymer system with miscibility gap[19] (a) and the phase diagram of a two-component solid solution system [20] (b).

I.2.2 Common Carriers for Manufacturing Drug-Polymer Solid Dispersions

The common polymeric carriers used for manufacturing ASD of poorly soluble drugs and some of their relevant physicochemical properties are listed in Table I.1. As mentioned in I.2.1, the choice of a proper carrier to formulate ASD is based on their physicochemical characteristics, phase behavior and also the intended method of preparation. For example, acceptable solubility in a wide range of volatile organic solvents and aqueous systems are prerequisite for the carriers to process by solvent methods. On the other hand, polymeric carriers should possess appreciable thermal stability to be used in heat-based methods.

Amorphous cellulosic derivatives such as hydroxypropyl methylcellulose (HPMC, hypromellose) of different viscosity grade/ degree of substitution and its esters are the most used carriers. The desirable solubility of HPMC is limited to only few organic solvents. However, esters of HPMC such as HPMC-acetate succinate (HPMC-AS) are soluble in a

wide range of solvents[21]. Due to the presence of unpaired electrons in ether oxygen, the molecules of these polymers can establish donor-acceptor interactions with a diverse H-bond donor drugs. The vinyl-pyrrolidone based linear polymers namely polyvinyl pyrrolidone (PVP) of different chain length and its copolymer with vinyl acetate i.e. PVPVA are also proven as the best carriers/ stabilizers for physicochemically stable ASD formulation of many structurally diverse drugs. This is because they are soluble in a wide range of polar and nonpolar volatile organic solvents and also show pH independent aqueous solubility. Also, they can establish H-bonding interactions with strong to weak H-bond donor compounds. The main concern on the use of the polymers from this category is their higher hygroscopicity which often proves deleterious to the stability of ASDs while preparation, downstream processing or storage. The semicrystalline polymers based on poly (oxyethylene) backbone such as polyethylene glycol (PEG) and its copolymers are also commonly used for solid dispersion preparation. Their excellent hydrophilicity, surface activity and availability of interacting groups aid for the solubilization, wetting and stabilization of drug during dissolution from solid dispersions. These polymers show very poor solubility in most of volatile organic solvents so not suitable for solvent methods. Because of their lower melting temperature (T_m), they are readily processed through fusion/melting methods. However, the complex and yet poorly understood behavior of PEG towards crystallization of drug and *vice versa* is a current setback towards the reproducible scalability for manufacturing solid dispersions based on them[22]. Methacrylic acid-methyl- or ethyl-methacrylate copolymers (marketed as Eudragit®) show pH dependent solubility hence ideal for targeted delivery in the GI tract. Furthermore, they are capable of forming solid dispersions with a wide variety of drugs and through diverse processes owing to their thermal stability, solubility in various solvents, and tendency of H-bonding as well as ionic interactions[23].

In view of the structural complexity and physicochemical diversity of inflowing drug candidates in the development pipeline and the essential need of processability, the number and type of carriers for manufacturing an enabling ASD are still limited. The efforts for modifying currently available carriers as well as seeking new carriers are continuing. Furthermore, the current paradigm is also shifting towards the use of multiple polymeric carriers to manufacture ASDs wherein individual components solubilize/stabilize by different mechanisms. The addition of other functional excipients such as surfactants or glidants in polymeric solid dispersions to aid dissolution or downstream processing is also prevalent. However, inadequate knowledge on the impact of these additional components on phase

behavior and processability of these multi-component systems has restricted the current selection procedures of these ingredients to *trial and error*[24].

Table I.1 The list of some common polymers used as the carriers in ASD and their relevant properties[25]

Polymer	T_a(or T_m) (°C)	Mol wt (KDa)	δ $(MPa)^{1/2}$	pH solubility	Moisture @75% RH/RT
Cellulosic derivatives					
Hypromellose 2910	170-180	10-50	23.8	1-10	~10%
Hydroxypropycellulose EF	100-150	80	31.5	1-10	12% @ 84% RH
Hydroxyethylcellulose LF		95	31		
HPMC-AS LF	113	55-93	40.5	>5.5	7-8%
HPMC-AS MF	113	55-93	31.2	>6.0	6-7%
HPMC-AS HF	113	55-93	_	>6.5	5-6%
Cellulose acetate phthalate	160-170(192)	N/A	27	>6.0	7-8%
Cellulose acetate butyrate	130(155-165)	30	28.7	Negligible	N/A
Cellulose actetate	170-190 (230-300)	30-60	25.8-26.2	NA	N/A
Hypromellose phthalate	133-137(150)	20-200	28	>5.0	7-8%
Ethyl cellulose	129-133	_	_	Insoluble	~3%
Vinyl pyrrolidone (co)polymers					
PVP K30	175	30-50	27.7	1-10	40%
PVP K90	180	1,100	27.7	1-10	40%
PVP VA 64	106	45-70	25.6	1-10	<10% @ 50%RH
Polyvinyl alcohol	(228,180-190)	20-200	_	1-10	_
Crospovidone		>1,000	_	Insoluble	Max. 60%
Soluplus	(60)	64	22.1	1-10	_
Oxyethylene (co)polymers					
PEG 6000	(55-63)	6	24	1-10.0	0.90%
PEG 35000 S	(64-66)	35	24	N/A	Nonhygroscopic
Poloxamer 188	(52-57)	7.68-9.51	23.7	1-10	<0.5%
Poloxamer 407	(52-57)	9.84-14.6	_	1-10	<0.5%
Solutol HS 15	(25-30)	0.34	_	1-10	N/A
Methacrylate (co)polymers					
Eudragit E100	48	147	19.3	<5.0	N/A
Eudragit L100-55	110	278	23.4	>5.5	
Eudragit L100	>150	123	23.5	>6.0	
Eudragit S100	>150	123		7	
Eudragit RL	70	31		Insoluble	
Eudragit RS	65	30	18.9	Insoluble	

I.2.3 Manufacturing of Amorphous Solid Dispersions

The manufacturing processes for ASD can be broadly classified into solvent and non-solvent methods. As illustrated in Figure I.1, solvent methods comprise various drying processes *viz.*, spray-drying, vacuum drying, freeze drying, supercritical fluid technology and precipitation[26]. The common steps in all these methods are the preparation of a drug-polymer solution in a liquid or supercritical solvent system(s) followed by the evaporation of the

solvent to generate solid state drug-polymer dispersions. However, the types of solvent, drying conditions and therefore the rate of evaporation drastically vary among different processes. For example, aqueous or hydroalcoholic solvents are preferred for freeze drying and processing temperature is generally far below the expected T_g of the solid dispersion. The precipitation method starts with a drug-polymer solution in organic solvent which is precipitated with the addition of organic non-solvent or water followed by drying. In vacuum drying, a drug-polymer solution is prepared in a volatile organic solvent and the same is dried under vacuum at ambient temperature (most of time below T_g). Industrially, spray-drying stands at the frontier of the solvent based methods for manufacturing ASD. A drug-polymer solution prepared in a common volatile organic solvent(s) is mechanically or pneumatically atomized into fine droplets followed by solvent evaporation at extremely fast rate using a drying gas inside a drying chamber and the solid particles formed are collected in a cyclone. The interest in other surrogate techniques of spray-drying such as electrospraying, electrospinning and pulse combustion drying is currently increasing for manufacturing ASD[27, 28]. Another unexplored but potential solvent based process is spray coating of a drug-polymer solution onto the surface of an inert carrier to form solid dispersion pellets[28].

The non-solvent methods are based on fusion/melting, milling or a combination. The fusion method involves heating a drug-polymer system beyond the melting or glass transition temperature followed by quench cooling the comelt to kinetically trap the disordered form in the solid-state. In milling processes, ASD are generated by breaking drug crystal lattices through mechanoactivation in presence of polymers as dispersants that will stabilize the system. This milling process is sometimes carried out in liquid nitrogen cooling environment (cryomilling at$<<T_g$) to avoid concomitant physical transformation of the generated amorphous state by localized heating during the milling process. The most promising non-solvent process for industrial scale manufacturing of ASD is hot melt extrusion[29]. In this method, the drug and polymer are mixed at or above the melting temperature of drug or T_g of polymer while passing through co- or counter-rotating screws that are often equipped with kneading and mixing elements and the extrudates are eluted through a die. The heat energy, shear force and dragging flow of polymer chains ensure intimate mixing of drug and polymer molecules.

Despite the availability of numerous manufacturing processes, the number of marketed formulations based on ASD is very limited[6]. The selection of a manufacturing process for a particular drug-carrier-additive is generally made intuitively. Moreover, many operating

parameters available within a particular process necessitate the comprehensive understanding on the impact of these parameters on the quality attributes of the resulting ASD which is currently lacking. At present, the process optimization activities for manufacturing ASD are merely based on statistical design of experiments[30]. In fact, this approach has only observational value and therefore redundant efforts are required for new systems.

I.2.4 Characterization of Solid Dispersions

As solid dispersions are composed of multiple components that too can be present in various solid states, the comprehensive characterization, best at the molecular level, requires the utilization of a gamut of analytical techniques. In case of ASD, the T_g is regarded as the primary indicator of miscibility and compositional homogeneity. An ideal set of characterization tools should provide both qualitative and quantitative information on miscibility, phase separation and size of the separated domains, crystallinity and the crystalline properties, molecular mobility, moisture/solvent and on the types/ strength of molecular interactions. These techniques should be capable of monitoring these characteristics of solid dispersions during manufacturing, stability and dissolution testing. Apart from molecular level properties, the analysis of particle and powder properties (size, morphology, surface and density) are equally important for solid dispersion downstream processing.

In this part, the focus is given to the tools for the characterization of the phase structure of solid dispersions. The thermoanalytical techniques mostly preferred for the analysis of solid dispersions. Baird and Taylor have recently published an excellent review on analysis of solid dispersion using thermal and thermoelectric tools[31]. The thermal analysis is complemented by X-ray diffractometric and various molecular and dielectric spectroscopic measurements at ambient/ non-ambient environment (higher humidity and/or temperature). Powder X-ray diffractometric analysis of amorphous composites using a high energy source generates high quality data to obtain miscibility information at subtle level by atomic-pair wise distribution (PDF) analysis[32]. Furthermore, light, electron and atomic force microscopic techniques provide abundant information on the surface topography, crystallinity, phase distribution etc. Gravimetric vapor sorption study of amorphous systems provides insight into moisture-induced crystallization kinetics and amorphous content. Also, there is increasing trend in the use of different tools in hyphenation to obtain an integrated and real time information. Table I.2 enlists the different types of molecular characterization tools for drug-polymer solid dispersions.

Table I.2 Some characterization techniques for ASDs, information therefrom and their pros and cons

Techniques	Information	Pros and Cons
Differential scanning calorimetry (DSC)	Glass transition, melting, crystallinity, (re)crystallization, polymorphic transitions, enthalpy recovery	Immiscibility reflected as multiple T_gs for separated domain size ≤30 nm[33], T_g shape and width important, local melting events undetectable for some heterogeneous systems
Thermogravimetric analysis (TGA)	Moisture/volatile content, kinetics of drying/desolvation, dehydration	Difficult to deconvolute concomitant moisture and solvent loss, hyphenatable with IR or MS
Powder X-ray diffractometry (pXRD)	Crystallinity, crystal forms, local structure, mesophases	Preferred orientation problem for crystallinity, amorphous halo interpretation of immiscible system complicated
X-ray photoelectron spectroscopy (XPS)	Surface chemical composition, phase distribution	Limited to drug-polymer with dissimilar elemental composition[34]
Vibrational spectrosocpy [Infrared (IR)/ Raman]	Homo/heteromolecular interaction (H-bonding, dipolar interaction), crystallinity, lattice vibration	Vibration bands broaden for amorphous phase, H-bonding interactions originate band shift, IR-phase resolution limited, interference by moisture, IR coupled with AFM[35], Raman profile not affected by water but by elastic scattering
Solid-state Nuclear Magnetic Resonance (NMR) Spectroscopy/ Relaxomerty	Molecular conformations, interactions, diffusion, mobility, relaxation times, separated domain size	Detection limit near to molecular size for separated domain[36], best tool for studying molecular dynamics, time intensive, expensive, bulk characterization indistinct from surface
Dielectric relaxation spectroscopy (DES)	T_g, molecular mobility (α, β and other processes) above and below T_g, crystallization	Technique of choice for studying local and global mobility originating from sub- and above-T_g processes, interfered by dc conductivity[37]
Polarized light microscopy (PLM)	Crystal form, size, morphology and transitions , desolvation, nucleation, crystallization	Insufficient illumination of trace/ small crystallites dispersed in polymer matrix, absence of birefringence in isotropic crystal eg. cubic
Scanning/transmission electron microscopy (SEM/TEM)	Surface, crystal form, size, morphology and transitions, internal structure	Surface crystallites easier to distinguish, less or no information on amorphous phase (separation) by SEM, TEM with staining helpful in studying phase distribution but tedious sample preparation
Atomic force microscopy (AFM)/ nano-thermal analysis	Surface topography, spatial T_g of phase separated systems, melting, phase distribution	Best technique for phase mapping and distribution analysis, complex for ternary systems, topographic information may suffer from thermal drift during slow imaging
Inverse gas chromatography (IGC)	Surface area, energy, mobility, crystallinity and interactions, porosity, diffusion	Method of choice for analyzing surface heterogeneity[38], equilibrium data interfered by the adsorption of probe gas on solid sample
Gravimetric vapor sorption (GVS)	Crystallization, amorphous content, hydrate formation, dehydration	Suitable to study the moisture-induced transitions[39], excess hygroscopicity poses problem of water condensation

I.3 Background of Spray-Drying

Spray-drying is a unit operation capable of transforming solutions or suspensions into a solid product. At present, it is operational in diverse industrial fields ranging from food and dairy processing, ceramics, paints, fertilizers, detergents and pharmaceutical industry. Spray-drying is a well utilized pharmaceutical unit operation for simple drying to particle

engineering of bulk API/excipient, granulation, encapsulation etc.[40]. One of the growing applications of spray-drying is for manufacturing amorphous solid dispersions, referred to as spray-dried dispersion (SDD) henceforth. The very fast solvent evaporation during spray-drying leads to rapid viscosity increase and permits kinetic trapping of the API in the carrier matrix[41].

An illustration of a typical spray-dryer installation is presented in Figure I.3. The spray-drying process consists of four basic stages: atomization of the liquid, mixing of the liquid with the drying gas, evaporation of the liquid and separation of the dried particles from the gas. The liquid solution or suspension is transported from the container to the nozzle entrance via a pump system. The solvent is mostly aqueous, but in case of solid dispersion preparation, organic solvents are mainly used. Hence appropriate equipment safeguards are mandatory.

Atomization transforms the liquid stream into fine droplets by applying a force. The high surface to volume ratio favors efficient and rapid drying of the droplets. Several types of atomization devices are available, depending on the type of energy that is involved: centrifugal energy, pressure energy, kinetic energy and vibrations. Centrifugal forces are generated in a rotary atomizer. The commonly used are kinetic energy or pneumatic nozzles (bifluid nozzles) where the fluid stream is broken in small droplets by interaction with a second fluid, usually pressurized air (Figure I.3). The droplet size is determined by the ratio of the pressurized gas flow rate to that of the liquid, density of the gas and the liquid, surface tension and viscosity of the liquid[42]. Pressure nozzles generate fine droplets by pressurizing a liquid feed by a pump and forcing the liquid feed through the nozzle orifice. Inserts produce a rotary motion of the liquid inside the nozzle leading to the desired cone-shaped spray pattern. Droplet size is inversely proportional to the pressure applied and directly proportional to the feed rate. Ultrasonic nozzles have become the focus of increasing interest in recent years. Buchi developed a lab scale spray-dryer based on vibration mesh spray technology which enables generation of very small and more uniformly sized droplets[43]. Droplets are generated based on a piezoelectric driven actuator, vibrating a thin, perforated stainless steel membrane in a small spray cap. The vibration of spray mesh featuring an array of micron-sized holes ejects millions of droplets with narrow size distribution.

The liquid spray is subsequently mixed with the drying gas, often air or in some cases nitrogen. The drying gas needs to be conditioned to have the right temperature and humidity in order to exert its heat and mass transfer properties. Perforated air dispersing systems

introduce the drying gas into the drying chamber. The dimensions of the drying chamber may vary from a diameter to length ratio of 1–5 in case of pressure nozzles or bifluid nozzles to 1–2 in case of rotary atomizers. Large droplets are most difficult to dry since they possess enough momentum to escape the gas whirl and lead to wall deposition. Hence, consideration of the drying chamber dimensions is important for process optimization. The contact between the liquid spray and the drying gas is mostly established via a co-current design, which indicates that the gas flow and spray is in the same direction. Drying gas inlet and atomizer are positioned at the top of the drying chamber. This configuration leads to contact between the feed and the highest temperature drying gas, since the latter has not yet exchanged its heat with the surroundings. Evaporative drying as in spray-drying can be monitored/described using psychrometric charts providing information concerning properties like dry and wet bulb temperature, relative and absolute humidity and enthalpy of the drying gas and the relationships between them (*Mollier diagrams*). These charts are available for air–water systems, but unfortunately less available for organic solvents-air or nitrogen systems.

A particulate aerosol is formed when droplets are dried and transformed to solid particles and the collection of the particles are separated from the drying gas stream and collected is using a cyclone separator and/or bag filtration. The cyclone is very efficient to separate dispersed particles from the continuous gas phase based on density differences between the two phases. When the solid particles and the gas are subjected to an accelerating flow field within a rotating vortex in the cyclone, a velocity lag is experienced by the dense particles compared to the lower density medium. The most common type of cyclone used is the reverse-flow type in which particle-air dispersion is introduced tangentially into the top part of the cyclone. The vortex that is produced by the high fluid velocity forces the particles to the walls of the cyclone and down to the conical section. At the end of the conical part, the gas stream reverses and leaves the cyclone through the vortex finder. Large particles separate from the vortex and are collected, whereas smaller particles are entrained with the gas stream. Larger the acceleration in the cyclone, the smaller the particles that can be separated from the drying gas. In case of using organic solvents in the feed, inert drying gases are used (e.g. dry nitrogen) in combination with a closed-cycle set-up. A condenser unit is applied to recover the solvents and to avoid pollution of the environment. Often, after completion of the process, the particles are further post-dried in a vacuum oven.

Spray-drying is a complicated process and understanding the interplay between process parameters on the one hand and formulation parameters on the other hand is crucial

for the desired product quality. Spray-drying process parameters include inlet temperature, humidity and flow rate of drying gas, feed rate and atomization conditions. On the other hand, formulation parameters to consider are composition (API, carrier, solvent) and solid content in the feed, solvent type, viscosity and surface tension of the drying solution.

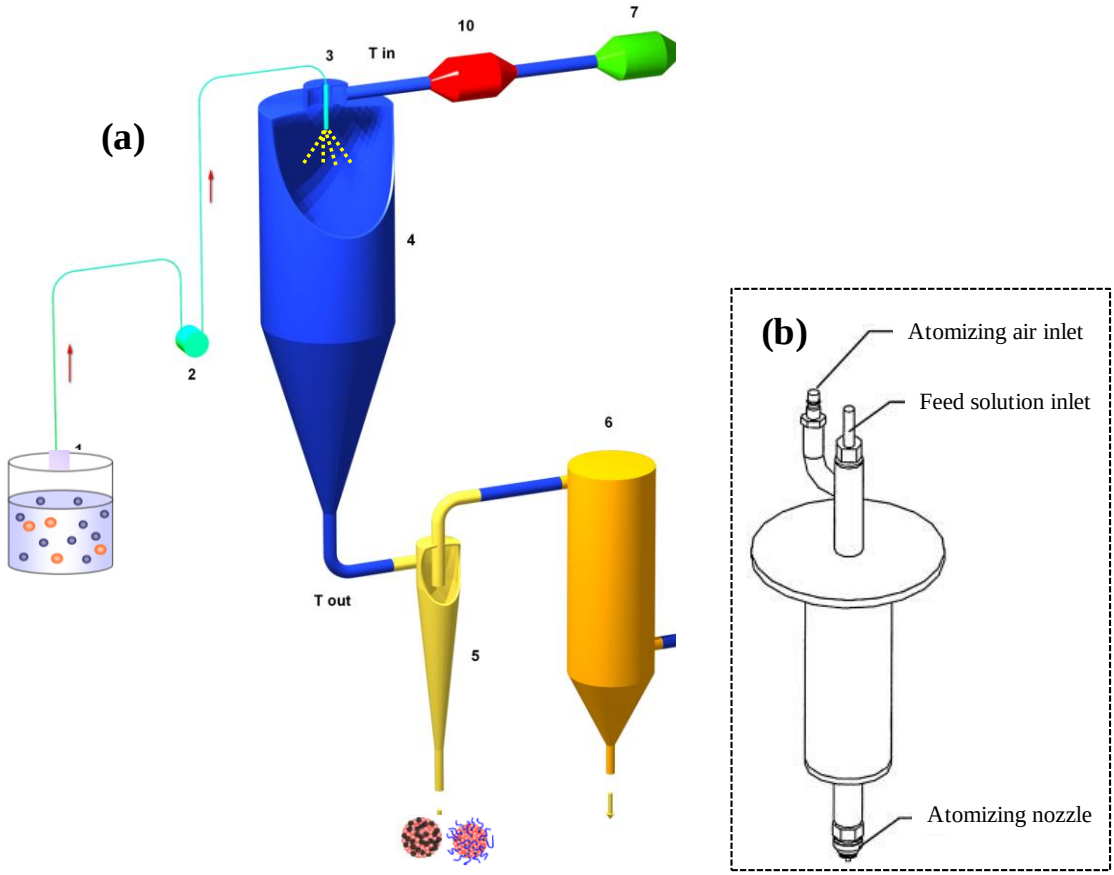

Figure I.3 (a) Spray-dryer with co-current orientation (1-Feed solution, 2-pump; 3-feed inlet and nozzle, 4-drying chamber, 5-cyclone collector, 6-filter and 7-heater) and (b) A bifluid nozzle assembly.

I.4 Solvent Systems for SDD Preparation

An adequate solvent system is a prerequisite for the generation of amorphous SDD of the desired phase structure and physicochemical attributes. The first indispensable condition is indeed to find out a common solvent (s) system to solubilize all feed components *viz*., API, carrier and other additives. The primary criteria for the selection of spray-drying solvent system include (i) high solubility of drug and carrier in the selected solvent (>50 mg/ml), (ii) the generation of a feed solution with acceptable viscosity, (iii) low toxicity, (iv) high volatility (v) appreciable chemical stability of feed components and (vi) non-combustive in the spray- drying environment[25].

Some relevant physical properties of the common spray-drying solvents are listed in Table I.3. Enthalpy of vaporization provides important information that can be helpful in

controlling the outlet temperature and energy consumption by the spray-dryer. Other solvent properties like viscosity and surface tension are determining factors for the feed atomization during spray-drying and are also indicators of molecular interaction among drug-carrier and solvent. Dielectric constant and polarizability are the polarity scales of a solvent; the higher the values, the more polar the solvent is. Sometimes, these properties are correlated with the phase structure in the resulting SDD. Solubility parameters can be an estimable guide for the spray solvent selection too. It can also provide an estimate for the solubility gap between drug and carrier in the feed solution. The Kamlet-Taft (KT) parameter is a traditionally used scale for getting insight into the possibility of having H-bond donor and acceptor pairs alongwith the strength of H-bonding in solution[44]. Solvents with higher α value, H-bond donor acidity, are protic solvents like normal alcohols that can efficiently disperse polymer or drug molecules with stronger H-bond acceptor in solution. In contrast, protophilic solvents with higher H-bond acceptor value (β) are suitable for stronger H-bond donor drugs/polymers.

Table I.3 ICH residual content limit and some relevant physical properties of spray-drying solvents[45]

Solvent	ICH limit (ppm)	B.P. (°C)	ΔH_v (kJ/mol)	P (hPa)	η (mPa.s)	γ (mJ/m^2)	ε	δ (cal/cm^3)$^{1/2}$	KT parameter	
									α	β
Water	Na	100.00	40.70	17.50	0.89	71.90	78.40	23.40	1.17	0.47
Methanol	3000	64.70	35.30	128.00	0.54	22.10	32.60	14.50	0.98	0.66
Ethanol	Na	78.30	38.70	59.00	1.08	22.00	24.30	12.70	0.86	0.75
Isopropanol	--	82.30	45.70	44.00	2.07	18.30	18.30	11.40	0.76	0.84
DCM	600	39.80	28.00	475.00	0.42	27.20	8.90	9.70	0.13	0.10
Acetone	Class 3	56.30	29.10	240.00	0.30	22.68	20.70	9.60	0.08	0.43
Dioxane	380	101.30	38.00	41.00	1.26	33.00	2.20	10.00	0.00	0.37
Tetrahydrofuran	720	66.00	26.90	200.00	0.46	26.40	7.50	9.100	0.00	0.55
Ethyl acetate	Class 3	77.10	31.90	97.00	0.43	23.20	6.00	9.00	0.00	0.45
Chloroform	60	61.20	30.80	210.00	0.54	26.60	4.70	9.30	0.20	0.10
Acetonitrile	410	81.60	33.80	97.00	0.34	28.45	37.50	11.9	3.44	--

B.P.: boiling point, ΔH_v: enthalpy of vaporization, P: vapor pressure at 20 ◦C, η: viscosity at 25 ◦C, γ: surface tension at 25 ◦C, ε: dielectric constant, δ: total solubility parameter, KT: Kamlet Taft, α: KT hydrogen bond donor acidity, β: KT hydrogen bond acceptor basicity.

Most of poorly water soluble API and polymeric carriers show acceptable solubility in a range of organic solvents or mixtures. However, the growing structural complexity of the molecules entering drug discovery and development programs render them insoluble not only in water but also in several spray-drying solvents. This necessitates a rigorous exercise in selecting the optimal solvent system for SDD manufacturing. Provided multiple choices, the spray-drying solvent is widely considered as one of the most important variables for pharmaceutical particle engineering to prepare tailor made products in terms of size

distribution, morphology and surface composition/topography and eventually drug release from the spray-dried products. Beyond the eminent impact on the particulate and bulk properties, the recent concern has been driven towards the understanding of the spray-drying solvent on the phase structure and therefore *in vitro*/*in vivo* performance and/or physical stability of amorphous SDDs. The solubility of API in the selected solvent can have an influence on the drug loading efficiency and hence release behavior of spray-dried particles. The use of solvent wherein the drug remains (partially) undissolved can result in remaining drug particles which possibly will not be enclosed in the spray-dried microspheres and if they will, they cause an inhomogeneous drug distribution in the microspheres, far from the often ambitioned molecular dispersion of the API in the polymeric matrix.

The importance of solvent selection on particle architecture can be explained by looking at the particle formation process. Particle formation in spray-drying and more precisely the distribution of the components in spray-dried materials has been described in detail by Vehring et al. The authors emphasized the use of the Peclet number (P_e) to predict compound distribution during the particle formation process[46] (eq I.6).

$$Pe_i = \frac{K_i}{8D_i} \quad \text{Equation I. 6}$$

In eq I.6, the evaporation rate is represented by K_i and D_i stands for the diffusion coefficient of solute *i*. The combination of these parameters will determine particle morphology and drug distribution in the particle, which is hence clearly influenced by the solvent selected, its evaporation rate and the distribution coefficient of the compounds in this solvent. Solvent selection has an influence on particle morphology and associated density through the solvent's evaporation rate. For a given feed concentration, a lower solvent evaporation rate (and thus lower P_e) allows the droplet surface to recede during the evaporation process, resulting in limited void spaces, denser particles and hence a higher bulk density of these microspheres. More rapid evaporation (higher P_e) and therefore faster solute deposition occurs in solvents which require low quantities of thermal energy to effect vaporization (solvents having a low boiling point) or in which the polymer has a low solubility. Consequently the solidification point will be reached faster, resulting in an increase in void volume and porosity. Shell formation will be likely due to the enrichment of solute at the droplet surface. Solvent can also have influence on the feed component distribution through the differential diffusion coefficient during droplet drying and hence affect the physical structure of the final SDD. With a constant evaporation rate, a lower diffusion

coefficient (and thus higher P_e) implies that the diffusional movement of the compound is slow compared to the speed of the receding droplet surface, resulting in enrichment of the compound at the droplet surface, leading towards shell formation. Compounds with a higher diffusion coefficient (and hence lower P_e) can follow the shrinkage of the droplet surface and will be distributed homogeneously throughout the particle. For immiscible compounds, the differences in diffusion coefficient will have an influence on their phase distribution: the compound with the lowest diffusion will most likely be situated at the microsphere surface (in the case that none of the compounds possesses surface activity). The diffusion coefficient of feed components can be correlated with various feed parameters using the Stokes Einstein equation[47] (eq I.7):

$$D = \frac{K_B T}{6\pi\eta r} \quad \text{Equation I. 7}$$

where D, r, T, η and K_B are the diffusion coefficient, the hydrodynamic radius of the diffusing component, the absolute temperature, the viscosity of the solution and Boltzmann constant, respectively. Viscosity of a polymer solution depends on the polymer concentration, molecular weight and is specific for a certain solvent/polymer pair. This specificity lies in the polymer dispersivity in a chosen solvent and non-covalent interaction between polymer–solvent. Moreover, the interplay between solvent evaporation rate and polymer solubility will influence the final particle size. With high evaporation rate and/or low polymer solubility, solidification of the droplet surface will be fast resulting in large particles. A slow evaporation rate and/or high polymer solubility will evoke slow shrinking of the droplets with a slower solidification rate (low P_e) whereby smaller but denser particles will be formed. Another important product quality influenced by solvent properties is the amount of residual solvent retained in the SDD. During the evaporation process the solvent removal rate will be dictated by the ratio between the boiling point of the solvent and the inlet temperature. A high ratio will be translated into a slower solvent evaporation and a higher amount of residual solvent. The foremost precaution related to solvent retention in SDD is indeed the toxicity issue of these solvents. Various solvents classified by ICH are allowed below a certain limit in the final product based on their toxicity[48]. In physicochemical perspectives, the residual solvent present will plasticize amorphous SDD hence lowers T_g of the SDD that can potentially lead to physical instability. Some authors described the benefits of using solvent mixtures, comprising increased drug–polymer miscibility, improved dissolution kinetics and enhanced stability[49]. The technological properties of powders can also be improved by using appropriate solvent blends for spray-drying.

I.5 Key Formulation and Process Parameters Influencing the Physical Structure of SDD

The current era of quality by design (QbD) conceptualization of the industrial manufacturing processes including pharmaceuticals in hyphenation with process analytical technology offer various opportunities of exploiting the knowledge space of precursor material properties and design space of underlying process variables for the development of a robust process as well as the desired quality attributes of the end products. The plethora of information available on the use pharmaceutical spray-drying is directed towards the built-in particulate or bulk level properties of the final product[30]. Nonetheless, there is paucity in literature information on the investigation of the impact of various formulation and/or processing variables of SDD on the final product quality. Few studies on SDDs attempted to relate the formulation and process variables on the yield, particulate/bulk properties or other derived properties therefrom of the obtained product that are important for the downstream product development process. In spite of copious information on the significant impact of evaporation rate on the characteristics of the generated supramolecular structures in spray-dried composites of food and dairy products, it is surprising that the pharmaceutical literature as such is silent on aspects of the nano to mesoscopic phase structures like homogeneity, amorphous miscibility, crystallinity, surface energy, hygroscopicity and on the physical stability of high energy amorphous SDDs resulted from the interplay of various process and formulation variables. The non-exhaustive information on the multivariate relationship of SDD quality attributes with formulation and process variables are presented in Figure I.4 and some literature examples are summarized in Table I.4.

I.5.1 Formulation Parameters

Understanding solution chemistry and control of the feed solution properties play a determining role on powder characteristics *viz.*, porosity, particle size/shape/morphology (distribution), surface charge/stickiness, volatile (residual solvent/moisture) content as well as phase homogeneity and surface/bulk energy of the resulting SDD. These outputs on the one hand affect several derived properties like powder flow (Carr index), bulk/tap density, tablettability, etc. and on the other hand determine the *in vitro* dissolution rate and/or *in vivo* performance, hygroscopicity, stressed and/or long term physical stability (structural relaxation, phase separation and/or crystallization rate). Additionally, final yield, experimental throughput and drying capacity can be notably affected[41]. Some critical feed solution properties and their contribution on various phenomena and quality attributes of the final formulation are illustrated in Figure I.4.

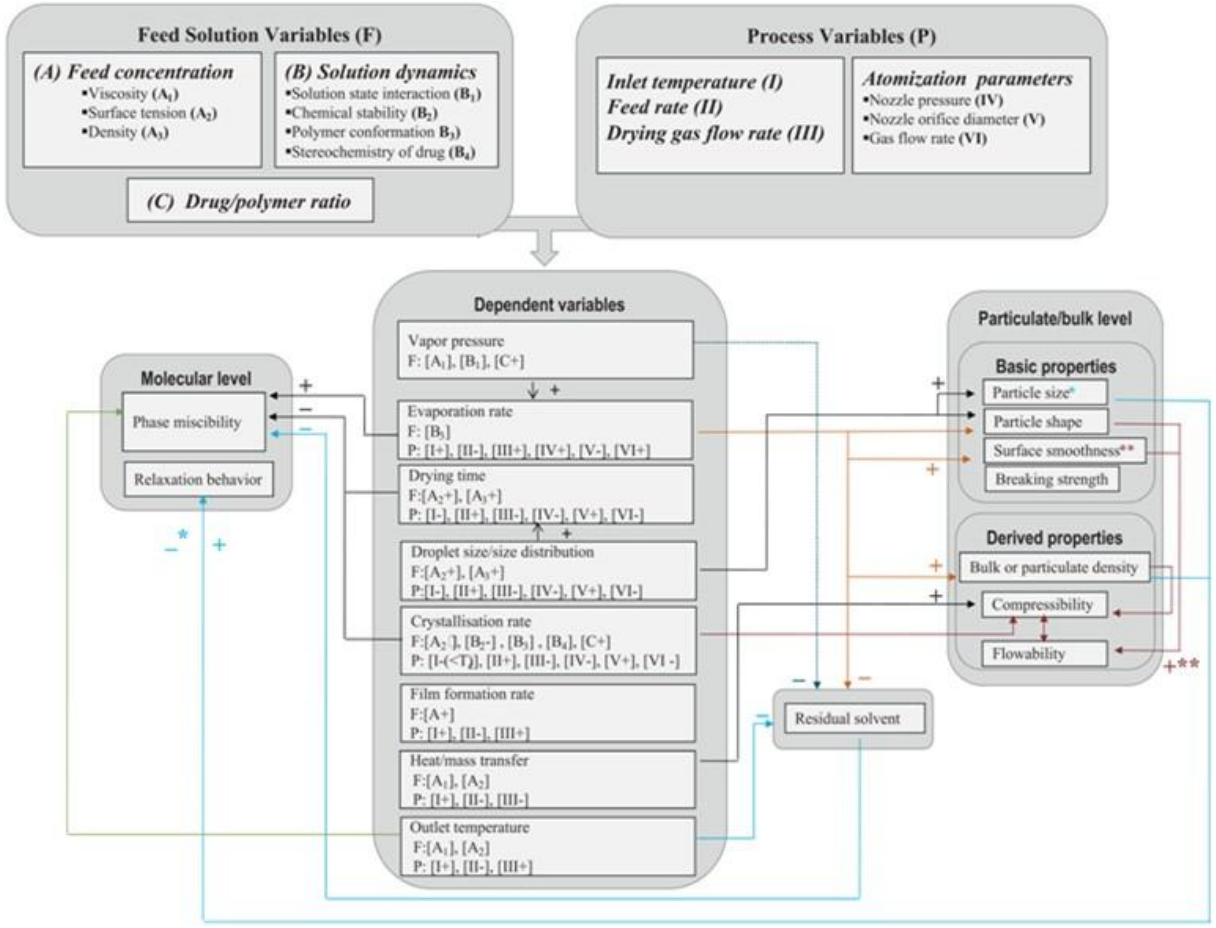

Figure I.4 A flowchart illustrating the influence of feed solution and process variables on underlying processes during spray-drying and thereby on the molecular and particulate/ bulk level properties of the SDD [(+): directly related, (−): inversely related, T_c: crystallization temperature and no notation (+ or−): variables can have a direct or an inverse relation with the effects).

I.5.1.1 Feed Composition

The rational selection of a suitable carrier, solvent and other possible additives in the right ratio is the foremost step in the development of a SDD of poorly water soluble drugs with the desired phase homogeneity and miscibility. Indeed, solid solubility is primarily the limiting factor for deciding the drug to polymer ratio to obtain homogenous amorphous SDD under the applied processing condition. The solubility difference among drug, carrier and other additives in a feed solution (solvent) leads to a different degree of saturation/supersaturation of these components[46]. This would expectedly influence several underlying phenomena during droplet drying. Moreover, the excessive gap in temperature dependent solubility between solute components can potentially induce radial demixing during particle formation as an insoluble component starts precipitating earlier at the shrinking droplet surface. The partial vapor pressure of the solvent in the feed solution is directly influenced by the solute content which has direct impact on the solvent evaporation

rate. The other feed solution properties that can be altered with the variation in drug to polymer ratio are viscosity, surface tension, specific gravity, pH, etc. This would impact the droplet size (distribution) during spray-drying and in turn the rate of solvent removal. The rate of core to surface transport of solvent and then evaporation from a droplet surface decrease with the increase in feed viscosity due to higher fraction and/or molecular weight of polymer present in solution. Also, breakup length of liquid jet during atomization increases with increasing feed viscosity resulting into larger droplets. The shift in rheological regime of feed solution can drastically change the spray rate and droplet size. The solution state properties such as polymer diffusion coefficient and solute–solvent molecular interactions are drastically altered with different drug to polymer ratio. For example, usually drug molecules of smaller size diffuse several orders of magnitude faster than bulky polymer molecules. These facts imply the utmost importance of composition dependent solution dynamics in predicting the phase behavior of the resulting SDD.

I.5.1.2 Feed Concentration

Typical feed concentration used for the preparation of amorphous pharmaceutical solid dispersions ranges from 10 to 20% (w/v)[25]. Apparently, feed concentration is directly proportional to P_e and hence inversely related to the evaporation time. The diffusivity ratio between feed solution components can alter markedly with the change in feed concentration. This is because in dilute solutions the drug is present as monomer while at higher concentration some drugs are able to form multimers[50]. At particle level, the geometric mean diameter of spray-dried particles is directly proportional to the feed concentration. The lower solute content in the feed solution typically generates spherical and smaller and highly electrostatic particles. In contrast, larger and often hollow particles are generated from concentrated and hence viscous solutions due to the formation of larger droplets[51]. The effect of solute concentration on the droplet size is less pronounced at higher settings of spray-drying process parameters.

I.5.2 Process Parameters

A large number of pharmaceutical publications emphasize the influence of processing parameters on the particulate and bulk properties of spray-dried products. However, there is almost no theoretical as well as experimental information in pharmaceutical literature dealing with the impact of different processing parameters on the phase structures as well as particulate and derived properties of the resulting SDD. Dobry et al. published an excellent

review providing a systemic flowchart on the spray-drying process development for manufacturing SDD[51].

I.5.2.1 Feed Flow Rate

The feed rate is the foremost parameter to start with for attaining a balance between throughput and proper drying[41]. It primarily governs the atomization pattern and droplet/particle residence time during the spray-drying operation. As feed rate directly affects the saturation degree of the exiting gas, it influences the outlet temperature at the given drying set up. Therefore the upper feed rate limit is set to attain sufficient drying of the particles.

I.5.2.2 Inlet and Outlet Temperature

The temperature of the drying gas encountering the droplets of the atomized feed is considered as the most important determinant of the internal structure of the resulting spray-dried particles. Next to feed solution development and feed rate setting, optimization of inlet temperature is crucial to maintain sufficient P_e value and to attain the targeted outlet temperature. Having direct impact on solvent evaporation kinetics from the drying droplet, it is a primary process variable responsible for the development of the unique phase structure and controlling the level of residual content and bulk/particulate level properties of the final product. The outlet temperature is also important to obtain the desired product quality. For amorphous formulations, it is of prime importance in relation to physical stability as this is practically the highest temperature to which the solidified product may be heated during spray-drying. The outlet temperature of the drying gas is a derived process parameter dependent upon inlet temperature, drying gas flow rate and enthalpy of evaporation of solvent in the feed[42]. The overall process efficiency of spray-drying is highly dependent on the ratio of inlet to outlet temperature. During spray-drying at higher temperature, hot/fast particle formation occurs with the temperature at the drying gas-droplet interface equivalent to or higher than the solvent boiling point wherein the vapor pressure built in by the solvent keeps the surface smoother. Hence, it results in materials with larger size, hollow core and dry hygroscopic particles with less residual solvent and the activated surface. In case of spray-drying at lower temperature (slow/cold), shrinking of particles leads to rough surface topography[51].

I.5.2.3 Drying/ Atomization Gas

Selection of proper drying as well as atomization gas type and flow rate ensures efficient drying capacity of a process with built-in product attributes. Other than for optimization of specific drying capacity of a spray-dryer, i.e. the mass ratio of drying gas flow rate to feed rate, drying gas is generally considered as the idle parameter in relation to the product properties. Slower rate of charging drying gas into the drying chamber leads to higher span of drying particles in the chamber which reduces the residual solvent content while higher drying gas flow rate leads to reduction of particle size due to higher gas-particle attrition. The nozzle airflow rate directly controls the droplet size and distribution during atomization. Dehumidified air is mostly used as the drying/atomization gas for the preparation of SDD. Inert gases are recommended for oxidatively labile feed and drying at higher temperature.

I.5.2.4 Atomization Nozzle Type

The atomization efficiency primarily relies on the selection of type, orientation and size of the atomization device. Mostly, bifluid nozzles are used to prepare pharmaceutical solid dispersions[42]. The selection of atomization nozzle type is important to consider in view of the subsequent scale up of the process to yield the matching droplet size distribution and evaporation profiles. Most of times, particle size distribution of the product is the main response to select the atomization parameters and nozzle types. The increasing interest towards the use of four fluid nozzles for the preparation of SDD is intended for feeding the drug and the carrier solution separately into an atomization nozzle and thus overcoming the problem related to the common solvent requirement for the feed components[52].

Table I.4 Examples of formulation and process effects on molecular properties of amorphous and SDDs

Drug (s)	Carrier (s)	Variable	Effect (s)	Ref
Macrolide antibiotic		Inlet temperatures (above and below T_g)	Product formed<T_g was partially crystalline while highly stable amorphous states formed between T_g-crystallization temperature	53
Furosemide		Inlet temperatures (above T_g)	The T_g of and the intermolecular interaction in the amorphous forms were directly linked to inlet temperatures	54
Ursodeoxy-cholic acid		Inlet temperatures	Inverse relationship of inlet temperature with the crystallinity, H-bonding and direct relation with the hygroscopicity	55
Cefditoren pivoxil		Inlet temperatures	At higher RH the amorphous state formed at lower temperature crystallizes/ sorbs more moisture but product formed at higher temperature remains intact/ sorbs less water	56
Griseofulvin	PVP /PHPMA	Solvents (acetone-water, acetone-methanol) and feed concentration	20°C higher T_g of SDD prepared from organic solvents mixture and lower feed concentration generates product with higher molecular mobility	49
Itraconazole,	Kollicoat IR	Solvent systems	Ternary solvent system broadened the applicability of Kollicoat IR by improving miscibility and decreasing crystallinity	57
Artemisinin	Malto-dextrin	Feed flow rate, inlet temperature	Crystallinity of artemisinin decreases with the increase of feed flow rate and inlet temperature	58
Itraconazole	Mannitol	Inlet temperature	Itraconazole crystallinity increased with inlet temperature	59
Acetaminophen	PVP	Outlet temperature, bifluid nozzle orifice diameter	Lower outlet temperature led to rougher surface topography whereas higher temperature formed smoother particles	60
Tetrahydro-cannabinol	Inulin	Drying gas (Nitrogen and air)	Nitrogen as drying gas markedly reduced the degradation of drug	61
Tolbutamide, salbutamol sulfate	HPMC, Eudragit (RL/ RS)	Nozzle type (bifluid and four fluid)	Feeding drug and polymer solution through a four fluid nozzle formed completely amorphous dispersion, partial crystallinity using a solution	52, 62
Nilvadipine or nifedipine	HPMC	Feed rate, concentration and nitrogen flow rate	Dispersions prepared with higher evaporation rate showed higher amorphous heterogeneity	63

I.6. Model Drug and Polymer System

The present project is designed to comprehensively investigate the influence of formulation and process parameters on the physical structure and related quality of amorphous solid dispersions prepared by spray-drying. The model poorly water soluble drug selected was naproxen and the model polymeric carrier selected was PVP.

Naproxen is a nonsteroidal anti-inflammatory drug (NSAID) of profen or aryl acetic acid class (*(S)-2-(6-methoxynaphthalen-2-yl) propanoic acid*) and therapeutically indicated

for the treatment of pain and musculoskeletal diseases[64]. Naproxen is currently the only marketed profen in an optically pure form. It is a nonselective inhibitor of cyclooxygenase (COX), the enzyme catalyzing the synthesis of prostaglandin, a messenger for the mediation of inflammation and pain pathway. Naproxen is marketed in tablet and oral suspension, administered as both free acid as well as sodium salt. Naproxen is a typical BCS class 2 drug with practical insolubility in aqueous medium (3mg/ml at pH 7.4 and < 20μg/ml at pH 1.2 and 25°C) and high GI membrane permeability (LogP: 3). This qualifies it as a model compound for the present investigation. Moreover, the molecular behavior of naproxen in solid- and solution-state has been extensively characterized. Only one reported crystal form of naproxen melts at ca. 156°C. In contrast to other profen congeners, its crystal structure lacks the cyclic H-bonded dimer[65]. Rather, it comprises the linear H-bonded catemer, hence non H-bonded carbonyl groups are also present. Naproxen exhibits variable solubility in organic solvents ranging in polarity and proticity *viz.*, methanol, ethanol, DCM, acetone etc. The molecular state of naproxen in solution is markedly solvent dependent[66]. It is mainly present as monomer in protophilic solvents and as dimer in aprotic solvent while both species uniformly exist in amphiphilic solvents[50]. Two conformers of naproxen molecules existing in solution have been characterized and their relative proportions show a distinct solvent dependence[67]. Another interesting structural feature of profens is their tendency to undergo temporal S↔R stereo-oscillation in organic and hydroalcoholic solutions[68]. The structural features are illustrated in Figure I.5.

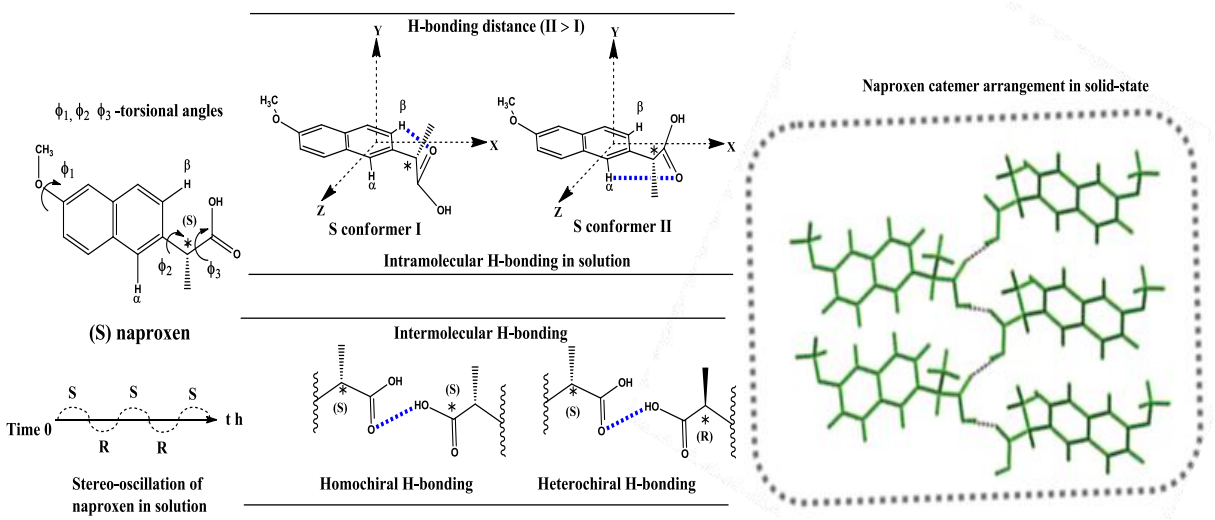

Figure I.5 Various solution- and solid-state molecular arrangements of naproxen (dashed blue line: H-bond)[50, 66-68].

The selected carrier for the present project, PVP, is an amorphous hydrophilic polymer soluble in water, methanol, dichloromethane etc[69]. It is a linear atactic polymer built up of N-vinyl pyrrolidone (VP) monomer units with random distribution of conformations with

adjacent pyrrolidone on the same (*meso*) and the opposite (*racemo*) side of a plane[70]. Overall, the viscosity of the polymer in solution and T_g are directly proportional to the molecular weight and hygroscopicity is inversely related to the chain length. Different molecular size PVPs are represented by their Fikentscher K-value derived from solution viscosity-concentration profiles. The T_g of pharmaceutical grade PVPs range from ca. 100°C (PVP K 12, average molar weight: 2400 Da) to ca. 180°C (PVP K 90, average molar weight: 1,100,000 Da). The VP contains two nucleophilic centres within the amide group *viz.*, non-bonded electron pairs of oxygen and of nitrogen. However, mostly only the carbonyl oxygen serves as the strong H-bond acceptor as the nitrogen is inaccessible due to steric hindrance. As shown in Figure I.6, the linear hydrocarbon backbone and freely suspended VP side groups provide substantial conformational flexibility through torsional and dihedral rotations in solution and solid-state[71]. Hence, highly heterogeneous intermolecular interactions can occur with solvents or cosolutes of different chemistry depending upon the availability and stability of the favourable conformations at varying temperature and concentration.

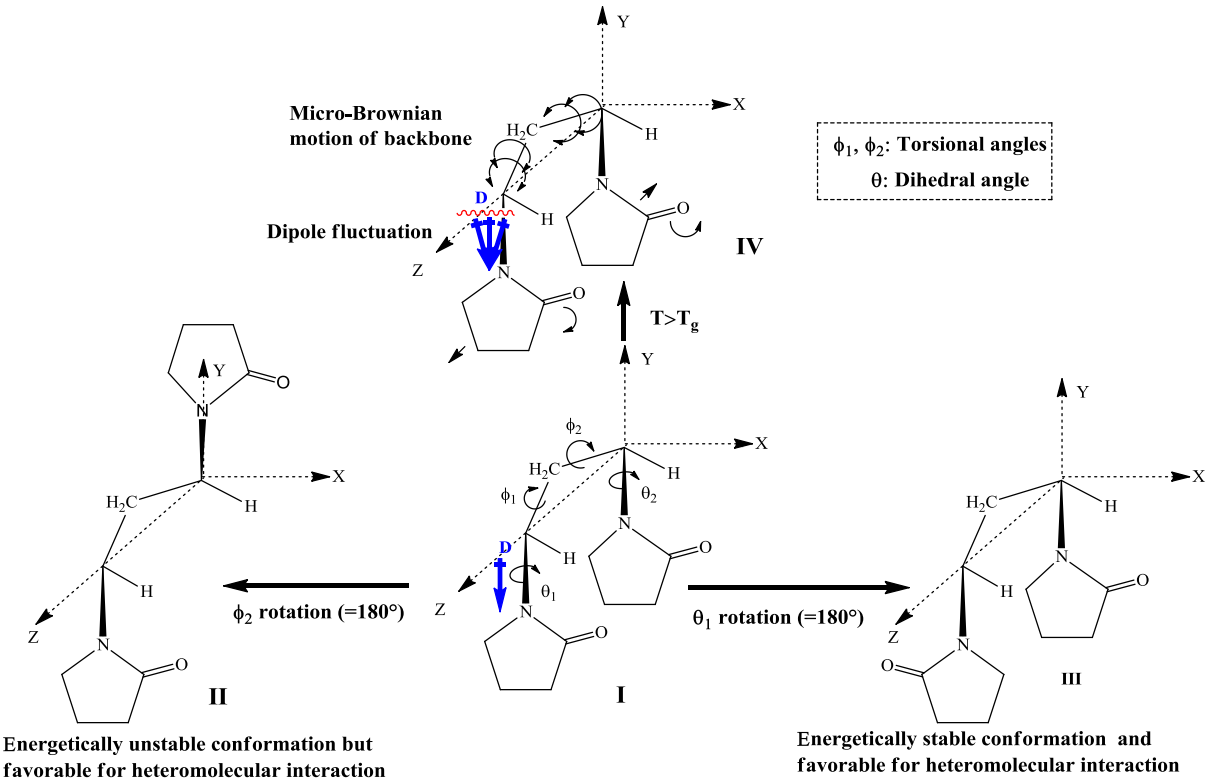

Figure I.6 Conformational characteristics of a VP meso-dyad[69-71].

I.7. References

1. Amidon, G.L.; Lennernas, H.; Shah, V.P. and Crison, J.R. A Theoretical Basis for a Biopharmaceutic Drug Classification: The Correlation of in Vitro Drug Product Dissolution and in Vivo Bioavailability. Pharm. Res. 1995, 12, 413-420.
2. Walters, W.P.; Green, J.; Weiss, J.R. and Murcko, M.A. What Do Medicinal Chemists Actually Make? A 50-Year Retrospective. J. Med. Chem. 2011, 54, 6405-6416.
3. Benet, L.Z.; Broccatelli, F. and Oprea, T.I. BDDCS Applied to over 900 Drugs. AAPS J 2011, 13, 519-547.
4. Williams, H.D.; Trevaskis, N.L.; Charman, S.A.; Shanker, R.M.; Charman, W.N.; Pouton, C.W. and Porter, C.J.H. Strategies to Address Low Drug Solubility in Discovery and Development. Pharmacol. Rev. 2013, 65, 315-499.
5. Noyes, A.A. and Whitney, W.R. The Rate of Solution of Solid Substances in Their Own Solutions. J. Am. Chem. Soc. 1897, 19, 930-934.
6. Van den Mooter, G. The Use of Amorphous Solid Dispersions: A Formulation Strategy to Overcome Poor Solubility and Dissolution Rate. Drug. Discov. Today Technol. 2012, 9, e79-e85.
7. Kawakami, K. Current Status of Amorphous Formulation and Other Special Dosage Forms as Formulations for Early Clinical Phases. J. Pharm. Sci. 2009, 98, 2875-2885.
8. Stevenson, J.D.; Schmalian, J. and Wolynes, P.G. The Shapes of Cooperatively Rearranging Regions in Glass-Forming Liquids. Nature Phys. 2006, 2, 268-274.
9. Nalawade, A.; Abukmail, A.; Hassan, M.K. and Mauritz, K.A. Sub-Tg Macromolecular Motions in Phosphoric Acid Doped Polybenzimidazole Membranes for High Temperature Fuel Cell Applications. ECS Trans. 2011, 41, 1449-1459.
10. Murdande, S.B.; Pikal, M.J.; Shanker, R.M. and Bogner, R.H. Solubility Advantage of Amorphous Pharmaceuticals: I. A Thermodynamic Analysis. J. Pharm. Sci. 2010, 99, 1254-1264.
11. Chiou, W.L. and Riegelman, S. Pharmaceutical Applications of Solid Dispersion Systems. J. Pharm. Sci. 1971, 60, 1281-1302.
12. Gordon, M. and Taylor, J.S. Ideal Copolymers and the Second-Order Transitions of Synthetic Rubbers. I. Non-Crystalline Copolymers. J. Appl. Chem. 1952, 2, 493-500.
13. Janssens, S. and Van den Mooter, G. Review: Physical Chemistry of Solid Dispersions. J. Pharm. Pharmacol. 2009, 61, 1571-1586.
14. Qian, F.; Huang, J. and Hussain, M.A. Drug-Polymer Solubility and Miscibility: Stability Consideration and Practical Challenges in Amorphous Solid Dispersion Development. J. Pharm. Sci. 2010, 99, 2941-2947.
15. Alonzo, D.E.; Zhang, G.G.Z.; Zhou, D.; Gao, Y. and Taylor, L.S. Understanding the Behavior of Amorphous Pharmaceutical Systems During Dissolution. Pharm. Res. 2010, 27, 608-618.
16. Pinal, R. Entropy of Mixing and the Glass Transition of Amorphous Mixtures. Entropy 2008, 10, 207-223.
17. Marsac, P.J.; Li, T. and Taylor, L.S. Estimation of Drug-Polymer Miscibility and Solubility in Amorphous Solid Dispersions Using Experimentally Determined Interaction Parameters. Pharm. Res. 2009, 26, 139-151.
18. Zhao, Y.; Inbar, P.; Chokshi, H.P.; Malick, A.W. and Choi, D.S. Prediction of the Thermal Phase Diagram of Amorphous Solid Dispersions by Flory-Huggins Theory. J. Pharm. Sci. 2011, 100, 3196-3207.
19. Vasanthavada, M.; Tong, W.-Q.T. and Serajuddin, A.T.M., Development of Solid Dispersion for Poorly Water-Soluble Drugs. In *Water-Insoluble Drug Formulation* Second ed.; Liu, R., Taylor & Francis: Florida, 2008; 'Vol.' 3 pp 499-529.
20. Huang, J. and Wigent., R.J. Determination of Drug and Polymer Miscibility and Solid Solubility for Design of Stable Amorphous Solid Dispersions. Am. Pharm. Rev. 2009, 12, 18-26.
21. Friesen, D.T.; Shanker, R.; Crew, M.; Smithey, D.T.; Curatolo, W.J. and Nightingale, J.A.S. Hydroxypropyl Methylcellulose Acetate Succinate-Based Spray-Dried Dispersions: An Overview. Mol. Pharmaceutics 2008, 5, 1003-1019.
22. Zhu, Q.; Harris, M.T. and Taylor, L.S. Time-Resolved SAXS/WAXS Study of the Phase Behavior and Microstructural Evolution of Drug/PEG Solid Dispersions. Mol. Pharmaceutics 2011, 8, 932-939.

23. Liu, H.; Zhang, X.; Suwardie, H.; Wang, P. and Gogos, C.G. Miscibility Studies of Indomethacin and Eudragit® E Po by Thermal, Rheological, and Spectroscopic Analysis. J. Pharm. Sci. 2012, 101, 2204-2212.
24. Yoo, S.; Krill, S.L.; Wang, Z. and Telang, C. Miscibility/Stability Considerations in Binary Solid Dispersion Systems Composed of Functional Excipients Towards the Design of Multi-Component Amorphous Systems. J. Pharm. Sci. 2009, 98, 4711-4723.
25. Shah, N.; Sandhu, H.; Choi, D.S.; Kalb, O.; Page, S. and Wyttenbach, N., Structured Development Approach for Amorphous Systems. In *Formulating Poorly Water Soluble Drugs*, ed.; III, R. O. W.; Watts, A. B.; Miller, D. A., Eds. Springer Science+Business Media: New York, 2012; 'Vol.' 3, pp 267-310.
26. Srinarong, P.; de Waard, H.; Frijlink, H.W. and Hinrichs, W.L.J. Improved Dissolution Behavior of Lipophilic Drugs by Solid Dispersions: The Production Process as Starting Point for Formulation Considerations. Expert. Opin. Drug Deliv. 2011, 8, 1121-1140.
27. Peltonen, L.; Valo, H.; Kolakovic, R.; Laaksonen, T. and Hirvonen, J. Electrospraying, Spray Drying and Related Techniques for Production and Formulation of Drug Nanoparticles. Expert. Opin. Drug Deliv. 2010, 7, 705-719.
28. Srivastava, S. and Mishra, G. Fluid Bed Technology: Overview and Parameters for Process Selection. Int. J. Pharma. Sci. Drug Res. 2010, 2, 236-246.
29. Repka, M.A.; Majumdar, S.; Kumar Battu, S.; Srirangam, R. and Upadhye, S.B. Applications of Hot-Melt Extrusion for Drug Delivery. Expert. Opin. Drug Deliv. 2008, 5, 1357-1376
30. Lebrun, P.; Krier, F.; Mantanus, J.; Grohganz, H.; Yang, M.; Rozet, E.; Boulanger, B.; Evrard, B.; Rantanen, J. and Hubert, P. Design Space Approach in the Optimization of the Spray-Drying Process. Eur. J. Pharm. Biopharm. 2012, 80, 226-234.
31. Baird, J.A. and Taylor, L.S. Evaluation of Amorphous Solid Dispersion Properties Using Thermal Analysis Techniques. Adv. Drug Deliv. Rev. 2012, 64, 396-421.
32. Rumondor, A.C.F.; Ivanisevic, I.; Bates, S.; Alonzo, D.E. and Taylor, L.S. Evaluation of Drug-Polymer Miscibility in Amorphous Solid Dispersion Systems. Pharm. Res. 2009, 26, 2523-2534.
33. Ivanisevic, I.; Bates, S. and Chen, P. Novel Methods for the Assessment of Miscibility of Amorphous Drug-Polymer Dispersions. J. Pharm. Sci. 2009, 98, 3373-3386.
34. Dahlberg, C.; Millqvist-Fureby, A. and Schuleit, M. Surface Composition and Contact Angle Relationships for Differently Prepared Solid Dispersions. Eur. J. Pharm. Biopharm. 2008, 70, 478-485.
35. Van Eerdenbrugh, B.; Lo, M.; Kjoller, K.; Marcott, C. and Taylor, L.S. Nanoscale Mid-Infrared Evaluation of the Miscibility Behavior of Blends of Dextran or Maltodextrin with Poly (Vinylpyrrolidone). Mol. Pharmaceutics 2012, 9, 1459-1469.
36. Dahlberg, C.; Dvinskikh, S.V.; Schuleit, M. and Furo', I. Polymer Swelling, Drug Mobilization and Drug Recrystallization in Hydrating Solid Dispersion Tablets Studied by Multinuclear NMR Microimaging and Spectroscopy. Mol. Pharmaceutics 2011, 8, 1247-1256.
37. Bhardwaj, S.P. and Suryanarayanan, R. Subtraction of Dc Conductivity and Annealing: Approaches to Identify Johari-Goldstein Relaxation in Amorphous Trehalose. Mol. Pharmaceutics 2011, 8, 1416-1422.
38. Ke, P.; Hasegawa, S.; Al-Obaidi, H. and Buckton, G. Investigation of Preparation Methods on Surface/Bulk Structural Relaxation and Glass Fragility of Amorphous Solid Dispersions. Int. J. Pharm. 2012 422, 170-178.
39. Van Drooge, D.J.; Hinrichs, W.L.J.; Visser, M.R. and Frijlink, H.W. Characterization of the Molecular Distribution of Drugs in Glassy Solid Dispersions at the Nano-Meter Scale, Using Differential Scanning Calorimetry and Gravimetric Water Vapour Sorption Techniques. Int. J. Pharm. 2006, 310, 220-229.
40. Snyder, H.E. Pharmaceutical Spray Drying: Solid-Dose Process Technology Platform for the 21st Century. Ther. Deliv. 2012, 3, 901-912.
41. Miller, D.A. and Gil, M., Spray-Drying Technology. In *Formulating Poorly Water Soluble Drugs*, ed.; III, R. O. W.; Watts, A. B.; Miller, D. A., Springer Science+Business Media: New York, 2012; 'Vol.' 3, pp 363-442.
42. Sollohub, K. and Cal, K. Spray Drying Technique: II. Current Applications in Pharmaceutical Technology. J. Pharm. Sci. 2009, 99, 587-597.

43. Heng, D.; Lee, S.H.; Ng, W.K. and Tan, R.B.H. The Nano Spray Dryer B-90. Expert. Opin. Drug Deliv. 2011, 8, 965-972.
44. Kamlet, M.J.; Abboud, J.L.M.; Abraham, M.H. and Taft, R.W. Linear Solvation Energy Relationships. 23. A Comprehensive Collection of the Solvatochromic Parameters,. Pi.*,. Alpha., And. Beta., and Some Methods for Simplifying the Generalized Solvatochromic Equation. J. Org. Chem. 1983, 48, 2877-2887.
45. Paudel, A.; Worku, Z.A.; Meeus, J.; Guns, S. and Van den Mooter, G. Manufacturing of Solid Dispersions of Poorly Water Soluble Drugs by Spray Drying: Formulation and Process Considerations. Int. J. Pharm. 2012, (In Press).
46. Vehring, R. Pharmaceutical Particle Engineering Via Spray Drying. Pharm. Res. 2008, 25, 999-1022.
47. Edward, J.T. Molecular Volumes and the Stokes-Einstein Equation. J. Chem. Educ. 1970, 47, 261.
48. ICHQ3(R5). Impurities Guideline for Residual Solvents, International Conference on Harmonisation. Geneva 2011.
49. Al-Obaidi, H.; Brocchini, S. and Buckton, G. Anomalous Properties of Spray Dried Solid Dispersions. J. Pharm. Sci. 2009, 98, 4724-4737.
50. Tomasko, D.L. and Timko, M.T. Tailoring of Specific Interactions to Modify the Morphology of Naproxen. J. Cryst. Growth 1999, 205, 233-243.
51. Dobry, D.E.; Settell, D.M.; Baumann, J.M.; Ray, R.J.; Graham, L.J. and Beyerinck, R.A. A Model-Based Methodology for Spray-Drying Process Development. J. Pharm. Innov. 2009, 4, 133-142.
52. Chen, R.; Tagawa, M.; Hoshi, N.; Ogura, T.; Okamoto, H. and Danjo, K. Improved Dissolution of an Insoluble Drug Using a 4-Fluid Nozzle Spray-Drying Technique. Chem. Pharm. Bull. 2004, 52, 1066-1070.
53. Yamaguchi, T.; Nishimura, M.; Okamoto, R.; Takeuchi, T. and Yamamoto, K. Glass Formation of 4-O-(4-Methoxyphenyl) Acetyltylosin and Physicochemical Stability of the Amorphous Solid. Int. J. Pharm. 1992, 85, 87-96.
54. Matsuda, Y.; Otsuka, M.; Onoe, M. and Tatsumi, E. Amorphism and Physicochemical Stability of Spray-Dried Frusemide. J. Pharm. Pharmacol. 1992, 44, 627-633.
55. Ueno, Y.; Yonemochi, E.; Tozuka, Y.; Yamamura, S.; Oguchi, T. and Yamamoto, K. Pharmaceutics: Characterization of Amorphous Ursodeoxycholic Acid Prepared by Spray-Drying. J. Pharm. Pharmacol. 1998, 50, 1213-1219.
56. Ohta, M. and Buckton, G. A Study of the Differences between Two Amorphous Spray-Dried Samples of Cefditoren Pivoxil Which Exhibited Different Physical Stabilities. Int. J. Pharm. 2005, 289, 31-38.
57. Janssens, S.; Anne′, M.; Rombaut, P. and Van den Mooter, G. Spray Drying from Complex Solvent Systems Broadens the Applicability of Kollicoat IR as a Carrier in the Formulation of Solid Dispersions. Eur. J. Pharm. Sci. 2009, 37, 241-248.
58. Sahoo, N.G.; Abbas, A.; Judeh, Z.; Li, C.M. and Yuen, K.H. Solubility Enhancement of a Poorly Water-Soluble Anti-Malarial Drug: Experimental Design and Use of a Modified Multifluid Nozzle Pilot Spray Drier. J. Pharm. Sci. 2008, 98, 281-296.
59. Duret, C.; Wauthoz, N.; Sebti, T.; Vanderbist, F. and Amighi, K. Solid Dispersions of Itraconazole for Inhalation with Enhanced Dissolution, Solubility and Dispersion Properties. Int. J. Pharm. 2012, 428, 103-113.
60. Thybo, P.; Hovgaard, L.; Lindelov, J.S.; Brask, A. and Andersen, S.K. Scaling up the Spray Drying Process from Pilot to Production Scale Using an Atomized Droplet Size Criterion. Pharm. Res. 2008, 25, 1610-1620.
61. Van Drooge, D.J.; Hinrichs, W.L.J.; Wegman, K.A.M.; Visser, M.R.; Eissens, A.C. and Frijlink, H.W. Solid Dispersions Based on Inulin for the Stabilization and Formulation of Δ^9-Tetrahydrocannabinol. Eur. J. Pharm. Sci. 2004, 21, 511-518.
62. Chen, R.; Okamoto, H. and Danjo, K. Preparation of Functional Composite Particles of Salbutamol Sulfate Using a 4-Fluid Nozzle Spray-Drying Technique. Chem. Pharm. Bull. 2008, 56, 254-259.

63. Kojima, Y.; Ohta, T.; Shiraki, K.; Takano, R.; Maeda, H. and Ogawa, Y. Effects of Spray Drying Process Parameters on the Solubility Behavior and Physical Stability of Solid Dispersions Prepared Using a Laboratory-Scale Spray Dryer. Drug Dev. Ind. Pharm. 2012, 1-10.
64. Patrono, C. and Rocca, B. Nonsteroidal Antiinflammatory Drugs: Past, Present and Future. Pharmacol. Res. 2009, 59, 285-289.
65. Bogdanova, S.; Pajeva, I.; Nikolova, P.; Tsakovska, I. and Muller, B. Interactions of Poly (Vinylpyrrolidone) with Ibuprofen and Naproxen: Experimental and Modeling Studies. Pharm. Res. 2005, 22, 806-815.
66. Velazquez, M.M.; Valero, M.; Rodriguez, L.J.; Costa, S. and Santos, M.A. Hydrogen Bonding in a Non-Steroidal Anti-Inflammatory Drug: Naproxen. J. Photochem. Photobiol. B. 1995, 29, 23-31.
67. Lahmani, F.; Le Barbu-Debus, K.; Seurre, N. and Zehnacker-Rentien, A. Laser Spectroscopy of a Chiral Drug in a Supersonic Beam: Conformation and Complexation of S-(+)-Naproxen. Chem. Phys. Lett. 2003, 375, 636-644.
68. Sajewicz, M.; Matlengiewicz, M.; Leda, M.; Gontarska, M.; Kronenbach, D.; Kowalska, T. and Epstein, I.R. Spontaneous Oscillatory in Vitro Chiral Conversion of Simple Carboxylic Acids and Its Possible Mechanism. J. Phys. Org. Chem. 23, 1066-1073.
69. Szaraz, I. and Forsling, W. A Spectroscopic Study of the Solvation of 1-Vinyl-2-Pyrrolidone and Poly (1-Vinyl-2-Pyrrolidone) in Different Solvents. Polymer 2000, 41, 4831-4839.
70. Tonelli, A.E. Conformational Characteristics of Poly (N-Vinyl Pyrrolidone). Polymer 1982, 23, 676-680.
71. Shinyashiki, N.; Spanoudaki, A.; Yamamoto, W.; Nambu, E.; Yoneda, K.; Kyritsis, A.; Pissis, P.; Kita, R. and Yagihara, S. Segmental Relaxation of Hydrophilic Poly (Vinylpyrrolidone) in Chloroform Studied by Broadband Dielectric Spectroscopy. Macromolecules 2011, 44, 2140-2148.

Chapter II: Objectives

The current setback behind the limited commercial success of amorphous solid dispersions as solubilizing strategy for poorly soluble drugs is the inadequate understanding of their manufacturability, stability and *in vitro* and *in vivo* performance. Selection of stabilizer(s), drug loading and manufacturing process is still iterative and empirically driven. The kinetic and thermodynamic manifestations alongwith the molecular interactions in amorphous systems in course of preparation, downstream process and storage are still poorly understood. Spray-drying stands at the frontier of the solvent based methods for preparation of amorphous solid dispersions. However, the information on the influence of various formulation and process parameters involved in spray-drying on the physical structure and physical stability of the resulting spray-dried dispersions is limited.

In order to transform the current *trial and error* practice of manufacturing spray-dried amorphous solid dispersions to a rational and scientifically based approach, a thorough investigation was designed with the selected model poorly water soluble drug (BCS class 2), naproxen and the commonly used hydrophilic solid dispersion carrier, polyvinylpyrrolidone (PVP). The model system was selected considering the extensive literature on the solution- and solid-state characteristics of the drug and the polymer as well as their combinations. The binary solid dispersions were intended to be prepared from feed solutions containing organic solvent(s) of different volatility, proticity and polarity using two laboratory scale spray-dryers of different drying capacities and hardware configurations. The following general objectives are defined in the current research project:

- *To envisage the applicability of different mixing thermodynamic models to designate the miscibility window (the gap between equilibrium solid solubility to kinetic miscibility) for the selected drug-polymer system*
- *To correlate the chemistry of the selected drug and polymer, the formulation variables (solvent type, concentration, composition), and physical processes inherent to spray-drying (evaporation, drying, atomization, phase distribution, crystallization etc) on the one hand and the resulting physical structure of the amorphous solid dispersions on the other hand*
- *To investigate the influence of various process parameters (inlet temperature, atomization conditions, spray rate and drying airflow rate) on the physical structure, stability and in vitro dissolution behavior of spray-dried amorphous solid dispersions prepared from the selected drug-polymer-solvent system*

Chapter III: Theoretical and Experimental Investigation on the Solid Solubility and Miscibility of Naproxen in Poly(vinylpyrrolidone)

The results described in this chapter are published in the following article:

Paudel, A.; Van Humbeeck, J. and Van den Mooter, G. (2010). Theoretical and Experimental Investigation on the Solid Solubility and Miscibility of Naproxen in Poly(vinylpyrrolidone). *Molecular Pharmaceutics*, 7 (4), 1133–1148.

III. 1 Abstract

The objective of the present study was to determine the solid state solubility and miscibility of naproxen in poly(vinylpyrrolidone) (PVP) and the mutual interaction using the standard thermodynamic models and thermal analysis. Solid dispersions were prepared by spray-drying several compositions of naproxen and PVP with different molecular weights, *viz*., PVP K 12, PVP K 25 and PVP K 90, and analyzed using modulated differential scanning calorimetry (mDSC). The kinetic miscibility limit in terms of a single mixed phase glass transition temperature was found to be relatively similar for the dispersions containing PVP with different chain lengths (≥50% w/w drug in PVP). But the systems with different PVP followed diverse patterns of composition dependent mixed phase glass transition temperature as well as the degree of plasticization by water. The crystalline solid solubility values of naproxen in PVP estimated by using its solubility data in n-methylpyrrolidone, a low molecular weight analogue of PVP, were 6.42, 5.85 and 5.81% w/w of drug in PVP K 12, PVP K 25 and PVP K 90 respectively. The values estimated for corresponding amorphous solubility showed no marked difference. The remarkable difference between thermodynamic solubility/miscibility and kinetic miscibility implied that naproxen was highly supersaturated in the PVP solid dispersions and only stabilized kinetically. The negative value of the drug-polymer interaction parameter (-0.36) signified the systems to be favorably mixing. The melting point depression data of naproxen in PVP pointed to the composition dependence and chain length effect on the interaction. The moisture sorption by the physical mixtures not only provided the composition dependent interaction parameter but also conferred an estimate of composition dependent miscibility of naproxen in PVP in the presence of water.

III. 2 Introduction

Amorphous forms of poorly water soluble drug substances are considered as one of the ultimate means to increase apparent solubilities and dissolution compared to their crystalline counterparts[1-4]. This results in higher systemic availability desired for the oral dosage form. However, due to higher tendency toward crystallization, these benefits are rarely sustained in formulating the purely amorphous active pharmaceutical ingredient. Therefore, the approach of formulating amorphous drugs in the form of amorphous solid dispersions with a polymeric carrier as a crystallization inhibitor has long been an active area of research[5,6]. Despite the extensive research, the development of a considerable number of stable and efficient formulations is yet to be achieved. The major challenge is to achieve molecule-level dispersions restraining favorable intermolecular interactions between the drug

substance and the polymeric matrix. The maximum crystallization inhibition of a drug in a solid dispersion can only be achieved when the drug is dispersed homogeneously or best at the molecular level in the matrix. This suggests that the basis of the selection of the right polymeric excipient for the formulation of amorphous solid dispersions should be the limit of solid state solubility of the drug in the selected polymer[7,8]. Knowledge of correct phase behavior of the drug-polymer system helps to avoid potential phase separation driven by supersaturation of the drug substance beyond the solubility/miscibility limit in a particular polymer. Thus, drug-polymer miscibility and solid solubility of drug in the polymer provide the right estimates of the drug loading to manufacture stable solid dispersion formulations.

The present study is aimed at investigating the solid state solubility/miscibility and the strength of drug-polymer interactions of a water insoluble drug in a polymeric carrier using a multimethodological approach. Naproxen (Figure III.1a) was selected as the model drug in the preparation of solid dispersions with three different molecular weight types of polyvinylpyrrolidone (PVP) (Figure III.1b). The dissolution enhancement of naproxen by the preparation of naproxen-PVP solid dispersions has been extensively investigated, but little has been reported on the solid solubility behavior of these systems. Selection of the proper molecular weight PVP is important for the preparation of solid dispersions with improved performance. Velaz et al. reported the interaction between naproxen and *n*-vinylpyrrolidone (the monomer of PVP) by complexation[9]. Bettinetti et al. studied the dissolution behavior of the naproxen with PVP K 15, 30, and 90 at different compositions[10]. There are several studies on the solid state interaction between naproxen and PVP. The carboxylic acid group of both the monomer and dimer of naproxen are reported to interact with PVP[11]. However, Bogdanova et al. suggested that the catemer arrangement (instead of dimer arrangement as of ibuprofen) and the intermolecular interactions in the crystal of naproxen do not presume favorable hydrogen bonding interactions with the PVP[12].

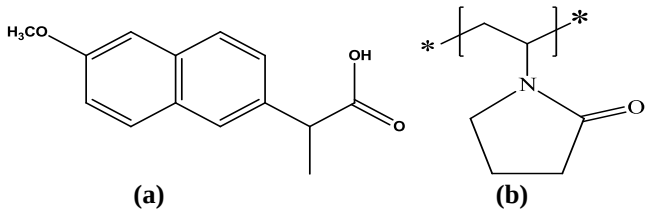

(a) **(b)**

Figure III.1 Chemical structure of naproxen (a) and PVP (b).

In the present study, we focused in finding out the kinetic as well as thermodynamic solubility/miscibility and interaction parameters of naproxen in PVP with different molecular weight. The apparent drug-polymer miscibility was determined by observing the glass

transition behavior of solid dispersions prepared by spray-drying. The commonly used thermodynamic relations derived from the Flory-Huggins (FH) lattice theory[13] and Hildebrand regular solution theory[14,15] were exploited together with the experimental solubility data in *n*-methylpyrrolidone, a low molecular weight analogue of PVP, to determine the equilibrium solid state solubility and interaction parameter of the drug in polymer. The composition dependent FH interaction parameters were estimated based on the extent of melting point depression of naproxen in the physical mixtures containing various compositions of PVP. The effect of water on the strength of composition dependent drug-polymer interaction was investigated based on the moisture sorption behavior of physical mixtures containing various compositions of naproxen and PVP.

III. 3 Materials and Methods

III. 3.1 Materials

Naproxen was obtained from CERTA Ltd. (Brain-l'Allend, Belgium). PVP K 12 (*Mw* = 2.4 kDa), PVP K 25 (*Mw* = 25 kDa) and PVP K 90 (*Mw* = 1,100 kDa) were kindly provided by BASF (Ludwigshafen, Germany). All other materials and solvents were of analytical or HPLC grade.

III. 3.2 Methods

III. 3.2.1 Spray-Drying

Spray-drying was used as the process to prepare the solid dispersions of naproxen in PVP at various compositions (5%, 10%, 15%, 20%, 30%, 40%, 50% and, 75% w/w drug in polymer) using a 5% w/v solution of powder blends in dichloromethane (Fisher Scientific UK Limited, Leicestershire, U.K.). A Buchi mini spray-dryer B191 (Buchi, Flawil, Switzerland) was used for spray-drying. The following process parameters were used: inlet temperature 50 °C, outlet temperature 30-40 °C, aspirator 100%, the pump 35%, and the air flow 800 L/h. All spray-dried powders were further dried in a vacuum oven (0.2 bar) at 25 °C in the presence of P_2O_5 for one week prior to analysis.

III. 3.2.1 Thermal Analysis

DSC experiments were performed using the 2920 differential scanning calorimeter (TA Instruments, Leatherhead, U.K.) in a dry nitrogen purged chamber at a flow rate of 150 mL/min and helium purge at 40 mL/ min. Samples were cooled using the refrigerated cooling system (RCS) accessory. The data analyses and processing were done using Universal

Analysis 2000 software (TA Instruments, Leatherhead, U.K.). The enthalpy was calibrated with an indium standard, and the temperature scale was calibrated with octadecane, indium and tin. The heat capacity signal was calibrated by comparing the response of a sapphire disk with the tabulated value at 106.85 °C. The validated measurements of temperature, enthalpy and heat capacity of the same standard materials showed deviations of <0.5 °C, <1% and <1% for the temperature, the enthalpy and the heat capacity at 106.5 °C, respectively. All samples were analyzed in duplicate using aluminum pans (samples weighed and crimped with the aluminum lid) in modulated mode (mDSC) using the method containing three cycles of heating sequence. Cycle 1: From -20 °C, samples were heated at 2 °C/min up to 160 °C, with a modulation of (±0.212 °C every 40 s. Cycle 2: The sample was cooled back to -20 °C at the instrument's preset rate and held isothermally for 2 min. Cycle 3: Cycle 1 was repeated up to a final temperature of 180 °C. For the measurement of heat capacity of amorphous naproxen during its T_g, 5-10 mg of sample was melted during heating until 160 °C in a DSC pan (crimped with the lid), quench cooled by transferring the pan into liquid nitrogen and immediately analyzed using the same mDSC method with only cycle 1.

The water content in the samples was estimated by thermogravimetric analysis using a TGA Q500 (TA-instruments, Leatherhead, U.K.). The sample was heated at 10 °C/ min from room temperature (30 °C) to 160 °C with a dry nitrogen purge at 100 mL/min. The data analysis was done using Universal Analysis 2000 software (TA Instruments, Leatherhead, U.K.).

III. 3.2.2 Melting Point Depression

The melting point depression was evaluated by running physical mixtures of naproxen with PVP at different compositions (95%, 90%, 85%, 80% and 75% w/w naproxen in PVP) in DSC. For this, the desired composition of drug and polymer was grinded in the mortar for approximately 2 min and run in DSC using the method that comprised equilibration at 120 °C followed by heating at 2 °C/min up to 160 °C. The pure ground drug was analyzed as the control using the same method.

III. 3.2.3 Density Determination by Helium Pycnometry

Density of the drug and PVPs was determined by helium pycnometry using a Beckman comparison pycnometer (model 930, Beckman Industries, Inc., Fullerton, CA). The drug and polymers used for the density measurements were dried in a vacuum oven at 40 °C for one week prior to the analysis. Measurements were performed in duplicate.

III. 3.2.4 Determination of the Drug Content in the Solid Dispersions by HPLC

The drug content in the spray-dried binary solid dispersions was assayed using HPLC made up of a Merck Hitachi pump L7100, an ultraviolet (UV) detector (L7400), an autosampler (L7200), an interface (D7000) and a LiChrospher 60 RP Select-B C-18 (5 μm, 12.5 × 0.4 cm) (all from Merck, Darmstadt, Germany) column. The method was isocratic with the mobile phase made up of 70% methanol (HiPerSolv Chromanorm, Belgium) and 30% 25 mM sodium acetate buffer (pH 3.5). The wavelength used for the detection was 270 nm. The samples were prepared by dissolving 5 mg of solid dispersion in 5 mL of diluents (mobile phase) to give 1 mg/mL concentration. The injection volume was 10 μL.

III. 3.2.5 Moisture Sorption Studies

The physical mixtures of naproxen were made using dried PVP K 25 and PVP K 90 with drug content of 75%, 50% and 25%. The samples (pure drug, polymers and physical mixtures thereof) were weighed and kept in a desiccator with controlled relative humidity of 94% maintained by a saturated aqueous solution of potassium nitrate. All samples were reweighed after 48 h. The differences were considered as the equilibrium moisture gain by the samples.

III. 3.2.6 Estimation of Equilibrium Solubility of Naproxen in n-Methylpyrrolidone (NMP)

The equilibrium solubility studies of naproxen in NMP (Aldrich, Steinheim, Germany), a small molecular weight analogue of PVP, were done by shaking excess drug in NMP for 72 h using a mechanical rotor (Snijders Scientific, Tinburg, The Netherlands) in amber colored test tubes (to avoid possible photodegradation as reported for NMP[16]). The samples were withdrawn, filtered using a syringe filter of 0.2 μm (Henke Sass Wolf, Tuttlingen, Germany) and properly diluted. The diluted samples were injected in the HPLC and analyzed using the aforementioned method.

III. 4 Results

III. 4.1 Mixed Phase Glass Transition and Phase Behavior of Naproxen-PVP Dispersions

The most apparent experimental indication of the miscibility of two amorphous components is the presence of a single glass transition temperature, often referred to as mixed phase glass transition temperature (T_{gm}). For a binary mixture containing components with a considerable difference between individual T_g values, the position of T_{gm} will be intermediate between the two T_gs as a function of composition. The position of T_{gm} for a miscible but non

interactive (athermal) system with merely equivalent cohesive and adhesive contributions between individual components can be estimated using various equations that follow a simple rule of mixing[17]. Of them, the Gordon-Taylor (GT) equation[18] with an implementation of the Simha-Boyler rule[19] is used extensively for pharmaceutical systems made up of drug and polymer. Equation III.1 is the GT expression for the ternary system.

$$T_{gm} = \frac{W_1 T_{g1} + K_1 W_2 T_{g2} + K_2 W_3 T_{g3}}{W_1 + K_1 W_2 + K_2 W_3} \quad \text{Equation III. 1}$$

where $K_1 \approx (\rho_1 T_{g1} / \rho_2 T_{g2})$ and $K_2 \approx (\rho_2 T_{g2} / \rho_3 T_{g3})$; W, T_g and ρ are weight fraction, glass transition temperature and density of individual components, respectively. The smaller value of subscripts denotes the components with lower T_g. The terms containing W_3 are excluded from eq III.1 in the case of binary systems.

In the case of pharmaceutical solid dispersions, phase separation is generally characterized by the presence of a melting endotherm or crystallization exotherm for the drug during heating[5]. Moreover, amorphous-amorphous separation or partial miscibility is indicated by the presence of multiple T_{gm}s corresponding to the heterogeneous drug polymer dispersion systems with different compositions or physical structures such as interaction densities (for example hydrogen bonding density)[20].

Correlating with the heating program, the thermal history of the co-spray-dried naproxen and PVP samples in first heating and second heating (after cooling) would indeed be different. The features observed in the first heating cycle represent the native thermal behavior of the spray-dried products. The thermal histories of the samples are generally changed on completion of the first cycle, and the formation of more homogeneous mixtures can be assumed. The average T_g values (K) obtained of pure drug and polymers were 279.34 (±0.40), 370.10 (±0.21), 430.05 (±0.38) and 451.84 (±0.24) for naproxen, PVP K 12, PVP K 25 and PVP K 90 respectively. Likewise, the ΔC_p (J/g · K) values obtained for naproxen, PVP K 12, PVP K 25 and PVP K 90 were 0.79 (±0.02), 0.20 (±0.03), 0.21 (±0.01) and 0.22 (±0.01), respectively. The densities (g/cm^3) measured were 1.25 (±0.00), 1.11 (±0.10), 1.14 (±0.18) and 1.18 (±0.15) for naproxen, PVP K 12, PVP K 25 and PVP K 90, respectively (the numbers in parentheses are the ranges obtained by duplicate measurements). The ΔC_p value of naproxen was calculated by normalizing the values obtained for the percentage amorphous material formed during the quench cooling experiments (ca. 35%). The T_g (K) and ΔC_p (J/g· K) values for water were assigned as 136 and 1.38, respectively from literature[21]. The drug contents in the dispersions used for the calculations were determined by HPLC analyses. The

experimental glass transition temperatures (T_{gm}) and the change in heat capacity during glass transition (ΔC_{pm}) of the spray-dried drug-polymer dispersions (first and second runs) are given in Table III.1.

Table III.1 The Naproxen Content in Solid Dispersions Assayed by HPLC, T_{gm} and ΔC_p Obtained in First and Second mDSC Heating Cycle and Moisture Content Data by TGA of Naproxen-PVP Solid Dispersions

	Second heating		First heating		
% naproxen in mixture	T_{gm} (K)	ΔC_p (J/g.K)	T_{gm} (K)	ΔC_p (J/g.K)	% water content
			Naproxen/PVP K 12[a]		
4.47 (±0.02)[b]	309.39 (±0.01)	0.18(±0.03)	293.18 (±1.65)	0.43 (±0.02)	7.15
9.64 (±0.04)	338.09 (±3.66)	0.24 (±0.06)	291.60 (±0.79)	0.54 (±0.01)	5.74
14.32 (±0.03)	345.09 (±1.96)	0.35 (±0.02)	294.27 (±2.50)	0.50 (±0.03)	4.35
20.93 (±0.15)	339.22 (±1.71)	0.36 (±0.02)	290.96 (±0.50)	0.49 (±0.01)	4.28
29.42 (±0.09)	316.37 (±3.36)	0.38 (±0.03)	298.45 (±2.02)	0.38 (±0.02)	3.36
38.94 (±1.02)	305.91 (±3.57)	0.34 (±0.00)	299.25 (±0.41)	0.40 (±0.01)	2.08
50.46 (±0.43)	314.62 (±0.38)	0.33 (±0.00)	298.75 (±3.47)	0.45 (±0.00)	1.00
72.57[c] (±2.16)	294.25 (±0.32)	0.32 (±0.15)	297.68 (±0.54)	0.20 (±0.01)	1.42
			Naproxen/PVP K 25[a]		
5.78 (±0.73)	414.62 (±1.78)	0.25 (±0.00)	410.25 (±1.56)	0.38 (±0.00)	7.79
10.39 (±0.70)	404.81 (±0.33)	0.23 (±0.01)	399.85 (±1.13)	0.42 (±0.02)	7.26
15.13 (±0.47)	390.06 (±3.67)	0.28 (±0.00)	389.42 (±0.51)	0.41 (±0.00)	6.57
21.31 (±0.56)	380.15 (±0.22)	0.28 (±0.01)	378.31 (±1.96)	0.34 (±0.03)	5.83
28.78 (±1.27)	360.70 (±1.94)	0.28 (±0.01)	315.09 (±1.59)	0.37 (±0.00)	4.27
40.09 (±0.62)	341.51 (±1.14)	0.35 (±0.01)	311.15 (±0.52)	0.38 (±0.00)	4.31
49.98 (±1.49)	330.07 (±0.24)	0.36 (±0.04)	295.68 (±2.91)	0.42 (±0.01)	3.24
78.10[c] (±3.70)	298.28 (±0.43)	0.36 (±0.00)	291.52 (±0.65)	0.37 (±0.08)	2.34
			Naproxen/PVP K 90[a]		
4.28 (±0.07)	433.77 (±0.12)	0.23 (±0.03)	433.98 (±0.62)	0.20 (±0.01)	1.30
9.92 (±0.00)	415.80 (±0.38)	0.26 (±0.01)	414.25 (±1.37)	0.20 (±0.01)	7.62
12.28 (±0.12)	404.65 (±0.64)	0.20 (±0.01)	402.00 (±0.31)	0.30 (±0.01)	7.44
20.06 (±0.17)	391.92 (±0.60)	0.30 (±0.02)	389.87 (±1.58)	0.22 (±0.03)	6.18
30.90 (±0.04)	370.24 (±0.55)	0.29 (±0.02)	370.81 (±1.38)	0.17 (±0.01)	6.27
39.94 (±0.30)	351.54 (±1.02)	0.22 (±0.00)	328.01 (±0.05)	0.26 (±0.03)	6.31
51.59 (±0.23)	333.36 (±0.72)	0.32 (±0.00)	316.39 (±0.61)	0.32 (±0.01)	3.11
73.79[c] (±0.94)	295.38 (±0.23)	0.38 (±0.01)	289.94 (±2.30)	0.32 (±0.02)	2.33

[a]Spray-dried mixture. [b]Numbers in parentheses represent range of duplicate measurements. [c]Melting endotherm observed corresponding to the fraction of crystalline drug phase separated from the dispersion rendering back ca. 58, 55 and 52% w/w drug dispersed into PVP K 12, PVP K 25 and PVP K 90 respectively in first heating while 48%, 51% and 47% respectively in the second heating.

III. 4.1.1 The First Heating Cycle and Glass Transition of the Spray-Dried Samples

The spray-dried products contained considerable amounts of water apparent from the TGA data and the broad endothermic peaks observed around the corresponding temperatures

in the thermograms. The type and state of water a system contains prior to or at the time of glass transition, namely, bound/unbound, surface/bulk water, discerns the degree of plasticization of a system. Moreover the strength of plasticization of a system by water is also a function of the glass forming ability of the plasticizer, the difference between its T_g and the particle temperature and so forth[17]. It has been well documented for PVP that it does not contain freezable water even at water content >20%[22]. Therefore, the T_{gm} values were systematically calculated by including the water as the third component in the GT equation for composites exhibiting T_{gm} < 100 °C and by normalizing the binary weight fractions excluding the water for composites with observed T_{gm} > 100 °C. Distinctive and single T_{gm} without other noticeable events were observed in the reversing heat flow signals for all the compositions except 25% polymer composition. In the case of the latter composition, the melting endotherm of the phase separated drug appeared along with a T_{gm} corresponding to the remaining mixed phase. Also, second glass transitions due to the existence of a phase separated polymer rich amorphous fraction were quite noticeable. They were almost merged with the melting endotherms in the case of PVP K 12 and PVP K 25 containing dispersions while quite pronounced for the mixture of drug in PVP K 90. The enthalpy of fusion values of the melting endotherms observed at 25% polymer containing composites were evaluated to measure the percentage of drug likely to be dispersed in PVP using the weight of drug alone in the dispersion. These values also ultimately indicate the kinetic miscibility of the drug with the polymer as given in Table III.1.

The plots of the difference between T_{gm} observed in the first heating cycle and that by the GT equation for the corresponding compositions against PVP weight fraction are given in Figure III.2a. The experimental T_{gm} showed negative deviations from the predicted values for all the naproxen-PVP dispersions. The observed T_{gm} of naproxen-PVP K 12 mixtures up to 80% polymer containing compositions showed higher deviation as compared to the subsequent mixture compositions. This suggested that the trace amount of water beyond this composition might have lesser plasticization effect. For naproxen dispersions with PVP K 25, a profound drop in T_{gm} values was observed below the 80% polymer content. By examining T_{gm} of an additionally spray-dried middle composition (75% polymer containing mixture) we could establish the consistent position in the trend (data not shown). Compositionally the dispersions can be divided into two regions above and below the 80% w/w polymer containing composite based on their T_{gm}. The predicted T_{gm} values of spray-dried naproxen-PVP K 90 mixtures showed a fairly similar trend as that of naproxen-PVP K 25 mixtures. The

curve of experimental T_{gm} against PVP weight fraction showed a steep slope up to 85% polymer containing composites followed by a jump analogous to naproxen-PVP K 25 systems beyond 70% PVP content. This suggests that mixtures with the three regions of T_{gm} exist across the selected composition range for the naproxen-PVP K 90 system.

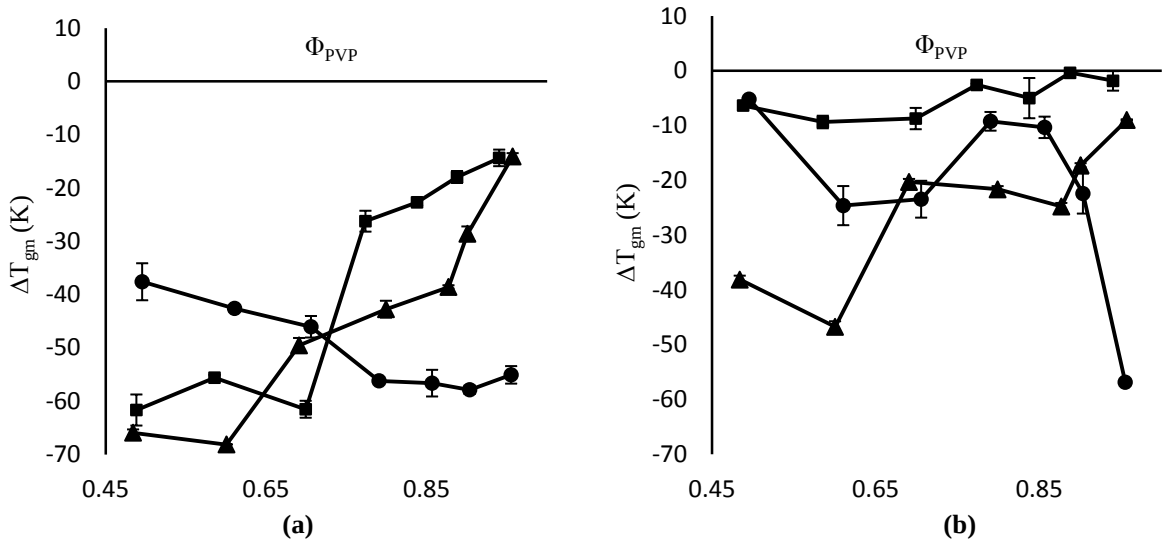

Figure III.2 The difference between the observed and predicted mixed phase glass transition temperatures predicted by the Gordon-Taylor equation (ΔT_{gm}) versus composition (polymer volume fraction, Φ_{PVP}) in first heating (a) and second heating (b) for spray-dried naproxen-PVP K 12 (●) (b), naproxen-PVP K 25 (■) and naproxen-PVP K 90 (▲) composites. The bars represent the difference between two measurements.

III. 4.1.2 The Second Heating Cycle and Glass Transition of the Spray-Dried Samples

The first anticipation for the mixture generated after cooling the spray-dried drug-polymer mixtures is the loss of moisture and other volatiles rendering them more homogeneous. The presence of comparably shallow endotherms observed in the second heating cycle of some mixtures indicated the permanent loss or trace remains of the water from the system. Thus T_{gm} values calculated for the naproxen-PVP binary systems were compared with the T_{gm} observed in the second run over the entire composition range. But, the nature and the extent of the moisture loss are not straightforward to project. The incompleteness of moisture loss due to the location of the moisture (inclusion within the polymer matrices, bound, hydrated with the drug/polymer) in the mixture cannot be overlooked.

The experimental T_{gm} values obtained in the second heating showed the negative deviation from the corresponding predicted values too across almost an entire composition range. However, the extent of deviation was much reduced except for the composites with PVP K 12 toward higher polymer content end (Figure III.2b). Surprisingly, the curve of

observed T_{gm} of naproxen-PVP K 12 mixtures still showed a noncompositional pattern. More precisely, the values of T_{gm} observed for the 95% and 90% PVP K 12 containing composites were lowered markedly compared to the corresponding T_{gm} values predicted by the GT equation, even lower than the subsequent T_{gm} of the mixtures containing higher drug content. The extent of negative deviations of experimental T_{gm} from predicted T_{gm} notably decreased in the case of naproxen-PVP K 25 dispersions to nearly fit with the predicted line up to 20% polymer content. The sigmoid-like T_{gm} pattern of the naproxen-PVP K 25 system observed in the first heating was almost not distinct in the second heating cycle, although the negative deviations were more evident beyond the same composition (20% polymer content). The T_{gm} pattern observed in naproxen-PVP K 90 reveals a symmetrical decrease in deviations from the predicted values as compared to the first heating. Though the curve of experimental T_{gm} fell sharply up to the 85% polymer containing composite, the curve showed parallel deviation from the predicted values for the further compositions. The melting endotherms of the drug in the samples containing 25% polymer were observed around the same region as in the first heating cycle, but the areas under the endotherms were considerably higher, indicating that the amount of drug remaining dispersed in the polymer was lower (Table III.1). However, the values of the melting endotherms were higher (by 20-25 J/g) than for the corresponding crystallization exotherms. This implies that the fraction of supersaturated drug dispersed in the polymer at this composition forms a separate amorphous fraction in addition to the partial amorphization of the phase separated crystals while cooling the comelts. This is evident from the presence of endotherms related to the enthalpy recovery and crystallization exotherms in the corresponding nonreversing heat flow signals. The crystallization temperature observed was in the order PVP K 90 g PVP K 25 > PVP K 12 (data not shown), indicating the effect of polymer chain length on kinetics of drug crystallization.

III. 4.1.3 Entropy of Mixing the Drug into the Polymer and the Composition Dependence

Though enthalpy of mixing is the dominantly used indicator for the miscibility of drug in polymer and for describing miscibility behavior of drug in polymer and possible drug-polymer interactions in solid dispersions, some of the recent publications emphasize employing the quantitative entropy of mixing as a significant scale in looking to the miscibility of pharmaceutical glass mixtures[17,23]. The Cauchman-Karasz (CK) equation predicts the T_{gm} of the drug-polymer mixtures utilizing the ΔC_p of the individual components as a part of the entropy contribution in mixing[24]. The mixed phase glass transition (T_{gm}^{CK}) is given by eq III.2:

$$lnT_{gm}^{CK} = \frac{x_1 \Delta C_{p1} lnT_{g1} + x_2 \Delta C_{p2} lnT_{g2}}{x_1 \Delta C_{p1} + x_2 \Delta C_{p2}} \ldots\ldots\ldots\ldots\ldots\ldots\ldots\ldots\ldots\ldots \text{Equation III. 2}$$

where T_{gm}^{CK}, x and ΔC_p are the mixed phase glass transition by the *CK* equation, the respective mole fraction of pure components, and heat capacity difference between glassy and liquid state of the pure components (subscript 1 denotes the values for the component with lower T_g) respectively. Hence, it is interesting to investigate the entropic contribution during mixing by correlating the predicted T_{gm}, observed T_{gm} and ΔC_{pm}. The ΔC_{pm} is a summation of conformational, free volume and cohesive interaction contributions[25]. If the drug-polymer miscibility is through hydrogen bonding which substantially influences the composition dependence of both free volume and cohesive interaction energy, it will also affect the ΔC_{pm} associated with the T_{gm}, and will affect the configurational entropy (ΔS_{mix}^{c}) of mixing. Pinal[17] has derived an expression for ΔS_{mix}^{c} that correlates the deviation and observed T_{gm} with T_{gm}^{CK} taking ΔC_{pm} into consideration (eq III.3).

$$T_{gm} = T_{gm}^{CK}[e^{-\left(\frac{\Delta S_{mix}^{c}}{\Delta C_{pm}}\right)}] \ldots\ldots\ldots\ldots\ldots\ldots\ldots\ldots\ldots\ldots\ldots\ldots \text{Equation III. 3}$$

In the present study, it was logical only to calculate ΔS_{mix}^{c} values with respect to the second heating cycle to omit the unpredictable entropic inputs of water content in miscibility.

As shown in Figure III. 3, the inspection of plots of ΔS_{mix}^{c} versus polymer content of the mixtures provided some further insight of the miscibility. The ΔS_{mix}^{c} pattern as a function of polymer weight fraction showed a defined entropy minimum of naproxen-PVP K 12 mixtures between 85% and 80% polymer containing composition. Two entropy minima were observed for naproxen dispersions with PVP K 25 and PVP K 90. In the case of naproxen mixtures with PVP K 25, the increasing entropy up to 90% polymer content followed by the fall toward 85% polymer content signifies the composition dependent abundance of energetic interaction. Similarly, the mixtures with entropy minima were those containing 90% and 80% polymer for naproxen-PVP K 90 system. These mixtures corresponded to the downward jumps displayed of the observed T_{gm} patterns below this polymer content (Figure III.2b).

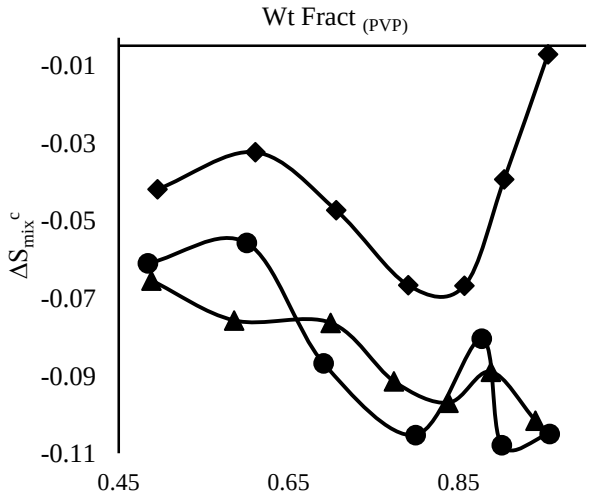

Figure III.3. Plots of configurational entropy of mixing (ΔS_{mix}^{c}) versus PVP weight fraction calculated for spray-dried naproxen-PVP K 12 (♦), naproxen-PVP K 25 (▲) and naproxen-PVP K 90 (●) composites based on data from second heating cycles in mDSC.

III. 4.2 Relating Solubility Data of Naproxen in n-Methylpyrrolidone to that in PVP Solid Dispersions

As proposed by Marsac and co-workers[7,8], it is reasonable to correlate the solubility of the drug in a polymer with that in the low molecular weight analogue or the monomer of the polymer which exists in the liquid state. Assuming the latter as the lattice of the polymer, its physical attributes like molecular weight and volume and the experimental solubility and activity coefficient of the drug can be introduced in the calculation of the solubility of the drug in the polymer. The expressions derived from Flory-Huggins (FH) lattice theory were used with assumptions of similar nature of interaction, and ideal combinatorial entropy of mixing in both drug-monomer and drug-polymer systems[13]. NMP (a low molecular weight analogue of PVP) was taken as the lattice in the FH lattice model, and its molecular volume was considered as lattice molecular volume ($MV_{lattice}$).

The equilibrium solubility of naproxen in NMP obtained from HPLC analysis was utilized to determine its activity coefficient (γ_{NMP}) in the same, which is the ratio of ideal mole fraction solubility (X_{id}) to the experimental mole fraction solubility (X_{exp}). X_{id} was calculated using eq III.4[26].

$$lnX_{id} = -\frac{\Delta H_f(T_m - T)}{R(T_m T)} + \frac{\Delta Cp(T_m - T)}{RT} - \frac{\Delta C_p}{R} ln\left(\frac{T_m}{T}\right) \dots\dots\dots\dots\dots \text{Equation III. 4}$$

where ΔH_f is the heat of fusion, T_m is the melting point of drug and ΔC_p is the heat capacity difference between liquid and crystal. R is the universal gas constant, and T is the absolute temperature for which the estimation is envisaged. The values of ΔH_f and T_m were obtained

from the DSC analysis of pure crystalline drug powder while that of ΔC_p was taken from the literature[27]. The calculated value of γ_{NMP} was thus employed in the calculation of the activity coefficient in the polymer (γ_{PVP}) at the solubility limit using eq III. 5.

$$ln\gamma_{PVP} = ln\left(\emptyset_{naproxen}/X_{exp}\right) + \left(1 - \frac{MV_{naproxen}}{MV_{PVP}}\right)\emptyset_{PVP} + ln\gamma_{NMP} \ldots\ldots\ldots \text{Equation III. 5}$$

Here Ø and MV denote the particular volume fraction and molar volume respectively. Consequently, the mole fraction solubility of crystalline naproxen in PVP (X_{PVP}), which is the ratio of X_{id} to γ_{PVP}, was estimated and converted to % w/w solubility (S_c). As it is debatable to compare the crystalline solubility of naproxen in amorphous PVP with its kinetic miscibility in the glassy solution, the solubility of amorphous naproxen in amorphous PVP or "amorphous solubility" (S_a) was approximated from the crystalline solubility and entropy of fusion (ΔS_f) using eq III.6[28,29].

$$S_a = S_c e^{\frac{\Delta S_f}{R} ln \frac{T_m}{T}} \ldots\ldots\ldots\ldots\ldots\ldots\ldots\ldots\ldots\ldots\ldots\ldots \text{Equation III. 6}$$

ΔS_f is the ratio of ΔH_f to T_m.

Furthermore, these values were exploited to estimate the FH interaction parameter (χ) for the naproxen-PVP system (eq III.7).

$$ln\gamma_{PVP} = ln\left(\frac{\emptyset_{naproxen}}{X_{exp}}\right) + \left(1 - \frac{MV_{naproxen}}{MV_{PVP}}\right)\emptyset_{PVP} + \left(\frac{MV_{naproxen}}{MV_{NMP}}\right)\chi\emptyset_{PVP}{}^{2} \ldots\ldots \text{Equation III. 7}$$

At last, the obtained χ value was implemented to profile the composition dependence of the Gibbs free energy of mixing (ΔG_{mix}) by applying eq III.8 (Figure III.4).

$$\frac{\Delta G_{mix}}{RT} = \frac{MV_{NMP}}{MV_{naproxen}}\phi_{naproxen} ln\phi_{naproxen} + \frac{MV_{NMP}}{MV_{PVP}}\phi_{PVP} ln\phi_{PVP} + \chi\phi_{naproxen}\phi_{PVP} \ldots \text{Equation III. 8}$$

The first two terms on the right-hand side of eq III.8 represent the entropy of mixing while the third represents the enthalpy of mixing. The ΔG_{mix} obtained would be composition dependent. The ΔG_{mix} for a system is reduced by the presence of a negative value of χ indicating exothermic (favorable) mixing. As entropy always favors mixing, for any drug-polymer system with enthalpy of mixing up to a certain unfavorable value, ΔG_{mix} will still remain negative. So, for athermal systems where there is no specific drug-polymer interaction ($\chi = 0$) also, ΔG_{mix} can still be negative. Beyond a positive value of interaction parameter, for an unfavorably (endothermic) interacting system, say $\chi_{critical}$, the value obtained for ΔG_{mix} will be positive at various compositions. Therefore the magnitude of is crucial in the predicted pattern of composition dependent drug-polymer miscibility.

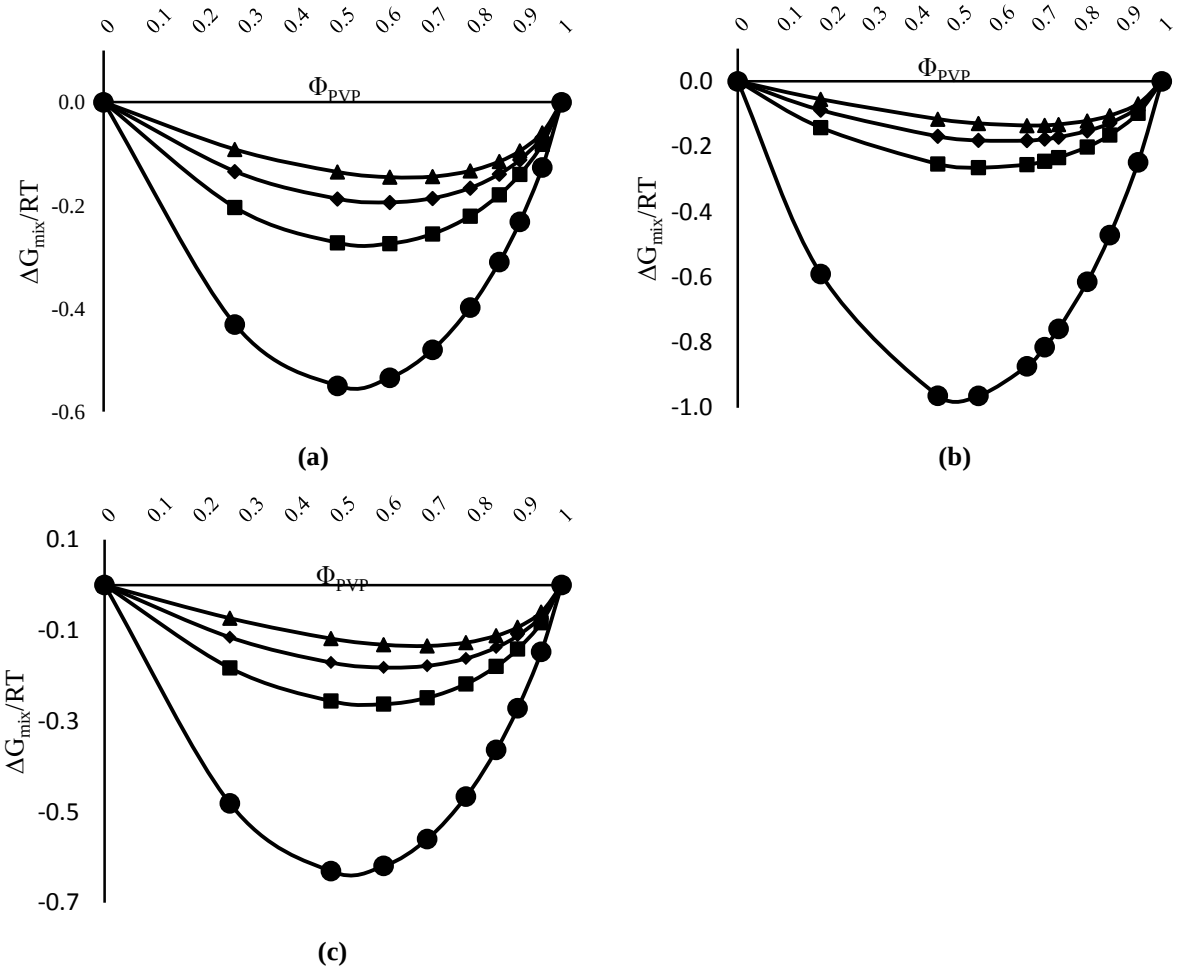

Figure III.4 Gibbs free energy of mixing (ΔG_{mix})/RT versus polymer volume fraction (Φ_{PVP}) for naproxen-PVP K 12 (a), naproxen-PVP K 25 (b) and naproxen-PVP K 90 (c) systems with Flory-Huggins interaction parameter determined by the melting point depression (●), experimental solubility (■), solubility parameters (▲) methods and athermal systems ($\chi = 0$) (♦).

In addition, the theoretical approach derived from Hildebrand regular solution theory based on solubility parameters of the solute and solvent components[14] was used to have more insight on the solid solubility of drug in polymer by comparing with the experimental values. It assumes the repeating unit of polymer (monomer or an interacting unit) as the solvent and the drug molecule as the solute. The different degrees of interaction between the drug and the polymers might result in variable drug-polymer miscibility, expressed in terms of eq III.9.

$$lnX_s = -lnX_{id} - \frac{\left(\delta_{PVP} - \delta_{naproxen}\right)^2 MV_{naproxen} \emptyset_{PVP}{}^2}{RT} \quad \text{... ... ... Equation III. 9}$$

X_s is molar fraction solubility of drug in PVP, and δ is the solubility parameter. The solubility parameters were calculated by the Fedors group contribution method[30]. The interaction parameter (χ_s) between drug and polymer was calculated using eq III.10:

$$\chi_s = \frac{V_{site}\left(\delta_{PVP} - \delta_{naproxen}\right)^2}{RT} \quad \text{... ... ... Equation III. 10}$$

Where, V_{site} is the volume of the hypothetical lattice. The value of MV_{NMP} was taken as V_{site} for relevant comparison.

The values related to various components used for calculations and results obtained based on the aforementioned analysis are given in Table III.2. The trend in solid solubility values of naproxen in PVP is in the order PVP K 12 > PVP K 25 > PVP K 90. The differences in the values of solid solubility, interaction parameter and activity coefficient of the drug in three PVPs are too small to account for the effect of chain length. The negative value obtained of χ from experimental solubility calculation agrees with the fact that naproxen is a favorably interacting drug with PVP in terms of mixing. Besides, this is even evident from the significant shifts reported of relevant peaks in infrared (IR) spectra of pure drug in the presence of PVP (in the form of colyophilized or physical mixtures) by Bettinetti et al[11]. Also, a less negative value of χ for the naproxen-PVP system compared to that reported for the indomethacin-PVP system obtained by the same methodology (-0.8)[8] reflects that it exhibits a comparatively weaker interaction with PVP. As mentioned in literature[8], the values beyond unity of activity coefficients of the drug obtained in PVP signify them to be regular solution systems. So, it is safe to compare these data with those calculated using the Hildebrand regular solution model. To some extent, the solubility of naproxen predicted by the solubility parameters method also matched with the experimentally obtained values. The value of the interaction parameter obtained nearer to zero (0.21) supported the naproxen-PVP system being an interactive system. Unsurprisingly, the value of χ_s cannot account for the exothermic mixing system as none of the components in the right-hand side of eq III.10 can be negative. As shown in Figure III.4, the ΔG_{mix} line drawn from the values using interaction parameters obtained by both methods are negative. This indicates that χ values calculated by both the methods are below $\chi_{critical}$.

The comparison of kinetic miscibility with both the crystalline and amorphous solubility in PVP implies that naproxen is highly supersaturated in solid dispersions. As a result, the existence of drug-polymer miscibility at the macroscopic level was only attributable to kinetic stabilization that might subsequently lead to the phase separation

Table III.2 Solid Solubility of Naproxen in PVP and the Related Values

Components	Values
Molar volume of drug (MV_d)	195.14 cm^3/mole
Molar volume of NMP (MV_{NMP})	96.43 cm^3/mole
Mole fraction solubility in NMP (X_{exp})	0.11
Heat of fusion (ΔH_f)	31578.51 J/mole
Melting temperature (T_m)	428.07 K
Absolute temperature (T)	298.00 K
Universal gas constant (R)	8.31 J/ mole.K
Heat capacity change (ΔC_p)	108.60 J/mole.K[a]
Entropy of fusion (ΔS_f)	73.77 J/ mole.K
Ideal mole fraction solubility (X_{id})	0.05
Activity coefficient of drug in NMP (γ_{NMP})	0.49
Solubility parameter of naproxen ($\delta_{naproxen}$)	23.37 $J^{1/2}/cm^{3/2}$
Solubility parameter of PVP (δ_{PVP})	20.56 $J^{1/2}/cm^{3/2}$

	naproxen-PVP K 12	naproxen-PVP K 25	naproxen-PVP K 90
Values estimated from experimental solubility			
Molar volume of PVP (MV_{PVP}) (cm^3/mole)	2252.25	20000.00	932203.39
Activity coefficient of drug in PVP (γ_{PVP})	2.01	2.14	2.15
Mole fraction solubility in PVP (X_{PVP})	0.029	0.026	0.026
FH interaction parameter ($\varkappa$)	-0.36	-0.36	-0.36
Crystalline solubility of drug in PVP (S_c) (%w/w)	6.42	5.85	5.81
Amorphous solubility of drug in PVP (S_a) (%w/w)	7.02	6.39	6.35
Values calculated from solubility parameters			
Mole fraction solubility in PVP (X_s)	0.04	0.04	0.04
Solute solvent interaction parameter ($\varkappa_s$)	0.21	0.21	0.21

[a]Taken from ref 27.

III. 4.3 Melting Point Depression of the Drug in the Presence of the Polymer as an Indicator of Drug-Polymer Miscibility

The melting point depression of drugs in polymeric matrices has been explored in deriving the possible solid state interaction between drug and polymer[7,8,31]. The drop in chemical potential of drug molecules in the presence of the polymer makes the system cross the smaller temperature interval and has an equal chemical potential as that of the liquid phase leading to a reduced melting point ($T_{m^{mix}}$) compared to the melting point in the pure state ($T_{m^{pure}}$). The extent of depression is more in the case of strong exothermic mixing, less for weak exothermic or athermal or endothermic mixing and no depression in a totally immiscible system[8]. The extensively used procedure for accessing interactions between the

components in the polymer blends described by Nishi and Wang[31] was used in the present studies. The interaction energy density, B, was estimated from the slopes of melting point depression (ΔT) plots (Figure III.5) against the second power of the polymer volume fraction ($\emptyset_{PVP}^2$) by using the Nishi and Wang equation (eq III.11). As evident from Figure III.5, the trends corresponding to ΔT versus $\emptyset_{PVP}^2$ plots exhibit feasible linearity for the calculations with R^2 values of 0.956, 0.966, and 0.816 for the naproxen-PVP K 12, naproxen-PVP K 25 and naproxen-PVP K 90 systems, respectively.

$$\Delta T = T_{m^{pure}} - T_{m^{mix}} = T_{m^{pure}} \left(\frac{MV_{naproxen}}{\Delta H_f} \right) B \emptyset_{PVP}^2 \ldots\ldots\ldots\ldots \text{Equation III. 11}$$

The value for the FH interaction parameter, χ was further computed using eq III.12:

$$B = RT_{m^{mix}} \left(\frac{\varkappa}{MV_{lattice}} \right) \ldots\ldots\ldots\ldots \text{Equation III. 12}$$

Here also the value of MV_{NMP} was taken as the lattice volume, $MV_{lattice}$. The value of B is independent of composition. Rather, it represents the intensity of molecular interaction during mixing as a function of molecular weight of the mixing components. So, it should rely on the molecular weight of the mixing components. As the latter is constant for the drug, the value of B would be more negative with the increase in the molecular weight of polymer up to certain critical value. On the other hand, the FH interaction parameter (χ) is truly composition and temperature dependent. The values obtained for B and composition dependence of χ are listed in Table III.3.

Table III.3 Composition dependent values of drug polymer interaction parameter obtained from melting point depression data by solving Nishi and Wang equation

Mixtures	% Naproxen	FH interaction parameter ($\varkappa$)	Interaction energy density (B) [J/cm^3]
Naproxen PVP K 12	95	-1.44	
	90	-1.44	-89.17
	85	-1.45	
	80	-1.45	
	75	-1.47	
Naproxen PVP K 25	95	-3.18	
	90	-3.19	-118.03
	85	-3.19	
	80	-3.19	
	75	-3.20	
Naproxen PVP K 90	95	-1.83	
	90	-1.83	-68.05
	85	-1.84	
	80	-1.84	
	75	-1.85	

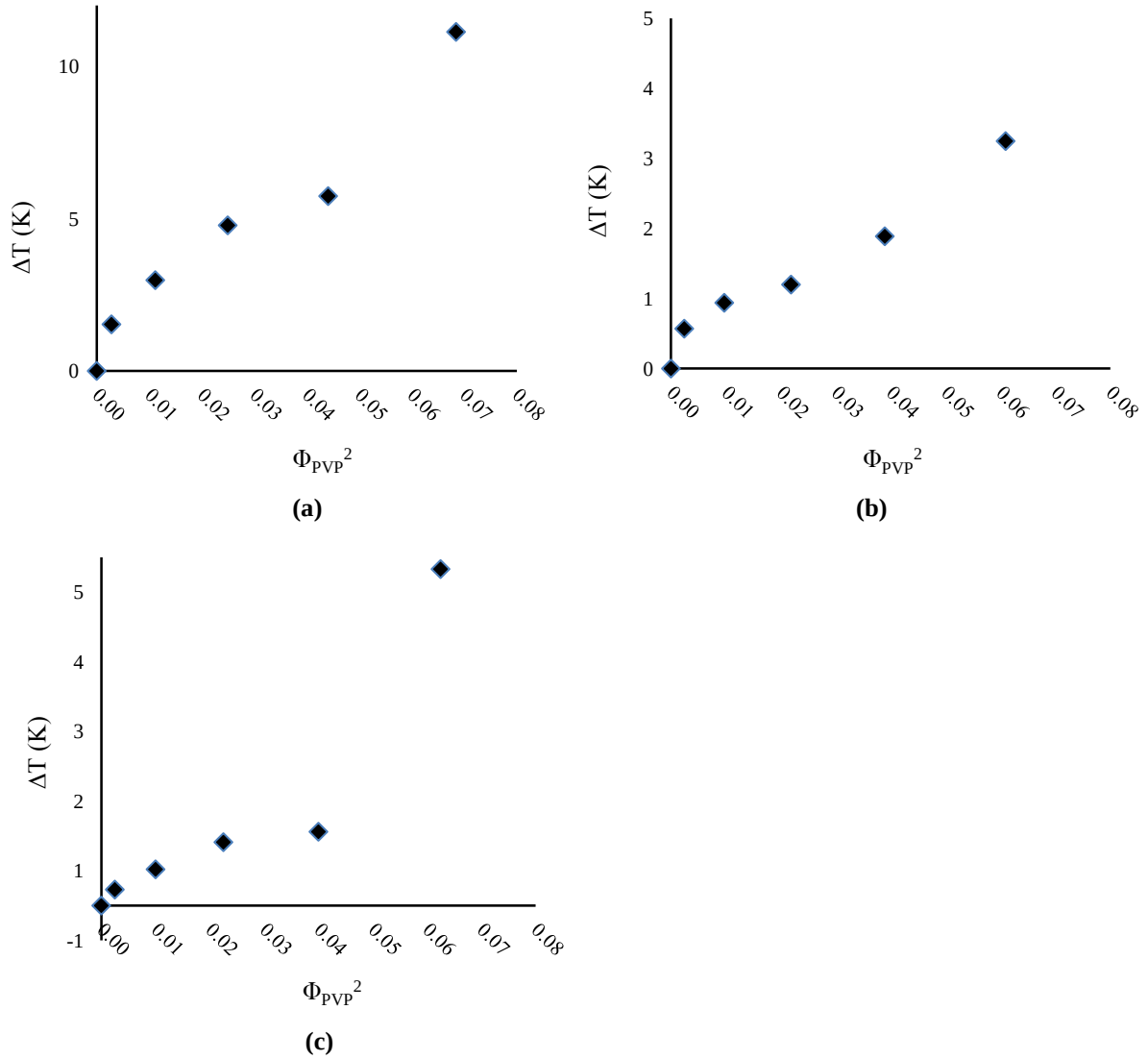

Figure III.5 The plot of melting point depression versus the second power of PVP volume fraction (Φ_{PVP}^2) for physical mixtures containing naproxen-PVP K 12 (a), naproxen-PVP K 25 (b) and naproxen-PVP K 90 (c).

The reduced melting point was calculated to consider the colligative melting point depression by the polymer in athermal mixtures by using a standard thermodynamic model excluding the interaction term (eq III.13).

$$\left(\frac{1}{T_{m^{mix}}} - \frac{1}{T_{m^{pure}}}\right) = -\frac{R}{\Delta H_f}\left[ln\,\emptyset_{naproxen} + \left(1 - \frac{MV_{naproxen}}{MV_{PVP}}\right)\emptyset_{PVP}\right] \ldots\ldots\ldots \text{Equation III. 13}$$

The offset temperatures of the melting endotherms were taken for the calculations since an intimate mixing can occur by this point. The calculated (for athermal system) and observed melting point depressions were plotted against polymer volume fraction of the composites (Figure III.6).

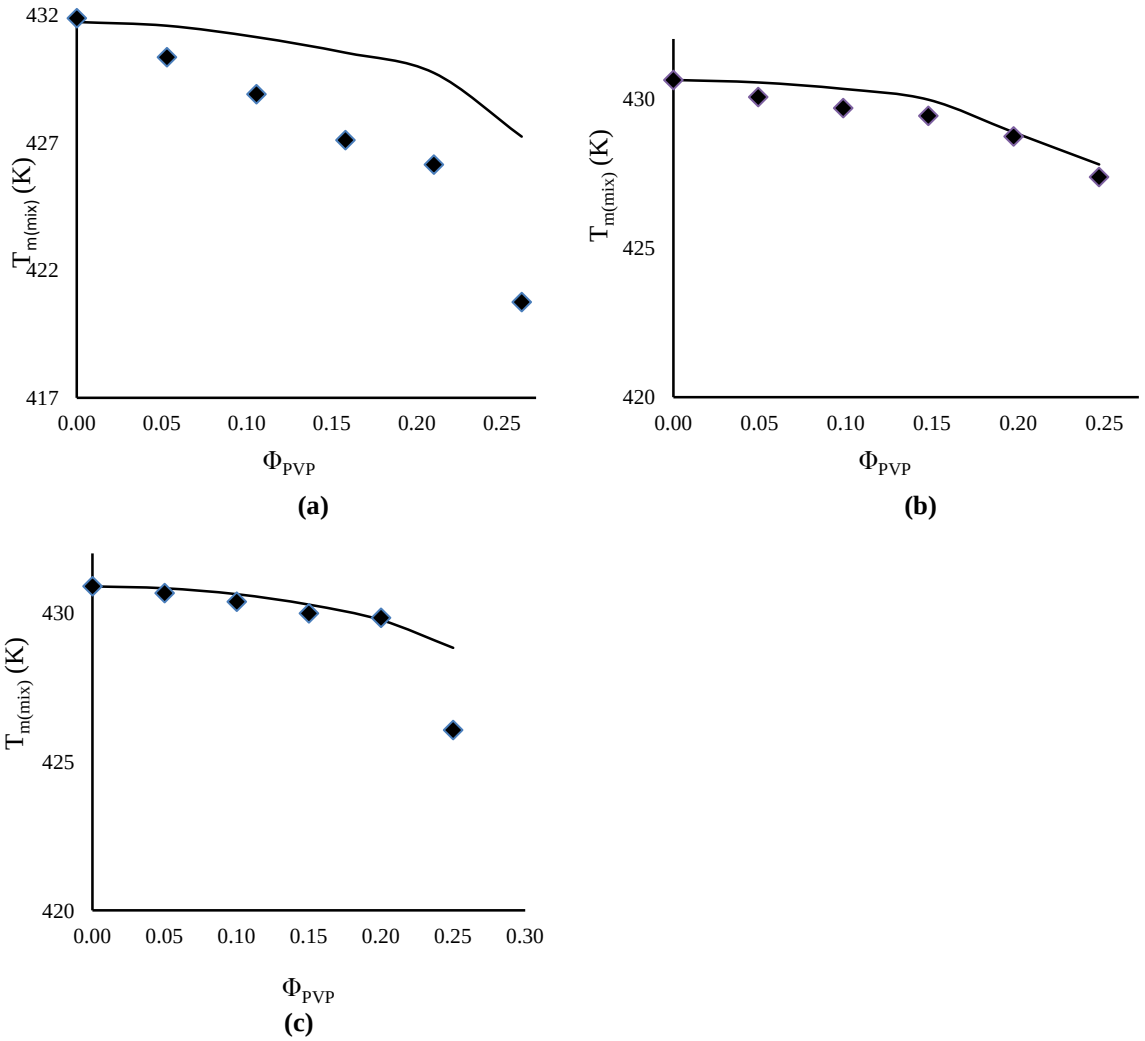

Figure III.6 The plot of reduced melting point of naproxen in presence of PVP versus the PVP volume fraction (Φ_{PVP}) for physical mixtures containing naproxen-PVP K 12 (a), naproxen-PVP K 25 (b) and naproxen-PVP K 90 (c). The lines represent the melting points for the corresponding athermal mixtures.

A remarkable compositional dependent depression in the melting point was observed. As observed in the plots, the melting point depressions calculated for the corresponding athermal systems using eq III.13 were smaller. For naproxen-PVP K12 system the differences were found to be higher while lower for naproxen-PVP K 25 systems. As discussed for similar cases by Marsac et al.[7], these results can be correlated with the difference between the melting region of mixtures and T_g values of PVPs. PVP K 12, having $T_g < T_{m^{mix}}$, exists in a liquid-like state bearing considerable molecular mobility leading to the better interaction and miscibility. Conversely, the glassy state of PVP K 90 with higher viscosity during melting of the drug in mixtures ($T_g > T_{m^{mix}}$) leads to less mixing and interaction.

The value of B was most negative for the systems made up of naproxen and PVP K 25. This signifies that the potential of interaction of drug is highest with PVP K 25. Also there should be some critical molecular weight or chain length of polymer wherefrom the strength of interaction would be reversed. As anticipated, the calculated χ values were found

appreciably negative for all the compositions. The negative value of χ increased consistently with an increase in polymer content in the mixtures. This can be taken as an indication of the compositional dependence of interaction. It would be logical to calculate the χ values of the system at the composition of solid solubility calculated by the experimental solubility method. But, for the mixtures from and beyond 50% PVP, there was no detectable melting endotherm present.

By virtue of comparing the value of χ with that obtained by the experimental solubility method, the lines were extrapolated to the drug content equivalent to the experimentally obtained solubility limits. The χ values obtained at the solubility limits for naproxen-PVP K 12, naproxen-PVP K 25 and naproxen-PVP K 90 systems are -2.02, -3.52, and -2.10 respectively. This reveals that the prediction of interaction between drug and polymer at ambient conditions needs to be corrected with respect to the temperature. This could be possible by reworking the values with the Wertheim thermodynamic perturbation theory which also correlated χ with the directional interaction apart from temperature[32,33]. The plots of ΔG_{mix} calculated by including the value of χ (the lowest of all the compositions for each polymer system) obtained by this method as function of polymer content were indeed deeper than that from the former ones (Figure III.4).

III. 4.4 Moisture Sorption Behavior of Physical Mixtures to Elucidate Drug-Polymer Interaction

The FH lattice model has been modified and extended to study the sorption behavior of the drug-polymer physical mixtures or solid dispersions[34,35]. This leads to the calculation of the composition dependent FH interaction parameter (χ) at a certain percentage relative humidity (% RH). This relationship can be expressed in terms of partial vapor pressures as given by eq III.14:

$$ln\left(\frac{P}{P_0}\right) = lnV_1 + \left(1 - \frac{1}{X_{12}}\right)V_2 + \varkappa V_2^2 \quad \ldots\ldots\ldots\ldots \text{Equation III. 14}$$

where V_1 and V_2 represent the volume fractions of solvent and solute respectively. P/P_o and X_{12} are the partial vapor pressure and the number of segments (monomer units) per solvent molecule. This relation was used first to calculate the drug water interaction parameter. A common expression derived from FH equation and Vrentas equation (eq III.15) includes mutual interaction parameters between drug-polymer, drug-water and polymer-water pairs in the drug-polymer-water ternary system as follows:

$$ln\left(\frac{P}{P_0}\right) = lnV_1 + (V_2+V_3) - \left(\frac{V_2}{X_{12}}\right) - \left(\frac{V_3}{X_{13}}\right) + [(\varkappa_{12}V_2 + \varkappa_{13}V_3)(V_2+V_3)] - \left(\frac{\varkappa_{23}V_2V_3}{X_{12}}\right) \ldots\ldots\ldots \text{Equation III. 15}$$

where χ_{12}, χ_{13} and χ_{23} are FH interaction parameters for naproxen-water, PVP-water and naproxen-PVP respectively. X_{12} and X_{13} are the number of molecules of naproxen and the number of segments (monomer units) of PVP per unit water molecule respectively. V_1, V_2 and V_3 are the volume fractions of water, naproxen and PVP respectively. As eq III.15 is reported to provide a better fit at the higher partial water vapor pressure, a 94% RH environment was used. The value of χ_{13} was taken as equal to 0.5 from literature[35]. X_{13} was taken as unity by assuming the interaction of one monomer unit of PVP with one molecule of water. The value of χ_{12} was calculated assuming X_{12} = 2 as reported for indomethacin[35], a molecule bearing a similar interacting functionality (carboxylic acid) as that of naproxen. Physical mixtures containing PVP K 12 were excluded from the moisture sorption study due to its excessive hygroscopicity that posed trouble in accuracy of the moisture gain measurement. The values obtained by the moisture sorption based calculation are given in Table III.4. The χ values obtained by this method showed pertinent composition dependence. The positive values of χ toward the higher drug content implied weaker or unfavorable drug-polymer interaction in them. However, at 25% w/w drug content the χ values are highly negative. Though these values from ternary systems are not precisely comparable with the drug-polymer binary system, an idea about the extent of interaction as a function of composition can be extracted in the presence of water.

The deviation of the moisture gain behavior of the mixtures from the theoretically calculated values as a function of composition is shown in Figure III.7. The negative deviations observed for all three compositions indicate the existence of favorable interaction between drug and polymer. The higher deviation seen at higher polymer content signifies the stronger interaction toward this composition.

Table III.4 Composition dependent values interaction parameter calculated from the moisture sorption based analysis

Mixture	%PVP in mixture	Interaction parameter between		
		$\varkappa_{13}$ (Polymer-water)	$\varkappa_{12}$ (Drug-water)	$\varkappa_{23}$ (Drug-polymer)
Naproxen-PVP K 25	25	0.5	5.73	12.02
	50			4.53
	75			-1.70
Naproxen-PVP K 90	25			11.05
	50			4.29
	75			-1.80

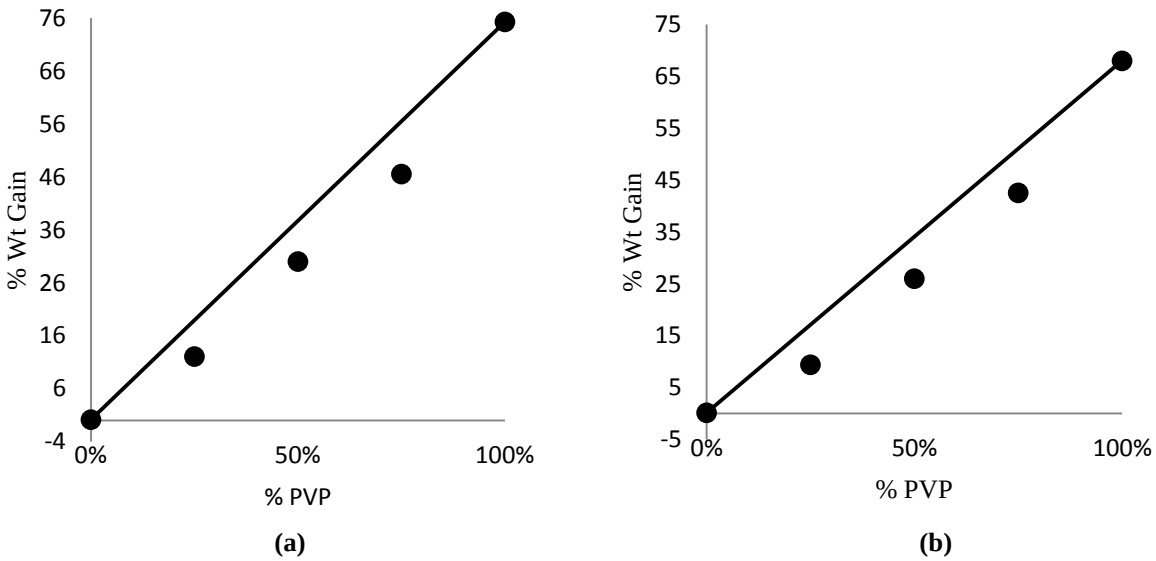

Figure III.7 Moisture gains versus % w/w PVP in physical mixtures containing naproxen-PVP K 25 (a) and naproxen-PVP K 90 (b). The solid lines represent the theoretical moisture gains.

III. 5 Discussion

The macroscopic examination of thermoanalytical data revealed that solid dispersions of naproxen and PVP prepared by spray-drying are miscible up to 1:1 compositions. The effect of water in mixing is more pronounced for the system containing the hygroscopic polymer PVP K 12. The exceedingly lower T_{gm} values obtained in the second heating cycle of solid dispersion of naproxen containing 95% and 90% PVP K 12 could be due to the *in situ* moisture absorption by the hygroscopic PVP K 12 while cooling the drug-polymer mixture in the DSC cell. If we assume that the extent of absorption is up to the theoretical equilibrium moisture content (EMC) of the system, then it will gradually decrease with the increase of the drug content in the mixture so that the plasticization will be less. The EMC of a mixture decreases gradually with the decrease in the polymer content, and hence the decrease of T_{gm} values below 15% polymer content may be due to the plasticization effect of the drug only. The observation of deeper endotherms remaining in the nonreversing heat flow signals of the corresponding mixtures provided additional evidence of the presence of moisture.

Disregarding this observation, there are always two groups of drug-polymer composites in terms of T_{gm}, especially in the case of naproxen-PVP K 25 and naproxen-PVP K 90 systems. The solo role of plasticization by the water content in the mixtures with T_{gm} below 100 °C was overruled as the patterns were consistent during the second heating cycle as well. Nevertheless, this behavior can be correlated to the composition dependent strength of the drug-polymer interaction and hence the miscibility in this system. The possible interactions of PVP with the drug molecules are electrostatic (ion-ion, ion-dipole, dipole-dipole), van der Waals and hydrogen bonding interactions[36]. Such behavior can further be

prevailed for the system with the prospect of potential saturable interaction between drug and polymer undergoing the mixing process. The term "saturable interaction" is implied to specific types of interaction such as hydrogen bonding which can get saturated with respect to mixture composition or mixing temperature. There is well documented evidence of the presence of saturable interactions between naproxen and PVP[11,37]. Here, the deviation of observed T_{gm} from that predicted using the GT equation reflects the strength of interaction which can render the integrity of miscibility. Also, it has been reported for naproxen that it can complex with *n*-vinylpyrrolidone (VP), a monomer unit of PVP, in 1:1 molar composition in solution[9]. However in solid state the scenario will not be the same as the molecular vicinity is different with comparable decrease in mobility. This is supported by the observation that the naproxen-PVP mixture with equimolar content of drug to VP molecules (67.47% w/w drug) already crosses the miscibility barrier. Thus, if the hydrogen bonding density (number of drug molecules hydrogen bonded with a monomer) is a function of composition for a system, the composition dependent deviation of T_{gm} from the predicted values can be due to the different types of structural mixtures. Interesting correlations have been drawn in a publication[22] for the composition dependent formation of single or double hydrogen bonds between the small units of PVP and PEG reflected by the deviation of T_{gm}. In a recent publication on interaction between PVP and aryl acetic acid NSAIDs[37], composition dependent miscibility behavior has been studied between naproxen and PVP K 30. As discussed by the authors, it is reasonable to assume an increase in the hydrogen bonding capacity as function of naproxen concentration with an increased diffusion of naproxen into the PVP chain due to its small molar volume. At a particular composition, the naproxen content in the mixture becomes excess apart from that interacts with PVP and immiscibility starts. However, it appears contradictory that naproxen is miscible through the whole composition range from 10% to 90% PVP K 30 containing mixtures. Besides these findings, more comprehensive spectroscopic investigations on the naproxen-PVP interaction and miscibility based on solid state ^{17}O-NMR[38] or pulsed field gradient (PFG) NMR[22] studies are necessary to ascertain the composition dependent hydrogen bonding behavior and its mechanistic explanation.

In comparison to ibuprofen, naproxen is considered as a weakly interacting molecule with PVP[12,37]. The weak interaction between naproxen and PVP due to the catemer arrangement of naproxen molecules in its crystal packing is reported[12]. However, the molecular geometry in the crystal structure rarely dictates the state of the drug after the

treatment with the molecular chaos provided by the processing solvents and other process parameters during the manufacture of the solid dispersion. The information on the intra- versus intermolecular hydrogen bonding behavior of naproxen has been studied in diverse solvents (protic, aprotic, alcoholic and polar/nonpolar)[39]. Rather, the persuasively supporting fact is that naproxen exhibits a higher number of self-assembling interactions (COOH… HOOC and COOH…-O-) as compared to ibuprofen (COOH…HOOC)[40]. This poses an increased competition of naproxen against itself toward hydrogen bonding with the polymer. For such weaker interactions, there would be a certain influence of the molecular weight and chain length of PVP on the probability of hetero-contact formation[23]. Up to a certain increase in molecular weight the number of drug-polymer hydrogen bonding increases. Beyond this, the higher molecular weight of PVP with longer chain length provides opportunity for more coiling. This leads to a lesser accessibility of the interacting groups for a random hetero-contact formation.

The drug-polymer miscibility analyzed with the vision of entropy contribution gives a different picture. The conformational rearrangements play a vital role in the local ordering effect against hetero-contact formation for the weakly interacting systems[23]. Hence, for the systems like naproxen-PVP, the entropic contribution to the miscibility is remarkable. These effects will contribute to an increase of the free volume and a corresponding decrease of the T_{gm} from predicted values. Negative entropy of mixing can be expected for strongly interacting mixture components in structured mixtures[17]. However, the energetic interactions that are prevailing in the lower naproxen containing mixtures will cause the denser packing of the mixture components due to decreased mobility and free volume leading to an increase in hetero-contact formation and in turn an increase in the T_{gm} values. This is apparent from the obtained U shaped entropy plots as a function of mixture composition (Figure III.3).

The equilibrium crystalline as well as the amorphous solubility obtained by the experimental solubility method over kinetic miscibility provided better insight about whether naproxen at certain composition is miscible with PVP on a molecular scale or is very close to being miscible in terms of supersaturation. The values obtained for amorphous miscibility ranged from 6.35 to 7.02% w/w while those obtained for crystalline solubility were 5.81-6.42% w/w. The values of the experimentally obtained amorphous solubility might be less than the calculated values at the given temperature due to simultaneous devitrification and plasticization effect on naproxen, a rapidly devitrifying molecule. The theoretical model is purely based upon the thermodynamics and, hence, does not take both phenomena into

account[41]. Though the amorphous miscibility is related to the balance between cohesive and adhesive forces between the mixing components and crystalline solubility is contributed by the crystal packing and cavitation energy, the difference in drug solubility was marginal. However both values are far below the observed kinetic miscibility. This suggests that the drug-polymer systems are markedly supersaturated. The negative values of FH interaction parameters (-0.36) provided a mechanistic indication for the naproxen-PVP mixtures being an exothermically mixing system. Though the interaction parameter looks more realistic as calculated from data at ambient temperature and with the drug composition at its solubility limits, its composition dependence cannot be worked out by this methodology. Based on the chemical structure of the drug substance, the chain length of PVP is crucial in deciding the interaction based miscibility[36,42]. The effect of chain length on the dynamic structure of PVP and PEG mixtures in a polar solvent has been conferred in terms of its contribution to relaxation processes, its change in complexation density in a mixture and its segmental motion[42]. However, the influence of the PVP chain length on the estimated solubility and interaction parameter values could not be revealed by this methodology. This could be due to the inappropriate use of the FH model or the assumptions made in deriving the expressions as discussed earlier. Moreover, the main setback of the FH model is that it does not take into account the directional interactions or hydrogen bond related parameter in the expression. So, the influence of the latter is missed in the course of the calculations. Conversely, the solid solubility values obtained by this method are approximately equivalent to that by the solubility parameter method. The difference in solubility parameter values between drug and polymer has also been used for accessing the drug-polymer miscibility[15,23]. However, it is a bolder assumption to make that all types of interactions (dispersive, dipolar and hydrogen bonding) that are included in the solubility parameter contribute similarly to the solid solubility. Thus, we assume that the Wertheim thermodynamic perturbation theory (WTPT)[33,34] can be a more appropriate model to describe the true phase behavior of the drug-polymer mixture exhibiting an existence of saturable interaction between the mixing components. This is the subject of our current investigation.

The other advanced mixing thermodynamics for modeling solute solubility in solvent and phase behavior are nonrandom hydrogen-bonding (NRHB) theory[43,44], the universal functional activity coefficient (UNIFAC) model[45], the nonrandom two liquid segment activity coefficient model (NRTL-SAC)[46] and the conductor-like screening model for real solvents (COSMO-RS)[47]. NRHB has recently been used for modeling the phase behavior in mixtures

of pharmaceuticals with liquid or supercritical solvents with promising results[40], and even COSMO-RS has also been used for the pharmaceutical systems[47]. The challenges posed in modeling the phase behavior of the drug-polymer systems are their complex hydrogen bonding and interaction behavior, the presence of chirality in drug and unavailability of fluid state data for polymers.

The technique based on melting point depression provided a better compositional dependent interaction. The popular methodology in studying miscibility of polymer blends based on the Nishi and Wang expression has also been used for the physical mixture and solid dispersion system containing a steroidal hormone and Eudragit®[48]. The B values determined by curve fitting indicated the interaction between the mixing components. The melting point depression method demonstrated the propensity of predicting the composition dependence and PVP chain length effect on the interaction and miscibility of naproxen and PVP. The less negative value of B for naproxen-PVP K 12 systems (-89.17) compared to the value of the naproxen-PVP K 25 system (-118.03) revealed that the molecular interaction is denser in the latter case. However, the decrease in the absolute value of B for the naproxen-PVP K 90 system is logical when considering the effect of the molecular weight of PVP beyond a certain value. The extrapolations of the composition dependent interaction parameter up to the solubility limit estimated from the experimental solubility limits provided an interesting insight. As naproxen showed the temperature dependent decrease in the number of intermolecular hydrogen bonding per molecule with ethanol and acetone with an increase in temperature[40], a similar scenario can be anticipated with PVP which in turn weakens the drug-polymer interaction. Hence, the value of the composition dependent interaction parameter would be less negative at ambient temperature as compared to that obtained from an extrapolation of the trend line to the desired composition by this method. The comparison of χ values from the experimental solubility method and melting point depression method can only be made after correction of this temperature term. However, the FH model does not offer preference for the same as it does not incorporate any hydrogen bonding related parameter in the calculation. Hence with this method, the temperature dependent interaction parameter cannot be obtained. So, WTPT will be capable of correlating the interaction parameter with the temperature[49].

The methodology based upon the moisture sorption analysis also provided the composition dependent interaction parameter. The outcome from this method in some way projects the fate of drug-polymer miscibility in the presence of moisture. The influence of

absorbed moisture in the miscibility of drug-polymer composites is well explored[34,35]. The solid solubility of drug in polymer at a particular composition decreases with an increase in supersaturation due to the sorbed moisture, a consequence commonly known as $\Delta\chi$ (χ_{12} - χ_{13}) effect. The composition dependent immiscibility can be induced due to the extreme difference between interaction of water with hydrophobic naproxen (unfavorable interaction, χ = 5.73) and hydrophilic PVP (favorable interaction, χ = 0.5). There are some examples on the moisture induced phase separation of pharmaceutical amorphous solid dispersions[50,51]. This can be more pronounced toward higher drug containing mixtures as they are already supersaturated. The interaction parameters obtained by this method are perhaps more qualitative.

As noticed from Figure III.4, the Gibbs free energy plots as a function of PVP molecular weight for the naproxen-PVP mixtures are highly comparable. All curves plotted from the values obtained with χ values except that from the solubility parameter method are lower than the corresponding athermal curves. The Gibbs free energy change minimum region that lies around the 50% w/w composition zone signifies the limit of kinetic miscibility.

III. 6 Conclusions

The thermodynamic solid solubility estimated of naproxen in PVP was considerably lower than the observed kinetic miscibility. Solid state behavior of the solid dispersions prepared using PVP with varying molecular weight showed marked differences in terms of composition dependence of mixed phase glass transition temperatures. The crystallization temperature in the phase separated systems indicated an identical extent of crystallization inhibition. The information derived from the configurational entropy is important for weakly interacting systems like naproxen and PVP. The difference in the estimated solid solubility of naproxen in PVPs with different molecular weights using experimental solubility in *n*-methylpyrrolidone was negligible. This implies that the currently used FH thermodynamic lattice model for drug-polymer mixing lacks the intended parameters to account for chain length effect on interaction and miscibility such as hydrogen bonding. The treatments of data with the models that really tender the chain length effect of polymer in solid solubility of drug like Wertheim thermodynamic perturbation theory are preferred. The extent of solid-solid solubility and the strength of the drug-polymer interaction estimated by different methods varied extensively. The method that uses the experimental solubility of drug in the low molecular weight analogue of the polymer to estimate the solubility in the corresponding

polymer offers more realistic values. This is due to the real time data generated for the downstream calculations at room temperature and toward lower drug content. It can be inferred from the melting point depression method that naproxen-PVP is a favorably interacting system with considerable negative values of the interaction parameter. Also, the composition dependent interaction parameters could be calculated by this method. However, it deals with mixing of the system around the melting point of the drug, which is practically very rare to reach, and the interaction parameter is truly composition/temperature dependent, especially for the systems exhibiting saturable interactions. The moisture sorption method provides an idea of the extent of weakening that water can cause to the drug-polymer interaction. It gives a qualitative estimate of the composition dependent interaction parameters.

III. 7 References

1. Chiou, W.L.; Riegelman S. Pharmaceutical Applications of Solid Dispersion Systems. J. Pharm. Sci. 1971, 60, 1281-1302.
2. Leuner, C.; Dressman, J. Improving Drug Solubility for Oral Delivery using Solid Dispersions. Eur. J. Pharm. Biopharm. 2000, 50, 47–60.
3. Sethia, S.; Squillante, E. Solid Dispersions: Revival with Greater Possibilities and Applications in Oral Drug Delivery. Crit. Rev. Ther. Drug. Carrier Syst. 2003, 20, 215-247.
4. Serajuddin, A.T.M. Solid Dispersion of poorly Water-soluble Drugs: Early Promises, Subsequent Problems, and Recent Breakthroughs. J. Pharm. Sci. 2000, 88, 1058-1066.
5. Khougaz, K.; Clas, S.D. Crystallization Inhibition in Solid Dispersions of MK-0591 and Poly (vinylpyrrolidone) Polymers. J. Pharm. Sci. 2000, 89, 1325-1334.
6. Janssens, S.; Van den Mooter, G. Review: Physical Chemistry of Solid Dispersions. J. Pharm. Pharmacol. 2009, 61, 1571-1586.
7. Marsac, P.J.; Shamblin, S.L.; Taylor, L.S. Theoretical and Practical Approaches for Prediction of Drug-Polymer Miscibility and Solubility. Pharm. Res. 2006, 23, 2417-2426.
8. Marsac, P.J.; Li, T.; Taylor, L.S. Estimation of Drug-Polymer Miscibility and Solubility in Amorphous Solid Dispersions using experimentally determined Interaction Parameters. Pharm Res. 2009, 26 139-151.
9. Velaz, I.; Sanchez M.; Martin, C.; Martinez-Oharriz, M.C.; Zornoza A. Interaction of Naproxen with Vinyl Pyrrolidone and β-Cyclodextrin: a Fluorimetric Study. Int. J. Pharm. 1997, 153, 211-217.
10. Bettinetti, G.P.; Mura, P. Dissolution Properties of Naproxen in Combinations with Polyvinlypyrrolidone. Drug Dev. Ind. Pharm. 1994, 20, 1353-1366.
11. Bettinetti, P.; Mura, P.; Liguori, A.; Bramanti, G. Solubilization and Interaction of naproxen with Polyvinylpyrrolidone in Aqueous Solution and in Solid State. Farmaco. [Prat.]. 1988, 43, 331-343.
12. Bogdanova, S.; Pajeva, I.; Nikolova, P.; Tsakovska, I.; Müller, B. Interactions of Poly(vinylpyrrolidone) with Ibuprofen and Nap roxen: Experimental and Modeling Studies. Pharm. Res. 2005, 22, 806-815.
13. Flory, P.J. Principles of Polymer Chemistry. Cornell University Press, Ithaca, 1953.
14. Hildebrand, H. The Term 'Regular Solution'. Nature. 1951, 168, 868.
15. Greenhalgh, D.J.; Williams, A.C.; Timmins, P.; York, P. Solubility Parameters as Predictors of Miscibility in Solid Dispersions. J. Pharm. Sci. 1999, 88, 1182-1190.
16. Muruganandham, M.; Chen, S.H.; Wu, J.J. Mineralization of N-methyl-2-pyrolidone by Advanced Oxidation Processes. Sep. Purif. Technol. 2007, 55, 360–367.

17. Pinal, R. Entropy of Mixing and the Glass Transition of Amorphous Mixtures. Entropy. 2008, 10, 207-223.
18. Gordon, M.; Taylor, J.S. Ideal Copolymers and the Second-order Transitions of Synthetic rubbers. I. Non-crystalline polymers. J. Appl. Chem. 1952, 2, 493-500.
19. Simha, R.; Boyer, R.F. On a General Relation Involving the Glass Temperature and Coefficients of Expansion of Polymers. J. Chem. Phys. 1962, 37, 1003-1007.
20. Vasanthavada, M.; Tong W.Q.; Joshi, Y.; Kislalioglu, M.S. Phase Behavior of Amorphous Molecular Dispersions II: Role of Hydrogen Bonding in Solid Solubility and Phase Separation Kinetics. Pharm. Res. 2005, 22, 440-448.
21. Forster, A.; Hempenstall, J.; Rades, T. Comparison of the Gordon-Taylor and Couchman-Karasz Equations for Prediction of the Glass Transition Temperature of Glass Solutions of Drug and Polyvinylpyrrolidone Prepared by Melt Extrusion. Pharmazie. 2003, 58, 838-839.
22. Feldsteina, M.M.; Roos, A.; Chevallier, C.; Creton, C.; Dormidontova, E.E. Relation of glass Transition Temperature to the Hydrogen Bonding degree and Energy in Poly (N-vinyl pyrrolidone) blends with Hydroxyl-containing Plasticizers: 3. Analysis of two Glass Transition Temperatures featured for PVP Solutions in liquid Poly (ethylene glycol). Polymer. 2003, 44, 1819–1834.
23. Schneider, H.A. Conformational Entropy Contributions to the Glass Temperature of Blends of Miscible Polymers. J. Res. Natl. Inst. Stand. Technol. 1997, 102, 229-248.
24. Couchman, P.R.; Karasz, F.E. A Classical Thermodynamic Discussion of the effect of Composition on Glass Transition Temperatures. Macromolecules. 1978, 11, 117-119.
25. Tanaka, N. Conformational effects on Glass Transition Temperature and Relaxation Phenomena of Polymers. Polymer. 1978, 19, 770-772.
26. Neau, S.H.; Flynn, G.L.; Yalkowsky, S.H. The influence of Heat Capacity Assumptions on the Estimation of Solubility Parameters from Solubility data. Int. J. Pharm. 1989, 49, 223-229.
27. Neau, S.H.; Bhandarkar, S.V.; Hellmuth, E.W. Differential Molar Heat Capacities to test Ideal Solubility Estimations. Pharm. Res. 1997, 14, 601-605.
28. Hancock, B.C.; Parks, M. What is the true Solubility Advantage for Amorphous Pharmaceuticals? Pharm. Res. 2000, 17, 397-404.
29. Lüder, K.; Lindfors, L.; Westergren, J.; Nordholm, S.; Kjellander, R. In Silico Prediction of Drug Solubility. 3. Free Energy of Solvation in pure Amorphous Matter. J. Phys. Chem. B. 2007, 111, 7303-7311.
30. Fedors, R.F. A Method for Estimating both the Solubility Parameters and Molecular Volumes of Liquids. Polym. Eng. Sci. 1974, 14, 147-154.
31. Nishi, T.; Wang, T.T. Melting-Point Depression and Kinetic Effects of Cooling on Crystallization in Poly (vinylidene fluoride)−Poly (methyl methacrylate) Mixtures. Macromolecules. 1975, 8, 909-915.
32. Wertheim, M.S. Fluids with highly Directional Attractive Forces. I. Statistical Thermodynamics. J Stat. Physics. 1984, 35, 19-34.
33. Wertheim, M.S. Fluids with highly Directional Attractive Forces. II. Thermodynamic Perturbation Theory and Integral Equations. J Stat. Physics. 1984, 35, 35-47.
34. Hancock, B.C.; Zografi, G. The use of Solution Theories for Predicting Water Vapor Absorption by Amorphous Pharmaceutical Solids: A test of the Flory-Huggins and Vrentas Models. Pharm. Res. 1993, 10, 1262-1267.
35. Crowley, K.J.; Zografi, G. Water Vapor Absorption into Amorphous Hydrophobic Drug/Poly (vinylpyrrolidone) Dispersions. J. Pharm. Sci. 2002, 91, 2150-2165.
36. Bühler, V. Polyvinylpyrrolidone Excipients for Pharmaceuticals Povidone, Crospovidone and Copovidone; Springer-Verlag Publishing Co.: Berlin Heidelberg, 2005; pp 88-108.
37. Gashi, Z.; Censi, R.; Malaj, L.; Gobetto, R.; Mozzicafreddo, M.; Angeletti, M.; Masic, A.; Di Martino, P. Differences in the Interaction between Aryl Propionic Acid Derivatives and Poly (vinylpyrrolidone) K30: A Multi-methodological Approach. J. Pharm. Sci. 2009, 11, 4216-4228.
38. Lemaître, V.; Smith, M.E.; Watts, A. A Review of Oxygen-17 Solid-State NMR of Organic Materials-Towards Biological Applications. Solid State Nucl. Magn. Reson. 2004, 26, 215-235.

39. Velazquez, M.M.; Valero, M.; Rodríguez, L.J.; Costa, S.M.; Santos, M.A. Hydrogen Bonding in a Non-Steroidal Anti-Inflammatory Drug-Naproxen. J. Photochem. Photobiol. B. 1995, 29, 23-31.
40. Tsivintzelis, I.; Economou, I.G.; Kontogeorgis, G.M. Modeling the Phase Behavior in Mixtures of Pharmaceuticals with Liquid or Supercritical solvents. J. Phys. Chem. B. 2009, 113, 6446-6458.
41. Chawla, G.; Bansal, A.K. A Comparative Assessment of Solubility Advantage from Glassy and Crystalline forms of a Water-insoluble Drug. Eur. J. Pharm. Sci. 2007, 32, 45-57.
42. Sengwa, R.J.; Sankhla, S. Chain Length Effect on Dynamical Structure of Poly (vinyl pyrrolidone)-Polar Solvent Mixtures in Dilute Solution of Dioxane Studied by Microwave Dielectric Relaxation Measurement. PRAMANA-J. Phys. 2006, 67, 375-381.
43. Panayiotou, C.; Pantoula, M.; Stefanis, E.; Tsivintzelis, I. Nonrandom Hydrogen-Bonding Model of Fluids and Their Mixtures. 1. Pure Fluids. Ind. Eng. Chem. Res. 2004, 43, 6592–6606.
44. Panayiotou, C.; Tsivintzelis, I.; Economou, I.G. Nonrandom Hydrogen-Bonding Model of Fluids and Their Mixtures. 2. Multicomponent Mixtures. Ind. Eng. Chem. Res. 2007, 46, 2628–2636.
45. Frank, T.C.; Downey, J.R.; Gupta, S.K. "Quickly Screen Solvents for Organic Solids." Chem. Eng. Prog. 1999, 95, 41–61.
46. Chen, C.; Song, Y. Solubility Modeling with a Nonrandom Two-Liquid Segment Activity Coefficient Model. Ind. Eng. Chem. Res. 2004, 43, 8354–8362.
47. Klamt, A.; Eckert, F.; Hornig, M.; Beck, M.E.; Burger, T. Prediction of Aqueous Solubility of Drugs and Pesticides with COSMO-RS. J. Comput. Chem. 2002, 23, 275–281.
48. Wiranidchaponga, C.; Rades, T.; Kulvanich, P.; Tucker, I.G. Method of Preparation does not Affect the Miscibility between Steroid Hormone and Polymethacrylate. Thermochim. Acta. 2009, 485, 57–64.
49. Available on https://lirias.kuleuven.be/bitstream/1979/2083/2/.pdf
50. Rumondor, A.C.; Marsac, P.J.; Stanford, L.A.; Taylor, L.S. Phase Behavior of Poly (vinylpyrrolidone) containing Amorphous Solid Dispersions in the Presence of Moisture. Mol. Pharm. 2009, 6, 1492-505.
51. Marsac, P.J.; Rumondor, A.C.; Nivens, D.E.; Kestur, U.S.; Stanciu, L.; Taylor, L.S. Effect of Temperature and Moisture on the Miscibility of Amorphous Dispersions of Felodipine and Poly (vinyl pyrrolidone). J. Pharm. Sci. 2010, 99, 169-185.

Chapter IV: Influence of Solvent Composition on the Miscibility and Physical Stability of Naproxen/PVP K 25 Solid Dispersions Prepared by Cosolvent Spray-Drying

The results described in this chapter are published in the following article:

Paudel, A. and Van den Mooter, G. (2010). Influence of Solvent Composition on the Miscibility and Physical Stability of Naproxen/PVP K 25 Solid Dispersions Prepared by Cosolvent Spray-Drying. *Pharmaceutical Research*, 29 (1), 251-270.

IV.1 Abstract

Purpose: To investigate the influence of solvent properties on the phase behavior and physical stability of spray-dried solid dispersions containing naproxen and PVP K 25 prepared from binary cosolvent systems containing methanol, acetone and dichloromethane.

Methods: The viscosity, polymer globular size and evaporation rate of the spray-drying feed solutions were characterized. The solid dispersions were prepared by spray-drying drug-polymer solutions in binary solvent blends containing different proportions of each solvent. The phase behavior was investigated with mDSC, pXRD, FT-IR and TGA. Further, physical stability of solid dispersions was assessed by analyzing after storage at 75% RH.

Results: The solid dispersions prepared from solvent/antisolvent mixture showed better miscibility and physical stability over those prepared from the mixtures of good solvents. Thus, solid dispersions prepared from dichloromethane-acetone exhibited the best physicochemical attributes followed by those prepared from methanol-acetone. FT-IR analysis revealed differential drug-polymer interaction in solid dispersions prepared from various solvent blends, upon the exposure to elevated humidity.

Conclusion: Spray-drying from a cocktail of good solvent and anti-solvent with narrower volatility difference produces solid dispersions with better miscibility and physical stability resulting from the simultaneous effect on the polymer conformation and better dispersivity of drug.

IV.2 Introduction

Amorphous solid dispersion (ASD) of a poorly water soluble active pharmaceutical ingredient (API) in a hydrophilic polymeric carrier is one of the most commonly applied strategies to increase the solubility, dissolution rate and hence systemic availability of drugs administered through the oral route[1,2]. In spite of these delivery benefits, the frequent problem with solid dispersion formulation is its higher physical and chemical instability. The solubility advantage of metastable ASD formulation often ceases due to the rapid crystallization of amorphous API, triggered upon exposure to an aqueous medium during administration or crystallization from the supersaturated solution[3,4]. The kinetically stabilized ASD with supersaturated drug loading is severely susceptible to crystallization upon storage. Molecularly dispersed systems provide maximum stabilization against crystallization[5]. In this respect, understanding of polymer-drug interaction and phase behavior of the binary system is of key importance for the selection of the most suitable carrier. Moreover, the method of

preparation, the range of process variables, and the drug/polymer ratio have a substantial influence on physical structure, the solid state solubility/miscibility of drug and polymer in an ASD[6,7]. Spray-drying of the mixture of a drug and a polymer from a solution/suspension in a solvent or solvent blend has been used for manufacturing ASD for many years. The morphological properties and drug release from an ASD prepared by spray-drying can be rationally correlated with the properties of dispersing solvents or solvent mixtures used during the process[8]. An improved in vitro performance of solid dispersions prepared by spray-drying from multiple solvents compared to that prepared from a single solvent has been reported through control of particle morphology (http://www.aapsj.org/abstracts/AM_2009AAPS2009-000990.PDF). The considerable difference in the solid state miscibility between polymer-polymer or drug-polymer in the film casted from different solvents has been reported[9,10]. Al-Obaidi et al. pointed on the significant role of solvent composition on the stability and dissolution rate of ternary ASD prepared by spray-drying[11]. Spray-drying from metastable solutions is reported to enhance miscibility of drug-polymer in solid dispersions[12]. Despite recent efforts, a deeper understanding on dispersing solvent chemistry and its impact on strength of the drug-carrier interaction, phase behaviour and solid state stability is still lacking. There are no reports in the literature on how a particular spray-drying solvent mixture leads to the development of an acceptable physical structure of the spray-dried products. The marked difference in physicochemical properties between drug and excipient used in solid dispersions also creates a considerable solubility gap in different solvent mixtures. Especially, polymer architecture such as chain folding/unfolding in a particular solvent mixture provides better opportunity to establish stronger drug-polymer interaction and hence optimal miscibility[11]. Hitherto, less emphasis has been given on the consequence of evaporation rate of different organic solvents used in spray-drying on molecular mixing of drug and polymer and also on the surface properties of the end products.

The present work aims to carry out a thorough investigation on the effect of initial solvent composition of the spray-drying feed solution on the phase behaviour and physical stability of the spray-dried dispersions (SDDs) of naproxen with PVP K 25 prepared from them. ASDs with two different drug loadings were prepared by spray-drying from the solutions in methanol, dichloromethane (DCM) and acetone and their binary mixtures at three different ratios. Thus, prepared SDDs were analyzed using modulated differential scanning calorimetry (mDSC), Fourier transform-infrared (FT-IR) spectroscopy and powder X-ray diffractometry (pXRD) to describe their phase behaviour/solid state miscibility/ crystal

growth and the strength of drug polymer interaction. The SDDs were stored at elevated humidity and analyzed by the above-mentioned techniques to gain further insight on their differential miscibility behaviour as an indicator of physical stability. The correlation of relevant solvent properties like evaporation rate, proticity, and solvent power with polymer solubility, polymeric globular size and solution viscosity was made to enlighten the mechanism underlying the observed difference in the miscibility and physical stability of the SDDs prepared from the corresponding solvent mixtures. A mechanistic explanation on the evolution of unique physical structures in SDDs prepared from a variety of solvent blends is postulated based on the observed results.

IV.3 Materials and Methods

IV.3.1 Materials

Naproxen was purchased from CERTA Ltd. (Brainl'Allend, Belgium). PVP K 25 (M_w = 25,000 Da) was kindly donated by BASF (Ludwigshafen, Germany). Methanol (HperSolv CHROMANORM, VWR, Belgium), DCM (J.T. Baker, The Nederland) and acetone (Chemlab, Belgium) were used single or as binary mixtures for spray-drying. The solvents used were of HPLC or analytical grade.

IV.3.2 Methods

IV.3.2.1 Spray-Drying

Volumetric combinations of methanol, DCM and acetone were prepared by mixing two solvents at 1:3, 1:1 and 3:1 ratio for each binary solvent system. Solid dispersions made up of 30%w/w and 55% w/w of naproxen in PVP K 25 were prepared by spray-drying 5%w/v solutions of drug and polymer in each solvent blend or pure solvents. The solid dispersion from acetone was not prepared due to insolubility of PVP in pure acetone. All solutions were spray-dried using a Buchi mini spray-dryer B191 (Buchi, Flawil, Switzerland) with 50°C inlet temperature, 100% aspirator rate (800 L/h heated nitrogen flow) and 12 ml/min feed rate using a peristaltic pump. The spray-dried samples were further dried to remove the residual solvent in a vacuum oven (0.2 bar) at 25°C for 1 week before analysis.

IV.3.2.2 Exposure to the Elevated Relative Humidity (RH) Storage Condition

Followed by the secondary vacuum drying, approximately 100 mg of the spray-dried samples were further stored in a desiccator containing a saturated sodium chloride solution in water at room temperature (25±2°C) to achieve the 75% RH condition. Samples were

removed after 1 week and 1 month and subsequently dried overnight in the presence of P_2O_5 at 40°C before analysis to avoid the interference of the condensed water.

IV.3.2.3 Thermal Analysis

mDSC was performed on a Q2000 DSC (TA Instruments, Leatherhead, U.K.) under a dry nitrogen purge at a flow rate of 50 mL/min. DSC was equipped with the refrigerated cooling system (RCS90) accessory. The data acquisition and analyses were carried out using Universal Analysis (version 4.4, TA Instruments, Leatherhead, U.K.). The enthalpy was calibrated with an indium standard, and the temperature scale was calibrated with octadecane, indium and tin. The total and reversing heat capacity signals in modulated heating mode (modulated with ±1°C amplitude every 40s) were calibrated by comparing the response of a sapphire disk with its standard values at 106.85°C. All samples were accurately weighed in aluminum pans and crimped with the aluminum lid. The samples were then heated from −20°C to 160°C at 2°C/min scan rate with the temperature modulation as that used in mDSC calibration. Glass transition temperature (T_g) was measured at half height of transition in the reversing heat flow curve. The large and broad transitions were precisely analyzed in the curve of the first derivative of the reversing heat flow. The optimum linear smoothing of the derivative curves was executed to obtain better resolution against baseline noise.

Further, DSC was calibrated with indium, and samples were run at 50°C/min linear heating rate from 0°C to 160°C to distinguish the melting event due to trace crystalline content in the samples that were not prominent at slow heating rate of 2°C/min.

The moisture and volatile content in the samples were determined by heating the samples at 2°C/min from 30°C to 160°C with a dry nitrogen purge at 100 mL/min in a thermogravimetric analyzer (TGA), SDT Q600 (TA-instruments, Leatherhead, U.K.). The data were analyzed using Universal Analysis 2000 software (TA Instruments, Leatherhead, U.K.). The recorded weight loss from the starting temperature to 100°C was considered as the loss due to the solvents and water.

IV.3.2.4 Evaporation Rate Measurement

The evaporation rates of spray-drying feed solutions and corresponding pure solvent mixtures were measured using TGA. Approximately 10–30 μl feed solutions were transferred into the ceramic crucible that was tared (with lid), covered with the lid and placed on the sample holder and enclosed inside the temperature-controlled furnace (23±0.5°C) constantly purged with nitrogen at 100 ml/min flow rate. The weight loss was recorded every minute for

25 min. The derivative of percentage weight loss as a function of time is presented as the evaporation rate of the system.

IV.3.2.5 Viscosity Measurement

Viscosity measurements of spray-drying feeds and pure PVP K 25 solution (5%w/v) were performed using a Vibration viscometer (vibration viscometer, SV-10, A & D Instruments, Oxfordshire, UK) equipped with a temperature-controlling water jacket assembly, AX-SV-37 set at 25±0.1°C. The instrument consists of two sensor plates positioned at a gap of 1 mm and oscillating in opposite directions with a frequency of 30 Hz and 1 mm amplitude that were dipped in the sample solution in a glass cup. All measurements were run until there was no fluctuation in the viscosity reading at constant temperature. The calibration was done at 25°C by using water as calibrant. The data acquisitions were carried out using the RSVisco program (A & D Instruments, Oxfordshire, UK). Additionally, intrinsic viscosity measurements of the solvent blends were performed using an Ostwald viscometer (Schott AG, Mainz, Germany) at 25°C using a water bath. All measurements were performed in triplicate.

IV.3.2.6 Dynamic Light Scattering

Globular size distribution of PVP K 25 in the naproxen-PVP K 25 solutions were measured using a BIC90Plus (Brookhaven Instruments Co., Holtsville, NY, USA). The measurement is based on the principle of photon correlation spectroscopy. All samples were properly filtered through 0.45 μm filter (Henke Sass Wolf, Tuttlingen, Germany) and measured at 25°C. The total solute content was always 5% w/v. The w/w ratio of naproxen to PVP K 25 was either 30/70 or 55/45. The volume-weighted mean particle diameters of the solutions were taken as the globular sizes for comparison and calculation.

IV.3.2.7 Powder X-ray Diffraction (pXRD) Studies

Spray-dried products were analyzed using an automated X'pert PRO diffractometer (PANalytical, Almelo, the Netherlands) with a Cu tube and the generator set at 45 kV and 40 mA. The samples were prepared by spreading over zero background plates or by clamping between Kapton foil. The analysis was performed in a continuous scan mode from 4° to 40° 2θ with 0.0021° step size and 19.685 s counting time. The X'pert Data Viewer (PANalytical, Almelo, The Netherlands) was used for processing and analysing the data. For the samples

that showed Braggs peaks, the relative degree of crystallinity was computed as the ratio of the net peak height above the amorphous halo to the total height at the same 2θ° (19.5±0.5°).

IV.3.2.8 Polarized Light Microscopy

Polarized light microscopy was performed with an Olympus BX60 polarizing optical microscope equipped with a LINKAM THMS600 hot stage and a LINKAM TMS93 programmable temperature controller. Sample powders were spread over a glass slide and covered with another slide. The specimens were visualized for the presence of birefringence under polarized light and pictured using a digital camera (Olympus). All images were taken at room temperature.

IV.3.2.9 Fourier Transform Infrared Spectroscopy (FT-IR)

Infrared spectra of spray-dried samples were collected using a Spectrum RX I FT-IR spectrometer (Perkin Elmer, Norwalk, CT, USA). Standard KBr disk method was applied to prepare samples. Approximately 1 mg of the sample and 200 mg of dried KBr was blended uniformly in an agate mortar and pressed into a translucent disk. The samples were scanned from 400 to 4,000 cm^{-1} with 32 scans per spectrum and a resolution of 4 cm^{-1} at room temperature. The spectra were analyzed with the Spectrum v2.00 software (Perkin Elmer, Norwalk, CT, USA). The optimum points Savitsky-Golay smoothing was performed on all the spectra to remove spikes and negative peaks. The relative peak intensities at the area of interest were further taken for the calculation of the interaction.

IV.4 Results

IV.4.1 Spray-Drying Feed Solution Properties

IV.4.1.1 Viscosity

As depicted in Table IV.1, the viscosities (η) of pure solvents and their mixtures provided a measure of the interaction between the components in the solvent blends, as all the binary mixtures have higher viscosity than the corresponding calculated values. For DCM-acetone system, η is progressively increasing with the increase of DCM content with higher values as compared to the pure components at each composition. The DCM-methanol mixtures also show an evident increase in η as compared to pure components or values calculated therefrom. But the mixture containing 1:1 ratio (by volume) exhibits the largest increase in η, indicating the strongest interaction at this composition. Likewise, methanol-acetone systems are also more viscous than the pure components. Pure PVP K 25 solution in

DCM has the highest viscosity and also higher in solvent blends containing DCM (Table IV.1). The viscosity of PVP in methanol-acetone systems was reduced as compared to that in pure methanol. In the case of feed solutions, the viscosity was lower in comparison to pure PVP solution, as they contain naproxen along with PVP. But the feed solutions with methanol-acetone system have lower viscosity than the pure solvent blends. This is evidence of the synergistic building of new binodal interaction in expense of solvent-solvent interaction. Also, PVP should remain compact in this system. This was also the case in the solutions containing lower proportion of DCM.

Table IV.1 Comparison of Viscosity and Diffusion Coefficient of Spray-Drying Feed Solutions with Varying Solvent Compositions [A: acetone, D: DCM and M: methanol]

Solvent System			30% w/w naproxen in PVP		55 %w/w naproxen in PVP	
	Viscosity *(η)* (cP) of pure solvents (n=3)	Viscosity *(η)* (cP) of PVP solution (5% w/v)	Viscosity *(η)* (cP)	Diffusion Coefficient (D) ($m^2/s \times 10^{-11}$)	Viscosity *(η)* (cP)	Diffusion Coefficient (D) ($m^2/s \times 10^{-11}$)
3D:1A	0.58±0.004	1.10	0.67	1.60	0.70	1.64
1D:1A	0.53±0.004	0.75	0.53	1.96	0.52	2.06
1D:3A	0.46±0.003	0.77	0.42	1.40	0.37	1.46
3D:1M	0.71±0.002	1.45	0.90	3.72	0.86	1.18
1D:1M	0.77±0.003	1.39	0.84	2.16	0.76	1.26
1D:3M	0.74±0.008	1.20	0.78	1.72	0.68	1.36
3M:1A	0.69±0.002	0.76	0.49	2.68	0.48	2.66
1M:1A	0.58±0.005	0.65	0.44	2.30	0.39	2.22
1M:3A	0.46±0.005	0.61	0.34	1.44	0.30	1.48
D	0.44±0.000	1.55	0.92	2.30	0.95	1.32
M	0.58±0.002	1.09	0.63	1.10	0.56	0.92
A	0.30±0.001					

IV.4.1.2 Polymeric Globular Size

The globular sizes of PVP measured in the spray-drying feed solutions of different solvent blends are shown in Figure IV.1. The mean diameter of the globules measured is higher in methanol as compared to DCM, which is in line with the viscosity results. This means that the more extended the polymeric chains are, the smaller the globular size. Moreover, the globular diameters in methanol, DCM and their binary mixtures are higher for the system containing 55% w/w naproxen compared to that of 30% w/w of naproxen. This might be due to the less inter-chain interaction of PVP at the latter composition. An increasing trend of globular size for 30% naproxen composition and decreasing trend of globular diameter for 55% naproxen content were observed with increasing proportion of methanol in DCM-methanol mixtures. This provides evidence of the composition dependent interaction.

For acetone-containing solvent blends, no marked PVP composition dependence of the globular size was observed. The trend of decreasing globular size of PVP with the decrease in acetone content in DCM-acetone as well as methanol-acetone solvent blends was observed, which is an indication of the increased PVP solubilization. Further, values of diffusion coefficient (*D*) of PVP globules in feed solution prepared in different solvent mixtures were calculated using Stokes-Einstein's equation (eq IV.1). This helps to correlate the rate of solute diffusion towards the core of the droplets during spray-drying[13].

$$D = \frac{KT}{6\pi\eta r} \ldots\ldots\ldots\ldots\ldots\ldots\ldots\ldots\ldots\ldots\ldots\ldots \text{Equation IV. 1}$$

where *K*, *T*, η and *r* are Boltzmann's constant, temperature, viscosity of solvent and hydrodynamic radius of polymeric globules, respectively. The *D* value is inversely related to the viscosity of the medium and PVP globular diameter as reflected from Table IV.1 and Figure IV.1.

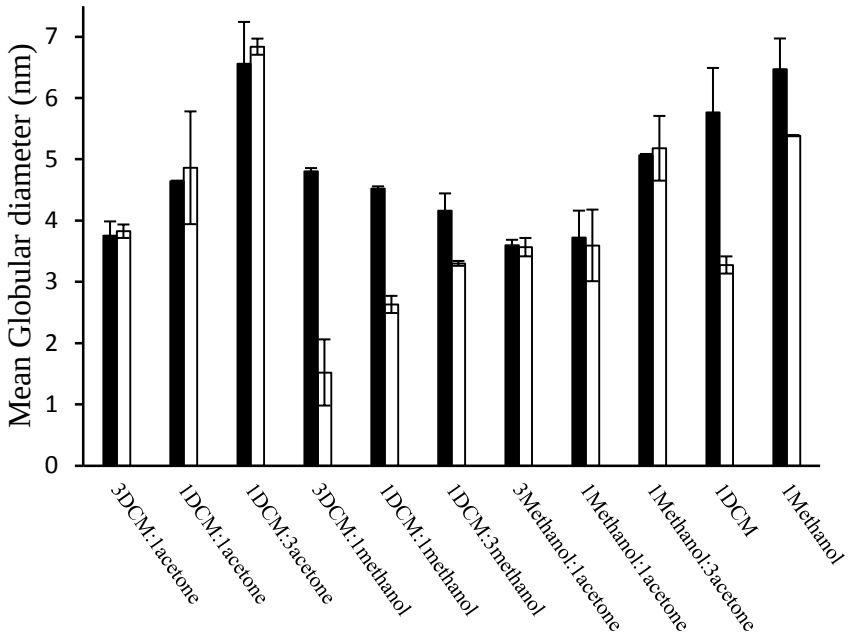

Figure IV.1 Mean globular diameter of PVP in spray-drying feed solutions (5% w/v) prepared in various solvent blends containing 30% w/w naproxen (white bar) and 55% w/w naproxen (black bar) in PVP K 25. Vertical lines represent the range of values obtained in two independent measurements.

IV.4.2 Rate of Solvent Evaporation from Spray-Drying Feed Solution

The miniaturized evaporation rate measurement of the feed solution is helpful in availing the insight of the relative evaporation time for different solvent blends and particle formation during spray-drying as well as the relative interaction strength. As depicted in Figure IV.2a–c, the evaporation rate of acetone-containing solvent blends remains constant throughout except the linear decrease for DCM-acetone (3:1) mixture. For DCM-methanol

system, the evaporation rate decreases nonlinearly, and the rate loss is more rapid with the higher DCM content.

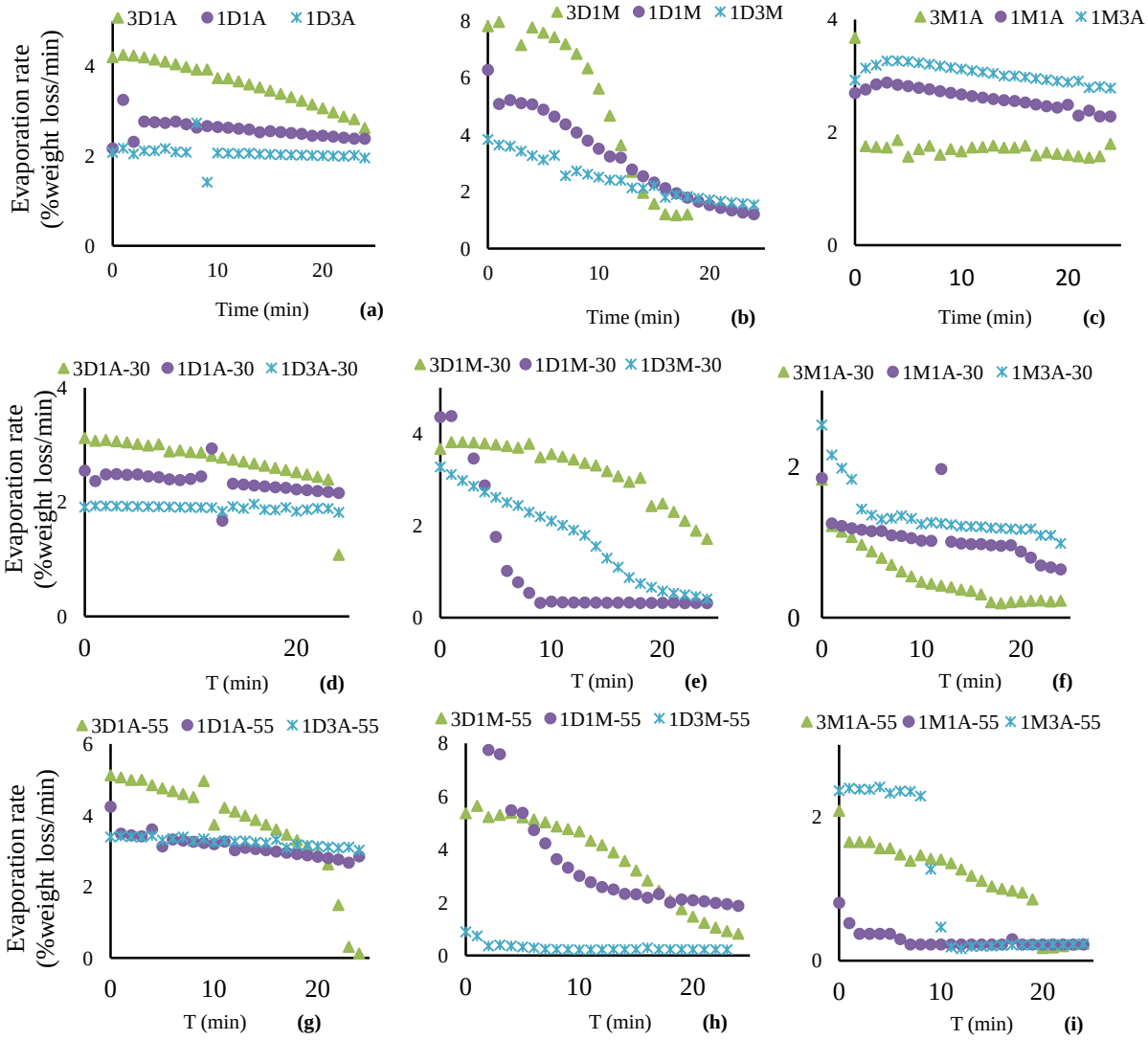

Figure IV.2 Evaporation rate (% weight loss/time) versus time of pure solvent blends (a–c), 30% w/w naproxen in PVP solution (d–f) and 55% w/w naproxen in PVP solutions (g–i) in various solvents. The legends on the plots represent the corresponding solvent composition where A: acetone, D: DCM and M: methanol.

As illustrated in Figure IV.2d–i, the evaporation rate profiles of solvents from different spray-drying feed solutions appeared more complicated. As anticipated, most of the systems showed a deviation from the pure solvent evaporation rates. DCM-acetone solutions containing 30%w/w naproxen in PVP showed almost similar weight loss profiles as that of pure solvent mixtures with overall decrease in evaporation rate. The polynomial evaporation rate loss behaviors are observed in methanol-acetone and DCM-methanol solutions containing same initial drug and polymer concentration. The sudden decrease in evaporation rates of the solutions in one part methanol with one part DCM or 3 parts acetone occurs at ca. 10 min. The solutions containing 55%w/w drug in PVP showed more complicated trends. The trends

of solutions in DCM-acetone were almost consistent with the preceding solutions, but overall evaporation rates increased. The average evaporation rate of solution in 1 methanol: 1 acetone was reduced the most, among the three mixtures, all showing step loss in evaporation rate after different time course. The evaporation rate trends exhibit more discrepancy in the solutions in DCM-methanol, the initial rate of 3 DCM: 1 methanol containing mixtures being higher than even that of pure DCM.

IV.4.3 Moisture and Solvent Content in Solid Dispersions

The thermogravimetric weight loss listed in Table IV.2 and Table IV.3 reveals that the moisture and volatile content in spray-dried dispersions after 1 week of secondary drying in vacuum varied with solvent compositions from which they originated.

Table IV.2 The Glass Transition Temperature (T_g) and the Width (ΔT_g) of Spray-Dried Dispersions with 30% w/w Drug Content Prepared from Different Solvent Systems, Before and After Exposure to Stress (75% RH) for Different Time Period (% Weight Loss Up to 100°C by TGA for Samples Immediately After Vacuum Drying) [A: acetone, D: DCM and M: methanol]

Solvent system	% Wt loss	As prepared				75% RH, 1W				75% RH, 1M					
		T_{g1} (°C)	ΔT_{g1} (°C)	T_{g2} (°C)	ΔT_{g2} (°C)	T_{g1} (°C)	ΔT_{g1} (°C)	T_{g2} (°C)	ΔT_{g2} (°C)	T_{g1} (°C)	ΔT_{g1} (°C)	$T_{g1'}$ (°C)	$\Delta T_{g1'}$ (°C)	T_{g2} (°C)	ΔT_{g2} (°C)
3D:1A	5.03	66.28	23.63	120.22	5.07	93.31	22.10	135.86	8.58	55.41	12.68	92.32	14.05	139.45	25.18
1D:1A	4.92	55.28	9.37	90.73	15.56	85.87	17.76	138.04	6.56	53.05	8.84	93.31	15.00	139.78	19.80
1D:3A	5.31	55.97	12.04	93.83	16.13	88.74	31.35	144.47	14.71	51.30	6.86	92.90	21.01	139.31	7.48
3D:1M	4.24	57.85	15.56	97.10	17.09	109.96	11.15	134.50	9.56	70.15	10.97	93.66	11.73	137.05	9.68
1D:1M	4.47	54.16	8.78	88.65	12.34	92.15	27.37	143.33	17.15	71.88	4.01	94.38	11.20	139.73	14.83
1D:3M	4.79	54.84	11.53	78.19	16.34	93.46	17.91	144.69	7.58	61.83	9.77	92.92	12.61	141.77	19.58
3M:1A	5.03	58.69	19.38	101.42	18.22	94.50	17.85	141.70	16.11	75.54	12.19	95.71	12.59	140.46	19.43
1M:1A	5.49	55.29	12.46	92.15	21.30	95.87	23.55	145.27	15.72	62.21	16.77	92.83	13.36	141.73	18.37
1M:3A	5.68	62.73	20.79	95.04	8.89	92.17	17.23	144.25	10.22	69.65	4.16	93.61	12.30	140.55	21.19
D	5.65	55.38	10.09	90.95	15.31	95.85	19.48	141.68	17.74	72.46	8.92	94.50	5.83	144.01	7.57
M	7.00	57.94	12.66	92.41	20.93	96.87	18.84	142.46	17.18	72.28	6.28	94.97	5.74	139.89	11.90

In general, the weight loss from 30% w/w drug containing composites was higher compared to that from 55% w/w compositions. This is reasonable, as due to less PVP content, the moisture and solvent retention in the dispersions with the latter composition is less. In general, the samples obtained by spray-drying from cosolvents contained relatively less residuals, which also indicate different extent of free and bound volatile and water in these samples. For 30% w/w drug content, the dispersions prepared from DCM-methanol blends showed the least weight loss. This might be due to faster evaporation rate of this system from

the end product (Figure IV.2). No marked differences were observed in the weight loss of the other samples.

Table IV.3 The Glass Transition Temperature (T_g) and the Width (ΔT_g) of Spray-Dried Dispersions with 55% w/w Drug Content Prepared from Different Solvent Systems, Before and After Exposure to Stress (75% RH) for Different Time Period (% Weight Loss Up to 100°C by TGA for Samples Immediately After Vacuum Drying) [A: acetone, D: DCM and M: methanol]

Solvent system	% Weight loss	As prepared				75% RH, 1W				75% RH, 1M			
		T_{g1} (°C)	ΔT_{g1} (°C)	T_{g2} (°C)	ΔT_{g2} (°C)	T_{g1} (°C)	ΔT_{g1} (°C)	T_{g2} (°C)	ΔT_{g2} (°C)	T_{g1} (°C)	ΔT_{g1} (°C)	T_{g2} (°C)	ΔT_{g2} (°C)
3D:1A	2.79	31.44	16.63	99.41	20.02	53.76	18.92	108.31	8.61	100.36	6.32	109.58	4.29
1D:1A	2.15	30.43	16.19	98.32	17.99	54.42	18.02	103.55	7.81	98.86	6.02	108.55	4.93
1D:3A	2.65	33.87	17.89	102.61	12.47	57.57	18.30	107.87	11.79	100.76	6.65	111.50	5.00
3D:1M	2.76	48.87	24.82	104.97	6.29	44.78	13.55	106.98	10.37	99.16	6.03	107.64	4.00
1D:1M	2.82	45.27	15.31	108.55	6.59	44.71	14.48	103.99	9.80	Na			
1D:3M	2.19	44.38	15.40	107.14	9.64	49.58	18.21	103.78	12.03	100.97	6.62	110.52	3.72
3M:1A	2.48	35.18	18.37	106.17	12.30	62.95	21.74	106.43	8.29	102.09	6.48	111.87	4.84
1M:1A	3.34	58.58	18.66	107.47	8.01	59.64	22.66	109.74	8.34	100.49	6.91	111.57	3.46
1M:3A	1.77	45.27	23.42	107.31	8.15	54.67	14.06	105.76	10.62	97.25	5.81	107.86	5.24
D	3.89	37.07	13.67	106.60	6.42	54.42	16.47	103.55	12.26	Na			
M	2.99	44.68	32.22	104.42	7.17	59.83	20.47	107.87	9.26	Na			

Na: not available

IV.4.4 Phase Analysis of Spray-Dried Dispersions

The selection of the two compositions for the current investigation was based upon their positions from equilibrium solid solubility in the miscibility window of the naproxen/PVP system. The 30% w/w naproxen-containing solid dispersions are metastable heterogeneous glass solutions at which an apparent jump in the composition-dependent T_g trend was observed in our earlier exploration[14]. Furthermore, the system heterogeneity increases to include two major amorphous domains and a crystalline phase at 55% drug content. So, it can be anticipated that the effect of solvent composition on the physical structures of solid dispersions with these two compositions should be representative for two different zones of miscibility.

Each set of thermogram includes a reversing heat flow signal and first derivative signal of reversing heat flow as a function of temperature. Accurate and reproducible measurement of heat capacity at T_g is difficult and induces uncertainty when using it for quantitative work. Alternatively, the endothermic depth at T_g in the derivative reversing flow signal provides a clearer reflection of the relative fraction of compositions in a phase-

separated system as well as visualization of the broadness of transitions. There exists a well-established relationship between the full width of the baseline shift at the T_g region measured in DSC (difference between extrapolated onset and endset temperature of transition) with the activation energy of structural relaxation and fragility of a glass[15]. For a glass mixture, the span of glass transition has been merely correlated with the degree of homogeneity of the system[16]. The broader T_g indicates the presence of concentration fluctuations that broaden the distribution of segmental relaxation times and also weaker interaction between the mixing components. Likewise, we consider here the width of a T_g (endset minus onset) as a measure of an individual phase homogeneity and the difference between two T_gs (midpoint values) to denote overall extent of phase separation for a system. The T_g corresponding to the drug-rich region (T_{g1}) with its width (ΔT_{g1}) and that corresponding to the polymer-rich region (T_{g2}) with its width (ΔT_{g2}) before and after exposure to the elevated humidity are given in Table IV.2 and Table IV.3 for spray-dried dispersions with 30% w/w and 55% w/w naproxen content, respectively. For 30% w/w drug-containing samples exposed to 75% RH for 1 month, a third T_g appeared (T_{g1}'). Further, Figure IV.3a and b depict the T_g difference (ΔT_g) between polymer-rich and drug-rich regions (T_{g2}-T_{g1}) for the spray-dried samples obtained from different solvent compositions with 30% w/w and 55% w/w naproxen content, respectively. The overlays of mDSC thermograms of spray-dried dispersions with 30% w/w naproxen content prepared from DCM before and after exposure to the elevated humidity are given in Figure IV.4a, while the same for spray-dried dispersions with 55% w/w naproxen content prepared from 3 DCM: 1 methanol mixture are given in Figure IV.4b.

IV.4.4.1 Solid Dispersions Containing 30%w/w Naproxen in PVP K 25

A broad glass transition event positioned between the T_g of pure naproxen (6°C) and that of pure PVP K 25 (157°C)[14] was observed in the reversing heat flow signal upon an initial analysis of the spray-dried dispersions prepared from different solvent blends. From the corresponding derivative reversing heat flow signals, it was apparent that the broad transition resulted due to the merger of two T_gs representing two different compositions. The solid dispersions prepared from pure methanol and DCM showed identical phase behavior revealing the similarity of their phase compositions. Among samples prepared from DCM-acetone blends, the sample prepared from 3 DCM: 1 acetone has a broader first T_g and a sharper second T_g both at higher temperatures, and also heterogeneity is higher as indicated with higher ΔT_g (Figure IV.3a). The two other compositions showed comparable miscibility. The DCM-methanol systems exhibited the first T_g at similar positions but a progressively

decreasing second T_g and hence decreasing ΔT_g with the increasing proportion of methanol in the blend. The extremely shallow endotherm at the second T_g position of samples derived from 1 DCM: 3 methanol in the derivate signals revealed a decreased proportion of the polymer-rich phase in this sample. In methanol-acetone systems, the phase heterogeneity decreases with an increase in the acetone content in the system. Also, the relative proportion of the two phases is opposite in the samples originating from 1:1 methanol-acetone blends compared to the extreme compositions of solvents (1:3 and 3:1).

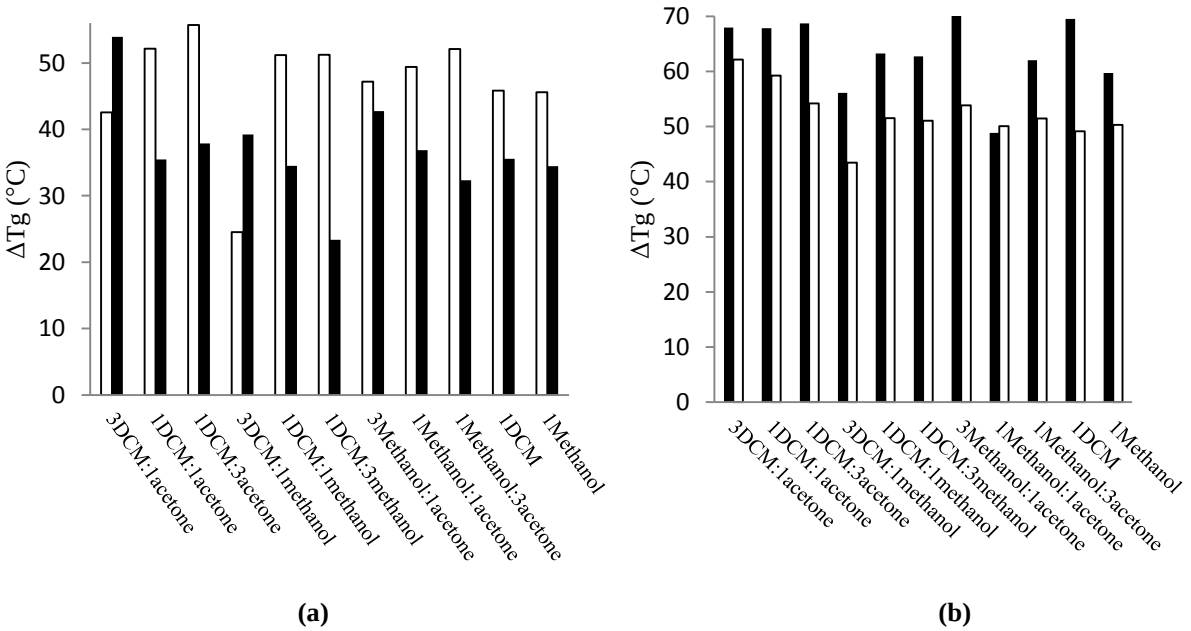

Figure IV.3 The difference between the glass transition temperatures (midpoint values) belonging to the polymer-rich region (T_{g2}) and drug-rich region (T_{g1}) of spray-dried solid dispersions prepared from various solvent blends with 30% w/w drug content (a) and 55% w/w drug content (b), before (black bars) and after (white bars) exposure to 75% RH for 1 week.

The positions of both of the T_gs (observed in untreated samples) shifted towards higher temperature, and clearly separated phases were perceived after the exposure to 75%RH for a week. Even after the exposure to the elevated humidity for a week, the shift in T_gs, individual T_g width and ΔT_g followed quite similar patterns for the samples generated from pure methanol and DCM, which is a further indication of similar solid state structure. However, the effect of exposure to the moisture for 1 week was markedly different among samples derived from the various solvent blends. The spray-dried dispersion from 1:3 and 1:1 solvent composition among that prepared from DCM: acetone system showed the least shift in T_{g1} values, which points to less reorganization of physical structure after the exposure to 75% RH. In samples from 3 DCM: 1 methanol, an abrupt increase in phase miscibility was observed as demonstrated by the discernible increase in both T_gs, decrease in ΔT_g and equivalent depth at both T_gs observed in derivative signal, while the moisture-induced phase

behavior was similar for the samples prepared from one part DCM with one part and three parts methanol. No considerable difference was found on the shift of T_gs among the dispersions prepared from different compositions of methanol: acetone system except slightly increasing trend of heterogeneity with an increased proportion of acetone in feed solution.

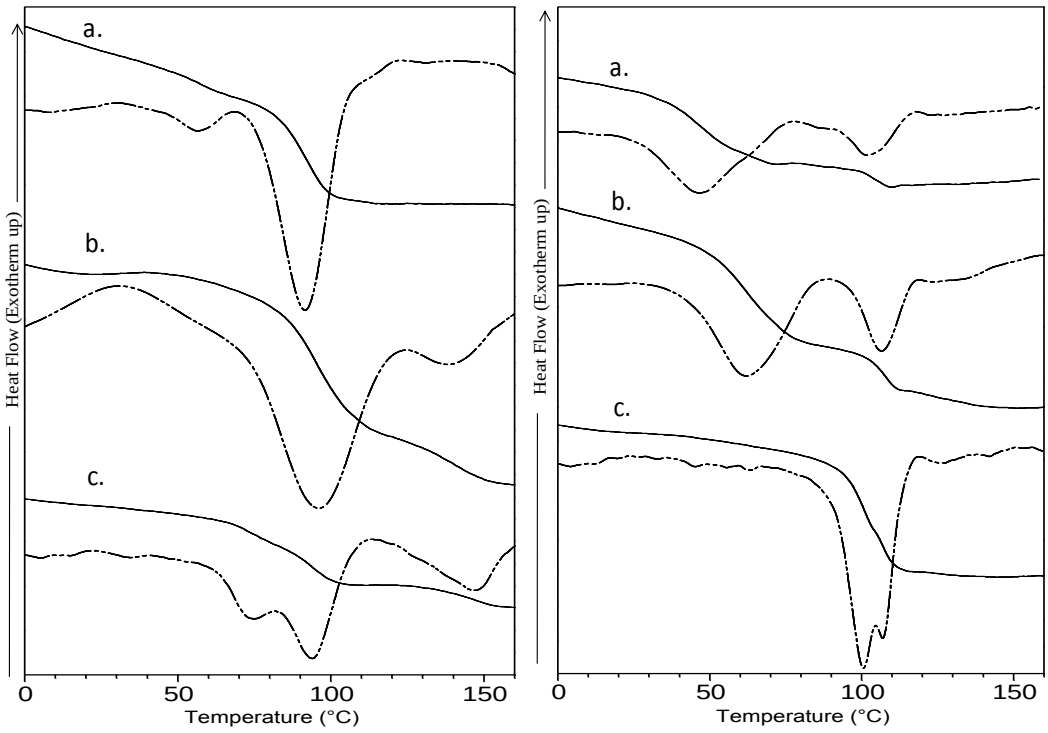

(a) **(b)**

Figure IV.4 (a) Reversing heat flow (continuous line) and derivative reversing heat flow (dashed line) versus temperature for spray-dried solid dispersions containing 30% w/w naproxen in PVP prepared from DCM (as prepared) (a**), after 1 week exposure to 75% RH (**b**) and after 1 month exposure to 75% RH (**c**). (b) Reversing heat flow (continuous line) and derivative reversing heat flow (dashed line) versus temperature for spray-dried solid dispersions containing 55% w/w naproxen in PVP prepared from 3 part DCM: 1 part methanol (as prepared) (**a**), after 1 week exposure to 75% RH (**b**) and after 1 month exposure to 75% RH (**c**).**

Upon exposure of samples to 75% RH further for one month, the first T_g was further split into two adjoining T_gs, while the position of the second T_g remained almost unaltered. This is supported by the crystallization of a fraction of naproxen from saturated composition corresponding to the first T_g discussed in the succeeding sections. The dispersions formulated from DCM: acetone mixture demonstrated increased phase heterogeneity at the split zone of the first T_g. The spray-dried dispersions from 1 DCM: 3 methanol and 1 methanol: 1 acetone exhibited the highest ΔT_g values in the split region, signifying the diverse effect of moisture in the group.

IV.4.4.2 Solid Dispersions Containing 55%w/w Naproxen in PVP K 25

The phase behavior of solid dispersions with 55% drug content is characterized by overlays of thermograms presented in Figure IV.4b. The transitions of the drug-rich and polymer-rich region are distinctly separated and also confirmed by the enthalpy recovery enotherms that appeared at the equivalent positions in non-reversing heat flow signals (data not shown). In all samples, a shallow transition corresponding to polymer-rich region (T_{g2}) positioned between ca. 100–110°C was observed in reversing heat flow signals. The first transitions due to drug-rich compositions within the dispersion matrix appeared at diverse positions depending upon the spray-drying solvent composition. T_{g1} was lower for the solid dispersion prepared from pure DCM as compared to that prepared from pure methanol, indicating high drug loading in the amorphous drug-rich region. Likewise, the solid dispersions prepared from DCM-acetone systems showed the lowest values of T_{g1} (Table IV.3), indicating relatively higher proportion of the amorphous drug loading in the matrix. The broader glass transitions related to the polymer-rich fractions (ΔT_{g2}) were located at lower temperature. This signifies that overall more drug is loaded in this region with higher heterogeneity. Conversely, solid dispersions generated from DCM-methanol systems showed relatively higher T_{g1} and T_{g2}, which is indicative for lower drug loading in both regions compared to the dispersions prepared from the other solvent compositions. The samples derived from methanol-acetone showed behavior between that of DCM-acetone and DCM-methanol systems, i. e. the drug loadings in the drug-rich region were in between that of the two systems. However, the sample from 1:1 methanol: acetone system was exceptional, as was the case for its evaporation rate. It showed lower drug content in the drug-rich region as compared to that prepared from the other compositions of this solvent system.

All the spray-dried dispersions exposed for one week to 75% RH showed a shift of T_g corresponding to the drug-rich part of the mixture (T_{g1}) towards higher temperature, which provided an indication of the crystallization of possibility of diffusion of naproxen from the drug-rich region to the unsaturated polymer-rich fraction was ruled out, as T_{g2} was also slightly shifted towards higher temperature for most of the samples. Rather, the latter observation refers to the crystallization of a small fraction of naproxen from the polymer region also, in the corresponding dispersion. The T_{g1} of the dispersion prepared from methanol was higher than that of the sample prepared from DCM. This indicates an increased conversion to the crystalline state. Among the spray-dried dispersions from solvent blends, the shift of T_{g2} towards the higher temperature was the least in the set of dispersions prepared

from DCM-acetone system pointing to comparatively lesser extent of crystalline conversion. The solid dispersion from 3 DCM: 1 methanol showed the highest shift in T_{g1} towards lower temperature among all solvent blends. A possible explanation is that the slight decrease in T_{g2} of samples from 1 DCM: 3 methanol and 1 DCM: 1 methanol might be due to the solid state diffusion of a small fraction of amorphous naproxen to the unsaturated polymer-rich region other than the major crystalline conversion. The dispersions produced from methanol-acetone also showed similar trend in increase of T_{g2} except that from 1:1 solvent mixture. Surprisingly, the sample from the latter mixture exhibited similar positions of T_g as that of the corresponding untreated sample. In spite of similar ΔT_g value, the relative depth of drug-rich and polymer-rich peaks observed in the derivative signal was reversed, indicating equivalent phase distributions. Prolonging the exposure of solid dispersions with 55% naproxen content to 75% RH for one month resulted in maximum crystallization of naproxen from the supersaturated drug-rich fractions of the dispersions. The T_{g1} was shifted and almost merged with T_{g2}, the latter also being slightly shifted to higher temperature, indicating further crystallization of a trace fraction of drug from the polymer-rich fraction.

IV.4.5 Evaluation of Relative Crystallinity in the Solid Dispersions

The 30% naproxen-containing samples were noncrystalline phase-separated amorphous dispersions up to one week exposure to 75% RH as confirmed by the absence of Bragg peaks in pXRD and birefringence in polarized light. Conversely, small peaks due to trace crystallinity were evident in pXRD of the samples exposed to 75% RH for one month. No striking difference was visible in amorphous halo patterns of the samples prepared from different solvents. Recently, the subtle difference in halo patterns of pharmaceutical solid dispersions has been statistically treated and analyzed using partial least-square (PLS) analysis for the quantification of phase separated fractions[17]. In our case, generation of the halo pattern of pure naproxen was not possible to attempt. We made an effort to obtain the pXRD pattern of molten naproxen that could be assumed to bear the structure nearly matching the amorphous halo. But no characteristic halo was observed as naproxen sublimated rapidly in the course of melting.

The crystallinity analysis was focused on the solid dispersions with 55% w/w drug content. The trace amount of small crystals spread over the polymer matrix was observed through the polarized light microscope of the initial samples and was more prevalent in the samples exposed to the elevated humidity. The micrographs of the samples prepared from methanol-acetone systems are given in Figure IV.5. Bragg peaks appeared on the top of an

amorphous halo in the diffractograms of the respective samples, except for the sample prepared from 3 DCM: 1 acetone. In line with the observation in the microscopic images, the relative increase in the intensity of crystalline peaks and decrease of the amorphous halo were noticed in samples exposed to 75% RH for one week and even more in that exposed for one month. The ratios of net intensity of the highest crystalline peak (2θ°=19.5±0.5°) on top of the amorphous halo to the total intensity for different samples are listed in Table IV.4. Although this is a not the measure of an exact crystallinity, and even the possible error due to preferred orientation cannot be ruled out, it provides an estimation of the crystallinity of a sample and enables comparison between samples. In mDSC analysis with 2°C/min heating rate, no melting event was observed in any sample, not even for the physically mixed drug-polymer composite with equivalent composition. The kinetically controlled solid-state dissolution, instead of melting of the drug, spread the polymer matrix upon slow heating of solid dispersion as reported before[18]. Similar phenomenon is assumed to be prevalent in the present case that is responsible for the undetectable melting event that can be surpassed by other events or spread through a broader temperature range. Nevertheless, the melting events were prominent in the DSC thermograms of the samples recorded at heating rate of 50°C/min. Depending upon the solvent composition used to prepare solid dispersions, the thermograms of the samples before humidity treatment showed the absence or the presence of very small endotherm following glass transition of the polymer-rich region in the samples. Just as expected, the endotherms due to melting increased with an increased exposure of the samples to 75% RH indicating the progressive increase in crystallization. The percentages of crystallinity derived from DSC data, assuming that drug-polymer interaction has ignorable impact on the heat of melting for trace crystalline content[18], are given in Table IV.4. As a whole, the crystallinity analysis is consistent with the positions of T_g and their shifts. The dispersion from pure methanol showed higher crystalline content than that from DCM. Solid dispersions prepared from DCM: methanol blends showed the highest initial crystalline drug content, and that from DCM: acetone systems contained the least. The exposure of samples to 75% RH for one week led to the increase of crystallinity, accordingly. But the extent of crystal growth was solvent-composition-dependent. Regardless of solvents, the exposure of samples at 75% RH for the period of one month led to a comparable extent of crystallization.

Table IV.4 The Relative Percentage Crystallinity Calculated Based on Enthalpy of Melting Observed in DSC and Relative Percentage Crystalline Peak Height Over Amorphous Halo for Spray-Dried Dispersions with 55% w/w Drug Content Prepared from Different Solvent Systems, Before and After Exposure to Stress (75% RH) for Different Time Period [A: acetone, D: DCM and M: methanol]

Solvent Systems	As prepared	75% RH, 1W			75% RH, 1M		
	% Peak height in pXRD	Melting enthalpy (J/g)	% Crystallinity by DSC	% Peak height in pXRD	Melting enthalpy (J/g)	% Crystallinity by DSC	% Peak height in pXRD
3D:1A	0.00	1.75	1.29	26.11	43.48	31.97	89.48
1D:1A	2.76	1.35	0.99	27.71	45.53	33.48	89.55
1D:3A	8.43	4.24	3.12	44.07	44.68	32.85	89.10
3D:1M	28.86	10.19	7.49	61.65	47.60	35.00	90.27
1D:1M	39.59	13.28	9.76	71.94		Na	
1D:3M	38.57	10.70	7.87	66.09	42.07	30.93	85.66
3M:1A	32.90	10.82	7.96	63.30	40.21	29.57	85.92
1M:1A	31.36	11.30	8.31	62.98	48.37	35.57	90.61
1M:3A	16.26	1.76	1.29	43.97	45.96	33.79	90.12
D	11.40	3.23	2.37	45.37		Na	
M	38.92	10.76	7.91	73.45		Na	

Na: Not available

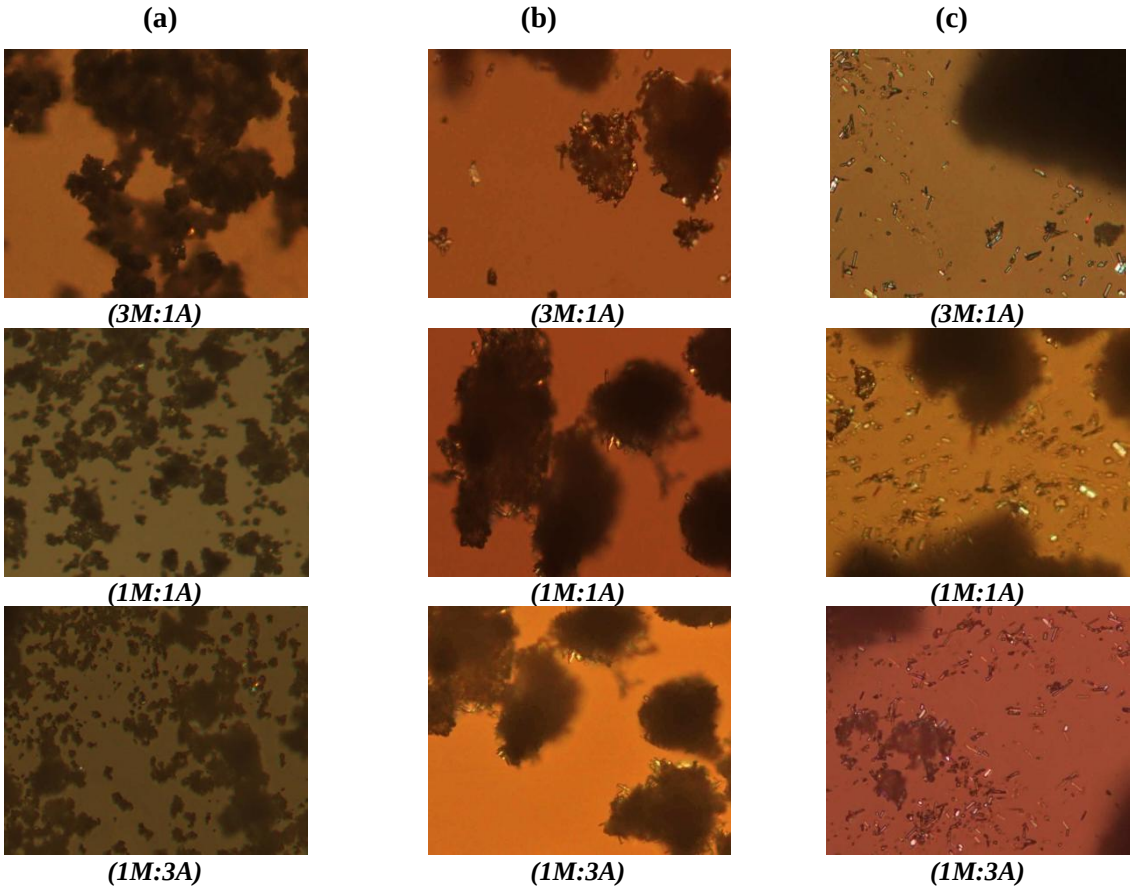

Figure IV.5 Polarized light micrographs of solid dispersions prepared from methanol: acetone systems with 55% naproxen content immediately after preparation (a), after 1 week storage at 75% RH (b) and after 1 month exposure at 75% RH (c). The notations in the parentheses correspond to the respective composition of solvent mixture where M: methanol and A: acetone.

IV.4.6 Spectroscopic Investigation on Drug-Polymer Interaction and Hydrogen Bonding

FTIR is one of the extensively used techniques for the study of solid-state interaction between drug and polymer in solid dispersions. The intermolecular hydrogen bonding in crystalline naproxen and naproxen solution in various organic solvents[19,20] as well as its solid dispersions with PVP[21] has been well documented. The crystal structure of naproxen reveals that it exists as a trimolecular catemer instead of cyclic dimeric congener as ibuprofen[22]. So, the fingerprint region in the FTIR spectrum of naproxen is mainly characterized by vibrations at 1,727 cm^{-1} and 1,686 cm^{-1} attributed to non-hydrogen-bonded –C=O stretching and hydrogen-bonded –C=O stretching of the catemer, respectively. The intensity of the vibrational band at 1,727 cm^{-1} is more dominant because most of the naproxen molecules are not engaged in hydrogen bonding. The bands observed at 3,206 cm^{-1} are assigned to the –OH stretching of –COOH group. The broad vibration band in the IR spectrum of pure PVP, with peak maximum at 1,654 cm^{-1}, is due to –C=O stretching of amide group that is hydrogen bonded with physically adsorbed water. It also shows the corresponding vibration at 3,446 cm^{-1} of hydroxyl groups due to the formation of the hydrogen bonds between PVP and water.

The FTIR spectra of solid dispersions containing 30% w/w naproxen are given in Figure IV.6. The carbonyl stretching region was more sensitive to the consequences of drug-polymer interaction. A new peak at 1,677 cm^{-1} appeared at the expense of the peak due to the hydrogen bonded carbonyl group of pure naproxen. This is an indication of the disruption of intermolecular hydrogen bonding between naproxen molecules. In addition, the peak due to non-hydrogen-bonded carbonyl stretching decreased appreciably. Though the PVP molecules would still be unsaturated in terms of hydrogen bonding, the vibration due to non-hydrogen-bonded carbonyl group of non-interacting PVP might have been masked by the intense peaks of the aromatic skeleton stretching of naproxen appearing around the same position. Generally, hydrogen bonding causes a shift to lower wave numbers of the vibration peaks. But the phenomenon depends on the self-association and interaction between molecules[23]. The percentages of hydrogen-bonded –C=O fraction between drug and polymer (% $F_{naproxen-PVP}$) listed in Table IV.5 for solid dispersions before and after exposure to humidity were calculated from the normalized height ratio of the corresponding peaks using eq IV.2.

$$\%F_{naproxen-PVP} = \frac{(I_{1677}) \times 100}{(I_{1677} + I_{1727})} \quad \text{Equation IV. 2}$$

where I_{1677} and I_{1727} are the normalized absorption intensity at the respective wave number in IR spectra. As total area of the carbonyl stretching region remained approximately constant

for the samples derived from various solvent blends, we assume that the ratio of molar absorption coefficient of free carbonyl group of naproxen to that of inter-associated carbonyl group of PVP (with drug) equals unity in eq IV. 2^{24}. No distinctive difference in % $F_{\text{naproxen-PVP}}$ was apparent within solid dispersions prepared from different solvent compositions stored at identical conditions, despite their dissimilar phase behavior observed from thermal analysis. No evidence of differences in hydrogen bonding was detected by FTIR between the samples. An average 75% intermolecular hydrogen-bonded –C=O was visualized up to one week exposure to 75% RH, which reduced to 55% on average after exposure for one month. Also, the vibration band due to naproxen-PVP intermolecular hydrogen bonding broadened after one month exposure to 75% RH, which is interpreted as an indication of weakening of the interaction. This can be well correlated with the fractional crystallization of the samples by this time.

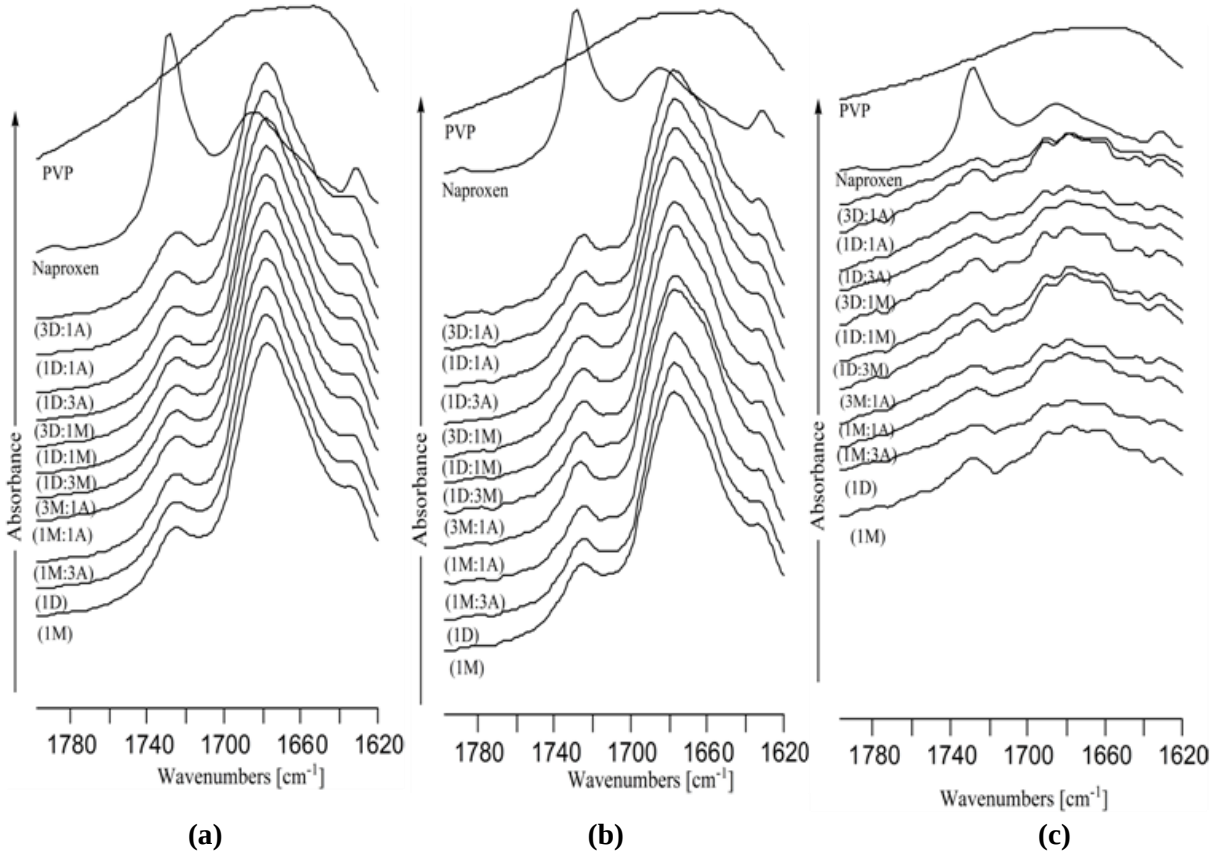

Figure IV.6 FTIR spectra for spray-dried solid dispersions containing 30% w/w naproxen in PVP prepared from various solvent blends after one vacuum drying (a), after 1 week exposure to 75% RH (b) and after 1 month exposure to 75% RH (c). The notations in parentheses correspond to the respective solvent mixture composition used to prepare solid dispersions where A: acetone, D: DCM and M: methanol.

Table IV.5 The Percentage of Hydrogen-Bonded –C=O Fraction Between Naproxen and PVP ($\%F_{naproxen\text{-}PVP}$) Calculated from FTIR Spectra Using eq IV.2 for Spray-Dried Dispersions with 30% w/w Drug Content Prepared from Different Solvent Systems, Before and After Exposure To Stress (75% RH) for Different Time Period [A: acetone, D: DCM and M: methanol]

Solvent System	As prepared	75% RH, 1 W	75% RH, 1 M
	$\%F_{naproxen\text{-}PVP}$	$\%F_{naproxen\text{-}PVP}$	$\%F_{naproxen\text{-}PVP}$
3D:1A	75.7	74.8	55.4
1D:1A	73.9	73.8	55.3
1D:3A	75.1	75.2	55.3
3D:1M	75.5	73.7	56.7
1D:1M	74.2	73.1	57.5
1D:3M	74.2	74.1	57.7
3M:1A	73.7	74.5	57.1
1M:1A	73.2	75.6	56.1
1M:3A	75.0	76.7	57.2
D	75.0	73.7	55.4
M	74.6	76.1	56.5

As shown in Figure IV.7, the spectral patterns of 55% w/ w naproxen containing solid dispersions in the carbonyl stretching region were strikingly different from those with 30% w/w naproxen content. An appearance of an extra vibration band at 1,632 cm^{-1} with the highest intensity was observed in the carbonyl region of the spectra of samples independent of solvent composition. This is assigned to the stronger intermolecular hydrogen bonding between naproxen and PVP molecules in the drug-rich region of solid dispersions. A shift to lower wave numbers of –C=O stretching band of PVP to a similar extent has been reported to be attributable to the –COOH group hydrogen bonded with the –C=O group of the amide functionality of PVP[25]. It is logical to hypothesize that the hydrogen bonding distance would be decreased with stoichiometrically increasing amount of interacting group. However, the peak observed at 1,677 cm^{-1} in spectra of 30% w/w drug containing dispersions is still present in dispersions with 5% w/w drug content, reflecting the presence of the polymer-rich phase with identical hydrogen bonding strength. Thus, in this case, the relative percentage of hydrogen-bonded –C=O belonging to drug-rich and polymer-rich region with respect to the non-hydrogen bonded –C=O stretching of drug was calculated using eq IV.3a–c. Here also, the ratio of molar extinction coefficient of free carbonyl group of drug and intermolecularly hydrogen-bonded –C=O of the amide group of PVP was assumed to be unity. The values are listed in Table IV.6.

$$\%F_{naproxen\ (non\ hydrogen\ bonded)} = \frac{(I_{1727}) \times 100}{(I_{1632} + I_{1677} + I_{1727})} \ldots\ldots\ldots\ldots\ldots\ldots\ldots\ldots \text{Equation IV. 3a}$$

$$\%F_{naproxen-PVP\ (polymer-rich)} = \frac{(I_{1677}) \times 100}{(I_{1632} + I_{1677} + I_{1727})} \ldots\ldots\ldots\ldots\ldots\ldots\ldots\ldots \text{Equation IV. 3b}$$

$$\%F_{naproxen-PVP\ (drug-rich)} = \frac{(I_{1632}) \times 100}{(I_{1632} + I_{1677} + I_{1727})} \ldots\ldots\ldots\ldots\ldots\ldots\ldots\ldots \text{Equation IV. 3c}$$

where the symbols carry their usual meanings.

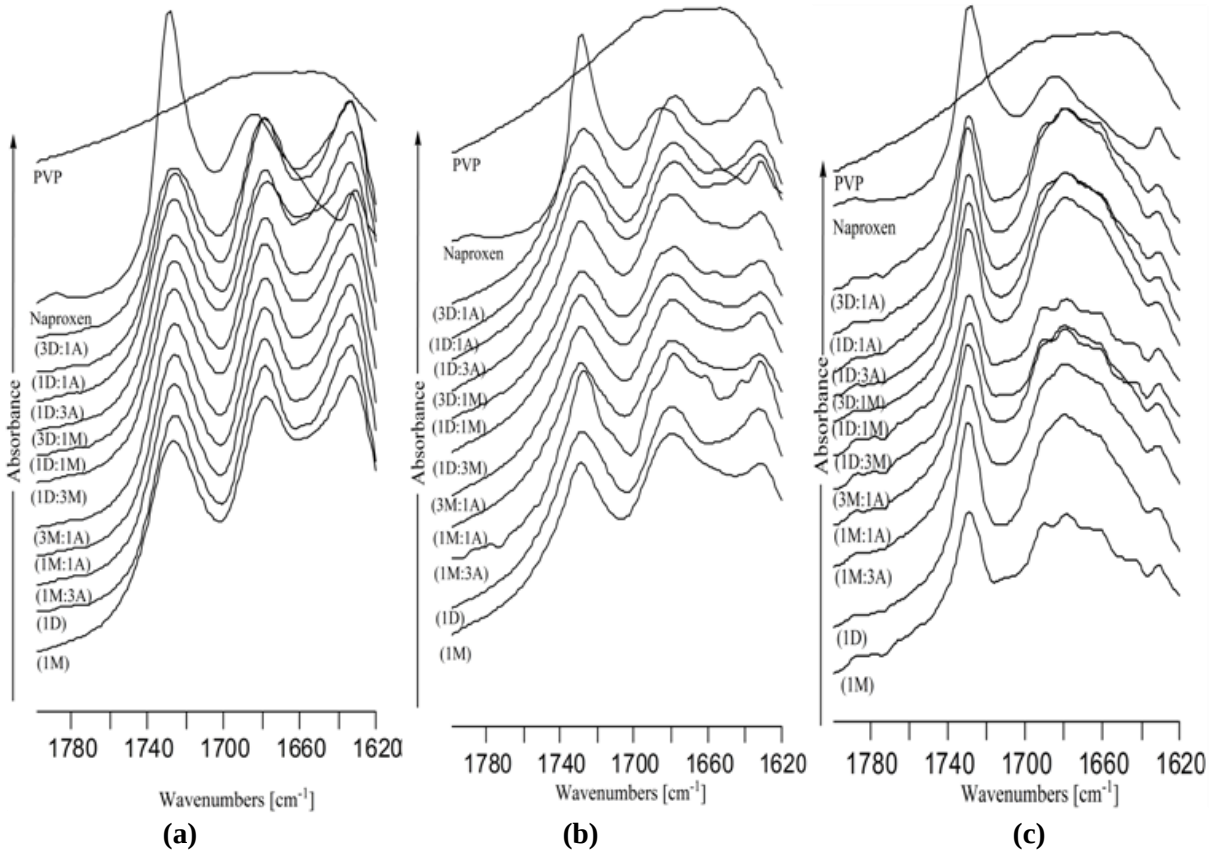

Figure IV.7 FTIR spectra for spray-dried solid dispersions containing 55% w/w naproxen in PVP prepared from various solvent blends after one vacuum drying (a), after 1 week exposure to 75% RH (b) and after 1 month exposure to 75% RH (c). The notations in parentheses correspond to the respective solvent mixture composition used to prepare solid dispersions where A: acetone, D: DCM and M: methanol.

Analysis of as prepared samples showed the highest percentage of –C=O hydrogen-bonded fraction belonging to the drug-rich region in samples derived from all solvent compositions, and no marked differences in the intensity ratio was observed among the samples. After stressing samples for one week at 75% RH, the scenario was different. All samples prepared from DCM-acetone showed a higher percentage of –C=O hydrogen-bonded fraction belonging to the drug-rich region as compared to that of the polymer-rich region, which was reverse in the case of all samples prepared from DCM-methanol system. The increase in peak intensity due to non-hydrogen-bonded –C=O compared to untreated samples also indirectly reflects an increase of crystallinity in the samples. The lesser percentage of

non-hydrogen-bonded –C=O in samples from one part acetone with one part and three parts DCM indicates their higher amorphicity. Samples after storage at 75%RH for one month showed a marked decrease in the percentage of –C=O hydrogen-bonded fraction belonging to the drug-rich region accompanied with an increase in the intensity of the vibration band attributed to non-hydrogen-bonded –C=O. This as a whole indicates an increased crystallinity in the samples comparable to that of the physical mixtures. The observations in FT-IR are in line with the phase behavior obtained from mDSC analysis. The intermolecular hydrogen bonding interaction between naproxen and PVP led to the shift to lower wave numbers of the hydroxyl band of naproxen up to 100 cm^{-1} in solid dispersions containing 55% w/w naproxen.

Table IV.5 The Percentage of Non-Hydrogen-Bonded –C=O Fraction (% $F_{naproxen(Non\text{-}Hydrogen\text{-}Bonded)}$), Hydrogen-Bonded –C=O Fraction Between Naproxen and PVP of Polymer-Rich Region (% $F_{naproxen\text{-}PVP(polymer\text{-}rich)}$) and Drug-Rich Region (% $F_{naproxen\text{-}PVP(drug\text{-}rich)}$) Calculated from FTIR Spectra Using eq IV. 3a–3c for Spray-Dried Dispersions with 55% w/w Drug Content Prepared from Different Solvent Systems, Before and After Exposure to Stress (75% RH) for Different Time Period [A: acetone, D: DCM and M: methanol]

Solvent System	As prepared			75% RH, 1 W			75% RH, 1 M		
	(%)								
	$F_{naproxen}$ (non hydrogen bonded)	$F_{naproxen}$ - PVP(polymer-rich)	$F_{naproxen}$ - PVP(drug-rich)	$F_{naproxen}$ (non hydrogen bonded)	$F_{naproxen}$ - PVP(polymer-rich)	$F_{naproxen}$ - PVP(drug-rich)	$F_{naproxen}$ (non hydrogen bonded)	$F_{naproxen}$ - PVP(polymer-rich	$F_{naproxen}$ - PVP(drug-rich)
3D:1A	27.0	35.0	38.0	30.0	34.5	35.6	36.4	37.4	26.2
1D:1A	27.7	35.1	37.2	31.2	34.2	34.6	36.8	39.5	23.8
1D:3A	28.8	33.0	38.2	31.2	33.9	34.9	36.8	37.4	25.8
3D:1M	27.8	34.9	37.3	31.8	35.3	32.9	35.7	40.3	24.0
1D:1M	28.1	34.2	37.7	32.3	35.2	32.6	35.7	40.3	24.0
1D:3M	28.0	34.5	37.5	32.3	35.2	32.6	34.7	38.4	26.9
3M:1A	28.2	34.4	37.4	31.6	35.0	33.4	38.2	34.8	27.0
1M:1A	28.0	34.5	37.5	31.9	35.0	33.1	35.2	38.5	26.3
1M:3A	28.1	34.3	37.5	32.2	34.5	33.3	35.3	38.5	26.2
D	28.7	34.4	36.8	31.3	34.4	34.3	37.3	38.4	24.3
M	28.9	34.3	36.8	32.1	35.9	32.1	36.2	35.7	28.1

IV.5 Discussion

IV.5.1 Solution Dynamics of Drug and Polymer Systems in Spray-Drying Feed Solutions

A variety of molecular interactions among the components, *viz*., drug, polymer and solvents, can be expected in the spray-drying feed solution. In a binary solvent mixture, there is potential opportunity for interaction as solvents can relatively behave as a proton donor and/or a proton acceptor. The interaction results in the deviation of the experimentally obtained physical attributes of the mixtures from the calculated values for their ideal solution. The extent and type of deviation depend upon the strength of interaction and composition of the solution. The methanol molecules undergo self-association in presence of DCM due to the

lack of mutual intermolecular hydrogen bonding. The methanol and acetone can interact through intermolecular hydrogen bonding as acetone is a weak proton acceptor. Thus, the binary mixtures of methanol with DCM and acetone show strong positive deviation from ideality[26,27]. The formation of electron donor-acceptor complexes and the absence of association in the pure components, and thereby the negative deviation from ideality, have been documented for the DCM-acetone system throughout a broad composition range[28]. The Kamlet–Taft (KT) polarity scale separately measures hydrogen bond donor acidity (α), hydrogen bond acceptor basicity (β), and polarizability of a solvent[29]. The α and β values for pure solvents, functional groups of naproxen and PVP used in this study were taken from literature[30]. The progressive increase in η of DCM-acetone system with the increase of DCM content could be the consequence of electron donor-acceptor complex formation as reported by Nath et al[31].

The solution dynamics of naproxen in various organic solvents has been extensively studied[19,20]. This information is relevant to understand the solution state interaction and also the physical state of the solid form resulting from the corresponding solution. The reported negative deviation from ideality (activity coefficient <1) of the naproxen solutions in methanol, DCM and acetone is evidence of its favorable interaction with these solvents. The solubility of naproxen in acetone is four times higher than that in methanol and DCM, in spite of the strength of hydrogen bonding being the highest in methanol[19]. The higher solubility of naproxen in acetone has been described as strongly dispersive with polar interactions[32]. According to Tomasko et al., naproxen majorly forms dimers in a proton-donating solvent and monomers in a proton-accepting solvent and both dimer/monomer are prevalent in the 1:1 mixtures of these solvent blends[19]. In our context, it should form dimers in DCM, monomers in acetone and both in the amphiprotic methanol, and apparently the effect should be synchronous in the solvent blends. Another interesting finding has been reported on the existence of intramolecular hydrogen bonding of naproxen in DCM, which is absent in methanol[20].

Solvents have vital influence on the conformation of the polymer in its solutions[11]. The solvent properties that provide an idea about the strength of polymer-solvent interaction can also provide the measure of a power of polymer solvation. The solvent polarity has been generally used as a correlating property to the polymer solvation in corresponding solution[30]. The benefit of better solvation should be reflected through the transport of drug molecules to the nearest proximity of PVP chain that provides a chance for stronger interaction. The

viscosity of a polymer in solution is considered as a good indicator of solvent power. The higher viscosity of PVP in DCM and DCM-containing blends could be due to the presence of weak hydrogen-donating power in DCM as well as the higher dispersive interaction with the hydrocarbon backbone of PVP. With methanol, there is propensity for hydrogen bonding with amide carbonyl function of PVP, but self association is also equally possible as the β value for methanol (α=0.98, β=0.66) itself is comparable with that of n-methyl pyrrolidone (NMP) (α=0.00, β=0.77), a small molecular analogue of PVP. There is no possibility of any type of donor-acceptor interaction between acetone (α=0.08, β=0.43) and PVP, as both are proton acceptors. Rather, the PVP chain should get more coiled due to self association through the pyrrolidone moiety. Hence, acetone is a typical anti-solvent for PVP. This can be visualized by the reduced viscosity of PVP in methanol-acetone systems. The lower viscosity of feed solutions in methanol-acetone system than the pure solvent blends is evidence of the synergistic building of new binodal interaction in expense of solvent-solvent interaction. Also, PVP should remain compact in this system. This was also the case in the solutions containing lower proportion of DCM.

The polymeric globular size provides additional information on ternary interaction in solution. This higher globular size of PVP in DCM could be because the more extended the polymeric chains are, the smaller the globular size. This higher globular diameter of PVP for the system containing 55% w/w naproxen compared to that of 30% w/w for naproxen in methanol, DCM and their binary mixtures might be due to the less inter-chain interaction of PVP at the latter composition. However, an increasing trend was observed. Moreover, the trend of increasing globular size for 30% naproxen composition and decreasing trend of globular diameter for 55% naproxen content with increasing proportion of methanol in DCM-methanol mixtures provides evidence of the composition-dependent interaction. The absence of marked difference in composition-dependent difference of the PVP globular size in acetone-containing solutions could be due to the acetone, being an anti-solvent for PVP but the best solvent for naproxen, which might give rise to the selective binodal interactions. However, the observed trend of decreasing globular size of PVP with the decrease in acetone content in DCM-acetone as well as methanol-acetone blends is an indication of the increased PVP solubilization. As the diffusion of small naproxen particles would be the fastest, the system producing smaller PVP globules that create the higher flux should provide the most intimate mixing between drug and polymer.

IV.5.2 Diverse Evaporation Rate Profiles of Feed Solutions in Solvent Blends

The evaporation rate profiles of pure solvent blends are in line with the relative volatility and binary composition. The methanol-acetone mixture is reported to form an azeotropic mixture at 88% w/w acetone content[27]. The relative volatilities of acetone and DCM decrease with increasing amount in methanolic solutions. The nonlinear decrease in the evaporation rate of DCM-methanol system could be due to the combination of the solvents with larger difference in volatility. The marked deviation in evaporation rate of feed solution from the pure solvent should be majorly contributed to the interaction of solvents with PVP in the solution as the vapor pressure of the polymeric solutions shows distinct concentration dependence[33]. The rapidly changing liquid composition in the binary solvents mixture during evaporation alters analogously the polymer concentration with respect to each solvent that leads to the nonlinear drop in the evaporation rate. Also, there exists a competitive hydrogen bonding among naproxen, PVP, and solvents. The abrupt drop in evaporation rates of the feed solutions might be due to the spontaneous vitrification of PVP at this stage. The overall increase in evaporation rates of feed solution with 55% naproxen content as compared to 30% drug content provided evidence of the disruption of the donor-acceptor-type solvent-solvent interaction by introducing drug-polymer solution in this system, which increases the relative volatilities of the solvents.

IV.5.3 Spray-Drying Solvent-Induced Variation in Phase Behaviour

The difference in physical structure of the solid dispersions prepared from diverse solvent compositions should be correlated with the relevant solvent properties. The major part of difference in the solid state architecture depends upon the type and extent of molecular chaos a solvent produces within the growing particles during the drying process. An entire pattern of inter-component interaction in solution state cannot be dictated exactly in solid state as molecular vicinity, type of interaction, especially nature of hydrogen bonding, drastically changes from solution to solid state. The main factors influencing the resulting solid structure are polymer conformation in the solvent and the rate of evaporation of the feed solution. These two factors can contribute favorably or unfavorably regarding the drug-polymer miscibility. For example, the solvent composition which results into better polymer chain conformation with smaller globular size thus producing higher flux could evaporate exceedingly fast so that particle formation occurs far before the drug-polymer interaction is established. Solvent evaporation from drug-polymer solution, which itself is an interplay between intra-droplet diffusion and gas phase mass transfer to drying air, is highly dependent

upon the droplet size, drying gas flow rate, solution feed rate and other parameters. For a constant set of process parameters, the evaporation rate is related with the rate of vitrification of the polymer from the solution and also with the interaction potential between solutes and solvents. An abrupt drop in evaporation rate should indicate the vitrification of the polymer in the growing particle.

Solutions containing 30% w/w drug in PVP in DCM-acetone showed an increase in globular size with the increase in acetone, an anti-solvent for PVP. Also, these systems showed relatively lower initial diffusional flux that avail sufficient span for polymer to stay in the right conformation for the interaction with the drug molecules. This is in line with higher miscibility observed in the solid dispersion prepared from these solvent mixtures. However, the higher heterogeneity in the sample prepared from 3 DCM: 1 acetone might be due to an increased dimerization of naproxen molecules with higher DCM content. The samples obtained by spray-drying drug-polymer solutions in methanol-acetone showed comparable miscibility as samples prepared from DCM-acetone. The same explanation fits for the increase in PVP globular size with the increase in acetone content in the feed solution for this system also. The phase heterogeneity decreases with an increase in acetone content. As methanol is an amphiprotic solvent, both monomer and dimer of naproxen can exist. But, with an increase in acetone, the monomer would again be prevalent, leading to increased possibility of interaction with PVP in the solid state. Drug-polymer solutions in DCM-methanol are different from aforementioned systems. As compared to acetone, both solvents are good solvents for PVP but poorer solvents for naproxen. The increase in globular size with an increase in methanol content could be due to increased self-aggregation of ethyl pyrrolidone groups of PVP. There is a potential chance in cooperativity in intermolecular hydrogen bonding between naproxen-PVP and methanol, as the latter can act as proton donor to the lone pair electron of the hydroxyl group of naproxen. This increases the strength of drug-polymer inter-association as an inter-molecular hydrogen bonding –COOH with the amide group is stronger than with the alcohol functionality[34]. But, at the same time, both solvents induce dimerization of naproxen, which is against drug-polymer miscibility. The dimerization would be less prevalent with an increase of methanol, hence leading to increased miscibility.

The effect of solvent composition is also viewed in terms of miscibility and crystallinity of resulting solid dispersions containing 55% naproxen. The drug-polymer solution in DCM-acetone systems exhibited an increasing trend of globular size with increase

in acetone content. The solid dispersions prepared from this solvent system showed higher drug content in the drug-rich domain, which was mainly amorphous. The same explanation as that given for the 30% w/w solid dispersions prepared from this solvent system holds for this system as well. The size of the PVP globules is smaller in the feed solutions in methanol-acetone blend, hence higher diffusion flux. So, there would be a balance between shrinking of droplets and receding solute transport to the core that generates higher crystallinity but comparable miscibility. The globular size decreases with increased methanol content, which is an opposite effect as compared to the solution containing 30% w/w drug in the same solvent system. This can be explained based upon the concentration dependency of polymer solvation with solvents in the presence of a hydrophobic drug[30]. The slower diffusional flux and faster evaporation rate can induce more crystallization as well as poor miscibility reflected by the phase behavior of the samples prepared by this solvent system.

As a whole, the presence of anti-solvent for the polymer in the spray-drying feed solution increases miscibility and decreases the crystalline content as compared to systems prepared from a binary mixture of good solvents. The latter can potentially generate radial demixing between naproxen and PVP during particle formation during spray-drying. Due to low affinity between the non-solvent and the polymer, the amorphicized drug can be rapidly embedded in the precipitating polymer, resulting in dispersions showing relatively low residual crystallinity. Recently, an increase in the strength of non-covalent interaction of a PVP-containing solid dispersion in the presence of a bad solvent for PVP in the feed solution has been discussed[11]. Addition of acetone in DCM or methanol possibly provides better interaction through solubilization of a maximum amount of drug in the acetone fraction. Conversely, a competing effect on solubility of drug and polymer in DCM-methanol blend would exist. Hence, more chance of self-aggregation of the individual component is possible. The solvent blend with lesser difference between the volatility of solvent and anti-solvent is preferable for better miscibility as the change of solvent composition in the course of drying could be more constant. Additionally, the consequence of solvent drug interaction is also important to decide the type of molecular chaos the solvent blend can impart on the end product. The solvent effect is also dependent upon the drug polymer ratio in the solution. The presence of a higher amount of hydrophobic drug in solution leads to an early and inhomogeneous precipitation of polymer during spray-drying, with decreasing miscibility as witnessed for 55% w/w solid dispersions. The straightforward correlation between dielectric constant and dipole moment of the solvents with the dispersion efficiency in the solid

dispersion is rather complicated as the polarity scale of solvent blends is not the weighted values of an individual solvent. Even so, simply correlating these properties has serious limitations, as they only account for the electrostatic solvent-solute interactions without considering whether the effective alignments of the solvent dipoles for the maximum interaction with the solute molecule are expected. Naproxen is reported to show oscillatory stereo-conversion from S to R in various solvents including methanol and DCM[35,36]. It is likely that the efficiency of molecular mixing is also sterically favored for one enantiomer over the other due to the reduced streric hindrance for interaction for chiral molecules like naproxen. This is the topic of our current investigation.

IV.5.4 Physical Stability of Solid Dispersions Inherited from Spray-Drying Solvents

Adsorption of moisture by solid dispersions initiates favorable water-PVP interaction in expense of non- covalent interactions between naproxen-PVP. The molecular mobility of the energetically trapped glassy phase increases with the weakening of intermolecular hydrogen bonding. The reorganization of the mixtures due to involvement of water is responsible for such behavior. The evolution of the new structure might be due to an increased mobility of the naproxen molecules below the activation energy of crystallization that led to an occurrence of solid state interdiffusion across the concentration gradient existing in the mixture. The diffusion of small molecules through the polymer matrix would indeed be very slow, even for non-interacting molecules. However, this process can be accelerated by water. The conformation change of the pyrrolidone ring from perpendicular with respect to the hydrocarbon backbone in hydrated PVP to the folded assembly in anhydrous PVP and the decrease in cohesion force between PVP chains due to H_2O molecules can enhance diffusivity of the drug between the domains[37].

A distinct polymer-rich region might be generated as moisture-induced surface binodal phase decomposition[38] that results into precipitation of PVP with a relatively low fraction of hydrophobic drug loading at the surface when exposed to the moisture. In this way, other than the strength of drug polymer interaction, the difference created in solid state physical stability among solid dispersions prepared from different solvent blends should be attributed to the surface composition and hydrophilicity, wettability, specific surface area and, of course, equilibrium moisture gain by the samples. In many instances, it is considered that the decrease in T_g in the presence of trace amounts of solvent is due to plasticization of the system by the same. It is not logical to believe the phenomena wherein the solvent present as a liquid in the sample is well above its melting temperature. So, the vitrification of the solvent is hard to

extrapolate at this temperature. Thus, the lower value of T_{g1} in 30% w/w naproxen containing spray-dried samples indicates that the specifically interacting composite is richer in drug content. The shift of T_g to higher temperature is due to reorganization in the presence of moisture with the change in polymer conformation as discussed above. The extent of phase separation would indeed be correlated with the different initial structure induced by solvent composition in the feed solution. The considerable shift of T_{g1} in dispersions prepared from 3 DCM: 1 acetone and 3 methanol: 1 acetone after humidification for one week could be due to weaker stabilizing interaction between drug and PVP due to solution state properties resulting in diffusion of a higher fraction of naproxen towards the polymer-rich surface. Moreover, after one month exposure to 75% RH, further phase separation occurred at the saturated drug-rich region to give three amorphous phases overall along with trace crystallinity observed in pXRD. As T_{g2} was at the same position, the mass balance between phases could be possibly explained through crystallization from the saturated region followed by the reorganization through water upon prolonged contact with moisture.

The increased vitrification of naproxen from naproxen-PVP K 30 physical mixture (1:1 composition) upon humidification has been reported due to the favorable conformation of PVP for interaction induced by water molecules[37]. The phenomenon is opposite in the solid dispersions as humidity led to the manifestation of crystal growth. The dispersions containing 55% w/w of naproxen exhibit a more precise picture. The lower extent of crystallization in samples prepared from DCM-acetone blends is due to the lesser availability of PVP for interaction with water when exposed to humidity. Hence, more drug molecules were rendered amorphous. Further, dimeric orientation of naproxen was so interrupted in the samples prepared by this solvent blends that it was hard to regain even after increase in molecular mobility in presence of water. In samples prepared from DCM-methanol, it is likely that more PVP was available (due to co-operativity between naproxen, PVP and methanol in solution state) for interaction with water so that the drug-rich matrix can easily be weakened to initiate crystallization. Further, dimeric orientation could be more preferential for naproxen to evolve towards crystals from the samples prepared from these solvent systems. The samples prepared from methanol-acetone show intermediate behavior, which is a reflection of the intermediary physical structure too. Moreover, the crystallization induction until one week of exposure to 75% RH might also be related with the initial crystalline content. This means more seeds in the initial sample, faster onset of crystallization and hence more crystallinity at the same time point. But after one month of humidification, it would already reach the secondary crystalline

state that samples lose the memory of initial physical structures due to spray-drying solvents. Overall, this resulted in identical crystallinity in the samples spray-dried from all solvent blends. Their mDSC behavior almost matches that of the physically mixed naproxen and PVP mixture (data not shown) with equivalent composition, which in fact reflects an exhaustive crystallization.

IV.6 Conclusion

The dependency of the phase behavior and physical stability of spray-dried solid dispersions between drug and polymer to the solvent properties was explored from the present investigation. The results showed that all complex supramolecular solution state interactions are not innately transferred to the solid state. The effects of solvent composition are different at different zone of miscibility. For the present system containing a hydrophobic drug, anti-solvent for PVP creates systems with better miscibility, lesser crystallinity and also higher physical stability. Nonetheless, it is more preferential that the anti-solvent is chosen to have favorable impact on solubility of the drug so that drug molecules can reach the nearest vicinity of interacting groups of the polymer in the right conformation. Based on all the results, the favorable solvent systems for manufacturing naproxen and PVP K 25 with improved physical attributes is in the order of DCM-acetone>methanol-acetone>DCM-methanol. In solvent mixtures containing the anti-solvent for PVP, acetone, 25% v/v content is favorable to produce the best mixing effect, amorphicity and physical stability.

IV.7 References

1. Nagapudi, K. and Jona, J. Amorphous Active Pharmaceutical Ingredients in Preclinical Studies: Preparation, Characterization, and Formulation. Curr. Bioact. Compd. 2008, 4, 213-224.
2. Leuner, C. and Dressman, J. Improving Drug Solubility for Oral Delivery Using Solid Dispersions. Eur. J. Pharm. Biopharm. 2000, 50, 47-60.
3. Rumondor, A.C. and Taylor, L.S. Effect of Polymer Hygroscopicity on the Phase Behavior of Amorphous Solid Dispersions in the Presence of Moisture. Mol. Pharmaceutics 2010, 7, 477-490.
4. Alonzo, D.E.; Zhang, G.G.; Zhou, D.; Gao, Y. and Taylor, L.S. Understanding the Behavior of Amorphous Pharmaceutical Systems During Dissolution. Pharm. Res. 2010, 27, 608-618.
5. Khougaz, K. and Clas, S.D. Crystallization Inhibition in Solid Dispersions of MK-0591 and Poly(Vinylpyrrolidone) Polymers. J. Pharm. Sci. 2000, 89, 1325-1334.
6. Janssens, S.; De Zeure, A.; Paudel, A.; Van Humbeeck, J.; Rombaut, P. and Van den Mooter, G. Influence of Preparation Methods on Solid State Supersaturation of Amorphous Solid Dispersions: A Case Study with Itraconazole and Eudragit E100. Pharm. Res. 2010, 27, 775-785.
7. Guns, S.; Dereymaker, A.; Kayaert, P.; Mathot, V.; Martens, J.A. and Van den Mooter, G. Comparison between Hot-Melt Extrusion and Spray-Drying for Manufacturing Solid Dispersions of the Graft Copolymer of Ethylene Glycol and Vinylalcohol. Pharm. Res. 2011, 28, 673-682.
8. Rizi, K.; Green, R.J.; Donaldson, M. and Williams, A.C. Production of pH-Responsive Microparticles by Spray Drying: Investigation of Experimental Parameter Effects on Morphological and Release Properties. J. Pharm. Sci. 2011, 100, 566-579.

9. Bank M, Leffingwell J, Thies C. The Influence of Solvent upon the Compatibility of Polystyrene and Poly (Vinyl Methyl Ether). Macromolecules. 1971, 4, 43–46.
10. Ansari, M.T. and Sunderland, V.B. Solid Dispersions of Dihydroartemisinin in Polyvinylpyrrolidone. Arch. Pharm. Res. 2008, 31, 390-398.
11. Al-Obaidi, H.; Brocchini, S. and Buckton, G. Anomalous Properties of Spray Dried Solid Dispersions. J. Pharm. Sci. 2009, 98, 4724-4737.
12. Janssens, S.; Anné, M.; Rombaut, P. and Van den Mooter, G. Spray Drying from Complex Solvent Systems Broadens the Applicability of Kollicoat IR as a Carrier in the Formulation of Solid Dispersions. Eur. J. Pharm. Sci. 2009, 37, 241-248.
13. Tsapis, N.; Bennett, D.; Jackson, B.; Weitz, D.A. and Edwards, D.A. Trojan Particles: Large Porous Carriers of Nanoparticles for Drug Delivery. Proc. Natl. Acad. Sci. U. S. A. 2002, 99, 12001-12005.
14. Paudel, A.; Van Humbeeck, J. and Van den Mooter, G. Theoretical and Experimental Investigation on the Solid Solubility and Miscibility of Naproxen in Poly(Vinylpyrrolidone). Mol. Pharmaceutics 2010, 7, 1133-1148.
15. Moynihan, C.T. Correlation between the Width of the Glass Transition Region and the Temperature Dependence of the Viscosity of High Tg Glasses. J. Am. Ceram. Soc. 1993, 76, 1081-1087.
16. Song, M.; Hammiche, A.; Pollock, H.M.; Hourston, D.J. and Reading, M. Modulated Differential Scanning Calorimetry: 4. Miscibility and Glass Transition Behaviour in Poly (Methyl Methacrylate) and Poly (Epichlorohydrin) Blends. Polymer 1996, 37, 5661-5665.
17. Rumondor, A.C. and Taylor, L.S. Application of Partial Least-Squares (PLS) Modeling in Quantifying Drug Crystallinity in Amorphous Solid Dispersions. Int. J. Pharm. 2010, 398, 155-160.
18. Tao, J.; Sun, Y.; Zhang, G.G. and Yu, L. Solubility of Small-Molecule Crystals in Polymers: D-Mannitol in PVP, Indomethacin in PVP/VA, and Nifedipine in PVP/VA. Pharm. Res. 2009, 26, 855-864.
19. Tomasko, D.L. and Timko, M.T. Tailoring of Specific Interactions to Modify the Morphology of Naproxen. J. Cryst. Growth 1999, 205, 233-243.
20. Velazquez, M.M.; Valero, M.; Rodriguez, L.J.; Costa, S. and Santos, M.A. Hydrogen Bonding in a Non-Steroidal Anti-Inflammatory Drug-Naproxen. J. Photochem. Photobio. B. 1995, 29, 23-31.
21. Nair, R.; Nyamweya, N.; Gönen, S.; Martinez-Miranda, L.J. and Hoag, S.W. Influence of Various Drugs on the Glass Transition Temperature of Poly (Vinylpyrrolidone): A Thermodynamic and Spectroscopic Investigation. Int. J. Pharm. 2001, 225, 83-96.
22. Bogdanova, S.; Pajeva, I.; Nikolova, P.; Tsakovska, I. and Müller, B. Interactions of Poly (Vinylpyrrolidone) with Ibuprofen and Naproxen: Experimental and Modeling Studies. Pharm. Res. 2005, 22, 806-815.
23. Painter PC, Park Y, Coleman MM. Thermodynamics of Hydrogen Bonding in Polymer Blends. 1. The Application of Association Models. Macromolecules. 1989, 22, 570–579.
24. Meaurio, E.; Velada, J.L.; Cesteros, L.C. and Katime, I. Blends and Complexes of Poly (Monomethyl Itaconate) with Polybases Poly (N, N-Dimethylacrylamide) and Poly (Ethyloxazoline). Association and Thermal Behavior. Macromolecules 1996, 29, 4598-4604.
25. Senatore, D.; Berix, M.J.A.; Laven, J.; van Benthem, R.A.T.M.; de With, G.; Mezari, B. and Magusin, P.C.M.M. Miscibility and Specific Interactions in Blends of Poly (N-Vinyl-2-Pyrrolidone) and Acid Functional Polyester Resins. Macromolecules 2008, 41, 8020-8029.
26. Maria C. Martin, M.J.C., and F. Mato. Vapor-Liquid Equilibrium Data at 25°C for Six Binary Systems Containing Methyl Acetate or Methanol, with Dichloromethane, Chloroform, or 1,2-Trans-Dichloroethylene. J. Solution. Chem. 1991, 20, 87-95.
27. Campbell, A.N. and Anand, S.C. Phase Equilibria in the Systems Acetone–Methanol, Acetone–Cyclohexane, Methanol–Cyclohexane, and Acetone–Methanol–Cyclohexane. Can. J. Chem. 1972, 50, 479-489.
28. Nath, J. and Prakash Dixit, A. Total Vapour Pressures for Binary Liquid Mixtures of Acetone with Tetrachloroethylene, Trichloroethylene, Methylene Chloride, 1, 2-Dichloroethane and Cyclohexane at 273.15 K. Fluid Phase. Equilibr. 1990, 60, 205-212.

29. Kamlet, M.J.; Abboud, J.L.M.; Abraham, M.H. and Taft, R.W. Linear Solvation Energy Relationships. 23. A Comprehensive Collection of the Solvatochromic Parameters,*, and, and Some Methods for Simplifying the Generalized Solvatochromic Equation. J. Org. Chem. 1983, 48, 2877–2887.
30. Malavolta, L.; Oliveira, E.; Cilli, E.M. and Nakaie, C.R. Solvation of Polymers as Model for Solvent Effect Investigation: Proposition of a Novel Polarity Scale* Tetrahedron 2002, 58, 4383-4394.
31. Nath, J. and Dixit, A.P. Binary Systems of Acetone with Tetrachloroethylene, Trichloroethylene, Methylene Chloride, 1, 2-Dichloroethane, and Cyclohexane. 2. Viscosities at 303.15 K. J. Chem. Eng. Data 1984, 29, 317-319.
32. Tsivintzelis, I.; Economou, I.G. and Kontogeorgis, G.M. Modeling the Phase Behavior in Mixtures of Pharmaceuticals with Liquid or Supercritical Solvents. J. Phys. Chem. B 2009, 113, 6446-6458.
33. Maria Bercea, J.E., and Bernhard A. Wolf. Vapor Pressure of Polymer Solutions and the Modeling of Their Composition Dependence. Ind. Eng. Chem. Res. 2009, 48, 4603-4606.
34. Kireeva, P.E.; Shandryuk, G.A.; Kostina, J.V.; Bondarenko, G.N.; Singh, P.; Cleary, G.W. and Feldstein, M.M. Competitive Hydrogen Bonding Mechanisms Underlying Phase Behavior of Triple Poly (N Vinyl Pyrrolidone)–Poly (Ethylene Glycol)–Poly (Methacrylic Acid Co Ethylacrylate) Blends. J. Appl. Polym. Sci. 2007, 105, 3017-3036.
35. Sajewicz M; Matlengiewicz M; Leda M; Gontarska M; Kronenbach D; Kowalska T and IR, E. Spontaneous Oscillatory *in Vitro* Chiral Conversion of Simple Carboxylic Acids and Its Possible Mechanism. J. Phys. Org. Chem. 2010, 23, 1066-1073.
36. Sajewicz, M.; Pietka, R.; Pienak, A. and Kowalska, T. Application of Thin-Layer Chromatography to Investigate Oscillatory Instability of the Selected Profen Enantiomers in Dichloromethane. J. Chromatogr. Sci. 2005, 43, 542-548.
37. Malaj, L.; Censi, R.; Mozzicafreddo, M.; Pellegrino, L.; Angeletti, M.; Gobetto, R. and Di Martino, P. Influence of Relative Humidity on the Interaction between Different Aryl Propionic Acid Derivatives and Poly (Vinylpyrrolydone) K30. Evaluation of the Effect on Drug Bioavailability. Int. J. Pharm. 2010, 398 61-72.
38. Van de Witte, P.; Dijkstra, P.J.; Van den Berg, J.W.A. and Feijen, J. Phase Separation Processes in Polymer Solutions in Relation to Membrane Formation. J. Membr. Sci. 1996, 117, 1-31.

Chapter V: Relating Hydrogen-Bonding Interactions with the Phase Behavior of Naproxen/PVP K 25 Solid Dispersions: Evaluation of Solution-Cast and Quench-Cooled Films

The results described in this chapter are published in the following article:

Paudel, A.; Nies, E., and Van den Mooter, G. (2012). Relating Hydrogen-Bonding Interactions with the Phase Behavior of Naproxen/PVP K 25 Solid Dispersions: Evaluation of Solution-Cast and Quench-Cooled Films. *Molecular Pharmaceutics*, 9 (11), 3301-3317.

V.1 Abstract

In this work, we investigated the relationship between various intermolecular hydrogen-bonding (H-bonding) interactions and the miscibility of the model hydrophobic drug naproxen with the hydrophilic polymer polyvinylpyrrolidone (PVP) across an entire composition range of solid dispersions prepared by quasi-equilibrium film casting and nonequilibrium melt quench cooling. The binary phase behavior in solid dispersions exhibited substantial processing method dependence. The solid state solubility of crystalline naproxen in PVP to form amorphous solid dispersions was 35% and 70% w/w naproxen in solution-cast films and quench-cooled films, respectively. However, the presence of a single mixed phase glass transition indicated the amorphous miscibility to be 20% w/w naproxen for the films, beyond which amorphous−amorphous and/or crystalline phase separations were apparent. This was further supported by the solution state interactions data such as PVP globular size distribution and solution infrared spectral profiles. The borderline melt composition showed cooling rate dependence of amorphization. The glass transition and melting point depression profiles of the system were treated with the analytical expressions based on Flory−Huggins mixing theory to interpolate the equilibrium solid solubility. FTIR analysis and subsequent spectral deconvolution revealed composition and miscibility dependent variations in the strength of drug−polymer intermolecular H-bonding. Two types of H-bonded populations were evidenced from 25% w/w and 35% w/w naproxen in solution-cast films and quench-cooled films, respectively, with the higher fraction of strongly H-bonded population in the drug rich domains of phase separated amorphous film compositions and highly drug loaded amorphous quench-cooled dispersions.

V.2 Introduction

There have been major strides in the last three decades toward formulating amorphous solid dispersion (ASD) of poorly water-soluble active pharmaceutical ingredients (APIs) with a hydrophilic polymeric carrier to improve the oral bioavailability, considering the higher solubility of the amorphous state and the crystallization inhibition power of such excipients[1,2]. Despite the potential solubility advantage, ASD suffer from poor physical and chemical stability. The common hurdle posed in developing ASD formulation is the propensity of API in amorphous form to undergo phase separation and/or crystallization during the intended lifetime of the product or administration and hence resulting in loss of the solubility advantage[3,4]. Molecular level understanding of the interaction between drug and polymeric carrier and their phase behavior in solid dispersion have now been realized as the critical

aspects in the development of physicochemically stable solid dispersion formulations[5]. The miscibility and physical stability of ASD result from the interplay between various thermodynamic factors, viz., extent and types of drug−polymer interaction, intrinsic solid solubility etc. and kinetic factors such as solidification rate involved in the formulation process[6]. The kinetic miscibility for a drug−polymer in ASD is generally found to be far higher compared to the equilibrium solid solubility of the system[7]. However, the failure to consider the contributions from specific and directional molecular interactions such as hydrogen-bonding (H-bonding) by frequently used thermodynamic models for solid solubility calculation often renders them deficient in predicting the real situations[8]. Conventionally, the deviations of the experimental glass transition temperature (T_g)−composition profiles from those predicted by expressions for mixing such as the Gordon−Taylor (GT) equation are considered as the confirmation of drug−polymer interaction[9]. Even so, this does not provide any specific information on the nature of noncovalent interactions, especially drug−polymer intermolecular H-bonding, which is considered the most important molecular interaction for improved miscibility and stabilization. In such cases, detailed spectroscopic investigation can reveal different types of composition dependent interactions between drug and polymer in solid dispersion[10].

The physical structure and stability of ASDs prepared by different methods can markedly differ due to the extent of energetic input during processing[7,11,12]. The common industrial screening methods for the development of ASD are high throughput film casting of a solution containing drug and polymer at different ratios or quench cooling the binary mixtures heated up to the melting temperature of the drug[13,14]. The miscibility in solution-cast films depends upon the mutual molecular interaction among drug, polymer and solvent while that in quench-cooled dispersion relies on applied heating/cooling rates and melt viscosity[15,16]. Nevertheless, the types and extent of stabilizing drug−polymer intermolecular interactions in the dispersions prepared with different (cooling/evaporation) rate processes, say by quasi-equilibrium to nonequilibrium conditions, are not well characterized.

Through this investigation, we aim to elucidate various types of saturable intermolecular interactions involved within the diverse zones of miscibility of naproxen, a poorly water-soluble NSAID, in polyvinylpyrrolidone (PVP), a hydrophilic polymeric carrier, and to correlate with their phase behavior. We prepared several solid dispersions of naproxen and PVP having different compositions by casting a methanolic solution and by slowly heating the same dispersions followed by quench cooling. Subsequently, *in situ*

characterizations using thermal, spectroscopic and diffractometric analysis and the information extracted from the thermal data treatments using thermodynamic models based on the Flory−Huggins (FH) theory, curve fitting and spectral deconvolutions provided molecular level information on the physical structures of solid dispersions with different compositions prepared by two different methods.

Based on the literature information on the relationship between the molecular interactions in solution state and the polymorphic diversity observed in the crystal forms[17], the potential effects of such interactions in multicomponent solutions on the physical structure of solid dispersions prepared by solvent processes can be projected. Therefore, the solid state structures of solution-cast films were additionally correlated with the composition dependent solution state interactions dictated by the globular size distributions of PVP in the solution states and infrared spectra of respective solutions.

V.3 Materials and Methods

V.3.1 Materials

(S)-Naproxen was procured from CERTA Ltd. (Brain-l'Alled, Belgium). PVP with average molar mass (M_w) of 2.5 × 104 g mol^{-1} (Kollidon K 25) was kindly donated by BASF (Ludwigshafen, Germany). HPLC grade methanol (MeOH) used in the solution-casting experiment was purchased from HperSolv Chromanorm, VWR, Belgium.

V.3.2 Methods

V.3.2.1 Preparation of Solid Dispersions by Solution Casting and Quench Cooling

Films of naproxen and PVP were prepared by solution casting (SC) for the whole composition range from 0 to 90% w/w naproxen. Naproxen and PVP were dissolved in MeOH at different drug to polymer ratios (the % w/w drug to polymer ratio mentioned henceforth is expressed as % naproxen). The solids concentration was 20% w/v for all the compositions. The solutions were filtered through syringe filters of 0.45 μm pore diameter (Henke Sass Wolf, Tuttlingen, Germany). For each composition a fixed volume of the solution was pipetted into multiple aluminum DSC pans (20 μL) and spread onto polyimide films (Kapton) (100 μL) to control the film thickness. The solvent was allowed to evaporate slowly at room temperature (quasi-equilibrium condition) by covering with a glass funnel with a diameter of 15cm inverted over the film casting assembly. The funnel was externally covered with aluminum foil to protect the solution from photochemical degradation. The

intact films formed in the pan and on the polyimide film were dried in a vacuum oven at 40 °C for several days until the samples attained a constant mass.

The quench-cooled (QC) samples were prepared by heating the SC films at 2 °C/min up to 160 °C and cooling back to −20 °C at 10 °C/min. The SC films prepared in the pans were processed in DSC as described in the Thermal Analysis section, and those prepared on Kapton films were processed on Linkam Hotstage THMS 600 (Linkam, Surrey, U.K.) for powder X-ray diffractometric analysis.

V.3.2.2 Polymeric Globular Size Measurement

The hydrodynamic diameters of PVP globules in casting solutions (in MeOH) with drug to polymer ratios up to 50% naproxen were determined by dynamic light scattering (DLS) using a BIC 90 plus model instrument (Brookhaven Instruments Co., USA) equipped with a 35 mW He−Ne laser as light source ($\lambda = 632.8$ nm) and detector configured to 90°. The solutions prepared at room temperature (ca. 25 °C) were filtered and measured for globular size distribution at 25 °C. The total solute content was always 20% w/v. The intensity-weighted mean diameter obtained from the DLS experiment was interpreted as the globular size, and in the case of bimodal distributions the percentage of light scattering intensity is expressed as the percentage volume for each diametric population.

V.3.2.3 Thermal Analysis

Temperature modulated differential scanning calorimetry (mDSC) experiments were performed using a Q2000 DSC (TA Instruments, Leatherhead, U.K.) equipped with the refrigerated cooling system (RCS90) under dry nitrogen purge at a rate of 50 mL/min. The instrument was calibrated for enthalpy and temperature measurement within the required temperature range using pure indium (heat of fusion 28.7 J/g, mp 156.6 °C) while heat capacity was calibrated using a sapphire disk. The SC film in the DSC pan that weighed 4 ± 0.5 mg was crimped with an aluminum lid having a vent hole and heated in the DSC from −20 °C to 160 °C at a constant heating rate of 2 °C/min and an amplitude/period of modulation of 1 °C/40 s. The QC films were prepared by in situ cooling the pans inside the DSC cell from 160 °C to −20 °C at 10 °C/min. Additionally, cooling at different lower rates down to 0.2 °C/min were tested for some compositions. The samples were reweighed and analyzed using the same heating programs as that of the SC films. The compositions exhibiting a melting peak in the respective thermograms were also analyzed at different heating rates (1.5, 1, and 0.5 °C/min) for the melting point depression assessment. Two

independent measurements were performed for all the samples. Analysis was carried out and monitored by TA Instrument explorer software (version 6.10). Data analysis was performed using Universal Analysis (version 4.7A) throughout the study.

V.3.2.4 Powder X-ray Diffractometry (pXRD)

For pXRD analysis, the films prepared on the Kapton foils were covered by another Kapton foil and clamped in between the Teflon rings of the sample holders. The samples were analyzed on an automated X'pert PRO diffractometer (PANalytical, Almelo, The Netherlands) with a Cu tube (Cu Kα, λ = 0.1542 nm) and the generator set at 45 kV and 40 mA in a continuous scan mode varying the diffraction angle 2θ from 4° to 40° with 0.0021° step size and 19.685 s counting time. The data was collected using X'Pert data collector and analyzed using the X'pert Data Viewer (PANalytical, Almelo, The Netherlands). After analysis, the SC films sandwiched between two Kapton foils were placed inside a hotstage to generate QC films by the heating program mentioned in section 2.2.1. The QC samples were also analyzed with the same instrument and method as for the SC films.

V.3.2.5 Attenuated Total Reflectance Fourier Transform Infrared (ATR-FTIR) Spectroscopy

An ATR-FTIR spectroscopic analysis of the drug−polymer solutions in MeOH, the resulting SC films and their QC dispersions was performed on a ThermoNicolet Avatar 370 FTIR spectrometer equipped with a DTGS detector and a horizontal Smart Orbit single-reflection ZnSe ATR assembly. A background spectrum was collected under the same experimental conditions without the sample and was subtracted from each subsequent sample spectrum. For each composition, a 10 μL solution in MeOH was pipetted over the ATR crystal and immediately covered with an inverted DSC pan to prevent the evaporation, and the FTIR spectrum was recorded. For solid state analysis, the DSC aluminum pan containing an intact film or melt quench sample was inverted over the ATR crystal and a holder tower was gently dialed down over the inverted bottom of the sample pan until the sample surface was in firm contact with the crystal. FTIR spectra of all samples were recorded from 4000 to 650 cm^{-1} with 32 scans at a spectral resolution of 4 cm^{-1} using Omnic program with Smart Performer ATR interface.

V.3.2.6 Spectral Deconvolutions

Since FTIR spectra of solid dispersions exhibited composition dependent increase or decrease of various superimposing bands, we applied curve fitting to the carbonyl stretching

regions using OriginPro software version 8 (OriginLab Corp., MA, USA) to deconvolute the contributing peaks. The iterative least-squares method using hybrid Gaussian−Lorentzian (pseudo-Voigt) function was employed for the curve fitting on the experimental spectra. The information extracted from the deconvolution, viz., central wavenumber, the Full Width at Half-Maximum (FWHM) and integrated area of the individual peak, was used for the semiquantitative interpretation of the composition-dependent H-bonding interactions. The fitting procedures are provided in detail as Appendix.

V.4 Results

V.4.1 Phase Behavior of Drug−Polymer in the Cast Films

V.4.1.1 Solution State Interactions

The cast films are obtained by the evaporation of the solvent from the cast solution. This makes it important to understand the molecular interactions among drug, polymer and casting solvent in the solution state for the justification of phase behavior in the resulting solid state. The hydrodynamic radius of polymer in the solution acts as a very specific representation to discern the extent of coil to globule transformation and solvation of polymer chain as well as the effect on the interaction of polymer with the other species present in the solution[15,18]. As shown in Figure V.1, the hydrodynamic diameter distributions of PVP globules in MeOH remarkably exhibited composition dependence in the presence of the increasing fraction of naproxen in the solution. The globular size of PVP in the presence of naproxen in the solution remained monodispersed having a similar size range, though slightly increased up to 15% naproxen. A clear bimodal size distribution of the PVP globules was observed from 20% naproxen content. The volume fraction of the populations with two different globular sizes also showed composition dependence from this composition. At the 20% naproxen composition, ca. 43% of total volume of PVP globules showed a decrease in hydrodynamic diameter compared to that in pure PVP solution while the rest remained as the size in pure PVP solution. With the further increase of naproxen content in the solutions, the population of PVP globules with smaller size exceeded 65% of total volume and the hydrodynamic diameter of this population showed gradually increasing trend with the increase in naproxen fraction. The size of larger globules remained identical (13−14 nm) up to 40% naproxen while a sharp increase in the same could be observed beyond this composition.

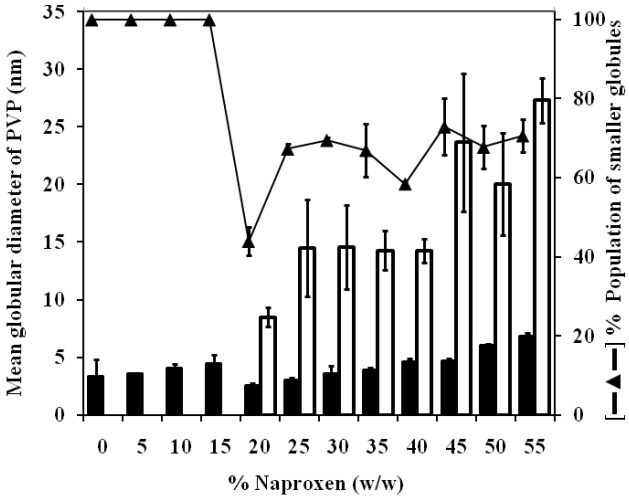

Figure V.1 Plot of hydrodynamic globular diameter distribution (bars) and % population of the globules with smaller diameter (▲) of PVP as a function of % naproxen (w/w) content in methanolic solution (20%w/v) of naproxen and PVP. Vertical error bars indicate ± standard deviation (*n = 3*).

The IR spectra of drug−polymer solutions in MeOH presented in Figure V.2 reveal the mutual binary or ternary interaction among the same or different components of solution. Figure V.2a demonstrates the crystallization driven alterations of the various intermolecular interactions in naproxen as a function of time. The interval between two subsequent measurements was the real difference between the scans, 30 s and the scan time for each time point, 15 s, therefore 45 s in total. Initially, there are prominent peaks corresponding respectively to the free C=O stretching at 1728 cm^{-1}, dimerized C=O stretching at 1710 cm^{-1} and at 1631 cm^{-1} and 1608 cm^{-1} attributable to aromatic skeleton stretching.19 With the evaporation of solvent, the relative intensity of the monomer peak increased as compared to that of dimer peak with the appearance of a new peak at 1686 cm^{-1}. Further, there was the shift in the position of dimeric C=O band (to 1704cm^{-1}) and an aromatic stretching band (to 1608 cm^{-1}) with the abrupt decrease in the relative peak intensities. The peak at 1704 cm^{-1} gradually shifted toward lower wavenumbers and finally vanished upon crystallization with the single crystalline dimeric C=O stretching peak remaining at 1681 cm^{-1}.[20] As illustrated in Figure V.2b,c, there was a composition dependent trend in the relative peak intensities of different vibration bands in naproxen−PVP solution. The relative peak intensities of dimer and monomer C=O stretching of naproxen normalized to that of PVP at 1662 cm^{-1} concurrently increased from 40% naproxen. Although the relative intensity of the dimeric C=O vibration band dominated over that of the monomer C=O throughout the compositions tested, the difference between dimer and monomer intensity of C=O stretching bands of naproxen gradually increased between 30 and 55% naproxen content followed by the rapid

rise further. These results indicate the drug/polymer composition dependent variations in the solution state interactions.

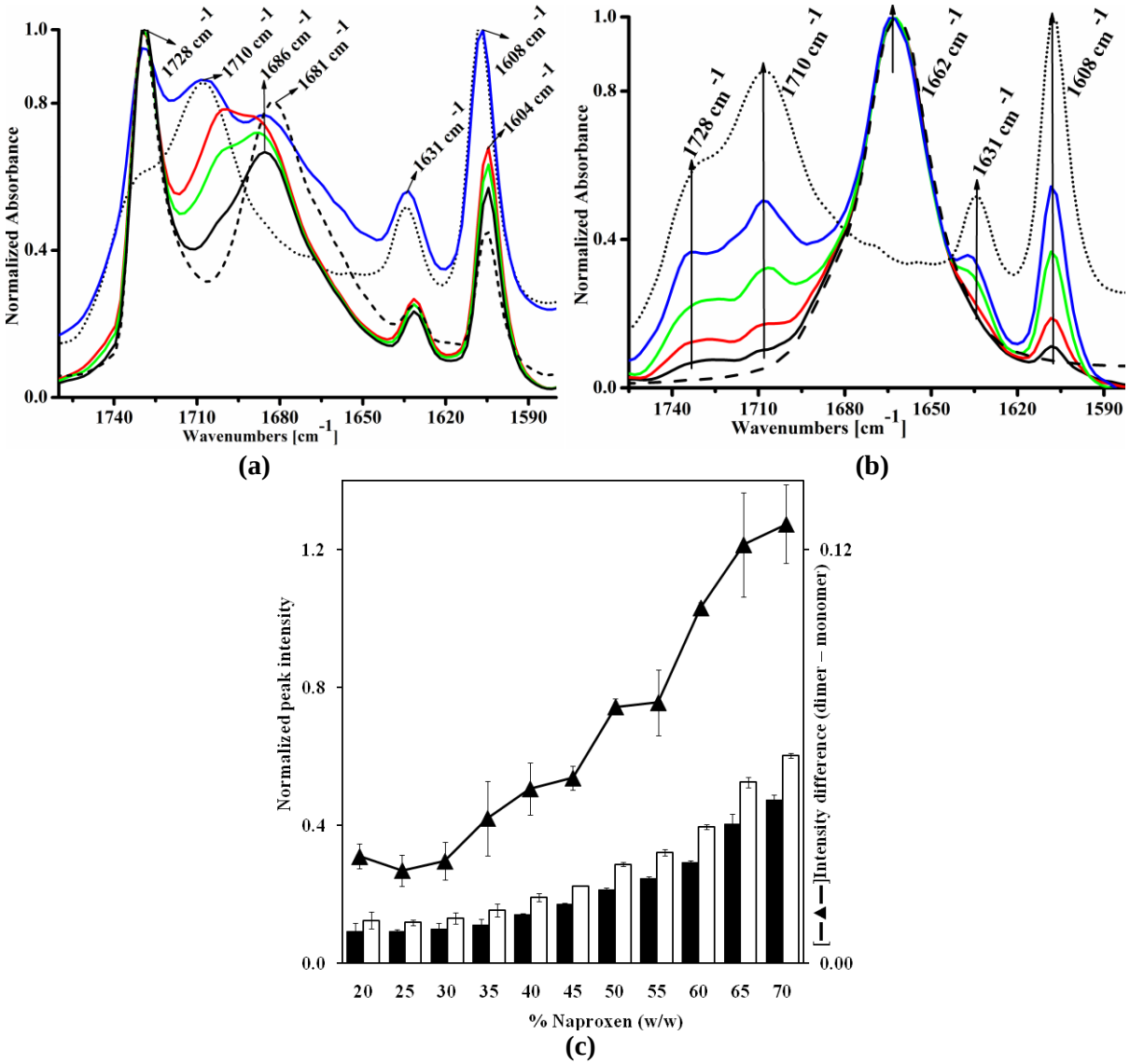

Figure V.2 (a) The normalized partial ATR-FTIR spectra of pure naproxen during evaporation (dotted line, at 15 s; blue, after 45 s; red, after 75 s; green, after 105 s; black, after 135 s; dashed, crystalline naproxen). (b) The normalized partial IR spectra of pure naproxen, pure PVP and naproxen−PVP solution with different drug to polymer composition (dotted line, pure naproxen; dashed, pure PVP; black, 20% w/w naproxen; red, 35% w/w naproxen; green, 55% w/w naproxen; blue, 65% w/w naproxen). (c) Normalized intensity of dimerized (white bar) and monomer (black bar) C=O stretching band of naproxen and the difference of intensity between dimer and monomer C=O peak of naproxen (▲) versus % w/w naproxen content (n = 3).

V.4.1.2 Solid State Phase Behavior

The macroscopic observation of the SC films prepared from the range of drug to polymer ratio showed aligned progression of the expected binary miscibility behavior as a function of composition. The photographs of SC films prepared from different drug to polymer ratios are available in the appendix. The SC films with drug content ≤20% were visually transparent. Distinct opaque islands appeared in the SC films with 25−35% naproxen

content. The films with ≥40% naproxen appeared to be fully opaque with the surface increasingly covered with naproxen crystals with increase in naproxen content. The presence of a diffuse halo without Bragg peaks in the pXRD patterns of the films with naproxen content ≤35% implied the complete XRD amorphous nature of the drug within this composition range while from 40% naproxen content crystalline peaks were superimposed on the amorphous halo and show increasing intensity with the increase of the naproxen content (data not shown).

The overlay of mDSC thermograms of SC films with representative compositions, depicted in Figure V.3, shows the complex composition dependent quasi-binary phase behavior of drug and polymer. The SC films with naproxen content ≤20% displayed a single mixed phase glass transition temperature (T_{gm}) implying them to be homogeneous vitrified mixtures. The positions of T_{gm} were identified in the first derivative signals of the reversing heat flow of the corresponding thermograms (not shown). For the films in the composition range 20% < naproxen ≤35%, two clearly separated T_{gm}s in the thermogram indicate the presence of two amorphous phases. The T_{gm} located toward the T_g of pure naproxen corresponds to that of drug rich domains (T_{gm1}) and that at higher temperature to the polymer rich domains (T_{gm2}). Similar observations in amorphous dispersions were apparent from the thermal profiles of films up to 35% drug content, with the gradual decrease in both T_{gm}s. At 40% drug content, both T_{gm}s shifted to higher temperatures, but the shift of T_{gm1} was higher than that of T_{gm2}. This is in agreement with the pXRD data as prominent crystalline peaks appearing over the amorphous halo are only observed for film compositions ≥40% naproxen. Further, the rapid increase of both T_{gm}s belonging to phase separated domains was observed with the increase in naproxen content along with the manifestation of a melting endotherm of the drug at lower temperature than that in the pure state. The glass transitions of both drug rich and polymer rich fractions merged at 60% drug content. From 65% onward, only one single T_{gm} at the temperature between T_{gm1} and T_{gm2} of the preceding composition and a melting endotherm were apparent. The T_{gm} gradually decreased while the maximum of the end part of the melting endotherm gradually increased with the further increase of the drug content in the SC film. The presence of polymer decreases the chemical potential of the drug leading to melting at lower temperature[21]. The practically observed extent of melting point depression depends upon the fraction of polymer present in the blend, the strength of drug−polymer interaction, the mutual diffusion and the polymer mobility. As the end temperature of the melting endotherm represents completion of melting process, it is also

referred to as dissolution end point (T_{end}) of the drug in polymer at particular composition[22]. The marked decrease in T_{end} was observed down to 65% naproxen content.

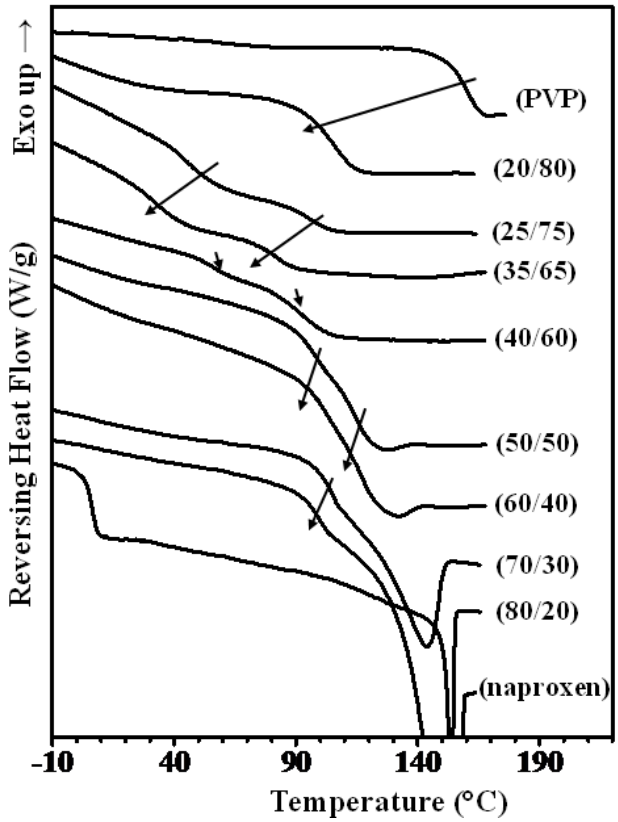

Figure V.3 mDSC traces recorded at 2 °C/min of the pure PVP, naproxen−PVP SC films prepared from the % w/w drug/polymer composition as indicated in the parentheses and partially amorphous naproxen (prepared by quench cooling naproxen melt in liquid N_2).The arrows denote the position and direction of T_{gm} progression as a function of % w/w naproxen.

V.4.2 Phase Behavior of the QC Dispersions

The mDSC thermograms of solid dispersions with representative compositions prepared by quench cooling are shown in Figure V.4. For the QC films showing only a glass transition event throughout the cooling and reheating cycle, the reversing heat flow signal is shown as function of temperature while the total heat flow signals are shown for some compositions with higher drug content that exhibited additional thermal events, viz., crystallization and melting. The solid dispersions up to 75% naproxen were X-ray amorphous and showed a single T_{gm} steadily decreasing with the increase in naproxen content. The glass transition was the only event visible in the cooling and reheating run up to 70% naproxen. The cooling curve recorded at 10 °C/min up to a composition of 75% naproxen showed only a single T_{gm} whereas upon heating the thermogram also showed a cold crystallization exotherm and the melting endotherm of an equal area indicating that the crystallinity only developed during heating. Considering the probable effect of cooling rate on the degree of amorphization

and the stability of the amorphous systems[23], slower cooling rates were tested to mimic the equilibrium cooling condition for the mixture compositions of 70% and 75% naproxen content.

As can be seen from the cooling curve, only a T_{gm} was apparent in the total heat flow signal of the melt with 70% naproxen, even down to the cooling rate of 0.2 °C/min. However, in the mixture with 75% naproxen two adjacent crystallization exotherms were noticed upon cooling at 4 °C/min. Upon further increasing the drug content to 80% naproxen again two but larger crystallization events were evident in the heat flow signal, even at faster cooling rate (10 °C/min), and prominent Bragg peaks corresponding to crystalline naproxen were visible in the pXRD patterns. For mixture compositions >85% similar trends were observed but a single crystallization exotherm was seen during cooling. The further decrease in T_{gm} evident in the heating curves of the compositions >80% naproxen indicated the more pronounced plasticization of drug rich amorphous domains, which is followed by the cold crystallization of the drug in excess to the kinetic solubilization capacity of the drug by polymer at the investigated composition. The onset of the melting peaks at higher drug content seemed to be accompanied by the glass transition event of pure PVP and/or polymer rich domains with very low drug loading. However, the positions of T_{end} points of the melting peak again showed consistent composition dependence as in the case of the corresponding SC films. Thus, here also we used T_{end} for the subsequent calculations related to the phase diagram, as explained in the Discussion section. The results overall reflect the impact of varying kinetics with the application of different solidification (cooling) rates and degree of solid state supersaturation of the drug−polymer mixtures on the extent of amorphization and kinetic miscibility in the resulting solid dispersions.

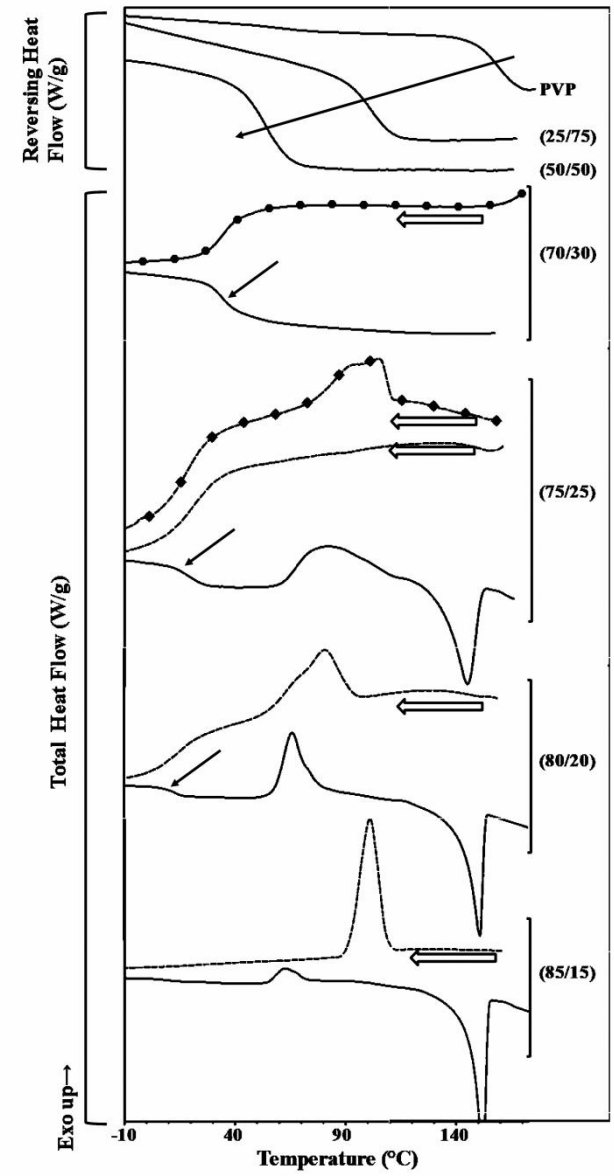

Figure V.4 mDSC thermograms of naproxen−PVP solid dispersions prepared by QC films with different drug to polymer ratio. The figures in the parentheses denote the respective drug to polymer compositions (% w/w). The thin arrow indicates the position and direction of T_{gm}, and thick arrows beside the curves denote the cooling cycles recorded at 10 °C/min (- - -), 4 °C/min (−■−) or 0.2 °C/min (−●−).

V.4.3 Spectroscopic Investigation on H-Bonding Interactions

The spectroscopic investigation of crystalline naproxen and PVP as well as their solutions in ranges of solvents has been extensively reported[24–27]. There are also spectroscopic studies occasionally reported for naproxen−PVP solid dispersions[15,28]. The carbonyl stretching regions of naproxen−PVP solid dispersions are characterized by several overlapping bands attributable to the residual peaks from uninteracted drug and/or polymer in addition to the peaks emerged from the composition dependent drug−polymer interactions. The characteristic vibration bands visible in the carbonyl region of pure naproxen, pure PVP or naproxen−PVP dispersion spectra are listed in Table V.1.

Table V.1 Peak positions of characteristic vibration bands observed in spectra of naproxen, PVP and naproxen-PVP solid dispersions

Spectrum of	Wavenumbers of the peak maxima (cm^{-1})	Assignments
Crystalline /partially amorphous naproxen	1718-1728	C=O stretching of non H-bonded –COOH of naproxen[25,29]
	1681-1686	C=O stretching of the H-bonded –COOH of naproxen catemer (linear dimer)[25]
	1604	Aromatic stretching band of naphthalene ring in naproxen[19]
	1394 and 1260	Bend/stretch and stretch/bend vibration band of free –COOH group of naproxen, respectively[30]
	3196 and 2670	O-H stretching band of free and intermolecularly H-bonded naproxen catemer respectively[25]
Pure PVP	1708	Vibration band of the completely unperturbed C=O group of PVP[31,32]
	1670 – 1680	Vibration band of C=O - C=O dipole interactions of PVP[33,34] (mostly in solution state)
	1648-1657	Vibration band due to strong dipolar interaction of C=O of PVP in solid state[35]
Naproxen-PVP systems (in addition to the pure component peaks)	1629 – 1631 (*dominant in drug rich composition*)	Vibration band of C=O stretching of PVP H-bonded with O-H of naproxen –COOH[15]
	1673 (*dominant in polymer rich composition*)	Weaker intermolecular H-bonding between C=O of PVP and O-H of naproxen –COOH[28,36]
	1706-1704	Stretching band assumed to be due to the C=O stretching of H-bonded cyclic dimer of drug[20]

In our recent study for the same drug−polymer system, we employed the relative intensities at the peak maxima of the different bands present in the carbonyl stretching region of the normalized spectra to approximate the fractions of each population in spray-dried solid dispersions[15]. In the present study, we applied an iterative least-squares curve fitting method using hybrid Gaussian−Lorentzian (GL) linear sum function (pseudo-Voigt) to decompose the multiple overlapping absorption bands across the normalized carbonyl stretching regions of the solid dispersions with different drug/polymer compositions to the individual peaks. The GL function describes the function "y_i" for the area of an individual peak as

$$y_i = y_0 + A_i\left[m_{u_i}\frac{2}{\pi}\frac{w_{L_i}}{4\left(x_i - x_{c_i}\right)^2 + w_{L_i}^2} + (1 - m_{u_i})\frac{\sqrt{4ln2}}{\sqrt{\pi}w_{G_i}}e^{-\frac{4ln2}{w_{G_i}^2}\left(x_i - x_{x_i}\right)^2}\right] \quad \text{.....Equation V.1}$$

where y_0, x_c, A, w_G, w_L, m_u are offset, center frequency with absorption maximum, amplitude, Gaussian width, Lorentzian width and profile shape factor (fraction of Lorentzian

contribution), respectively, for the ith peak. The FWHM of an individual peak is determined by both w_G and w_L. The second derivative method with second order Savitsky−Golay smoothing (20 points) was implemented to find locations of absorption bands. The area percentage of individual vibration band was calculated from the integrated normalized areas of the bands corresponding to different C=O stretching (eq V.2).

$$\%Area = \frac{A_i \times 100}{\sum n(A_1 + A_2 + \cdots A_n)} \quad \text{..... Equation V.2}$$

where A_i is the area under the i^{ith} peak and n is the number of peaks in the spectrum of particular composition.

A pure Gaussian profile is associated with faster molecular relaxation of coherently vibrating populations with much higher coherence lifetime compared to the amplitude correlation time, the characteristic feature of solids (with higher order)[37,38]. As an another extreme, in the systems with the highest disorder like liquids and gases, molecular vibrations attain faster dephasing with rotations and collisions and their profiles follow Lorentzian shape. A hybrid GL function was employed for spectral deconvolution with the assumption that these systems behaved non-homogeneously due to amorphous or crystalline phase separation [38,39].

V.4.3.1 ATR-FTIR Characterization of SC Films

The normalized C=O stretching regions of the FTIR spectra along with the respective deconvoluted peaks of the naproxen−PVP SC films compositions representing different miscibility zones (solid solution zone, phase separated amorphous zone, phase separated amorphous plus partially crystalline zone, single amorphous phase plus partially crystalline zone) are displayed in Figure V.5. The deconvoluted peak at 1604 cm^{-1} is the contribution from the aromatic skeleton stretching of naproxen (Table V.1) and is not displayed and also not taken into account for the calculation of area percentage of the vibration bands attributable to various C=O stretching.

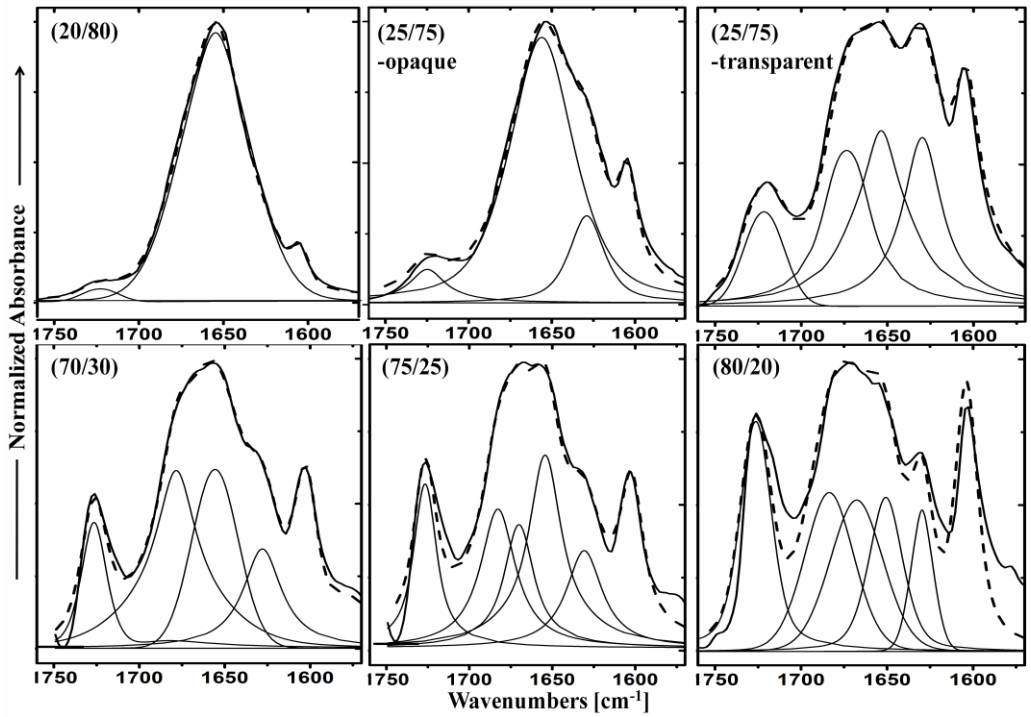

Figure V.5 Partial normalized ATR-FTIR spectra (1760−1560 cm^{-1}) of naproxen−PVP SC films prepared from different drug to polymer ratios as indicated in the figures in the parentheses. The deconvoluted peaks correspond to different C=O vibration bands belonging to naproxen, PVP and/or naproxen−PVP interaction as described in Table 1. The peak with maximum at 1604 cm^{-1} has been removed for clarity (see text for details). The dashed lines correspond to the sum curves of the decomposed peaks derived from fitting of the respective spectra.

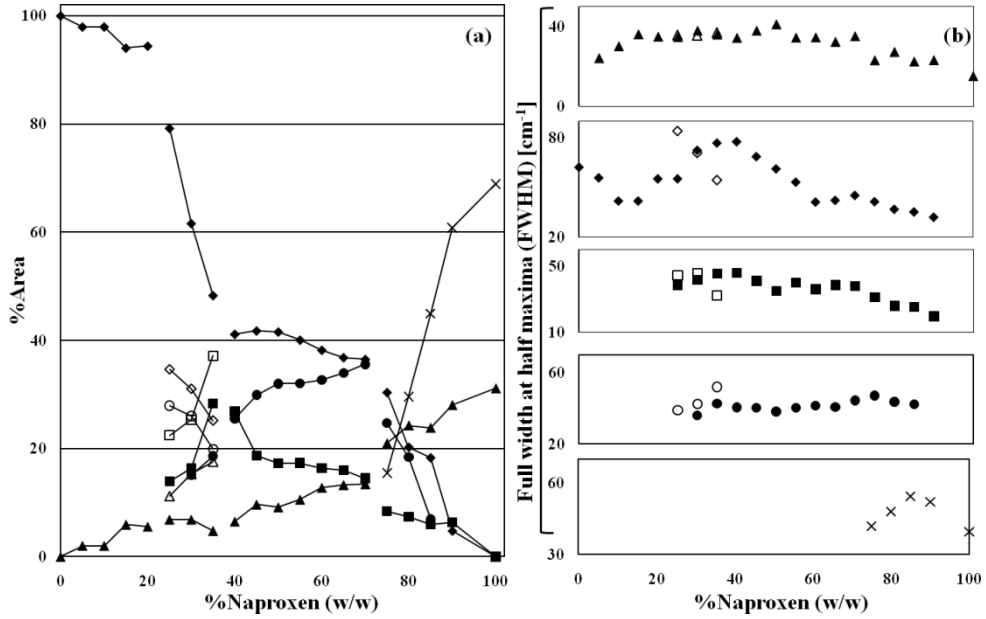

Figure V.6 Plot of normalized % peak area (a) and Full Width at Half-Maximum (FWHM) [cm^{-1}] (b) of vibration bands corresponding to C=O stretching of non-H-bonded naproxen (▲), non-H-bonded PVP (◆), strongly H-bonded (■) and weakly H-bonded (●) PVP with naproxen O−H, and H-bonded naproxen catemer (×) as the function of % w/w naproxen in naproxen−PVP SC films. The open symbols represent the corresponding peaks observed in the transparent portion of the particular compositions.

The progression of the area contributions from the various peaks with increase of the naproxen content in the SC films is illustrated by the plot in Figure V.6a. Up to 20%

naproxen, the C=O stretching peak of uninteracted naproxen increases with the concurrent decrease of the C=O stretching peak of uninteracted PVP. For the films containing 25−35% naproxen, containing distinct transparent and opaque portions, spectral profiles were recorded from the distinct regions. In addition to the vibration bands that appeared in the preceding compositions, the spectrum of the opaque section shows two additional peaks at 1630 cm^{-1} and 1670 cm^{-1} attributable to stronger and weaker H-bonding between naproxen and PVP respectively (will be referred as strongly and weakly H-bonded fraction henceforth) (Figure V.5). Across this composition range, the increase in naproxen content leads to a gradual increase of the area percentage of the 1630 cm^{-1} peak with a remarkable decrease of $(C=O)_{PVP}$ peak. In the films with 30% and 35% naproxen the peak at 1672 cm^{-1} observed in the opaque parts and attributable to the weak H-bonding increases with the increase of the naproxen content (Table V.1). On the other hand, the spectra of the transparent portions of the films in the range of 25−35% naproxen content showed completely different compositions of various –C=O stretching bands compared to those of the corresponding opaque portions. Here, the area of the strongly H-bonded peak showed a sharp increase with the increase of naproxen and became dominant at 35% naproxen content, together with the simultaneous decrease of the weakly H-bonded fraction. The film with 40% naproxen appeared excessively opaque, and the surface became increasingly covered with naproxen crystals, making it difficult to probe the location with different fraction or strength of H-bonded fraction. IR scans of multiple points across the entire film area in the DSC pan of samples with ≤40% naproxen, considering the existence of two T_{gm}s, resulted in similar spectral profiles for the particular composition.

At 40% naproxen content, the areas of peaks belonging to strongly and weakly H-bonded fractions were equivalent. In 40−70% composition range of naproxen, the gradual decrease of the peak area of the uninteracted $(C=O)_{PVP}$ band and that of the strongly H-bonded fraction was accompanied by the opposite trend of the peak areas of uninteracted $(C=O)_{naproxen}$ bands and weakly H-bonded fraction. From ≥75% naproxen, the films with higher crystalline fraction showed the appearance and thenafter the rise in the vibration band attributable to $(C=O)_{naproxen\ catemer}$. Furthermore, the rapid decrease in the peak area of free $(C=O)_{PVP}$ band and weakly H-bonded fraction as well as gradual decrease of strongly H-bonded fraction was accompanied by the steady increase in the peak area of the uninteracted $(C=O)_{naproxen}$.

Apart from the peak area, the composition dependent variations in the peak broadness observed for some of the vibration bands in the C=O stretching regions of the SC films are represented by the plot in Figure V.6b. The peak related to non-H-bonded $(C=O)_{naproxen}$ broadened up to 15% naproxen and almost leveled off until 70% drug content, after which this peak started appearing sharper and turning narrowest for the pure crystalline naproxen. The peak of uninteracted $(C=O)_{PVP}$ showed decrease in FWHM up to 15% naproxen followed by rapid increase up to 35% naproxen. The steep decrease of FWHM of this peak was observed from 40% naproxen which almost remained quiescent from 60% naproxen. The peak width of strongly H-bonded C=O fraction remained more or less constant up to 40% naproxen and gradually declined up to 50% naproxen, and a steep decrease started from 70% drug content, while the FWHM for the peak of weakly H-bonded C=O fraction remained almost unchanged throughout. The peak broadness of H-bonded C=O stretching vibration band of naproxen catemer that appeared from 75% naproxen increased up to 85% naproxen and then decreased in the succeeding compositions, turning narrowest for the pure crystalline naproxen.

The varying positions of the peak maxima of C=O stretching of the uninteracted naproxen (Figure V.7) and O−H stretching of naproxen −COOH were observed as a function of film composition. The amorphous films containing ≤35% naproxen exhibited the peak maximum of the non-H-bonded $(C=O)_{naproxen}$ at 1718 cm^{-1} with a shoulder peak of 1728 cm^{-1}, the latter showing continuous increase with the increase in naproxen. Immediately with the development of partial crystallinity, i.e., in the film with 40% naproxen, the shoulder at 1728 cm^{-1} in the preceding composition became the peak maximum with the shouldering of peak at 1718 cm^{-1} that consistently decreased with the increase in naproxen concentration. The vibration band that belongs to $(O-H)_{naproxen}$ is very broad and diffuse up to 50% naproxen, and the peak maximum for this vibration band could only be identified in mixtures with >55% naproxen. In the SC films with naproxen content of 55−80% naproxen, the peak maximum of the latter vibration band was located at 3170−3174 cm^{-1}, which shifted to 3196 cm^{-1} from 85% naproxen content. Also, a shallow H-bonded O−H vibration band at 2570−2670 cm^{-1} attributable to the naproxen catemer was prevalent in the film compositions bearing the same. Another peak maximum that shifted as a function of naproxen composition was that of C=O stretching vibration band of naproxen catemer that moved from 1684 cm^{-1} in solid dispersions to 1681 cm^{-1} in pure crystalline naproxen.

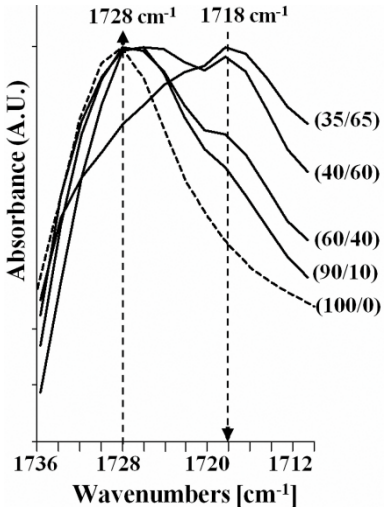

Figure V.7 The detailed spectral part of non-H-bonded C=O stretching region of naproxen in naproxen−PVP SC films with varying drug to polymer ratio (mentioned in parentheses). The dotted arrows guide the peak maximum and its direction of change in intensity with composition.

V.4.3.2 ATR-FTIR Characterization of QC Films

As revealed by Figure V.8, the C=O stretching regions of the naproxen−PVP dispersions with representative compositions prepared by melt quenching displayed completely different phase−spectral profile relationships compared to that of the corresponding cast films. This can be further discerned from plots of peak area and FWHM as functions of naproxen content in the QC films (Figure V.9). The C=O stretching spectral regions of melt quenches up to 20% naproxen were characterized by an increasing trend for uninteracted $(C=O)_{naproxen}$ and decreasing trend for that of uninteracted PVP. Further, the spectra of dispersions with 25 and 30% naproxen additionally contained the strongly H-bonded C=O stretching band. In the spectrum of QC dispersion with 35% naproxen, the sharp drop in the peak area of uninteracted $(C=O)_{PVP}$ was replenished by the appearance of the C=O stretching bands of the strongly and weakly interacting H-bonded fractions. From this composition on, the peak area of uninteracted and weakly H-bonded C=O stretching bands of PVP steadily decreased with increase in naproxen concentration in the QC films. This behavior was accompanied by the persistent rise in the peak area of non-H-bonded $(C=O)_{naproxen}$ up to the dispersion containing 70% drug. Conversely, there was an abrupt increase in the peak area of the strongly H-bonded fraction when moving from 40 to 45% naproxen which then flattened up to the 70% naproxen containing dispersion. As observed for the SC films, the C=O stretching band of H-bonded naproxen catemer started to appear from 75% naproxen content, which increased expectedly with a further increase of naproxen concentration. The peak area of uninteracted $(C=O)_{PVP}$ band markedly reduced by 75% naproxen content compared to previous composition and remained constant up to the highest

drug content. The relative contribution of the peak area of strongly H-bonded fraction is also reduced remarkably by this composition and kept on decreasing with the increase of the naproxen concentration while the vibration band of the weakly H-bonded fraction is absent for >85% drug content. More interestingly, the C=O stretching regions of QC dispersions with 75 and 80% naproxen also exhibited an additional vibration band with the peak maximum at 1704 cm^{-1} (Figure V.8) that was more prevalent in the latter composition. Note that a vibration band was also evolved at 1704 cm^{-1} as the contribution from naproxen catemer in the course of naproxen crystallization from methanolic solution (Figure V.2a).

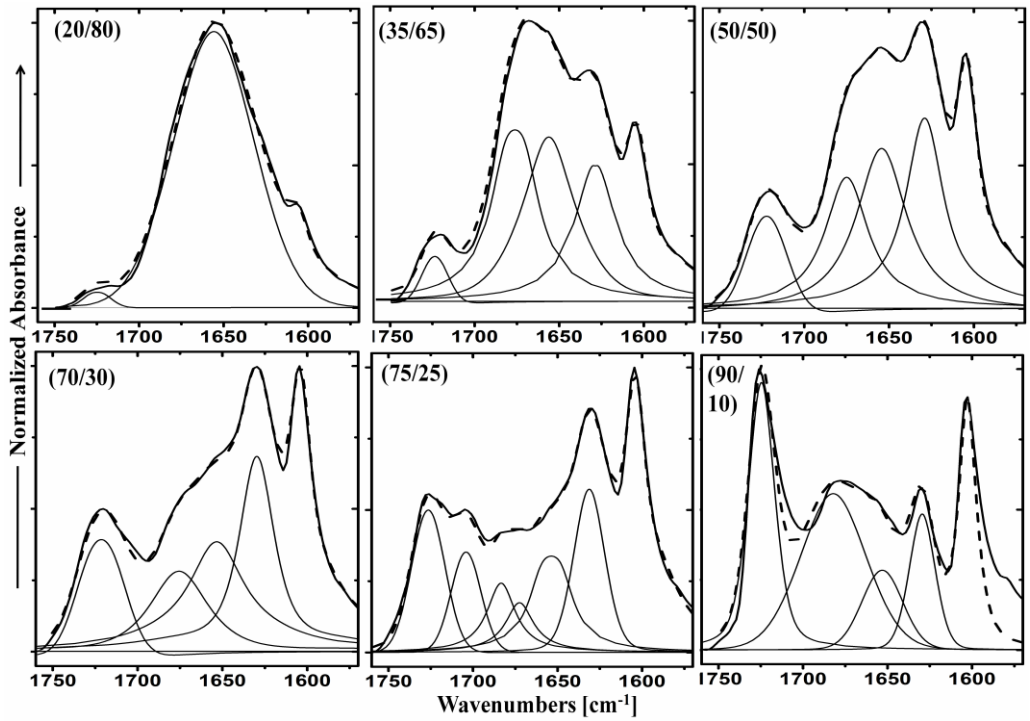

Figure V.8 Partial normalized ATR-FTIR spectra (1760−1560 cm^{-1}) of naproxen−PVP QC films prepared from different drug to polymer ratios as indicated in the figures in parentheses. The deconvoluted peaks correspond to different C=O vibration bands belonging to naproxen, PVP and/or naproxen−PVP interaction as described in Table V.1. The peak with maximum at 1604 cm^{-1} has been removed for clarity (see the text for details). The dashed lines correspond to the sum curves of the decomposed peaks derived from fitting of the respective spectra.

Figure V.9b shows the increase of the FWHM of non-H-bonded $(C=O)_{naproxen}$ peak from 10 to 15% naproxen content that remained almost invariable up to 70% naproxen content and decreased for the dispersions from 75% naproxen. The FWHM of uninteracted $(C=O)_{PVP}$ peak was more or less constant up to 70% naproxen and decreased onward. Likewise, the H-bonded C=O peaks also became narrower for higher drug content. The broadness of the H-bonded C=O stretching peak of naproxen catemer increased with the higher drug containing QC films.

As observed for the cast films, the reversal of the peak maximum of the non-H-bonded $(C=O)_{naproxen}$ band was witnessed upon increasing naproxen concentration across the borderline composition range, i.e., from 70 to 75% naproxen content (Figure V.10). The peak maximum of the $(O-H)_{naproxen}$ band could only be assigned from 75% naproxen containing dispersion. The peak maximum of this peak was 3124 cm^{-1}, 3138 cm^{-1}, 3160 cm^{-1} and 3178 cm^{-1} for the dispersions with 75%, 80%, 85% and 90% naproxen content, respectively. The composition dependent peak position of the C=O and O−H stretching bands of H-bonded naproxen catemer followed a similar trend as that of the cast films.

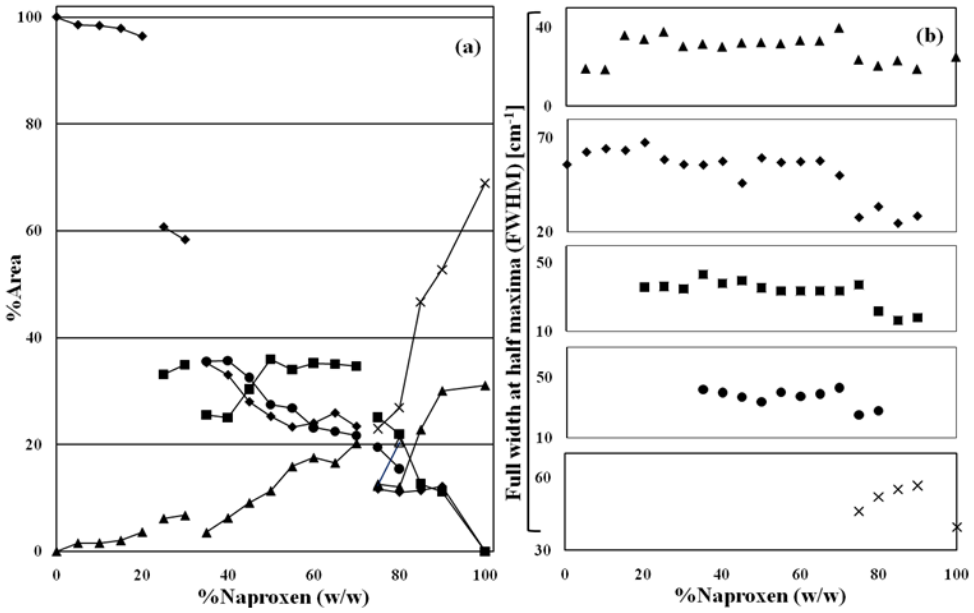

Figure V.9 Plot of normalized % peak area (a) and Full Width at Half-Maximum (FWHM) [cm^{-1}] (b) of vibration bands corresponding to C=O stretching of non-H-bonded naproxen (▲), non-H-bonded PVP (◆), strongly H-bonded (■) and weakly H-bonded (●) PVP with naproxen O−H, H-bonded naproxen catemer (×) and an additional peak (Δ) as functions of % w/w naproxen in naproxen−PVP QC films.

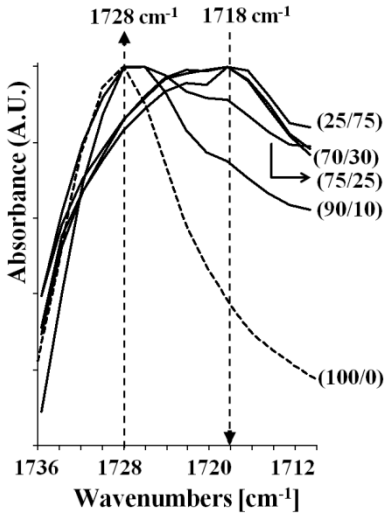

Figure V.10 The zoomed spectral part of non-H-bonded C=O stretching region of naproxen in naproxen−PVP QC films with varying drug to polymer ratio (mentioned in parentheses). The dotted arrows guide the peak maximum and its direction of change in intensity with composition.

V.5 Discussion

V.5.1 Molecular Interactions in Solution State to Forecast Miscibility in Cast Films

It has been documented that the composition specific physical structure (miscibility, solid state interactions and physical stability) of solid dispersions prepared by solvent processes largely relies on the various types of thermodynamic, dynamic and kinetic processes such as self-associative and interassociative interactions among drug, polymer and solvent, mutual interdiffusion of drug and solvent into polymeric chains, and on the solvent evaporation rate from the starting solution[15,18]. From the study on the dynamics of pure PVP in methanolic solution, it has been reported that the local chain motion of the polymer is 2 orders of magnitude slower than the rotational motion of MeOH dipoles[40]. Thus, the dilute polymeric solution is expected to facilitate rapid diffusion of the solvent into the volume pervaded by the side chains leading to the increased solvation, with some of the solvent also engaged in H-bonding with C=O of PVP and hence smaller globular sizes. However, upon adding naproxen (≤15% w/w) in the solution the trend in globular size was found opposite that expected in the pure polymeric solution. This may indicate that the −COOH group of naproxen either establishes H-bonding with its O−H group to C=O of PVP or to "O" group of MeOH, thus depriving PVP from solvation and leading to the increase of globular size. The latter is certainly possible and also evident from solution IR[24]. Compared to the vibration frequency reported for non-H-bonded C=O and H-bonded C=O of the catemer of naproxen in weakly H-bond acceptor solvents[25], both peaks shifted to lower wavenumbers, evidencing the existence of cooperative H-bonding. On the other hand, no position shifts of $(O-H)_{naproxen}$ and $(C=O)_{PVP}$ were observed in drug−polymer solution as compared to the peak positions in their pure solutions. This ruled out the formation of H-bonding between drug and polymer in the starting solution. Also, monomer-multimer (catemer) equilibrium of naproxen in MeOH showed a higher fraction of catemer over monomer as apparent from Figure V.2a. Additionally, no change in the vibration position of aromatic skeleton stretching band (at 1608 cm^{-1}) observed in the drug−polymer solution may point to the absence of the strong hydrophobic interaction of naproxen with the hydrocarbon backbone of PVP. So, the increase in globular size should be contributed to the decrease in the extent of solvation.

The bimodal distribution of the PVP globular populations from ≤20% w/w naproxen content suggests that this composition is the threshold tolerance concentration. At this composition, the larger size globules could be generated from interchain self-aggregation of PVP with decreased solvation caused by the higher fraction of MeOH engaged with naproxen

in the vicinity. On the other hand, the smaller globules could be due to the sustained open chain PVP with a higher degree of solvation and physical presence of naproxen molecules between pyrrolidone free spaces.10 Similar composition dependent DLS behavior has been recently reported for the solution of a polymer blend which dictates the varying degree of homogeneity in the resulting solid state structure[41]. In our SC films also, 20% w/w naproxen was the threshold amorphous composition exhibiting a single T_{gm}. With further increase of the naproxen content, this phenomenon continues in the unsaturated smaller globules, whose size shows a gradually increasing trend while the self-aggregation in the larger globules levels off. From 45% w/w naproxen onward, the increased dimerization of naproxen (Figure V.2c) decreases its diffusivity toward the self-aggregating PVP that makes the latter grow further. As a consequence of higher extent of dimerization from 30 to 55% naproxen, the probability of nucleation increases compared to preceding compositions. The further increase in dimerization ≤60% naproxen could initiate concomitant nucleation and crystal growth leading to the higher extent of crystallization obtained from this composition in the films.

The time-resolved IR−crystallization profile of naproxen from solution (Figure V.2a) shows the evolution of the stronger H-bonded dimers with the gradual red shift in peak position and progressive increased fraction of the same at the expense of the weakly H-bonded random solution state dimers positioned at higher vibration frequency which totally transforms to the former one upon complete solidification. Likewise, the dominating vibration intensity of the aromatic stretching peak of the naphthalene ring of naproxen in solution state drastically dropped and consistently showed a red shift of 4 cm^{-1} upon solidification. This provides the evidence on the course of hydrophobic interaction development due to the increased ordering of molecular layers of naproxen during crystallization[42].

V.5.2 Relationship between the Quasi-Equilibrium Drug−Polymer Miscibility Limit and H-Bonding Interactions in SC Films

The melting temperature of a small organic molecule is depressed upon dispersing it in a solvent due to the drop of overall chemical potential in solution with particular concentration[43]. Analogously, polymer carriers, by acting as a solvent in drug−polymer solid dispersion, can reduce the melting temperature of a crystalline drug dispersed in the matrix[44]. This is often considered as the dissolution temperature of drug crystals in the polymeric solid dispersion system[45]. This drug dissolution merely follows the kinetic process or heating rate dependence in contrast to the melting of the pure crystal being solely the thermodynamic phase transition. It can be envisioned for the films that the increase of polymer concentration

sharply increases the heating rate dependence of T_{end} (Figure V.11a). The decreased viscosity of the saturated solid solution of the compositions with the higher drug content renders its dissolution process kinetically dormant, hence less dependent upon rate process as observed for films with ≤85% naproxen content. In contrary, due to the increased viscosity of dispersions with lower drug concentration (≥65% naproxen), T_{end} shows drastic heating rate dependence. This can justify the absence of a distinct melting endotherm of naproxen in the crystalline film compositions with <50% drug content, in the thermograms at <2 °C/min, which can otherwise be visualized with the faster scan rates[15]. Further, the inability of DSC to detect drug melting events for these compositions also points out the presence of small crystallites of naproxen in the finely suspended state within the solid dispersion[46]. Thus, the extrapolated T_{end} (to 0 °C/min heating rate), which is also assumed to be an equilibrium melting temperature, can be utilized to calculate the thermodynamic activity of naproxen in PVP (γ_{naproxen}) for the particular composition using eq V.3:[22]

$$ln\gamma_{naproxen} = \frac{\Delta H_f}{R}\left(\frac{1}{T_m} - \frac{1}{T_{end}}\right) \text{ ... ... Equation V. 3}$$

where ΔH_f, R, T_m and T_{end} are heat of fusion of pure drug, universal gas constant, melting (end) temperature of pure naproxen and dissolution end point of naproxen in PVP, respectively. The obtained γ_{naproxen} at different compositions can be fitted to the Flory−Huggins (FH) model (eq V.4) as shown in Figure V.11b[47,48].

$$ln\gamma_{naproxen} = ln\emptyset_{naproxen} + (1 - \frac{1}{m})\emptyset_{PVP} + \varkappa\emptyset_{PVP}^2 \text{.....Equation V.4}$$

where $\emptyset_{naproxen}$ and $\emptyset_{PVP}$ are respectively the volume fraction of naproxen and PVP, m is the molar volume ratio of polymer to drug and χ is the FH binary interaction parameter between naproxen and PVP. The negative value obtained for χ (−2.54) signifies the contribution of favorable adhesive (heteromolecular) mixing interaction between drug and polymer compared to the cohesive (homomolecular) interaction[21]. The melting point depression line interpolated toward the compositions with the lower drug content using the obtained χ value back in eqs V.3 and V.4 gives the solid−liquid boundary line for the system. As shown in Figure V.11c, the plot of composition−T_{gm} profile together with the melting point depression line provides the complete thermal phase diagram for the naproxen−PVP films. The crossing of the solid−liquid line with the declining T_{gm} line of the homogeneous amorphous dispersion (x, y = 17% w/w naproxen, 112 °C) can be assumed as equilibrium solid solubility of naproxen in PVP at that particular temperature[22]. This means, in the white region below T_{gm} (≤20%

naproxen) in Figure V.11c, the amorphous naproxen is undersaturated in PVP rendering it physically stable with reduced molecular mobility. Interestingly, this composition is also recently reported by us as the threshold composition for the same system, which maintained blend homogeneity upon compression.[49]. In the range of 20−35% naproxen, both drug rich and polymer rich domains are thermodynamically supersaturated, predominantly the former one, but could sustain nucleation during film formation by the hindered molecular mobility in the presence of sufficient PVP. From 40 to 60% naproxen, inability to maintain increasing supersaturation by the lower amount of polymer causes the excess naproxen to nucleate, which can further act as seeds for ripening the supersaturated solid solutions. This could be the reason for increasingly antiplasticized T_{gm}s and leveling off from 50% naproxen, observed in this region with the increase of naproxen content, hence the increase of seed during film formation. Due to the large concentration gradient built ≥65% naproxen, there could be prominent interdiffusion resulting in slightly plasticized T_{gm} from this composition. Interestingly, the interpolated straight line of the T_{gm} corresponding to the single amorphous−crystalline phase separated compositions also passes through the point of intersection of the T_{gm} line of homogeneous solid solution and solid−liquid line (Figure V.11c). Thus, the T_{gm} values of solid dispersions with the latter compositions (≥65% naproxen) indeed provide an estimate of the amorphous drug loading possible with the solubilization capacity of the amount of polymer present and thus the crystallization inhibition against the seed crystals present therewith. The starting composition of crystallization in our case, i.e., 40% naproxen, coincides with the data from Nair et al. for the crystallization of naproxen in the films with PVP K 90 developed by methanolic solution casting[28], which is further supported by similar limit of kinetic miscibility of naproxen reported in PVP K 25 and K 90.[6]

The SC films were developed with the control of evaporation rate to the lowest possible and also analyzed with firm cautions for its structural integrity. The solid dispersions prepared by film casting or rotary evaporation are often subjected to grinding or micronization for sample preparation before the analysis or performance testing ignoring the severe risk of changing the physical structure of the system by doing so. The marked increase in the extent and the rate of crystallization induced by simply creating cracks or a scratch on the quench cooled amorphous indomethacin has been reported[50]. Moreover, we recently reported compression induced demixing of amorphous solid dispersions made up of naproxen and PVP K 25[49]. Especially, for films separately developed in bulk with morphologically

visible inhomogeneity, large uncertainty rises in maintaining the same level of bulk heterogeneity while sampling them for analysis.

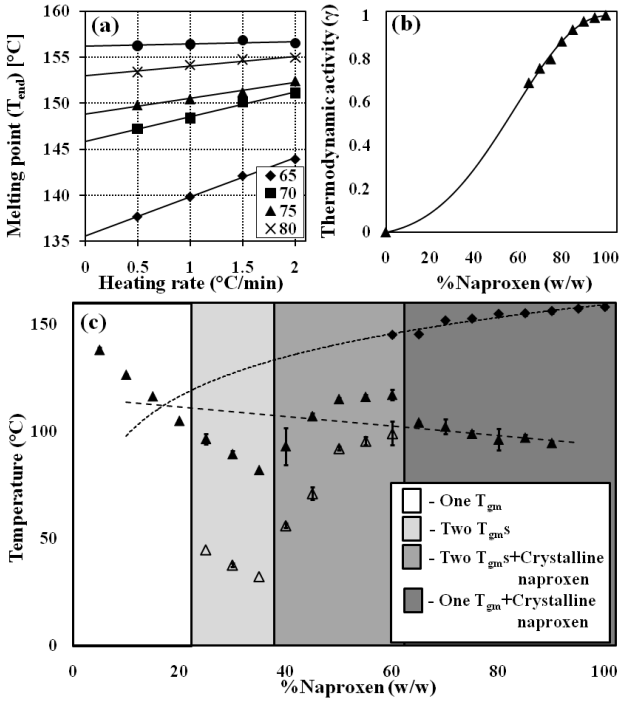

Figure V.11 (a) Heating rate dependence of melting point (T_{end}) of drug in the SC films at different composition, (b) the plot of thermodynamic activity of naproxen in PVP as the function of % w/w naproxen content (▲, estimated $\gamma_{naproxen}$; solid line, the fitted line using eq V.4) (R^2 = 0.98 and χ = −2.54) and (c) thermal phase diagram of naproxen (▲, T_{gm} or T_{gm2} for the phase separated composition; Δ, T_{gm1}; ◆, T_{end}; (⋯), T_{end} calculated by combining eqs V.3 and V.4 and (- - -), linear T_{gm} interpolation using T_{gm} of compositions from 65% naproxen). The vertical error bars represent the range between the values from two independent measurements.

Despite utmost care taken in sample preparation, the role of several kinetic processes involved during the film formation process itself cannot be disregarded. The effect of composition dependent evaporation rates of solvent from the polymer solution or drug−polymer solution on the miscibility and amorphicity in the resulting physical structure has been reported[15,18,51]. At higher polymer concentration, faster film formation leads to a decrease of overall evaporation rate hence providing sufficient time for the interacting groups of the drug and polymer to reach in mutual vicinity and establish favorable mixing interactions. Conversely, solvent evaporates so fast at lower polymer content (≤35% PVP) that an exceedingly higher fraction of amorphous naproxen above its solid solubility, even in the presence of surplus seed crystals, could be trapped as witnessed by the gradual plasticization. Additionally, other solution state properties such as viscosity and surface tension of PVP solution have been shown to follow erratic concentration dependent behavior in the presence of extraneous materials[52].This could eventually lead to the differential rate of interfacial nucleation and rate of surface enrichment by naproxen during film formation from

solution containing different drug to polymer ratio. With the conformation flexibility possible due to the easily rotatable bonds present in naproxen and PVP, they can rapidly interconvert among different conformers with a smaller energy barrier for interconversion present in solution[24,27,53−55]. In addition, the unique time dependent stereo-oscillating behavior (converting from "R" to "S" and vice versa) demonstrated for naproxen in MeOH[56] and different extent of interaction of naproxen enantiomer and racemate reported with PVP[57] poses a challenge in directly linking the starting solution state interactions and solid state phase behavior. Rather, the film formation end point can be viewed as the snapshot of one of many solution state conformations and thereby the molecular interactions wherein only certain conformations are frozen out. The conformational states and intermolecular interactions developed in solid state thus can be the interplay of complex kinetic processes. Currently, we are actively investigating to unravel the fate of the time dependent drug−polymer solution state interactions on the phase behavior of solid dispersions prepared by solvent process.

The information of drug−polymer solid dispersions from FTIR analysis has long been utilized to explore the type and strength of intermolecular interaction profiles between drug−drug and drug−polymer and relate them with miscibility[58,59]. The appearance of a vibration band at 1630 cm^{-1} as the consequence of strong intermolecular H-bonding of PVP with −COOH functionality has been reported before[15]. Although the peak assignment ranging from 1687 cm^{-1} to 1654 cm^{-1} is found in the literature for the non-H-bonded $(C=O)_{PVP}$ band, the same for neat or unperturbed C=O is reported at 1708 cm^{-1} (Table V.1)[31,32]. So, the peak position observed of this band at 1662 cm^{-1} in MeOH solution could be due to self-aggregation of pyrrolidone and/or solvent−polymer H-bonding[40]. This way the vibration band occurring at 1672 cm^{-1} could be assigned for weak H-bonding of naproxen to the unperturbed C=O of PVP during film formation[15,28].

Note that none of the peaks ascribed to naproxen−PVP interaction are visible up to 20% naproxen. This peak could have been eclipsed by the maintenance of the large fraction of uninteracted PVP, hence not even visible as the dip in the second derivative spectrum. Alternatively, there might be non-H-bonding interactions such as dipolar interaction between $C=O_{naproxen}$ and $C=O_{PVP}$ leading to the slower progression of the former band with composition up to ≤20% naproxen. Alternatively, as suggested by the globular size profiles and solution IR, the drug molecules might have been immobilized as amorphous clusters filled within the free volume among the PVP chains by mixing due to the extreme

composition regime. As the pXRD amorphous films were macroscopically biphasic solid dispersions from 25 to 35% naproxen, the two different spectral profiles witnessed from the corresponding regions seem justified. The lower uninteracted $(C=O)_{PVP}$ and higher H-bonded fractions observed for the transparent section of the film suggest it to be rich in amorphous drug exhibiting corresponding T_{gm1} while the respective opaque counterpart at the same compositions with the opposite ratios of peaks should be the polymer rich region contributing to T_{gm2}. However, the presence of both strongly and weakly H-bonded fractions for a single domain itself suggested that drug and polymer are demixed at the single T_{gm} level as well, in fact, with the domain size much lower than the detection limit of DSC (<30 nm)[60,61]. Nevertheless, it was noticeable that the spectral profiles of phase separated regions started appearing identical with the decrease in the T_{gm} difference between the phase separated domains. Moreover, partially crystalline films with 40−60% naproxen with two T_{gm} exhibited identical spectral profiles, even upon scanning at different locations. This could be because of either an identical H-bonding behavior of the phase separated compositions or poor spatial resolution of FTIR. So, even for XRD amorphous dispersions appearing homogeneous by DSC analysis, it is challenging to detect the state (molecule or cluster) and size of the dispersed domains[46]. Even though DSC and pXRD analysis confirmed the composition from 40 to 70% naproxen to be partially crystalline, the vibration band ascribed to C=O stretching of H-bonded naproxen catemer in the crystal was not perceptible. This could be due to the presence of smaller crystals finely embedded in the PVP matrix possibly also with a different habit compared to bulk crystal having different surface to volume mode of vibration. Tomasko and Timko have explained the variation of the relative intensity of non-H-bonded and H-bonded C=O peak of crystalline naproxen with the difference in crystal habit[25]. Accordingly, the crystal habit with predominant internal O−H groups (volume modes) would be involved in catemer formation and that with only external −OH groups (surface modes) could exist as monomers. Furthermore, the presence of the C=O peak maximum of naproxen at lower wavenumber for the completely amorphous films pointed toward the differential vibration strength of the same, in the disordered system. It is likely that, due to their increased mobility, a large fraction of amorphous naproxen can diffuse to the residual −OH group present at the end of the PVP molecule. The intermolecular dispersion interactions that are present, such as London-type dispersion forces, exchange-repulsion and induction energies, are major contributors to the true long-range order in crystalline state of naproxen[42]. These interactions would be highly altered in amorphous state lacking the long-range order. The observed frequency shift of C=O of naproxen upon amorphization could be due to the global

competition among different noncovalent interactions (dispersion, dipolar, H-bonding) in determining short-range order in the amorphous state. Also, the gradual peak shift of the C=O stretching band of H-bonded naproxen dimer toward lower wavenumber, upon increased crystalline content or crystallization (Figure V.2a), could be due to the strengthening of H-bond upon increasing molecular vicinity and ordering during crystallization[20,62].

Peak width of a vibration band, often expressed in terms of FWHM, carries an asset of information on the local chemical environment, molecular disorder, motion and to some extent the strength of H-bonding of the vibrating functional group[37,38]. As a general convention, peak width is inversely related to the vibration lifetime, and therefore, the higher the degree of disorder or the stronger the H-bonding, the faster the molecular relaxation, hence resulting in larger bandwidth. The sharper peaks of non-H-bonded $(C=O)_{naproxen}$ for the SC films with >70% naproxen resulted from the increased fraction of the ordered system, crystalline form. The same explanation holds for the H-bonded $(C=O)_{PVP}$, specifically strongly H-bonded fractions. Further, the trend is more apparent for the peak width of the C=O band of H-bonded naproxen catemer which broadens with higher amorphous drug loading and eventually narrowed down again for the crystal[62]. The variation in FWHM of uninteracted $(C=O)_{PVP}$ could be potentially due to the differential dipolar contribution of the heterogeneous states of molecular, amorphous and crystalline naproxen at different composition.

V.5.3 Relationship between the Kinetic Drug−Polymer Miscibility Limit and H-Bonding Interactions in QC Films

Considering the physical structure in QC dispersions being developed from the binary liquid state, i.e., molten drug and supercooled polymer ($>T_g$), it should represent the native behavior of the system that is unaffected by a third component like solvent in the case of SC films[14]. Heating the SC films, even the phase separated and partially crystalline ones, and rapidly cooling them ensures the trapping of the mixed state into the solid state[16,23,39]. Thus, the miscibility obtained by nonequilibrium kinetic input to the system is nominated as kinetic miscibility[6]. Likewise in SC films, heating rate dependence for T_{end} for different compositions was observed in QC films. A similar profile as that of SC films was apparent of the $\gamma_{naproxen}$ in PVP as a function of composition, obtained by the use of equilibrium melting points. The χ obtained for QC system by fitting eq V.4 was −2.40 (R^2 = 0.99), comparable to that for SC films. This value of χ was further used in eqs V.3 and V.4 to derive the solid liquid line for melt quenches as shown in the thermal phase diagram given in Figure V.12a. The comparable

intersection point of melting point depression line with T_{gm} line (x, y = 18% w/w naproxen, 115 °C) of the QC systems to that of SC films was in accordance with their identical χ value and T_{end} profile. As mentioned earlier, the slight negative deviation from the composition−T_{gm} profile calculated using the GT equation indicates the involvement of noncombinatorial drug−polymer interaction for the mixing in the binary system with the overwhelming contribution of increased free volume of mixing over the intercomponent interactions in solid solution[63].

Kalogeras has recently tested a quadratic polynomial expression, known as the BCKV (Brostow, Chiu, Kalogeras, Vassilikou-Dova) equation[64], to successfully describe the complex T_{gm} (% w/w) profile for the wide diversity of pharmaceutical solid dispersion systems[65]. The BCKV equation for naproxen−PVP system can be written as

$$T_{gm} = w_{naproxen}T_{g(naproxen)} + (1 - w_{naproxen})T_{g(PVP)} + w_{naproxen}(1 - w_{naproxen})[a_0 + a_1(2w_{naproxen} - 1) + a_2(2w_{naproxen} - 1)^2] \quad \text{Equation V.5}$$

where $T_{g(naproxen)}$, $T_{g(PVP)}$ and T_{gm} correspond to the T_g of pure naproxen, pure PVP and their blend, respectively, with w_{naproxen} being the weight fraction of naproxen. The empirical parameter a_0 along with its normalized expression ($a_0/\Delta T_g[(T_{g(\text{PVP})} - T_{g(\text{naproxen})}]$) has been explained as the representation of the differences between the cohesive and adhesive molecular interaction energies of the mixing components while a_1 and a_2 represent the strength of asymmetric contributions in mixing. Thus, the sign and magnitude of these adjustable parameters obtained by fitting eq V.5 to the experimental T_{gm} (% w/w) profile fairly provide a measure of the composition dependent energetic contribution of heteromolecular interaction, noncombinatorial entropy of mixing and hence the observed structural heterogeneities across the composition range[66]. The values of a_0, $a_0/\Delta T_g$, a_1 and a_2 estimated for our system were −91.63, −0.61, −11.18 and −22.52, respectively. Our BCKV fitting results are partly in agreement with that reported for naproxen−PVP K 90[65]. The negative values estimated for a_0 and $a_0/\Delta T_g$ indicate the prevailing entropic effect (excess volume of mixing) over the enthalpic one (H-bonding), as the case explained for another NSAID congener, ketoprofen with PVP K30.67 The asymmetric molar contributions due to smaller molar volume of naproxen molecules compared to that of PVP could have created the complex phase behavior of the system (a_1, $a_2 \neq 0$) leading to the induction of drug crystallization at higher naproxen content (≥75%). In contrast to the wide conformational flexibility in solution, the PVP molecules align in a finite number of conformations through

the dihedral angles across hydrocarbon backbone as well as the specific direction of dipole moment along the pyrrolidone side chain of PVP molecules as a function of temperature[54]. More precisely, the component of dipole moment that is fixed perpendicular to main chain contour of PVP coherently fluctuates with micro-Brownian motion of the main chain of the majority of PVP molecules with the increase in the distance between adjacent pyrrolidone rings during glass transition[54,55]. Thus, despite the increased kinetics of small naproxen molecules in its molten state (prominent rotational and diffusional motions) that can facilitate the penetration within interchain voids of polymer, the favorable polymer conformation for the establishment of specific H-bonding interaction would not be accessible to all the naproxen molecules present in the melt at certain composition. This is evident from the progressive increase in the heterogeneity in the QC films with the increase of naproxen as reflected from the increase in the T_{gm} width, the difference between the temperature at the starting of the step change (onset) and the end (endset), observed in the corresponding cooling curves depicted in Figure V.12b[68]. The declining trend of T_{gm} width from the melt composition with ≥45% w/w naproxen evidenced the apparent saturation of the sterically favorable PVP conformation for the establishment of the specific interaction. Thus, mixing upon further increase of naproxen content should be essentially kinetically driven[23].

Even at higher drug content, polymers are commonly demonstrated to act as effective kinetic crystallization inhibitors by marked reduction in nucleation rate provided the sufficiently faster rate processes, for example the solidification rate[69,70]. Rapid cooling of almost homogeneously mixed molten drug with the polymer in its supercooled liquid state ($>T_g$) in the melt results in an abrupt drop in the melt viscosity, which inhibits the diffusion of the drug molecules that are extensively screened between the polymer chains, hence inhibiting the growth of amorphous clusters to evolve into the nuclear size[70]. By testing cooling rate dependent crystalline demixing from the melt, the borderline composition was possible to be distinguished for QC dispersions of naproxen−PVP K 25. Specifically, cooling the melt with 70% naproxen, even at 0.2 °C/min, still renders it amorphous while that with 75% naproxen started showing a crystallization exotherm in the cooling curve when lowering the cooling rate down to 4 °C/min. Moreover, the two merged crystallization exotherms witnessed in the cooling and reheating curves of compositions up to 80% drug content imply the heterogeneous drug distributions at these compositions experiencing two different extents of crystallization inhibition related to the amount of polymer present at the local environment[45]. The change in crystalline modification at these compositions was ruled out by

the presence of identical peak height and positions in pXRD of naproxen crystals as that of pure naproxen.

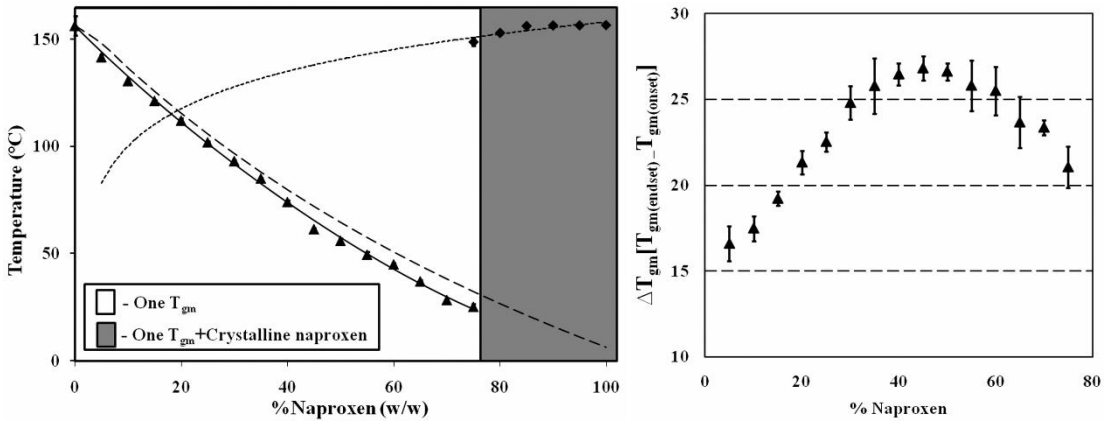

(a) **(b)**

Figure V.11 (a) Thermal phase diagram of naproxen−PVP in QC films (▲, T_{gm}; ◆, T_{end}; (⋯), T_{end} calculated by combining eqs V.3 and V.4; (- - -), theoretical T_{gm} predicted by GT equation; (-), fit to BCKV equation; a_0, −91.63 ± 2.24; a_1, −11.18 ± 5.64; a_2, −22.52 ± 13.83 (R^2 = 0.99)). (b) The plot of span of glass transition observed during quench cooling the melts (ΔT_{gm}) as a function of composition. The vertical error bars represent the range between the values from two independent measurements.

The spectral profiles for QC films point toward remarkably different fractions of intermolecular interactions built up as a function of composition. Up to 20% naproxen, a similar trend of peak area in the C=O stretching region as that of cast films was observed for QC samples. The dispersions obtained by heat cool cycle were visibly transparent without macroscopically distinct appearance across the wide composition range. The appearance of C=O vibration band ascribed to the strongly H-bonded fraction with a higher fraction of peak area compared to that in SC film with 25% naproxen suggests the involvement of a higher number of naproxen molecules H-bonded with PVP. The appearance of two (strong and weak) H-bonded fractions from 35% naproxen on suggests gradual increase in the saturation of favorable PVP conformations for naproxen to establish stronger H-bonding. The leveling off of the % peak area of the strongly H-bonded fraction from 45% naproxen suggests the apparent saturation of sterically suitable C=O of PVP for additional naproxen molecules to undergo such strong H-bonding. This is in agreement with the DSC data wherein from 45% naproxen T_{gm} width started decreasing. Additionally, the different C=O band composition observed from 75% naproxen also reflects it to be at the borderline of miscibility. Especially, from this composition there is a drastic decrease of H-bonded fractions along with the appearance of the C=O band of the naproxen dimer. The same explanation as that for the SC films also holds true here except for an additional vibration band observed at 1704 cm^{-1} for 75% and 80% naproxen. This could be from the fraction of crystalline naproxen which could have been more finely embedded in PVP to create the weaker catemer as developed in course

of crystallization of naproxen with the vibration band at the same position (Figure V.2b). This could be the reason for the appearance of two crystallization exotherms in cooling curves exclusively for these two compositions. We prepared quench-cooled naproxen with methods reported earlier that are claimed to generate amorphous naproxen[49,62]. However, only amorphicity up to 35−40% could be obtained with this method[6]. Thus, the difference observed was a broader catemer C=O peak and a higher intensity of the aromatic skeleton band compared to that in untreated crystalline naproxen powder which indicates increased disorder. In this way, the absence of the peak at 1704 cm^{-1} even in quench-cooled naproxen indicates the vital role of polymer in dissipating the crystallites into different populations with the same crystal structure but either a different habit or degree of order. Nevertheless, the use of thermal-FTIR for naproxen−PVP solid dispersions could clarify the temperature dependent evolution of different H-bonded interactions. The reversal of the peak maximum of non-H-bonded $(C=O)_{naproxen}$ band from 1718 cm^{-1} to 1728 cm^{-1} from the composition which is at or near to crystallization, i.e., 75% naproxen, could have the same origin as that discussed for SC films. The increased red shift in peak positions of the O−H stretching band of H-bonded naproxen in QC films as compared to SC films reflects slightly stronger overall H-bonding in the latter. The sharp decrease of FWHM of all C=O vibration bands, except that of H-bonded C=O stretching of the naproxen catemer, in QC dispersions with composition ≥75% naproxen points to the impact of the increased ordering or crystallization transition of higher fraction of drugs. However, the increasing FWHM of H-bonded C=O stretching band of naproxen could be also associated with the contribution from increasing amount of amorphous loading in PVP[62].

V.6 Conclusions

We prepared the naproxen/PVP K 25 solid dispersion films with several compositions through solution casting and quench cooling and then characterized them by thermal, spectroscopic and diffractometric analysis without preprocessing. The results revealed that SC films prepared by a near to equilibrium evaporation process provide information on the lower boundary of the kinetic miscibility (≤20% w/w naproxen in PVP), near to the interpolated equilibrium solid solubility along with the crystalline solubility to be ≤35% w/w naproxen. The solution state data such as PVP globular size and solution spectral profile in parts forecast the phase behavior in the resulting SC film. On the other hand, QC films generated from rapid cooling from the melt provide an estimate for the upper limit of kinetic miscibility (≤75% w/w naproxen) of the system. Accordingly, the different behaviors of composition dependent

strength and type of drug−drug and drug−polymer intermolecular H-bonding interactions were evidenced by ATR−FTIR analysis for the dispersions prepared by two different methods. The appearance of two (strongly and weakly) H-bonded fractions was observed at 25% naproxen for SC film and 35% for QC film. The favorable PVP conformation for specific drug−polymer interaction is saturated at 45% naproxen for QC dispersion. The different extent of conformational flexibility available for mixing components, especially PVP, in solution and at higher temperature is postulated as a plausible mechanistic explanation for the different phase and drug−polymer interaction behavior in solid dispersions prepared by solution casting and quench cooling. Thus, a substantial influence of the processing methods and parameters on the physical structure and stability for the solid dispersions can be expected for the compositions positioned within the obtained miscibility window (20−75% w/w naproxen).

V.7 References

1. Van den Mooter, G. The Use of Amorphous Solid Dispersions: A Formulation Strategy to Overcome Poor Solubility and Dissolution Rate. Drug Discov. Today: Tech. 2012, 9, e79–e85.
2. Padden, B. E.; Mill, J. M.; Robbins, T.; Zocharski, P. D.; Prasad, L.; Spence, J. K.; LaFountaine, J. Amorphous Solid Dispersions as Enabling Formulations for Discovery and Early Development. Amer. Pharm. Rev. 2011, 1, 66-73.
3. Alonzo, D. E.; Gao, Y.; Zhou, D.; Mo, H.; Zhang, G. G. Z.; Taylor, L. S. Dissolution and Precipitation Behavior of Amorphous Solid Dispersions. J. Pharm. Sci. 2011, 100, 3316-3331.
4. Newman, A.; Knipp, G.; Zografi, G. Assessing the Performance of Amorphous Solid Dispersions. J. Pharm. Sci. 2012, 101, 1355-1377.
5. Qian, F.; Huang, J.; Hussain, M. A. Drug-Polymer Solubility and Miscibility: Stability Consideration and Practical Challenges in Amorphous Solid Dispersion Development. J. Pharm. Sci. 2010, 99, 2941-2947.
6. Paudel, A.; Van Humbeeck, J.; Van den Mooter, G. Theoretical and Experimental Investigation on the Solid Solubility and Miscibility of Naproxen in Poly(vinylpyrrolidone). Mol. Pharmaceutics 2010, 7, 1133-1148.
7. Janssens, S.; De Zeure, A.; Paudel, A.; Van Humbeeck, J.; Rombaut, P.; Van den Mooter, G. Influence of Preparation Methods on Solid State Supersaturation of Amorphous Solid Dispersions: A Case Study with Itraconazole and Eudragit E100. Pharm. Res. 2010, 27, 775-785.
8. Albers, J.; Matthée, K.; Knop, K.; Kleinebudde, P. Evaluation of Predictive Models for Stable Solid Solution Formation. J. Pharm. Sci. 2011, 100, 667-680.
9. Gordon, M.; Taylor, J. S. Ideal Copolymers and the Second-order Transitions of Synthetic rubbers. i. Non-crystalline Copolymers. J. Appl. Chem. 1952, 2, 493-500.
10. Tobyn, M.; Brown, J.; Dennis, A. B.; Fakes, M.; Gao, Q.; Gamble, J.; Khimyak, Y. Z.; McGeorge, G.; Patel, C.; Sinclair, W.; Timmins, P.; Yin, S. Amorphous Drug–PVP Dispersions: Application of Theoretical, Thermal and Spectroscopic Analytical Techniques to the Study of a Molecule with Intermolecular Bonds in both the Crystalline and pure Amorphous State. J. Pharm. Sci. 2009, 98, 3456-3468.
11. Huang, J.; Li, Y.; Wigent, R. J.; Malick, W. A.; Sandhu, H. K.; Singhal, D.; Shah, N. H. Interplay of Formulation and Process Methodology on the Extent of Nifedipine Molecular Dispersion in Polymers. Int. J. Pharm. 2011, 420, 59-67.
12. Dalwadi S.; Soni T.; Thakkar V.; T., G. Silymarin-Solid Dispersions: Characterization and Influence of Preparation Methods on Dissolution. Acta. Pharm. 2010, 60, 427–443.

13. Weuts, I.; Van Dycke, F.; Voorspoels, J.; De Cort, S.; Stokbroekx, S.; Leemans, R.; Brewster, M. E.; Xu, D.; Segmuller, B.; Turner, Y. T. A. Physicochemical Properties of the Amorphous Drug, Cast films, and Spray Dried Powders to Predict Formulation Probability of Success for Solid Dispersions: Etravirine. J. Pharm. Sci. 2011, 100, 260-274.
14. Lauer, M. E.; Grassmann, O.; Siam, M.; Tardio, J.; Jacob, L.; Page, S.; Kindt, J. H.; Engel, A.; Alsenz, J. Atomic Force Microscopy-Based Screening of Drug-Excipient Miscibility and Stability of Solid Dispersions. Pharm. Res. 2011, 28, 1-13.
15. Paudel, A.; Van den Mooter, G. Influence of Solvent Composition on the Miscibility and Physical Stability of Naproxen/PVP K 25 Solid Dispersions Prepared by Cosolvent Spray-Drying. Pharm. Res. 2012, 29, 251-270.
16. Forster, A.; Hempenstall, J.; Tucker, I.; Rades, T. Selection of Excipients for Melt Extrusion with two Poorly Water-Soluble Drugs by Solubility Parameter Calculation and Thermal Analysis. Int. J. Pharm. 2001, 226, 147-161.
17. Desiraju, G. R. Supramolecular Synthons in Crystal Engineering—A New Organic Synthesis. Angew. Chem. Int. Edit. 1995, 34, 2311-2327.
18. Al-Obaidi, H.; Brocchini, S.; Buckton, G. Anomalous Properties of Spray Dried Solid Dispersions. J. Pharm. Sci. 2009, 98, 4724-4737.
19. Jubert, A.; Legarto, M. L.; Massa, N. E.; Tevez, L. L.; Okulik, N. B. Vibrational and Theoretical Studies of Non-Steroidal Anti-Inflammatory Drugs Ibuprofen [2-(4-isobutylphenyl) propionic acid]; Naproxen [6-methoxy-[alpha]-methyl-2-naphthalene acetic acid] and Tolmetin acids [1-methyl-5-(4-methylbenzoyl)-1H-pyrrole-2-acetic acid]. J. Mol. Struct. 2006, 783, 34-51.
20. Loebmann, K. A. M.; Laitinen, R.; Grohganz, H.; Gordon, K. C.; Strachan, C. J.; Rades, T. Co-amorphous Drug Systems: Enhanced Physical Stability and Dissolution Rate of Indomethacin and Naproxen. Mol. Pharmaceutics 2011, 8, 1919-1928.
21. Marsac, P. J.; Li, T.; Taylor, L. S. Estimation of Drug-Polymer Miscibility and Solubility in Amorphous Solid Dispersions using Experimentally Determined Interaction Parameters. Pharm. Res. 2009, 26, 139-151.
22. Tao, J.; Sun, Y.; Zhang, G. G. Z.; Yu, L. Solubility of Small-Molecule Crystals in Polymers: D-mannitol in PVP, Indomethacin in PVP/VA, and Nifedipine in PVP/VA. Pharm. Res. 2009, 26, 855-864.
23. Pinal, R. Entropy of Mixing and the Glass Transition of Amorphous Mixtures. Entropy. 2008, 10, 207-223.
24. Velazquez, M. M.; Valero, M.; Rodriguez, L. J.; Costa, S.; Santos, M. A. Hydrogen Bonding in a Non-Steroidal Anti-Inflammatory Drug-Naproxen. J. Photochem. Photobiol. B. 1995, 29, 23-31.
25. Tomasko, D. L.; Timko, M. T. Tailoring of Specific Interactions to modify the Morphology of Naproxen. J. Crystl. Growth 1999, 205, 233-243.
26. Taylor, L. S.; Langkilde, F. W.; Zografi, G. Fourier Transform Raman Spectroscopic Study of the Interaction of Water Vapor with Amorphous Polymers. J. Pharm. Sci. 2001, 90, 888-901.
27. Szaraz, I.; Forsling, W. A Spectroscopic Study of the Solvation of 1-vinyl-2-pyrrolidone and Poly (1-vinyl-2-pyrrolidone) in Different Solvents. Polymer. 2000, 41, 4831-4839.
28. Nair, R.; Nyamweya, N.; Gonen, S.; Martinez-Miranda, L. J.; Hoag, S. W. Influence of Various Drugs on the Glass Transition Temperature of Poly (vinylpyrrolidone): a Thermodynamic and Spectroscopic Investigation. Int. J. Pharm. 2001, 225, 83-96.
29. Halamova, D.; Zelenak, V. NSAID Naproxen in Mesoporous Matrix MCM-41: Drug Uptake and Release Properties. J. Incl. Phenom. Macrocycl. Chem. 2012, 1-9.
30. Wei, M.; Shi, S.; Wang, J.; Li, Y.; Duan, X. Studies on the Intercalation of Naproxen into Layered Double Hydroxide and its Thermal Decomposition by in situ FT-IR and in situ HT-XRD. J. Solid State Chem. 2004, 177, 2534-2541.
31. Painter, P. C.; Pehlert, G. J.; Hu, Y.; Coleman, M. M. Infrared Band Broadening and Interactions in Polar Systems. Macromolecules. 1999, 32, 2055-2057.
32. Hu, Y.; Motzer, H. R.; Etxeberria, A. M.; Fernandez-Berridi, M. J.; Iruin, J. J.; Painter, P. C.; Coleman, M. M. Concerning the Self-association of N-Vinyl Pyrrolidone and its Effect on the Determination of Equilibrium Constants and the Thermodynamics of Mixing. Macromol. Chem. Phys. 2000, 201, 705-714.

33. Chiu, C. Y.; Yen, Y. J.; Kuo, S. W.; Chen, H. W.; Chang, F. C. Complicated Phase Behavior and Ionic Conductivities of PVP-co-PMMA-Based Polymer Electrolytes. Polymer 2007, 48, 1329-1342.
34. Fleming, O. S.; Chan, K. L. A.; Kazarian, S. G. High-Pressure CO_2-Enhanced Polymer Interdiffusion and Dissolution Studied with in situ ATR-FTIR Spectroscopic Imaging. Polymer. 2006, 47, 4649-4658.
35. Martinez de Ilarduya, A.; Iruin, J. J.; Fernandez-Berridi, M. J. Hydrogen Bonding in Blends of Phenoxy Resin and Poly (vinylpyrrolidone). Macromolecules. 1995, 28, 3707-3712.
36. Hirasawa, N.; Danjo, K.; Haruna, M.; Otsuka, A. Physicochemical Characterization and Drug Release Studies of Naproxen Solid Dispersions using Lactose as a Carrier. Chem. Pharm. Bull. 1998, 46, 1027-1030.
37. Choperena, A.; Painter, P. Hydrogen Bonding in Polymers: Effect of Temperature on the OH Stretching Bands of Poly (vinylphenol). Macromolecules. 2009, 42, 6159-6165.
38. Reilly, J. T.; Walsh, J. M.; Greenfield, M. L.; Donohue, M. D. Analysis of FT-IR Spectroscopic Data: The Voigt Profile. Spectrochim. Acta A 1992, 48, 1459-1479.
39. Gordon, S. H.; Cao, X.; Mohamed, A.; Willett, J. L. Infrared Spectroscopy Method Reveals Hydrogen Bonding and Intermolecular Interaction Between Components in Polymer Blends. J. Appl. Polym. Sci. 2005, 97, 813-821.
40. Shinyashiki, N.; Imoto, D.; Yagihara, S. Broadband Dielectric Study of Dynamics of Polymer and Solvent in Poly (vinyl pyrrolidone)/Normal Alcohol Mixtures. J. Phys. Chem. B 2007, 111, 2181-2187.
41. Chen, S. C.; Kuo, S. W.; Chang, F. C. On Modulating the Self-Assembly Behaviors of Poly (styrene-b-4-vinylpyridine)/Octyl Gallate Blends in Solution State via Hydrogen Bonding from Different Common Solvents. Langmuir. 2011, 27, 10197–10205.
42. King, M. D.; Buchanan, W. D.; Korter, T. M. Application of London-type Dispersion Corrections to the Solid-state Density Functional Theory Simulation of the Terahertz Spectra of Crystalline Pharmaceuticals. Phys. Chem. Chem. Phys. 2011, 13, 4250–4259.
43. Mohan, R.; Lorenz, H.; Myerson, A. S. Solubility Measurement using Differential Scanning Calorimetry. Ind. Eng. Chem. Res. 2002, 41, 4854-4862.
44. Marsac, P. J.; Shamblin, S. L.; Taylor, L. S. Theoretical and Practical Approaches for Prediction of Drug-Polymer Miscibility and Solubility. Pharm. Res. 2006, 23, 2417-2426.
45. Sun, Y.; Tao, J.; Zhang, G. G. Z.; Yu, L. Solubilities of Crystalline Drugs in Polymers: An Improved Analytical Method and Comparison of Solubilities of Indomethacin and Nifedipine in PVP, PVP/VA, and PVAc. J. Pharm. Sci. 2010, 99, 4023-4031.
46. Dahlberg, C.; Dvinskikh, S.; Schuleit, M.; Furo, I. Polymer Swelling, Drug Mobilization and Drug Recrystallization in Hydrating Solid Dispersion Tablets Studied by Multinuclear NMR Microimaging and Spectroscopy. Mol. Pharmaceutics 2011, 8, 1247–1256.
47. Flory, P. J. Thermodynamics of High Polymer Solutions. J. Chem. Phys. 1941, 9, 660-661.
48. Huggins, M. L. Thermodynamic Properties of Solutions of Long Chain Compounds. Ann. N. Y. Acad. Sci. 1941, 43, 1-32.
49. Ayenew, Z.; Paudel, A.; Van den Mooter, G. Can Compression Induce Demixing in Amorphous Solid Dispersions? A Case Study of Naproxen-PVP K 25. Eur. J. Pharm. Biopharm. 2012, 81, 207-213.
50. Bhugra, C.; Shmeis, R.; Pikal, M. J. Role of Mechanical Stress in Crystallization and Relaxation Behavior of Amorphous Indomethacin. J. Pharm. Sci. 2008, 97, 4446-4458.
51. Bercea, M.; Eckelt, J.; Wolf, B. A. Vapor Pressures of Polymer Solutions and the Modeling of their Composition Dependence. Ind. Eng. Chem. Res. 2009, 48, 4603-4606.
52. Bolten, D.; Turk, M. Experimental Study on the Surface Tension, Density, and Viscosity of Aqueous Poly (vinylpyrrolidone) Solutions. J. Chem. Eng. Data 2011, 56, 582–588.
53. Lahmani, F.; Le Barbu-Debus, K.; Seurre, N.; Zehnacker-Rentien, A. Laser Spectroscopy of a Chiral Drug in a Supersonic Beam: Conformation and Complexation of S-(+)-Naproxen. Chem. Phy. Lett. 2003, 375, 636-644.
54. Tonelli, A. E. Conformational Characteristics of Poly (N-vinyl pyrrolidone). Polymer. 1982, 23, 676-680.

55. Shinyashiki, N.; Spanoudaki, A.; Yamamoto, W.; Nambu, E.; Yoneda, K.; Kyritsis, A.; Pissis, P.; Kita, R.; Yagihara, S. Segmental Relaxation of Hydrophilic Poly (vinylpyrrolidone) in Chloroform Studied by Broadband Dielectric Spectroscopy. Macromolecules. 2011, 44, 2140–2148.
56. Sajewicz, M.; Matlengiewicz, M.; Leda, M.; Gontarska, M.; Kronenbach, D.; Kowalska, T.; Epstein, I. R. Spontaneous Oscillatory in vitro Chiral Conversion of Simple Carboxylic Acids and its Possible Mechanism. J. Phys. Org. Chem. 2010, 23, 1066-1073.
57. Ivanov, I. T.; Tsokeva, Z. Effect of Chirality on PVP/Drug Interaction within Binary Physical Mixtures of Ibuprofen, Ketoprofen, and Naproxen: A DSC Study. Chirality. 2009, 21, 719-727.
58. Gupta, P.; Thilagavathi, R.; Chakraborti, A. K.; Bansal, A. K. Role of Molecular Interaction in Stability of Celecoxib-PVP Amorphous Systems. Mol. Pharmaceutics 2005, 2, 384-391.
59. Rumondor, A. C. F.; Wikstrom, H.; Van Eerdenbrugh, B.; Taylor, L. S. Understanding the Tendency of Amorphous Solid Dispersions to Undergo Amorphous-Amorphous Phase Separation in the Presence of Absorbed Moisture. AAPS PharmSciTech. 2011, 12, 1-11.
60. Ann Newman; David Engers; Simon Bates; Igor Ivanisevic; Ron C. Kelly; Zografi, G. Characterization of Amorphous API:Polymer Mixtures Using X-Ray Powder Diffraction. J. Pharm. Sci. 2008, 97, 4840-4856.
61. Qian, F.; Huang, J.; Zhu, Q.; Haddadin, R.; Gawel, J.; Garmise, R.; Hussain, M. Is a Distinctive Single T_g a Reliable Indicator for the Homogeneity of Amorphous Solid Dispersion? Int. J. Pharm. 2010, 395, 232-235.
62. Gupta, M. K.; Bogner, R. H.; Goldman, D.; Tseng, Y. C. Mechanism for Further Enhancement in Drug Dissolution From Solid-Dispersion Granules upon Storage. Pharm. Dev. Technol. 2002, 7, 103-112.
63. Schneider, H. A. Conformational Entropy Contributions to the Glass Temperature of Blends of Miscible Polymers. J. Res. Natl. Inst. Std. Technol. 1997, 102, 229-248.
64. Kalogeras, I. M. Description and Molecular Interpretations of Anomalous Compositional Dependences of the Glass Transition Temperatures in Binary Organic Mixtures. Thermochim. Acta. 2010, 509, 135-146.
65. Kalogeras, I. M. A Novel Approach for Analyzing Glass-Transition Temperature vs. Composition Patterns: Application to Pharmaceutical Compound+Polymer Systems. Eur. J. Pharm. Sci. 2011, 42, 470–483.
66. Brostow, W.; Chiu, R.; Kalogeras, I. M.; Vassilikou-Dova, A. Prediction of Glass Transition Temperatures: Binary Blends and Copolymers. Mater. Lett. 2008, 62, 3152-3155.
67. Di Martino, P.; Joiris, E.; Gobetto, R.; Masic, A.; Palmieri, G. F.; Martelli, S. Ketoprofen-Poly (vinylpyrrolidone) Physical Interaction. J. Cryst. Growth. 2004, 265, 302-308.
68. Mok, M. M.; Liu, X.; Bai, Z.; Lei, Y.; Lodge, T. P. Effect of Concentration on the Glass Transition and Viscoelastic Properties of Poly (methyl methacrylate)/Ionic Liquid Solutions. Macromolecules. 2011, 44, 1016–1025.
69. Van Eerdenbrugh, B.; Taylor, L. S. Small Scale Screening to Determine the Ability of Different Polymers to Inhibit Drug Crystallization upon Rapid Solvent Evaporation. Mol. Pharmaceutics 2010, 7, 1328-1337.
70. Kestur, U. S.; Taylor, L. S. Role of Polymer Chemistry in Influencing Crystal Growth Rates from Amorphous Felodipine. CrystEngComm. 2010, 12, 2390-2397.

Chapter VI: An Investigation into the Effect of Spray-Drying Temperature and Atomizing Conditions on Miscibility, Physical Stability, and Performance of Naproxen–PVP K 25 Solid Dispersions

The results described in this chapter are published in the following article:

Paudel, A.; Loyson, Y.; and Van den Mooter, G. (2013). An Investigation into the Effect of Spray-Drying Temperature and Atomizing Conditions on Miscibility, Physical Stability, and Performance of Naproxen–PVP K 25 Solid Dispersions. *Journal of Pharmaceutical Sciences*, 102 (4), 1249-1267.

VI. 1 Abstracts

The present study investigates the effect of changing spray-drying temperature (40°C–120°C) and/or atomizing airflow rate (AR; 5–15 L/min) on the phase structure, physical stability, and performance of spray-dried naproxen–polyvinylpyrrolidone (PVP) K25 amorphous solid dispersions. The modulated differential scanning calorimetry, attenuated total internal reflectance–Fourier transform infrared, and powder X-ray diffractometry (pXRD) studies revealed that higher inlet temperature (IT) or atomization airflow leads to the formation of amorphous phase-separated dispersions with higher strongly H-bonded and free PVP fractions, whereas that prepared with the lowest IT was more homogeneous. The dispersion prepared with the lowest atomization AR showed trace crystallinity. Upon exposure to 75% relative humidity (RH) for 3 weeks, the phase-separated dispersions generated by spray-drying at higher temperature or higher atomization airflow retained relatively higher amorphous drug fraction compared with those prepared at slow evaporation conditions. The humidity-controlled pXRD analysis at 98% RH showed that the dispersion prepared with highest atomization AR displayed the slowest kinetics of crystallization. The molecular-level changes occurring during crystallization at 98% RH was elucidated by spectroscopic monitoring at the same humidity. The rate and extent of the drug dissolution was the highest for dispersions prepared at the highest atomizing AR and the lowest for that prepared with the slowest atomizing condition.

VI.2 Introduction

In view of the progressive increase in the number of poorly water-soluble drug substances entering the early development phase, optimizing the oral bioavailability remains a major challenge to the pharmaceutical industry[1,2]. Over three decades, formulating poorly soluble active pharmaceutical ingredients (APIs) as amorphous solid dispersions in a polymer matrix has become one of the most preferred approaches for improving solubility- and dissolution rate-limited oral bioavailability[3]. Despite the accumulation of enormous research efforts, very few products based on this approach have been marketed. The reluctance of pharmaceutical companies to exploit this solubilization strategy is the inherently poor physical and chemical stability of the amorphous state of an API compared with its crystalline counterparts[4]. More specifically, phase separation and/or crystallization of API from amorphous dispersions diminish the claimed solubility advantage upon exposure to the elevated humidity and/or temperature during shelf life or with the exposure to the aqueous environment during product development or administration. On one hand, it has been realized

that the ultimate molecular miscibility and compositional homogeneity guarantee physically stable amorphous solid dispersions[5]. On the other hand, various thermodynamic and kinetic interplays introduced by the formulation variables and method of preparation are anticipated to have substantial influence on the initial phase structure and miscibility in the resulting multicomponent amorphous composites[6]. However, selection of formulation variables and manufacturing process for amorphous solid dispersions are still driven by trial and error, which makes it an expensive and time consuming process without guarantee of success. Particularly, the inadequate understanding on the impact of selecting a particular manufacturing process, processing conditions, as well as formulation variables on the phase structure and consequently on the stability of resulting amorphous systems has turned to be the current bottleneck behind the limited commercial success of this potent solubilization approach.

Spray-drying is a well-established and scalable unit operation with multiple applications in pharmaceutical industry[7]. Ultrafast solvent evaporation from the atomized solution makes one of the preferred preparation processes for supersaturated amorphous solid dispersion of poorly soluble drugs[8]. Countless research has been performed in the past focusing on the efficient process development of spray-dried amorphous solid dispersions (SDDs) of poorly soluble drugs[9]. Nevertheless, major efforts are made on the particle engineering aspects and on tailoring the micromeritic properties[9,10]. In spite of SDD being the subject of investigation for many years, only few attempts have been made to mechanistically characterize the role of process variables on the physical structure of SDD products[11,12]. Despite the well-known role of kinetic history applied during amorphization on phase homogeneity and physical stability of amorphous systems, a very limited number of attempts have been made in exploring the molecular level effects of multiple spray-drying process parameters on the resulting end products[13]. It is important to have an in-depth understanding of the variation in the molecular level miscibility and physical structure of SDD originating from the alteration of spray-drying temperature, spray rate, drying gas flow rate, atomization conditions, and so on, or their combination, as this is vital for the development of physicochemically stable SDD and subsequent scale up.

The present work aims to investigate the influence of spray-drying at different inlet temperature (IT) or rates of atomization airflow on the molecular level miscibility and moisture-induced phase-separation behavior/crystallization kinetics of naproxen–polyvinylpyrrolidone (PVP) K 25 SDDs. Naproxen–PVP K 25 with drug to polymer ratio of

4:6 (w/w) SDDs were prepared by spray-drying at three different ITs or three different atomization airflow rates (ARs) to identify independently the effect of these variables on the phase structure of the end product. Modulated temperature differential scanning calorimetry (mDSC), Fourier transform infrared (FTIR), and powder X-ray diffractometry (pXRD) were performed to evaluate the compositional homogeneity, drug–polymer interactions, and crystallinity of as prepared SDDs, respectively. The drug dissolution from SDDs prepared using different process parameters revealed the role of process parameters on the in vitro performance of the end products. Further, the solid-state analysis of SDD powders after the exposure to 75% relative humidity (RH) for 3 weeks or after subjecting to high compression pressure (565MPa) provided information on the influence of down-stream processing on the physical stability. pXRD measurements of samples at particular time interval at high RH (98%) was performed to examine the impact of spray-drying process parameters on the crystallization kinetics. This was complemented by time-resolved FTIR measurement at 98% RH of a SDD powder to understand the fate of molecular interactions during moisture-induced destabilization.

VI. 3 Materials and Methods

VI. 3.1 Materials

S-naproxen was obtained from CERTA Ltd. (Brainl'Allend, Belgium). PVP K 25 [molecular weight (MW) = 25 kDa] was kindly provided by BASF (Ludwigshafen, Germany). All other materials and solvents were of analytical or high-performance liquid chromatography (HPLC) grade.

VI. 3.2 Methods

VI. 3.2.1 Preparation of SDDs

The Pro-C-epT Micro spray-dryer (Zelzate, Belgium) was used to prepare the spray-dried products. The spray-dryer was built up with a large drying chamber, conveyer tube, cyclone, and product collector running in cocurrent mode. Compressed air was used as the drying gas. The process parameters except flow rate were precisely controlled using FIX MMIR$^{(R)}$ (version 7.0) (Intellution Inc., Reno, Nevada, USA). The solution was pumped using a peristaltic pump (Masterflex L/S, Cole-Parmer Instrument Company, London, UK), and feed rate was calibrated and set manually. A bifluid nozzle with an orifice diameter of 0.4mm was used. The spray-drying solution was prepared by dissolving 40% (w/w) naproxen and 60% (w/w) PVP K 25 in methanol (MeOH). The feed concentration was 10% (w/v) for all

experiments. The dispersions were prepared at three inlet air temperatures (ITs), *viz.* 40°C, 80°C, and 120°C or three atomization ARs, *viz.* 5, 10, and 15 L/min. The feed rate (1.5L/h) and drying AR (400 L/min) were set constant throughout the experiments. The final products were sieved through 300μm mesh and further dried at 25°C in a vacuum oven till constant weight. Subsequently, the samples were analyzed or otherwise stored airtight in an evacuated desiccator with P_2O_5 at 4°C.

VI. 3.2.2 Evaluation of Physical Stability upon Compression

The SDD powders were compressed using a manual hydraulic press (PerkinElmer, Norwalk, Connecticut) in a die of 13mm diameter with evacuation to prepare discs. The sample powders were compressed at approximately 565MPa with a dwell time of 1 min. Compressed samples were analyzed using mDSC and FTIR.

VI. 3.2.3 Storage at Elevated Relative Humidity

Equal weight of SDD powders, prepared using different process parameters, were transferred to DSC pans and stored inside the desiccator containing a saturated sodium chloride solution in water (75% RH) at room temperature. Samples were removed after 3 weeks, subsequently dried overnight in the presence of P_2O_5 at 40°C and analyzed using mDSC, FTIR, and pXRD to evaluate the physical stability.

VI. 3.2.4 Study of Moisture-Induced Crystallization of Drug from SDDs

The SDD powder was filled in DSC pans and placed on the custom-made aluminum holder (Appendix Figure 1). The well in the sample holder surrounding the sample was filled with saturated potassium sulfate solution in water and covered by a polyimide foil (Kapton®, DuPont Electronic Technologies, Rue General Patton, Luxembourg). The pXRD measurement was performed every 30 min on the sample, thus exposed to the highly humid environment (98% RH at 25°C) for several hours until no marked increase in crystallinity was observed. A similar procedure was followed for SDDs, prepared under all different IT or AR. The extent of moisture induced crystallization (EOC) at different time intervals was calculated by dividing the degree of crystallinity (DOC) at that time by the same at the plateau time point. The obtained crystallization profiles were fitted with the kinetic model proposed by Yang et al.[14] Also, the time-dependent micrographs were captured using light microscopy with cross-polarized light (Olympus, Center Valley, Pennsylvania, USA) of SDD powder

specimen enclosed inside a custom-made setup wherein moist air (98% RH) was circulated using a peristaltic pump.

A similar setup was used to measure the temporal attenuated total internal reflectance (ATR)–FTIR of a SDD sample prepared at IT of 80°C and AR of 10 L/min to understand the moisture-induced alteration of molecular interactions in the SDD. The SDD powder was directly mounted over the ATR crystal, and the sample holder well filled with saturated potassium sulfate solution was covered by inverting a glass vessel over it. FTIR scans were taken every 30 min interval for 8 h.

VI. 3.2.5 Analysis of Compositional Homogeneity by Modulated Differential Scanning Calorimetry

The modulated temperature DSC (mDSC) analysis of SDD powders was performed on a Q2000 DSC (TA Instruments, Leatherhead, UK) equipped with a refrigerated cooling system (RCS90) and a dry nitrogen purge (50mL/min). Indium was used to calibrate enthalpy and temperature, and sapphire disks were used to calibrate heat capacity. The temperature modulated heating program consisted of an amplitude 1°C and a period of 40 s at underlying heating rate of 2°C/min from −20°C to 160°C. Samples were prepared in crimped aluminum pans. The data acquisition and analyses were carried out using TA Instrument explorer software (version 6.10) and Universal Analysis, respectively (version 4.4; TA Instruments). The glass transition temperature (T_g) was analyzed in reversing heat flow (RHF) signal. Additionally, more information on T_g such as T_g width and relative proportions of T_gs was extracted from the first derivative of the RHF (dRHF) signal with respect to the temperature after optimum smoothing to remove baseline noise.

VI. 3.2.6 Thermogravimetric Analysis

The as prepared SDDs were analyzed using SDT Q600 (TA Instruments) to determine the moisture and volatile contents before vacuum drying. The samples were heated at 2°C/min from 30°C to 160°C in an inert environment maintained by dry N_2 purge at 100 mL/min. The percentage weight loss integrated up to 100°C was accounted for the moisture and solvent loss.

VI. 3.2.7 Assessment of Molecular Interactions by ATR–FTIR Spectroscopy

An ATR–FTIR spectrometer equipped with a deuterated triglycine sulfate detector and a horizontal single-reflection Zn–Se ATR assembly (Avatar 370 FT-IR with Smart endurance option, Thermo Nicolet, Thermo Scientific, Clintonpark Keppekouter, Erembodegem-Aalst,

Belgium) was used. The powder samples were placed over the ATR crystal and held by gently pressing a holder tower over it. The IR spectrum was collected as an average of 32 scans in the range of 4000–650 cm^{-1} at the spectral resolution of 4 cm^{-1} for each sample. Additionally, an evaporative- IR analysis of the feed solution was carried out using the same spectrometer assembly to mimic the fate of molecular interactions during solvent evaporation and particle formation in the course of spray-drying. A 50 μL solution containing 10% (w/v) solute (4% naproxen and 6% PVP) in MeOH was dispensed over the ATR crystal and covered by the perforated lid. An IR spectral acquisition was made at the defined time interval up to the maximum solvent evaporation and film formation at room temperature.

VI. 3.2.8 Powder X-Ray Diffractometry Analysis

The SDD powders before and after exposure to 75% RH were analyzed on an automated X'pert PRO diffractometer (PANalytical, Almelo, The Netherlands) in transmission mode with a Cu Kα source and the generator set at 45 kV and 40 mA. The samples were placed between two Kapton$^{(R)}$ foils and clamped on the Teflon ring of sample holders. All samples were analyzed in continuous scan mode in the range of $4° \leq 2\theta \leq 40°$ with the step size and time of 0.0021° and 19.685 s, respectively. The X'Pert HighScore Plus version 2.2a (PANalytical) was used to analyze pXRD data and to obtain the area under peaks. The ratio of the net area under the curve (AUC) of the most intense Bragg peak above the amorphous halo to the total area at 19.5± 0.5° 2θ was compared for the relative crystallinity in the dispersions after exposure to 75% RH.

For the moisture-induced crystallization study at 98% RH, the measurements were carried out in the same 2θ range using 0.0170° step size and 20.029 s counting time. The areas of all Bragg peaks appearing at a particular time were used to estimate the DOC. The area of aluminum diffraction peak at 38.26° 2θ from DSC pan was taken as an internal standard and the DOC at different time interval was estimated by:

$$Degree\ of\ Crystallinity\ (DOC) = \frac{\sum_i^n AUC_{Bragg\ peak}}{\sum_i^n AUC_{Bragg\ peak} + \sum_i^n AUC_{amorphous\ halo}} \times 100 \ldots\ldots \text{Equation VI.1}$$

where *AUC* is area under curve at i^{th} Bragg peak or halo beneath at particular 2θ and *n* is total number of peaks present over amorphous halo in a diffractogram.

VI. 3.2.9 In Vitro Drug Dissolution Testing

The *in vitro* dissolution studies were performed using USP II dissolution apparatus (SR8 dissolution test station; Hanson Virtual Instruments, Chatsworth, California, USA) consisting of a temperature controlled water bath maintained at 37°C. The stirring speed of the paddles was set to 100 rpm. Three hundred milliliters of simulated gastric fluid without pepsin (2 g NaCl in 7mL HCl diluted to 1000mL with deionized water and adjusted to pH of 1.2) containing 0.02% (w/v) sodium dodecyl sulfate was used as the dissolution medium for all experiments. The total SDD content in the dissolution vessel was fixed to 75mg so that a maximum concentration of naproxen is 0.1mg/mL, which is above the equilibrium solubility of naproxen in the selected medium (0.014 mg/ mL). One-milliliter samples were withdrawn during 60 min and always replaced by the same volume of fresh medium. The samples were filtered through 0.45μm polytetrafluoroethylene membrane filter (Henke Sass Wolf, Tuttlingen, Germany) and assayed by HPLC for naproxen content. All experiments were preformed in triplicate.

VI. 3.2.10 HPLC Analysis

The drug content was assayed using an HPLC made up of a Merck Hitachi pump L7100, an ultraviolet detector (L7400), an autosampler (L7200), an interface (D7000), and a LiChrospher 60 RP Select-B C-18 column (5μm, 12.5× 0.4 cm) (all from Merck, Darmstadt, Germany). The method was isocratic with the mobile phase made up of 70% MeOH (HiPerSolv Chromanorm, Research Park, Haasrode, Leuven, Belgium) and 30% 25mM sodium acetate buffer (pH 3.5). The wavelength used for the detection was 270 nm.

VI. 4 Results

VI.4.1 Miscibility, Infrared Spectroscopy, and Dissolution Profiles of SDDs

As mentioned in Table VI.1, SDDs are provided with a code as per the process parameters set during the preparation. Henceforth, these codes are used to represent the respective SDD for simplicity. All SDDs prepared with 40% (w/w) naproxen in this study were X-ray amorphous except $IT_{80}AR_5$. A small Bragg peak at 19.5° 2θ over the amorphous halo in the pXRD profile of the latter indicated the presence of trace crystallinity (Figure VI.1). In general, two major diffuse halos at the positions related to that for amorphous PVP (ca. 15° and 20° 2θ) were dominant in all pXRD patterns[15]. As mentioned in Table VI.1, the thermogravimetric analysis (TGA) data for the moisture and/or solvent retained in the obtained SDDs (before secondary drying) showed the dependence of the process parameters

employed to prepare them. Expectedly, the process parameters resulting in the slowest solvent evaporation rate, *viz*. lowest IT or AR (larger droplets) led to the dispersions with the highest residual solvent content.

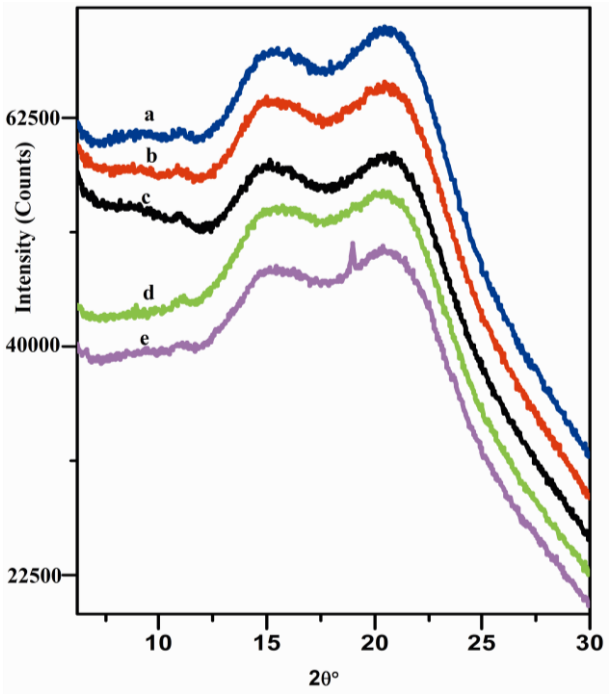

Figure VI.1 The pXRD patterns of $IT_{80}AR_{15}$ (a), $IT_{120}AR_{10}$ (b), $IT_{80}AR_{10}$ (c), $IT_{40}AR_{10}$ (d), and $IT_{80}AR_{5}$ (e).

Table VI.1 Glass Transition Temperature (T_g) and Width of T_g, Percentage FTIR Relative Peak Intensity of Vibration Bands at 1658 and 1631 cm^{-1} in $\upsilon_{C=O}$ Regions Normalized with Respect to Peak at 1672 cm^{-1}, Drug Content and Percentage Residual Content Before Secondary Drying, the Initial Rate of Dissolution Estimated from the Slope of Cumulative Amount Dissolved Versus Time up to 20 min and Maximum Percentage of Naproxen Dissolved During Drug Dissolution from SDDs Prepared with Different Process Parameters

Process parameters					%relative intensity of IR peak at[a]		%w/w naproxen by HPLC[b]	% Initial residual content by TGA[a]	Dissolution rate up to 20 min ($\times10^6$ g/mL.min)	Maximum %naproxen dissolved[b]
IT (°C)	AR (L/min)	Process Code	T_g (°C)[a]	T_g width (°C)[a]	1658 cm^{-1}	1631 cm^{-1}				
40	10	$IT_{40}AR_{10}$	70.51±0.24	21.51±1.42	83.74±0.27	83.39±0.17	41.89±0.24	5.03±0.27	0.75	34.84±1.34
80	5	$IT_{80}AR_{5}$	72.74±0.59	25.90±1.25	79.26±0.00	79.12±0.03	38.67±0.44	4.79±0.12	0.85	28.95±0.96
80	10	$IT_{80}AR_{10}$	68.29±0.41	28.21±1.50	90.53±0.18	90.26±0.24	39.18±0.86	4.41±0.22	0.73	35.34±2.02
80	15	$IT_{80}AR_{15}$	64.22±1.90	32.90±0.29	98.31±0.03	92.61±0.05	39.55±0.93	4.08±0.14	1.11	43.19±0.59
120	10	$IT_{120}AR_{10}$	61.52±1.99	29.68±0.14	93.30±0.01	98.16±0.28	38.88±0.45	3.60±0.37	1.03	35.21±1.13

[a]Average ± range (n = 2), [b]Average ± SD (n = 3).

Figure VI.2 depicts the overlay of mDSC thermograms of SDDs prepared with the different process parameters. The RHF signals of all dispersions showed slightly discontinuous glass transition step changes except for that of $IT_{40}AR_{10}$. This is more apparent in the corresponding first dRHF signals. The dRHF signals suggested that the SDDs prepared with higher IT or AR were phase separated to a higher extent compared with those prepared

with the lower values of processing parameters. Although the T_g of phase-separated SDDs were not sufficiently distinct to integrate individually, it can be visualized from the corresponding dRHF signals that the predominant contribution in overall T_g is from the drug-rich domain with the lower local T_g value (higher dips). As listed in Table VI.1, the overall T_g values of SDDs prepared with the higher IT and AR were comparatively lower indicating the presence of a higher fraction of drug-rich domain. The compositional heterogeneity was further compared based on the width of the glass transition event observed for different SDDs. The $IT_{80}AR_{15}$ displayed the widest T_g region indicating the highest extent of phase inhomogeneity. This was followed by $IT_{120}AR_{10}$, whereas $IT_{40}AR_{10}$ displayed the narrowest T_g. The information on relative contributions from the domains rich in drug and rich in polymer in the T_g region of inhomogeneous dispersions were further apparent from the ratio taken of the height of drug-rich dip to that of polymer-rich dip obtained along the T_g region in the dRHF signals of respective SDDs, as reported in Table VI.2. The results overall indicated that the process parameters leading to the higher rate of solvent evaporation results in amorphous–amorphous-phase separated dispersions. In contrast, the slower solvent evaporating conditions did generate SDDs with comparatively higher amorphous miscibility but also with some trace crystallinity in case of $IT_{80}AR_5$.

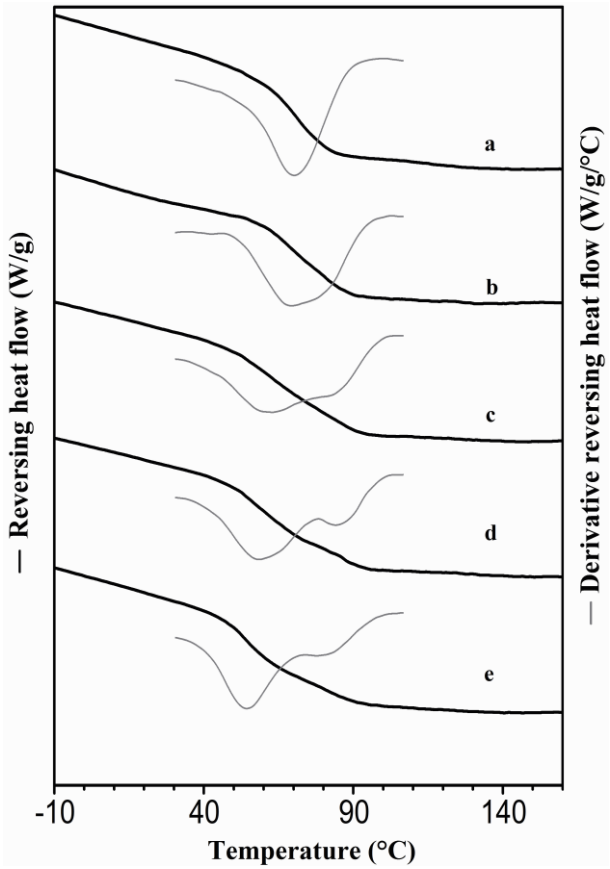

Figure VI.2 An overlay of mDSC thermograms of $IT_{40}AR_{10}$ (a), $IT_{80}AR_5$ (b), $IT_{80}AR_{10}$ (c), $IT_{80}AR_{15}$ (d), and $IT_{120}AR_{10}$ (e).

Table VI.2 The Average Values ± Range (n = 2) of Peak Temperatures Obtained in the Derivative RHF (dRHF) and Ratio of Peak Height of Drug-Rich to Polymer-Rich Dips Along T_g in (dRHF) Signals of SDDs Prepared with Different Process Parameters; as Prepared and After Compression at 565MPa with 1 min Dwell Time

Process code	As prepared			After compression at 565 MPa for 1 min		
	T_g drug rich (°C)	T_g polymer rich (°C)	Ratio of dRHF height ($\frac{\text{drug rich}}{\text{polymer rich}}$)	T_g drug Rich (°C)	T_g polymer rich (°C)	Ratio of dRHF height ($\frac{\text{drug rich}}{\text{polymer rich}}$)
$IT_{40}AR_{10}$		-Na-		55.73±0.37	72.17±0.37	0.75±0.37
$IT_{80}AR_{5}$	70.52±1.71	77.15±0.37	1.06±0.03	54.03±0.97	79.37±0.78	1.99±0.06
$IT_{80}AR_{10}$	63.56±2.30	81.71±2.17	1.24±0.11	53.30±1.99	76.15±1.29	1.57±0.14
$IT_{80}AR_{15}$	58.81±0.86	72.33±1.04	1.69±0.01	54.20±1.47	72.33±1.77	0.97±0.06
$IT_{120}AR_{10}$	54.77±1.37	75.03±2.88	2.29±0.34	57.17±2.28	75.03±1.81	1.18±0.02

Na, not applicable.

The alteration in solid-state intermolecular interactions in the resulting SDDs due to the underlying processing parameters is demonstrated by the overlay of normalized partial FTIR spectra in the carbonyl stretching ($\upsilon_{C=O}$) in Figure VI.3. Naproxen–PVP K 25 solid dispersion has been extensively characterized by FTIR spectroscopy before[16]. The spectrum of crystalline naproxen (dashed line) is characterized by the presence of vibrational bands attributable $\upsilon_{C=O\ (nap\ monomer)}$ and $\upsilon_{C=O\ (nap\ dimer)}$ positioned respectively at 1728 and 1681 cm^{-1}, whereas the PVP spectrum (dotted line) showed a single $\upsilon_{C=O\ (PVP\ amide)}$ peak at 1658 cm^{-1}. The spectra of SDDs showed a decrease in the relative peak intensity and position of $\upsilon_{C=O\ (nap\ monomer)}$, disappearance of $\upsilon_{C=O\ (nap\ dimer)}$, presence of $\upsilon_{C=O\ (PVP\ amide)}$ because of the residual unperturbed functionality of PVP as well as the appearance of two new vibration bands. These additional peaks are the contribution from the stretching of hydrogen- bonded $C=O_{PVP\ amide}$ with naproxen (COOH). The vibration band at 1672 cm^{-1} is attributable to the weakly H-bonded fraction, whereas that at 1631 cm^{-1} is from the strongly H-bonded fraction. The relative peak intensity of of $\upsilon_{C=O\ (nap\ monomer)}$ band appeared similar for all SDDs. The spectra normalized to the most intense peak at 1672 cm^{-1} exhibited the marked difference in relative peak intensities of vibration bands corresponding to strongly H-bonded fraction and free $C=O_{PVP\ amide}$ fraction appearing as a shoulder. The percentage relative peak intensities of these bands with respect to the highest band at 1672 cm^{-1} are given in Table VI.1. The spectra of $IT_{120}AR_{10}$ showed that the strongly H-bonded band had almost the same intensity of that of the weakly H-bonded band. The relative peak intensity of this peak was lesser for SDDs prepared at low IT and/or AR; the lowest intensity was observed for the $IT_{80}AR_{5}$ condition, which also exhibited trace crystallinity. The relative peak intensity of free $C=O_{PVP\ amide}$ band

was in order of $IT_{80}AR_{15}$> $IT_{120}AR_{10}$> $IT_{80}AR_{10}$> $IT_{40}AR_{10}$> $IT_{80}AR_5$. In correlation with DSC data, these spectroscopic results implied that the SDDs prepared with higher IT or AR showing higher extent of separated (drug rich) phase also showed the presence of higher fraction of strongly H-bonded and free $C=O_{PVP\ amide}$ fraction.

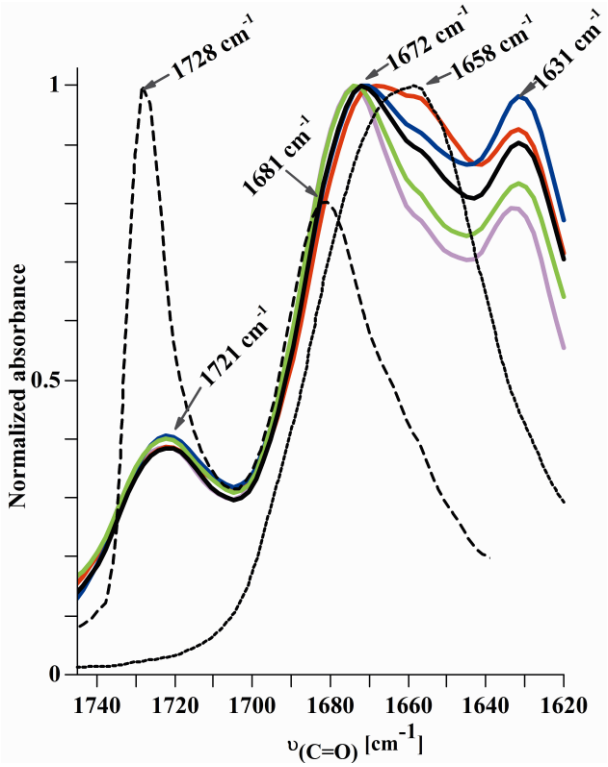

Figure VI. 3 An overlay of partial ATR–FTIR spectra ($\upsilon_{C=O}$ regions) of SDDs prepared with different process parameters; $IT_{40}AR_{10}$ (green), $IT_{80}AR_5$ (pink), $IT_{80}AR_{10}$ (black), $IT_{80}AR_{15}$, and $IT_{120}AR_{10}$ (blue). The spectra of crystalline (dashed line) and PVP (dotted line) are overlayed for comparison. The spectra of SDDs are normalized with respect to the most intense vibration band at 1672 cm^{-1}.

The drug dissolution profiles from SDDs prepared by different process parameters are illustrated in Figure VI.4. The drug dissolution from naproxen–PVP solid dispersions is reported before[17]. The dissolution profiles obtained from SDDs prepared with different process parameters were not drastically different; especially, the initial rates of dissolution up to 20 min were similar. The maximum percentage cumulative drug dissolved and the rate of dissolution obtained by regressing (R^2:>0.98) the initial linear dissolution profiles from different SDDs are reported in Table VI.1. The extent as well as the rate of drug dissolution from $IT_{80}AR_{15}$ is the highest, and the maximum drug dissolved was the least from slightly crystalline $IT_{80}AR_5$. More precisely, the cumulative percentage drug dissolved was higher during initial time points for $IT_{120}AR_{10}$ and $IT_{80}AR_{15}$, whereas the same was the lowest for $IT_{80}AR_5$, the dispersion with trace crystallinity in the beginning. The declining trend of the dissolved naproxen was observed thereafter, which indicated the precipitation of drug due to crystallization from the supersaturated solution. This was evidenced from the visible haziness

of dissolution media as well as from the birefringence in the hazy samples when observed through polarized light microscopy (see appendix).

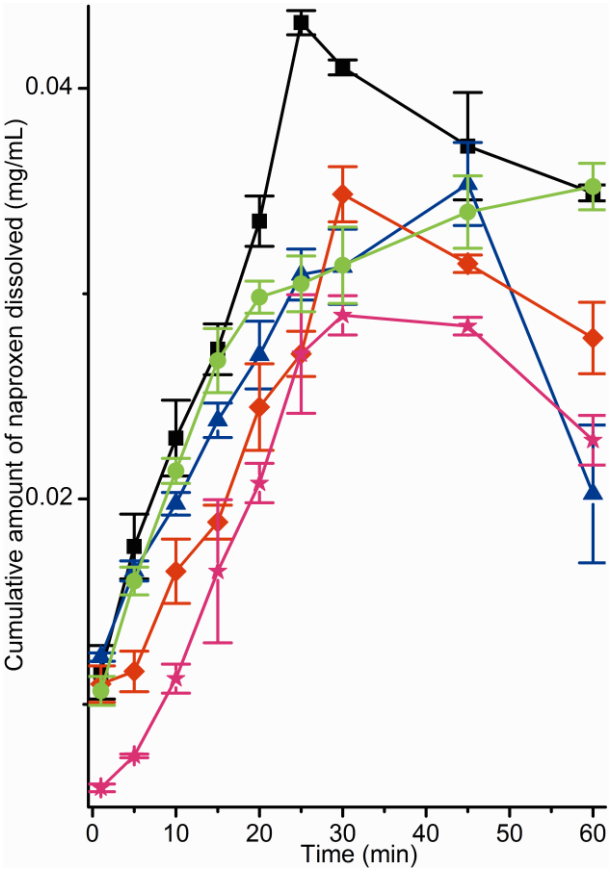

Figure VI. 4 The plots of cumulative amount of naproxen dissolved versus time obtained during powder dissolution studies of $IT_{40}AR_{10}$ (-♦-), $IT_{80}AR_{5}$ (-★-), $IT_{80}AR_{10}$ (-▲-), $IT_{80}AR_{15}$ (-■-), and $IT_{120}AR_{10}$ (-●-). The error bars are the standard deviation of the replicate measurements (n = 3).

VI.4.2 Phase Separation and/or Crystallization under Stress Conditions

The compression force and dwell time higher than that relevant to pharmaceutical tableting were initially tested to assess the stability of SDDs based on our previous experience on the compression-induced demixing of naproxen–PVP K 25 SDDs[18]. As apparent from the broad T_g and two peaks in respective dRHF signals (Figure VI.5), compression-induced phase separation or altered phase composition in SDDs. $IT_{40}AR_{10}$ previously exhibiting a continuous step change exhibited a discontinuous glass transition upon compression with the higher polymer-rich fraction. In comparison with the uncompressed dispersions, the marked increase in polymer-rich fraction was apparent from thermograms of $IT_{120}AR_{10}$ and $IT_{80}AR_{15}$, whereas the drug-rich fraction appeared predominant in $IT_{80}AR_{10}$ and $IT_{80}AR_{5}$ upon compression. As for the untreated samples, the compression induced restructuring of drug-rich and polymer-rich phase composition in SDDs prepared with various process parameters are presented in Table VI.2 as the ratio of drug-rich to polymer-rich height of dRHF dips

along T_g regions of respective dispersions. The changes in phase composition of amorphous SDDs upon compression were also supported by the alteration in molecular interaction evidenced in the corresponding FTIR spectra (Figure VI.6). In general, compression facilitated the increase in the relative peak intensity of free $\upsilon_{C=O\ (PVP\ amide)}$ for all SDDs. Likewise mDSC thermograms, the different relative intensities of the peaks in $\upsilon_{C=O}$ region for the SDDs prepared by different process parameters upon application of the same compression force pointed toward the diverse extent of distortion in H-bonding interactions. The compression initiated phase heterogeneity in $IT_{40}AR_{10}$ was evidenced by the marked decrease in the normalized intensity of strongly H-bonded peak was adjunct to the concurrent increase in free $\upsilon_{C=O\ (PVP\ amide)}$ band intensity. The relative increase in the contribution of polymer-rich fraction in T_g after compression is supported by the decrease in relative intensity of weakly H-bonded peaks and concomitant increase in the free $\upsilon_{C=O\ (PVP\ amide)}$ for $IT_{120}AR_{10}$ and $IT_{80}AR_{15}$.

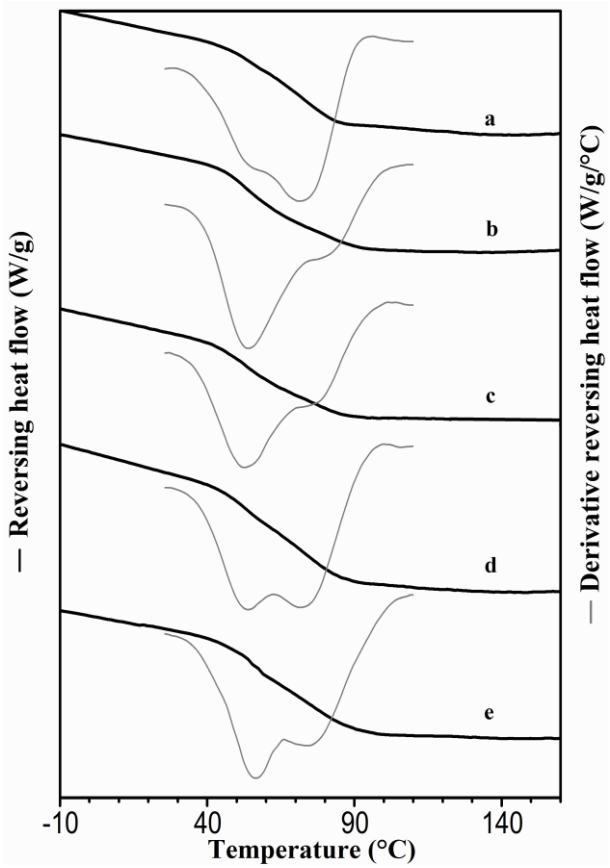

Figure VI. 5 An overlay of mDSC thermograms of SDDs prepared with different process parameters recorded after subjecting to the compression pressure of 565MPa. $IT_{40}AR_{10}$ (a), $IT_{80}AR_5$ (b), $IT_{80}AR_{10}$ (c), $IT_{80}AR_{15}$ (d), and $IT_{120}AR_{10}$ (e).

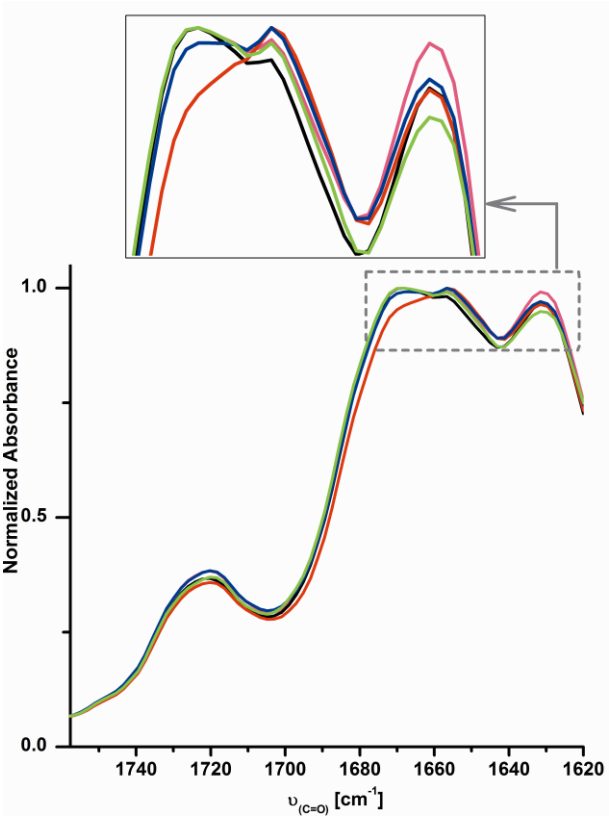

Figure VI. 6 An overlay of partial ATR–FTIR spectra ($\upsilon_{C=O}$ regions) of SDDs prepared with different process parameters after subjecting to the compression pressure of 565MPa; $IT_{40}AR_{10}$ (green), $IT_{80}AR_5$ (pink), $IT_{80}AR_{10}$ (black), $IT_{80}AR_{15}$, and $IT_{120}AR_{10}$ (blue). The spectra are normalized with respect to the most intense vibration band at 1672 or 1658 cm^{-1}.

Regardless of process parameters, the storage of SDDs at 75% RH for 3 weeks led to the extensive amorphous–amorphous phase separation, accompanied by partial crystallization of naproxen. As illustrated in mDSC overlay in Figure VI.7, three very distinct T_gs were apparent in the thermograms of all SDDs. In addition, appearance of sharp Bragg peaks superimposed over amorphous halo indicated the notable fraction of naproxen crystallization induced by moisture. The position of lower (T_{g1}), middle (T_{g2}), and higher (T_{g3}) glass transition temperature were slightly different for the SDDs originating from different processing conditions. As listed in Table VI.3, T_{g1}values were comparatively lower for $IT_{120}AR_{10}$ and $IT_{80}AR_{15}$ when compared to that of $IT_{40}AR_{10}$ and $IT_{80}AR_5$. This denotes that SDDs prepared with higher IT or AR still retained a higher fraction of amorphous naproxen in the drug-rich domain. The value of T_{g2} was comparable for all dispersions except that for $IT_{40}AR_{10}$. The highest value of T_{g3} was observed for $IT_{120}AR_{10}$ and the lowest for $IT_{80}AR_5$. Apart from the positions of different T_gs the relative contributions from different phase-separated domains can be semi-quantitatively compared among SDDs prepared with different process parameters from the calculated percentage *AUC* of T_g in dRHF (eq VI.2).

$$\%\, dAUC_i = \left(\frac{dAUC_i}{dAUC_1 + dAUC_2 + dAUC_3}\right) \times 100 \quad \text{……Equation VI.2}$$

where $\%dAUC_i$ is the percentage *AUC* in dRHF of i^{th} T_g (i = 1, 2, or 3). The *%dAUC* values for different T_gs of SDDs prepared by different process parameters are listed in Table VI.3. The $\%dAUC_1$ (of T_{g1}) was the highest for $IT_{80}AR_{15}$ followed by that for $IT_{120}AR_{10}$, again indicating that these dispersions are constituted of a higher fraction of amorphous drug-rich domain compared with those prepared with lower IT or AR. The comparatively higher values of$\%dAUC_2$ and$\%dAUC_3$ of $IT_{80}AR_5$ and $IT_{40}AR_{10}$ than that of SDDs prepared by higher IT or AR implied a higher relative fraction of polymer-rich domains. In addition to the amorphous phase compositions, the crystallinity induced by moisture in these partially crystalline dispersions was also comparatively different (Figure VI.8). The comparison of percentage relative peak intensity of the most intense Bragg peak (at 19.5°2θ) signified that the highest relative crystallinity was developed in $IT_{80}AR_5$, which already exhibited trace crystallinity upon preparation. Despite the higher initial compositional heterogeneity, $IT_{80}AR_{15}$ exhibited the lowest relative crystallinity, followed by $IT_{120}AR_{10}$. This is in agreement with the mDSC data indicating the higher fraction of amorphous drug-rich domains in the latter dispersions. In comparison with the pXRD patterns of the freshly prepared dispersions, the decreased relative intensity of low-angle PVP amorphous halo at 15°2θ was apparent in the pXRD patterns of all SDDs after exposure to elevated humidity. As illustrated in the overlay of FTIR spectra of SDDs after storage at elevated humidity (Figure VI.9), notable changes could be observed in the intermolecular interaction profiles. Overall, the $\upsilon_{C=O\ (PVP\ amide)}$ appeared as the most abundant vibration band in the normalized $\upsilon_{C=O}$ spectral region indicating the increased fraction of unperturbed C=O (PVP amide) freed upon the partial crystallization of the H-bonded naproxen with the same. Relative to this band, the normalized intensity of other characteristic peaks for different SDDs showed alteration with process parameters applied. The peak maximum of $\upsilon_{C=O\ (nap\ monomer)}$ shifted toward that of crystalline naproxen at 1728 from 1721 cm^{-1} for $IT_{80}AR_5$ and $IT_{40}AR_{10}$. The shoulders due to the vibration band attributable to weakly H-bonded $C{=}O_{PVP\ amide}$ for $IT_{80}AR_{15}$ and $IT_{120}AR_{10}$ were distinct, and the relative peak intensities of the same were higher as compared with that prepared with lower IT or AR. Also, the relative peak intensities of the vibration band from strongly H-bonded $C{=}O_{PVP\ amide}$ were comparatively higher for $IT_{80}AR_{15}$ and $IT_{120}AR_{10}$ (Table VI.3). These results again pointed toward the higher fraction of amorphous naproxen remained in

moisture-ridden partially crystalline SDDs prepared with higher IT or AR compared with those prepared with the lower values of these parameters.

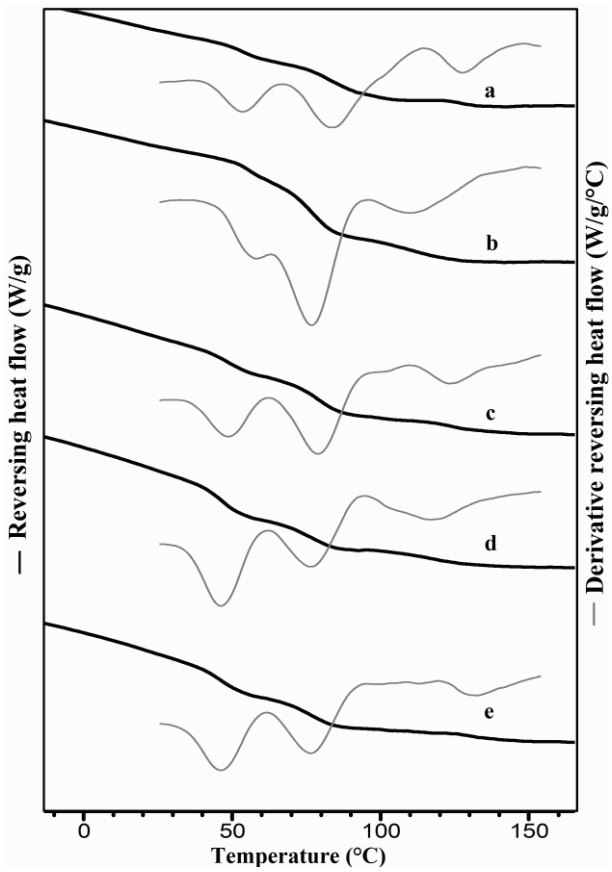

Figure VI. 7 An overlay of mDSC thermograms of SDDs prepared with different process parameters recorded after storage at 75% RH for 3 weeks. $IT_{40}AR_{10}$ (a), $IT_{80}AR_{5}$ (b), $IT_{80}AR_{10}$ (c), $IT_{80}AR_{15}$ (d), and $IT_{120}AR_{10}$ (e).

Table VI.3 The Average Values ± Range (n = 2) of Glass Transition Temperatures (T_gs) and Percentage Area Under Curves in dRHF (*%dAUC*) of T_gs, Percentage FTIR Relative Peak Intensity of Vibration Bands at 1672 and 1631 cm^{-1} in $\upsilon_{C=O}$ Regions Normalized with Respect to Peak at 1658 cm^{-1} and Percentage pXRD Relative Peak Intensity at 19.5° 2θ of SDDs Prepared with Different Process Parameters Analyzed After Exposure to 75% RH for 3 Weeks

Process code	T_g (°C)			% area under curve (AUC) of dRHF[a]			%relative intensity of IR peak at		% relative crystallinity calculated at 19.5° 2θ
	T_{g1}	T_{g2}	T_{g3}	% $dAUC_1$	% $dAUC_2$	% $dAUC_3$	1672 cm^{-1}	1631 cm^{-1}	$(=\frac{AUC_{peak} \times 100}{AUC_{peak} + AUC_{halo}})$
$IT_{40}AR_{10}$	53.14±0.85	82.21±1.59	126.91±1.59	25.63	50.00	24.38	85.25±0.22	82.85±1.08	18.03±1.59
$IT_{80}AR_{5}$	55.72±2.03	76.45±1.36	108.76±3.35	13.86	67.42	18.73	83.79±0.41	78.76±0.43	25.11±2.80
$IT_{80}AR_{10}$	48.25±1.19	78.11±2.40	122.21±0.91	30.82	53.76	15.41	90.85±0.80	85.81±0.54	15.93±1.79
$IT_{80}AR_{15}$	47.53±1.22	77.56±1.80	119.40±2.74	42.94	39.88	17.18	94.91±0.32	93.12±0.71	9.54±2.44
$IT_{120}AR_{10}$	46.61±0.79	76.28±2.21	131.86±1.28	40.68	47.46	11.86	92.80±0.15	92.76±0.35	13.70±0.83

[a]Calculated using average dAUC [(J/g ◦C) and (n = 2)] using eq VI.2.

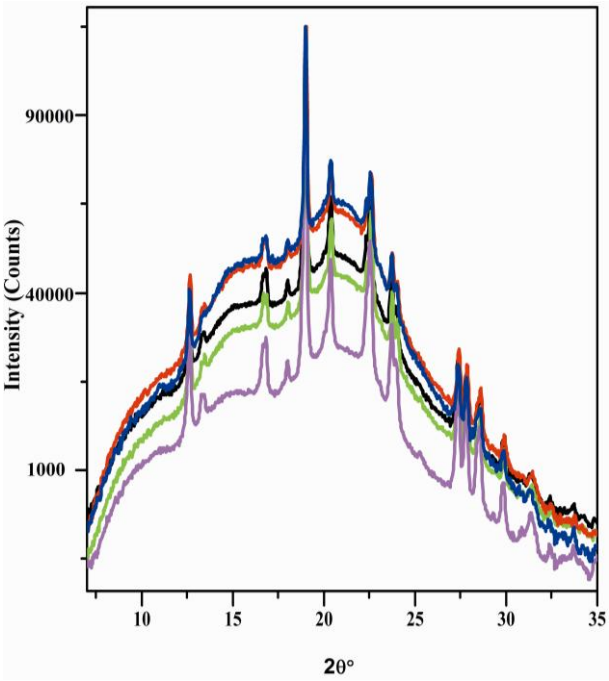

Figure VI. 8 An overlay of pXRD patterns of SDDs prepared with different process parameters recorded after storage at 75% RH for 3 weeks; $IT_{40}AR_{10}$ (green), $IT_{80}AR_{5}$ (pink), $IT_{80}AR_{10}$ (black), $IT_{80}AR_{15}$, and $IT_{120}AR_{10}$ (blue). The diffractograms are normalized with respect to the most intense Bragg peak at 19.5° 2*θ*.

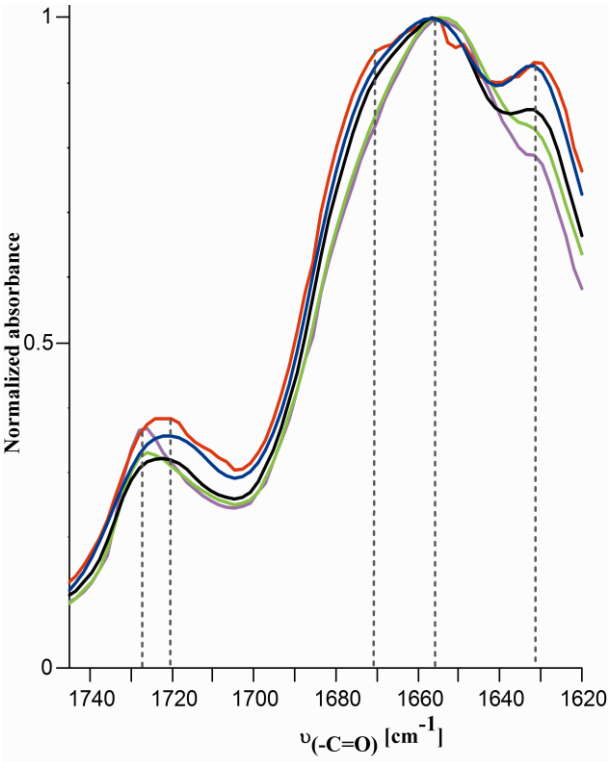

Figure VI. 9 An overlay of partial ATR–FTIR spectra ($\upsilon_{C=O}$ regions) of SDDs prepared with different process parameters after storage at 75% RH for 3 weeks; $IT_{40}AR_{10}$ (green), $IT_{80}AR_{5}$ (pink), $IT_{80}AR_{10}$ (black), $IT_{80}AR_{15}$, and $IT_{120}AR_{10}$ (blue). The spectra are normalized with respect to the most intense vibration band at 1658 cm^{-1}.

The moisture-induced isothermal crystallization profiles of naproxen from SDDs prepared using different process parameters are plotted as function of time in Figure VI.10a. The progression of crystal growth in different planes due to moisture is illustrated in the time-

dependent pXRD patterns given in Figure VI.10b.The maximum DOC estimated for all SDDs were similar except that for $IT_{80}AR_5$. The latter dispersion consisting of trace crystallinity already at the beginning (Figure VI.1) underwent faster crystallization and to a considerably higher extent when compared with the rest of the SDDs. The crystallization from $IT_{80}AR_{15}$ started half an hour later than the remaining three SDDs and progressed with the slowest rate. Overall, the individual amorphous halo of PVP was not distinguishable in SDDs in presence of sorbed moisture.

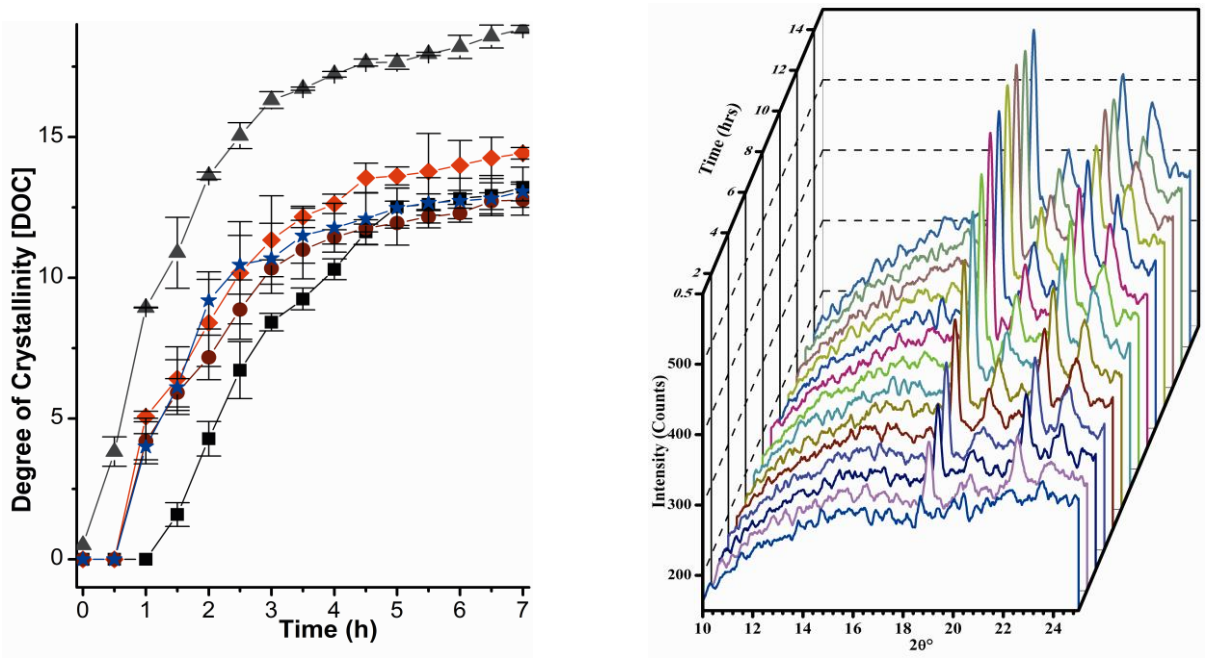

(a) **(b)**

Figure VI. 10 (a) The plots of DOC (mean values) of naproxen versus the time of exposure to 98% RH of SDDs prepared with different process parameters. $IT_{40}AR_{10}$ (-★-), $IT_{80}AR_5$ (-▲-), $IT_{80}AR_{10}$ (-♦-), $IT_{80}AR_{15}$ (-■-), and $IT_{120}AR_{10}$ (-●-). The vertical bars are the range between two independent measurements. (b) The pXRD patterns of IT80AR10 recorded at different time point at 98% RH.

VI.5 Discussion

VI. 5.1 Process Parameters Mediated Compositional Heterogeneity–Molecular Interaction of SDDs

The composition selected for the present investigation was based on our previous studies of the binary phase behavior of the selected drug–polymer system[16,19]. The SDDs of naproxen prepared with three very different MWPVPs (2.4–1100 kDa) under a set of process parameters were amorphous up to 50% (w/w) drug content.19 A drug loading of ≥40% (w/w) naproxen is required to obtain partially crystalline naproxen in naproxen–PVP K 25 cast films prepared from MeOH with the slowest evaporation rate possible thus providing a clue on the worst case scenario[16]. The phase structures of SDDs prepared preliminarily with ≤35% (w/w) naproxen content were less responsive to the alteration in spray-drying process parameters. This means applying multiple processing conditions to prepare SDD with <40% (w/w)

naproxen can generate acceptable physical structure. The presence of surface crystallites of naproxen in amorphous naproxen–PVP K 17 SDD particles prepared with ≥40% (w/w) naproxen from alcoholic solution has been reported before[20]. This information points to the suitability of 40% (w/w) drug loading for investigating the molecular level effects such as miscibility and physical stability of the process parameters of the naproxen–PVP K 25 SDDs.

The three ITs here are higher than (120°C), near to (80°C), and lower (40°C) than the T_g of the amorphous quench-cooled film of same drug–polymer composition (ca. 74°C)[16]. The IT_{40} is even lower than the boiling point of MeOH (ca. 65°C). The straightforward interpretation of the effect of IT is on the rate of solvent evaporation from the droplets during particle formation. Furthermore, the other complex rate processes would be highly altered at these three temperatures. With faster evaporation rate, very rapid diffusion rate of solute molecules accompanied by turbulent molecular motions hinder the reorganization or ordering; hence, low possibility of crystallization[13]. In contrast, slow solvent evaporation allows sufficient time or the molecular stacking or reorganization that can mediate nucleation/crystallization. A significant reduction in crystallinity is reported upon spray-drying of a poorly water-soluble crystalline ursodeoxycholic acid at higher IT compared with lower temperature[21]. This was attributed to higher extent of disruption in intermolecular H-bonding during spray-drying at higher temperature. The influence of IT on the underlying phenomena during particle formation could be more pronounced for multicomponent systems, for example, (amorphous) solid dispersion preparation. Spray-drying of artemisinin with maltodextrin at higher IT resulted in microparticles with lesser drug crystallinity leading to a proportional increase in drug solubility compared with those produced at lower IT[12]. The dissolved solutes in multicomponent droplets with significantly different Peclet numbers tend to phase separate macroscopically or at molecular level due to their different diffusional velocities during particle formation process[8]. Moreover, the gap in conformational flexibility and molecular diffusivity between small molecular-sized drugs and polymers can markedly increase at higher temperature, which can mediate amorphous–amorphous phase separation in SDDs prepared at very high temperature as observed in the present case[22].

The atomization nozzle ARs employed in the present study were well controlled within the working range of the spray-dryer. Process parameters such as IT, feed rate, as well as atomizing conditions have vital influence on atomization intensity and droplet characteristics[13]. In the bifluid nozzle used in the present study, the compressed atomizing air flows through an outer tube, whereas the feed solution is dispensed through the inner tube.

Both of these fluids encounter/mix at the nozzle tip immediately leading to the atomization of liquid feed into droplets. The variation made in nozzle AR has direct influence on the droplet size and distribution. Higher AR results in smaller droplet size as well as higher shear forces in the liquid feed during droplet formation. Assuming uniform droplet formation, the diameter of an uncoalesced droplet (*D*) can be approximated from the feed rate (FR) and nozzle AR using eq VI.3 (the derivation of this expression is provided in appendix):

$$D = \sqrt[1/2]{\frac{6\times FR}{AR}\times (d_{ic}^2 - d_{on}^2)} \ldots\ldots\ldots\ldots\text{Equation VI.3}$$

where d_{ic} and d_{on} are the inner orifice diameter of the nozzle cap and outer orifice diameter of the nozzle, respectively. The calculated droplet diameters obtained upon spraying the feed at AR_5, AR_{10}, and AR_{15} are about 101, 71, and 58 μm, respectively. The rapid solvent evaporation from smaller multicomponent droplets is reported to generate smaller or coalesced particles wherein the spatial phase composition can be a function of the radius[23]. Therefore, the local T_g can also be expected to differ. The very fast diffusion rate of naproxen molecules as compared with that of PVP could mediate the different mechanisms and extent of spatial liquid–liquid phase separation during extremely faster evaporation from smaller droplets; thus, possibly resulting in a difference in the spatial phase distribution in SDD particles originating from varying drying temperature and/or atomizing conditions. The varying degree of drug enrichment at the surface of PVP-based amorphous dispersion particles prepared by solvent methods has been characterized for the dispersions prepared by different solvent evaporation rates[24]. The degree of plasticization from surface to core has been excellently modeled based on the dRHF profiles of spatial T_g for maltodextrin particles exposed to moisture[25]. Additionally, localized nanothermal analysis or surface selective analytical techniques such as atomic force microscopy or time-of-flight secondary ion mass spectrometry (SIMS) of SDD particles could further provide evidence of spatial phase composition/ distribution[11,26]. During slower solvent evaporation from larger droplets resulting from medium AR and at the lowest IT could allow sufficient time for the conformational fluctuation for PVP, and transport of PVP molecules get sufficient vicinity with fast moving drug molecules, both favoring the molecular mixing process. This could be the reason for higher homogeneity of $IT_{40}AR_{10}$. However, decreasing the nozzle AR further to 5L/min might produce the largest droplets wherein very slow solvent evaporation might have favored trace crystallinity in spite of higher IT, as observed in case of $IT_{80}AR_5$.

Apart from IT and AR, the outlet temperature (T_{out}) attained while spray- drying at a particular set of process parameters can have vital influence on the phase structure of the resulting SDD particles[27]. As mentioned in Table VI.4, all process combinations resulted in T_{out} below the boiling point of MeOH. The higher T_{out} ensures lower residual solvent levels in the final product. The relative solvent saturation of drying gas at T_{out} ($\%RS_{out}$) and energy input by drying gas (E_D) can be calculated for different sets of process parameter combinations by eqs. VI.4 and VI.5, respectively[9]:

$$\%RS_{out} = \frac{\left(\frac{P_{chamber}}{P_{MeOH}}\right)}{\left(1+\frac{\left(\frac{DR}{MW_{air}}\right)}{\frac{FR\times(1-X_{solid})}{MW_{MeOH}}}\right)} \times 100 \text{.....Equation VI.4}$$

$$E_D = DR \times C_P^{air} \times (IT - T_{out}) \text{ .....Equation VI.5}$$

where $P_{chamber}$ is absolute pressure within the drying zone, P_{MeOH} is equilibrium vapor pressure of *MeOH* at the respective T_{out}. *DR* and FR are drying airflow and feed rate, respectively. *MW*, *Cp*, and X_{solid} are molecular weight, specific heat capacity, and solid mass fraction in the feed, respectively. The relative degree of solvent saturation at outlet temperature reflects the residual solvent content in the final particles prepared by a different process parameter set (Table VI.1). The highest solvent saturation and the lowest energy input for $IT_{40}AR_{10}$ and the lowest solvent saturation and the highest energy input for $IT_{120}AR_{10}$ are in agreement with the residual solvent content in the same. As $T_{outlet} < T_g$, none of the glassy dispersions generated should have underwent supercooling while exiting from the outlet of the drying zone assuming negligible exposure of solid SDD particles to IT environment. As T_{out} is dependent on a combination of FR, drying gas flow rate, and nozzle AR, T_{out} was found different for three IT values. At a constant IT, T_{out} was found similar for three AR values. The theoretical droplet-to-particle residence time (T_D) inside the drying chamber within the known distance between drying gas inlet and outlet in a spray-dryer (*H*) and radius of drying chamber (*R*) can be calculated using eq VI. 6[28]:

$$T_D = \pi \times R^2 \times H \times \left(\frac{IT}{T_{outlet}}\right) \times (1 - X_{MeOH}) \text{ .....Equation VI.6}$$

where X_{MeOH} is the mole fraction of solvent in the drying gas at the outlet. As mentioned in Table VI.4, at different IT or AR, the residence time of particles would be markedly dependent upon the outlet temperature. Especially, with faster solvent evaporation immediately after liquid atomization, less dense and hollow particles formed might entrain for longer time in the drying zone. Kojima et al[11]. Recently demonstrated with the spatial T_g

mapping using nanothermal analysis that SDDs prepared with higher evaporation rate constitute of higher extent of heterogeneity despite of indistinguishable bulk T_g from that of SDD prepared under the slower evaporating conditions. The authors cited Sen et al[29]. to explain the observation that hollow particles formed during immediate droplet drying under very fast evaporating condition due to the insufficient solute diffusion time toward the core (Peclet number>>1) can subsequently undergo heteromolecular phase segregation while spanning longer duration at higher temperature. Similar explanation is most likely valid for the current scenario.

Table VI. 4 The Outlet Temperature Recorded at Different Process Conditions During Spray Drying and Percentage Relative Solvent Saturation of Drying Gas at Outlet Temperature, Drying Energy Input, and Residence Time of Particles in Drying Zone Calculated Therefrom Using Eqs VI.4, VI.5, and VI.6

Process code	T_{outlet} (°C)	%Relative solvent saturation at outlet ($\times 10^4$)	Energy input by drying gas (KJ/min)	Residence time in drying zone (s)
$IT_{40}AR_{10}$	28	4.12	5.76	5.60
$IT_{80}AR_{15}$	38	2.09	20.16	8.25
$IT_{80}AR_{5}$	41	2.52	18.72	7.64
$IT_{80}AR_{10}$	40	2.19	18.96	7.84
$IT_{120}AR_{10}$	53	1.29	32.16	8.87

To anticipate the fate of intermolecular H-bonding interactions in the course of SDD particle formation to a certain extent, the solvent evaporation from a small volume of feed solution at ambient condition was monitored spectroscopically. Complete film formation was visualized in 10 min. The normalized absorbance profiles of solute peaks in $\upsilon_{C=O}$ region and CH_3 peak of MeOH at 1022 cm^{-1} are presented in Figure VI.11. As expected, the most intense peak at the beginning was from the solvent. Apart from the solvent peak, free and strongly H-bonded $\upsilon_{C=O(PVP\ amide)}$ are visible initially (ca. <1 min), which could be the characteristic saturation time of these states of PVP. From this time onward, the abrupt evolution and progression of most of the solute vibration bands points to a high rate of solidification. The rate of free $\upsilon_{C=O(PVP\ amide)}$ predominated over concomitantly rising strongly and weakly H-bonded $\upsilon_{C=O(PVP\ amide)}$ while free $\upsilon_{C=O(naproxen\ \ monomer)}$ progressed the slowest. The molecular interaction profiles from this experiment are not absolutely representative for the contactless droplet drying process as drying AR used during spray-drying is several magnitudes higher. However, it provides evidence of the fact that for the current drug–polymer–solvent combination the alteration in polymer vitrification/film formation kinetics or other rate processes originated from the different solvent evaporation temperature, and/or the size of droplets generated can potentially alter the molecular interactions in the resulting solid state; hence, developing diverse physical structures of SDDs. MeOH can form multiple H-bonds

with a single naproxen molecule or its dimer existing in solution. The number of H-bonding of ethanol per naproxen molecule is reported to linearly decrease with the increase in temperature over a wide temperature range[30]. This evidenced that the higher fraction of naproxen molecules should be able to H-bond strongly upon MeOH evaporation at higher IT than at lower IT. This resulted in the higher fraction strongly H-bonded domain in $IT_{120}AR_{10}$. Also, the solution characteristics of PVP might be markedly influenced by different process parameters employed. Especially, an increased degree of rotational freedom for the pyrrolidone group through the C–C backbone of PVP chains at higher temperature could generate conformational microheterogeneties in solution with which naproxen and MeOH molecules would get a differential extent of interaction accessibilities[16]. The higher electron density on C=O for a certain conformation of PVP in aqueous solution has been reported due to the migration of lone pair electrons from N toward C=O at higher temperature[31]. Likewise, in the present case a fraction of accessible PVP conformations with higher electron density at higher IT might have generated strongly H-bonded fractions with naproxen while naproxen molecules entrapped within the free space of PVP chains might have weakly H-bonded with less favorable PVP conformations. Simultaneous thermal, spectroscopic, microscopic and diffractometric online monitoring (possible inside an acoustic levitator) of the evolution of molecular interactions and phase structure in the course of drying of the levitated feed droplet of different size at varying temperature and/ or speed of drying gas could further improve our scientific understanding[32].

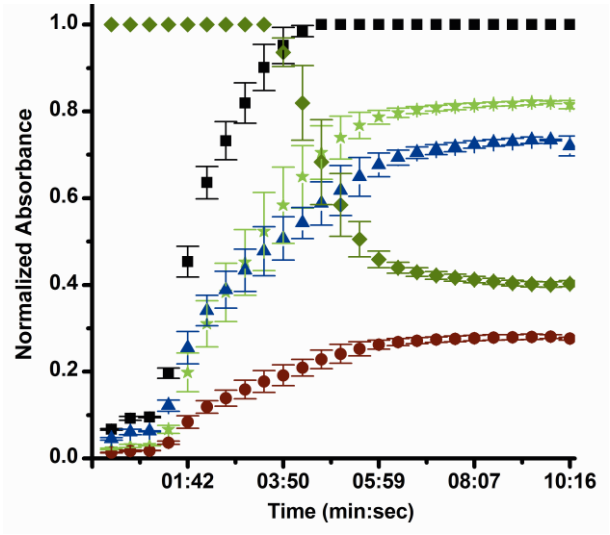

Figure VI. 11 The relative normalized peak intensities recorded of the vibration bands appearing in υC O regions of feed solution used in spray drying [naproxen–PVP (4:6) solution in MeOH (10%, w/v)] as function of time during solvent evaporation. $\upsilon_{C=O(naproxen\ monomer)}$ (-●-), strongly (-★-) and weakly (-▲-) H-bonded $C=O_{PVP\ amide}$ with naproxen, free $\upsilon_{C=O(PVP\ amide)}$ (-■-) and CH_3 of MeOH (-♦-). The error bars represent the standard deviation of three measurements.

VI. 5.2 Relating Phase-Separation Behavior to Initial Phase Structure and Preparation Conditions

The diverse physical stability of SDDs generated with different process parameters an indeed originate primarily from their different extent of initial phase heterogeneity. However, the particle properties such as morphology, size (distribution), surface topography and energy, density, and hygroscopicity that are directly inherited by SDD particles from a particular set of process parameters could contribute in parts to the altered physical stability upon exposure to the extreme compression force or elevated humidity.

The induction of molecular demixing between naproxen and PVP K 25 from homogenous amorphous SDD with different drug to polymer ratio subjected to different compression force is recently reported by us[18]. The evidence of the overall increase in free $C{=}O_{PVP\ amide}$ in compressed samples was observed in comparison with the uncompressed dispersions. The varying extent of segmental motion of PVP chains expected in SDDs with different miscibility might result in a diverse extent of conformational flexibility during plastic deformation. The comparatively higher fraction of free PVP after the compression of $IT_{120}AR_{10}$ and $IT_{80}AR_{15}$ might be due the presence of higher initial H-bonded fractions. The increase in polymer-rich fraction in $IT_{40}AR_{10}$ is supported by the smallest relative intensity of strongly H-bonded peak. The increased extent of compression induced structural relaxation is reported in amorphous solids having higher bulk volume[33]. In this way, the variation in a range of particulate level properties of SDDs prepared with different process parameters will contribute at least in parts to the diverse molecular level effect of compression observed in naproxen–PVP amorphous dispersions. Recently, through the dynamic-SIMS depth profiling on tablet prepared by amorphous ibipinabant–PVP dispersion, Leane et al[34]. revealed that compression induces PVP surface enrichment. The ease of surface enrichment by free $C{=}O_{PVP\ amide}$ should be possible during compression of hollow SDD particles prepared under fast solvent evaporating condition wherein radial phase separation can exist. This could be the reason for the relatively higher free $C{=}O_{PVP\ amide}$ in $IT_{120}AR_{10}$ and $IT_{80}AR_{15}$. The higher proportion of strongly H-bonded fraction generated upon compression of $IT_{80}AR_{5}$ could be attributable to the further densification of strongly H-bonded domains upon intermolecular diffusion in the denser particles formed under slower solvent evaporation.

The phase-separated naproxen–PVP dispersions generated after isothermal conditioning of amorphous SDDs prepared with varying process parameters at elevated humidity (75% RH) for 3 weeks showed different phase distributions. The concomitant

presence of three amorphous domains with different fractions of amorphous naproxen mixed with PVP (three T_gs) along with a part of crystallized naproxen fraction (pXRD) certainly indicate the nonequilibrium state of these heterogeneous composites[35]. The time-dependent moisture-induced phase separation and crystallization in naproxen–PVP K 25 SDD with different feed composition is reported before[36]. On the basis of the initial status of miscibility, the extent of phase separation/crystallization could be anticipated to a lesser extent from SDD with higher blend homogeneity, for example, from $IT_{40}AR_{10}$. As such, it was counterintuitive that the fraction of amorphous drug-rich domain was higher and relative crystallinity was lower in SDDs with higher initial heterogeneity, *viz*. $IT_{120}AR_{10}$ and $IT_{80}AR_{15}$ upon exposure to elevated humidity. However, this could be molecularly explained on the basis of higher fraction of free $C{=}O_{PVP\ amide}$ present in these phase-separated dispersions and with the unique behavior reported for unperturbed PVP in presence of moisture. Provided the uninteracted state of the pyrrolidone moiety, the presence of moisture leads to the open chain structure of PVP with the pyrrolidone ring perpendicular to the hydrocarbon backbone compared with an anhydrous environment wherein these interacting side chains are entangled within the folded main chain[37]. The authors have proposed this as the mechanism behind the increased amorphization of naproxen and other profens in drug–PVP physical mixtures after exposure to higher humidity as a function of time. The marked decrease in relative intensity of the low angle amorphous halo at 15° 2θ (the characteristic scattering distance attributable to a short range order parameter between chain segments mainly belonging to different interpenetrating chains of PVP) compared with that in pure PVP as well as that in the corresponding as prepared SDDs support similar effects of moisture in the present case as well[15]. On the other hand, the glass transition of PVP K 25 is reported to occur at 25°C upon equilibration at or beyond 65% RH, hence it transforms into a mobile rubbery state[38]. This moisture-induced rubbery and favorable conformational state of excess unperturbed PVP, available in phase-separated SDDs prepared at fast solvent evaporating conditions, could be available to a certain extent for the reestablishment of H-bonding with the free naproxen molecules that are generated by the simultaneous moisture-induced breaching of weakly H-bonded domains and thus inhibiting nucleation and crystal growth. Upon exposure to humidity, this might result in a higher fraction of amorphous naproxen and drug-rich amorphous domain in SDDs with higher initial free $C{=}O_{PVP\ amide}$ content. Although in case of homogeneous $T_{40}AR_{10}$ with comparatively lesser fraction of free $C{=}O_{PVP\ amide}$ and predominant weakly H-bonded fractions, there would be insufficient PVP in a favorable conformational state to rescue highly mobile naproxen molecules that are liberated upon moisture-induced distortion of existing H-

bonding with PVP from crystallization. In addition, with the initial trace crystallites acting as seed nuclei in presence of moisture, the highest extent of crystallization was evident from $T_{80}AR_5$. We acknowledge here that further spatial and temporal analysis by advanced surface analytical tools in hyphenation with chemical depth profiling techniques is necessary for better understanding of the contribution of the process-dependent particulate level properties on the diverse phase-separation (distribution) behavior of respective SDDs.

VI. 5.3 Moisture-Induced Crystallization Kinetics and Dissolution Profiles of Naproxen from SDDs

The moisture-induced crystallization kinetics of drug from SDDs prepared with varying process parameters were studied at high RH (98% RH) to accelerate the process so that nucleation/crystal growth triumph the amorphous–amorphous-phase-separation process. The excess sorbed water at higher %RH can act as the solvent for a fraction of PVP in the rubbery state[15]. This could facilitate the clustering of water molecules around naproxen–PVP phases wherein water molecules potentially compete or supersede for H-bonding with PVP in parallel to weakening or breakage of the existing naproxen–PVP H-bonds. The condensation of water was not visible in any sample up to the period of monitoring. This is also evident from pXRD patterns in Figure VI.10b wherein no halo corresponding to the phase separated/bulk water could be visualized. The simplified power equation proposed by Yang et al.[14] was utilized to fit the experimental data on crystallization kinetics (eq VI.7).

$$EOC = \frac{K \times t^n}{(1+K \times t^n)} \quad \text{.....Equation VI.7}$$

where *EOC* is the extent of crystallization representing the fraction of crystalline drug at storage time *t*. *K* and *n* are the apparent temperature-dependent rate constant and the temperature-independent order parameter depending upon nucleation/growth mechanism and the fractal of crystal growth dimension.

The plots of drug crystallization kinetics from different SDDs with the fitting parameters (*K* and *n*) are displayed in Figure VI.12. The longest induction time for crystallization was observed for $IT_{80}AR_{15}$ whereas $IT_{80}AR_5$ was already slightly crystalline at time zero. Likewise, the value of *K* was the lowest for $IT_{80}AR_{15}$, the highest for $IT_{80}AR_5$, and medium and comparable among the rest of the SDDs. This is in agreement with the moisture-induced phase separation observed in different SDDs. The order parameters obtained should correspond to the dimensionality of crystal growth from SDDs[39]. In all cases, the values of *n* obtained are around two signifying the nearly disc-like crystal growth except for $IT_{80}AR_{15}$

where *n* is >3. Therefore, the growth of spherulite like crystals could be anticipated from the latter. The time-dependent photographs taken using polarized light microscopy under similar humidity conditions revealed the distinct spherules-like fractal of crystal growth from $IT_{80}AR_{15}$ as compared to the disc-like growth from the rest of the SDDs. Some representative micrographs are included in the appendix. The difference in the kinetics and the EOC observed from SDDs prepared with varying process parameters can be related in parts with the initial phase structure of SDDs.

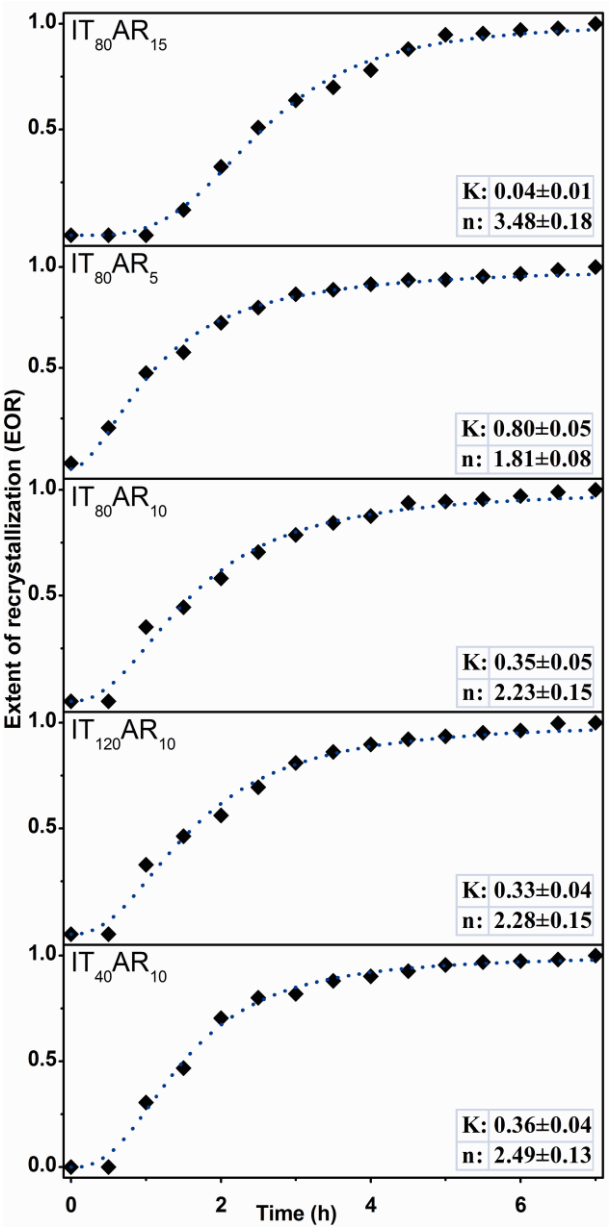

Figure VI. 12 The plots of the extent of crystallization calculated as the ratio of the mean DOC at a time and the mean DOC at plateau (7 h) versus the time of exposure to 98% RH for SDDs prepared with different process parameters mentioned at the left upper corner in each plot. K (h^{-1}) and n (dimensionless) are the fitting parameters obtained by fitting experimental values (♦) using eq VI.7 (. . .) (R^2 > 0.98). See text for the explanation of *K* and *n*.

To further unravel the molecular manifestation during moisture-induced crystallization, a temporal ATR–FTIR analysis was performed on one of SDDs ($IT_{80}AR_{10}$) under similar humidity condition as that of pXRD. The overlay of time-dependent partial FTIR spectra in the $\upsilon_{C=O}$ region is presented in Figure VI.13. With the increase in the time of exposure to moisture, the concomitant decrease in the relative peak intensity of strongly and weakly H-bonded fractions accompanied the increase in that of $\upsilon_{C=O(PVP\ amide)}$. The gradual blue shift of the latter peak due to increased extent of water–PVP H-bonding was observed with time, which stabilized at 1640 $cm^{-1.}$ By one and a half hour, the remarkable broadening and decrease in peak maxima of $\upsilon_{C=O\ (naproxen\ monomer)}$ region was observed, whereas the shoulder attributable to weakly H-bonded fraction at 1672 cm^{-1} almost vanished due to the disruption of the latter. The prominent peak maximum of crystalline $\upsilon_{C=O\ (naproxen\ monomer)}$ appeared at 2 hours and slightly increased further. This time point is also near to the crystallization plateau time according to pXRD. Further, the shoulder attributable to naproxen dimer at 1681 cm^{-1} was apparent at the time points corresponding to the maximum crystallization. The fractal and kinetic of crystallization could be highly affected by the particulate level properties (morphology, surface properties, etc.) apart from molecular level variations. The higher extent of crystallization of amorphous cefditoren pivoxil prepared at lower IT than that prepared at higher temperature is reported to be due to the alteration in the short range order and energetics of particle surface[40]. Also, for a macrolide antibiotic, higher physical stability against crystallization was observed for the morphologically distinct spray-dried amorphous state prepared at higher IT compared with that prepared at lower temperature upon exposure to 40°C/75% RH[41]. Wu et al.[42] have recently reported the dependence of solvent evaporation rate applied during the preparation of piroxicam–PVP amorphous solid dispersions by solution casting at different temperature on the crystallization behavior. The heterogeneity due to the surface channel formation owing to the folding of PVP resulting from the inhomogeneous viscosity distribution at lower evaporation temperature is proposed as the precursor of accelerated crystallization of drug compared to less or no crystallization from the dispersion prepared at higher temperature. Likewise, the smoother surface topography of SDD particles generated at faster solvent evaporation provided by higher IT or AR could be more resistant to heterogeneous nucleation as compared to the higher crystallization rate possible from the shrunken particles that are obtained by spray-drying at lower temperature or larger droplets[9].

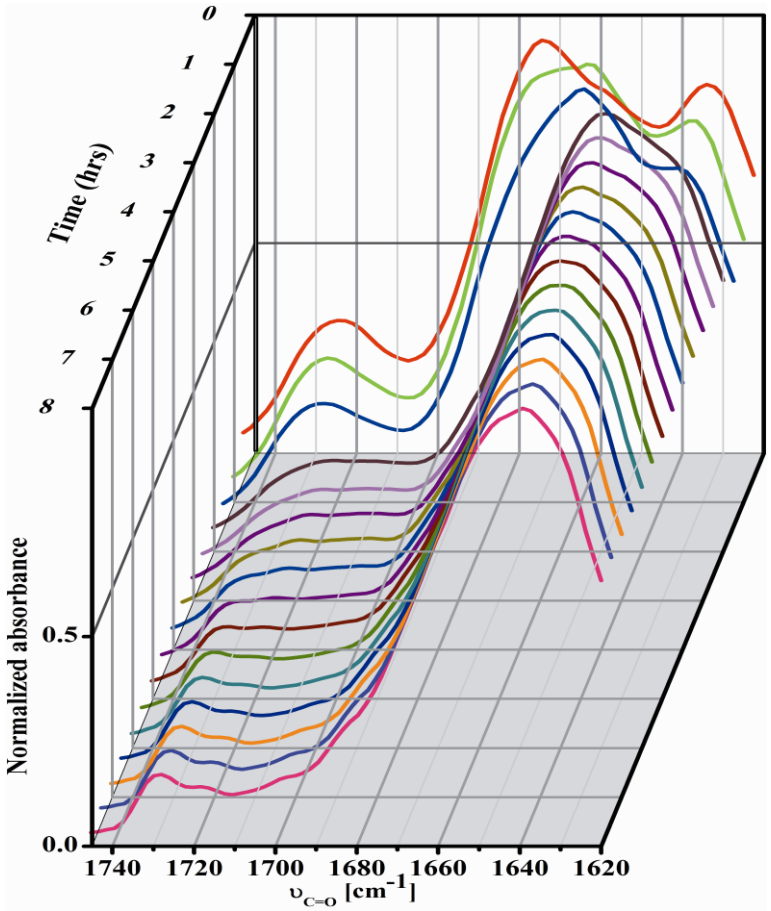

Figure VI. 13 An overlay of partial ATR–FTIR spectra ($\upsilon_{C=O}$ regions) of $IT_{80}AR_{10}$ recorded at different time in 98% RH environment. (The peak assignments for different vibration bands are explained in text).

The drug dissolution profiles from SDDs are, to an extent, correlated with the initial compositional heterogeneity and physical stability. None of the dispersions were able to dissolve even half of the total amount of naproxen loaded. In an earlier study, poor intrinsic dissolution of naproxen from quench cooled amorphous naproxen–PVP dispersion was attributed to the significant surface crystallization of naproxen from supersaturated solution during dissolution[43]. Despite increasing PVP content up to 80% (w/w), the intrinsic dissolution rate from amorphous dispersions could only be increased by 2–3-folds as of crystalline naproxen. The maintenance of relatively higher degree of supersaturation by the phase-separated $IT_{80}AR_{15}$ over more homogenous $IT_{40}AR_{10}$ poses the question on the universal requirement of molecular level miscibility in amorphous solid dispersions for optimal performance. Accompanied by multiple solid- and solution-state phase transformations and other physical processes, the drug dissolution behavior from amorphous solid dispersions is very complex process[44]. The mechanistic difference in the drug dissolution/crystallization from drug-rich and polymer-rich domains of phase-separated SDD is not yet understood. Also, it is not clear that whether the presence of stronger drug–carrier interaction or the higher extent of antiplasticization is important for higher extent of

stabilization against drug crystallization during dissolution. Although, the higher solid-state supersaturation of a drug-rich phase favors crystallization, the dissolution process from the same can be speculated to be faster due to lesser local microviscosity. The role of polymer microviscosity is reported to be vital over bulk during dissolution process from amorphous solid dispersion[45]. The particle size distribution along with the other process specific particulate level properties as described above could also be important contributors for the observed difference in the drug dissolution profiles from SDDs prepared by different processing conditions.

VI.6 Conclusions

Through this study, we showed that the alteration in spray-drying process parameters primarily influencing the solvent evaporation rate and droplet size, resulted in different miscibility, crystallinity, and hence physical stability in the SDDs. Fast evaporation/ drying conditions using higher IT or atomization AR generated SDDs with a wider miscibility gradient but still retain higher amorphicity upon exposure to a humid environment thus presents superior physical stability. The difference in the physical (in) stability of SDDs when subjected to higher compression force was also dependent upon the physical structure generated by a particular set of preparation process parameters. The crystallization kinetics and dissolution profiles to some extent showed a correlation with the initial phase structure of SDDs inherited from the applied process parameters. These findings on a process sensitive naproxen–PVP SDD system point towards the need of a better understanding of the relationship between spray-drying process parameters and physical structure of the final product to ensure successful scalability and commercialization.

VI.7 References

1. Walters, W.P.; Green, J.; Weiss, J.R. and Murcko, M.A. What Do Medicinal Chemists Actually Make? A 50-Year Retrospective. J. Med. Chem. 2011, 54, 6405-6416.
2. Benet, L.Z.; Broccatelli, F. and Oprea, T.I. BDDCS Applied to over 900 Drugs. AAPS J. 13, 519-547.
3. Van den Mooter, G. The Use of Amorphous Solid Dispersions: A Formulation Strategy to Overcome Poor Solubility and Dissolution Rate. Drug Discov. Today: Technol. 2012, 9, e79–e85.
4. Available at http://www.pharma-iq.com/pre-clinical-discovery-and-development/articles/ensuring-stability-the-biggest-amorphous-challenge/ (accessed on 29/10/2012).
5. Qian, F.; Huang, J. and Hussain, M.A. Drug-Polymer Solubility and Miscibility: Stability Consideration and Practical Challenges in Amorphous Solid Dispersion Development. J. Pharm. Sci. 2010, 99, 2941-2947.
6. Janssens, S. and Van den Mooter, G. Review: Physical Chemistry of Solid Dispersions. J. Pharm. Pharmacol. 2009, 61, 1571-1586.
7. Snyder, H.E. Pharmaceutical Spray Drying: Solid-Dose Process Technology Platform for the 21st Century. Ther. Deliv. 2012, 3, 901-912.

8. Vehring, R. Pharmaceutical Particle Engineering Via Spray Drying. Pharm. Res. 2008, 25, 999-1022.
9. Dobry, D.E.; Settell, D.M.; Baumann, J.M.; Ray, R.J.; Graham, L.J. and Beyerinck, R.A. A Model-Based Methodology for Spray-Drying Process Development. J. Pharm. Innov. 2009, 4, 133-142.
10. Baldinger, A.; Clerdent, L.; Rantanen, J.; Yang, M. and Grohganz, H. Quality by Design Approach in the Optimization of the Spray-Drying Process. Pharm. Dev. Technol. 2012, 17, 389-397.
11. Kojima, Y.; Ohta, T.; Shiraki, K.; Takano, R.; Maeda, H. and Ogawa, Y. Effects of Spray Drying Process Parameters on the Solubility Behavior and Physical Stability of Solid Dispersions Prepared Using a Laboratory-Scale Spray Dryer. Drug Dev. Ind. Pharm. 2012, 0, 1-10.
12. Sahoo, N.G.; Abbas, A.; Judeh, Z.; Li, C.M. and Yuen, K.H. Solubility Enhancement of a Poorly Water-Soluble Anti-Malarial Drug: Experimental Design and Use of a Modified Multifluid Nozzle Pilot Spray Drier. J. Pharm. Sci. 2008, 98, 281-296.
13. Paudel, A.; Worku, Z.A.; Meeus, J.; Guns, S. and Van den Mooter, G. Manufacturing of Solid Dispersions of Poorly Water Soluble Drugs by Spray Drying: Formulation and Process Considerations. Int. J. Pharm. 2012 (In press).
14. Yang, J.; Grey, K. and Doney, J. An Improved Kinetics Approach to Describe the Physical Stability of Amorphous Solid Dispersions. Int. J. Pharm. 2010, 384, 24-31.
15. Teng, J.; Bates, S.; Engers, D.A.; Leach, K.; Schields, P. and Yang, Y. Effect of Water Vapor Sorption on Local Structure of Poly (Vinylpyrrolidone). J. Pharm. Sci. 2010, 99, 3815-3825.
16. Paudel, A.; Nies, E. and Van den Mooter, G. Relating Hydrogen-Bonding Interactions with the Phase Behavior of Naproxen/PVP K 25 Solid Dispersions: Evaluation of Solution-Cast and Quench-Cooled Films. Mol. Pharmaceutics 2012, 9, 3301-3317.
17. Bettinetti, G. and Mura, P. Dissolution Properties of Naproxen in Combinations with Polyvinylpyrrolidone. Drug Dev. Ind. Pharm. 1994, 20, 1353-1366.
18. Ayenew, Z.; Paudel, A. and Van den Mooter, G. Can Compression Induce Demixing in Amorphous Solid Dispersions? A Case Study of Naproxen-PVP K 25. Eur. J. Pharm. Biopharm. 2012, 81, 207–213.
19. Paudel, A.; Van Humbeeck, J. and Van den Mooter, G. Theoretical and Experimental Investigation on the Solid Solubility and Miscibility of Naproxen in Poly (Vinylpyrrolidone). Mol. Pharmaceutics 2010, 7, 1133-1148.
20. Corrigan, O.I.; Holohan, E.M. and Reilly, M.R. Physicochemical Properties of Indomethacin and Related Compounds Co-Spray Dried with Polyvinylpyrrolidone. Drug Dev. Ind. Pharm. 1985, 11, 677-695.
21. Ueno, Y.; Yonemochi, E.; Tozuka, Y.; Yamamura, S.; Oguchi, T. and Yamamoto, K. Pharmaceutics: Characterization of Amorphous Ursodeoxycholic Acid Prepared by Spray-Drying. J. Pharm. Pharmacol. 1998, 50, 1213-1219.
22. Wang, S. and Langrish, T. A Review of Process Simulations and the Use of Additives in Spray Drying. Food Res. Int. 2009, 42, 13-25.
23. Adhikari, B.; Howes, T.; Bhandari, B.R. and Troung, V. Surface Stickiness of Drops of Carbohydrate and Organic Acid Solutions During Convective Drying: Experiments and Modeling. Drying Technol. 2003, 21, 839-873.
24. Dahlberg, C.; Millqvist-Fureby, A. and Schuleit, M. Surface Composition and Contact Angle Relationships for Differently Prepared Solid Dispersions. Eur. J. Pharm. Biopharm. 2008, 70, 478-485.
25. van Sleeuwen, R.M.T.; Zhang, S. and Normand, V. Spatial Glass Transition Temperature Variations in Polymer Glass: Application to a Maltodextrin-Water System. Biomacromolecules 2012, 13, 787-797.
26. Meeus, J.; Chen, X.; Scurr, D.J.; Ciarnelli, V.; Amssoms, K.; Roberts, C.J.; Davies, M.C. and Den Mooter, G.v. Nanoscale Surface Characterization and Miscibility Study of a Spray-Dried Injectable Polymeric Matrix Consisting of Poly(Lactic-Co-Glycolic Acid) and Polyvinylpyrrolidone. J. Pharm. Sci. 2012, 101, 3473-3485.
27. Thybo, P.; Hovgaard, L.; Lindelov, J.S.; Brask, A. and Andersen, S.K. Scaling up the Spray Drying Process from Pilot to Production Scale Using an Atomized Droplet Size Criterion. Pharm. Res. 2008, 25, 1610-1620.

28. Eslamian, M.; Ahmed, M. and Ashgriz, N. Modeling of Solution Droplet Evaporation and Particle Evolution in Droplet-to-Particle Spray Methods. Drying Technol. 2009, 27, 3-13.
29. Sen, D.; Spalla, O.; Tache, O.; Haltebourg, P. and Thill, A. Slow Drying of a Spray of Nanoparticles Dispersion. In Situ Saxs Investigation. Langmuir 2007, 23, 4296-4302.
30. Tsivintzelis, I.; Economou, I.G. and Kontogeorgis, G.M. Modeling the Phase Behavior in Mixtures of Pharmaceuticals with Liquid or Supercritical Solvents. J. Phys. Chem. B 2009, 113, 6446-6458.
31. Singh, M. and Kumar, S. Activation Energy, Free Energy, Enthalpy, and Entropy Changes Associated with Viscometric Changes of Extremely to Moderately Dilute Aqueous Solutions of Polyvinylpyrrolidone at 288.15–313.15 K. J. Appl. Polym. Sci. 2004, 93, 47-55.
32. Wulsten, E.; Kiekens, F.; van Dycke, F.; Voorspoels, J. and Lee, G. Levitated Single-Droplet Drying: Case Study with Itraconazole Dried in Binary Organic Solvent Mixtures. Int. J. Pharm. 2009, 378, 116-121.
33. Imamura, K.; Kagotani, R.; Nomura, M.; Tanaka, K.; Kinugawa, K. and Nakanishi, K. Influence of Compression on Water Sorption, Glass Transition, and Enthalpy Relaxation Behavior of Freeze-Dried Amorphous Sugar Matrices. Int. J. Pharm. 2011, 408, 76-83.
34. Leane, M.M.; Sinclair, W.; Qian, F.; Haddadin, R.; Brown, A.; Tobyn, M. and Dennis, A.B. Formulation and Process Design for a Solid Dosage Form Containing a Spray-Dried Amorphous Dispersion of Ibipinabant. Pharm. Dev. Technol. 2013, 18, 359-366.
35. Sun, Y.; Tao, J.; Zhang, G.G.Z. and Yu, L. Solubilities of Crystalline Drugs in Polymers: An Improved Analytical Method and Comparison of Solubilities of Indomethacin and Nifedipine in PVP, PVP/VA, and PVAc. J. Pharm. Sci. 2010, 99, 4023-4031.
36. Paudel, A. and Van den Mooter, G. Influence of Solvent Composition on the Miscibility and Physical Stability of Naproxen/PVP K 25 Solid Dispersions Prepared by Cosolvent Spray-Drying. Pharm. Res. 2012, 29, 251-270.
37. Malaj, L.; Censi, R.; Mozzicafreddo, M.; Pellegrino, L.; Angeletti, M.; Gobetto, R. and Di Martino, P. Influence of Relative Humidity on the Interaction between Different Aryl Propionic Acid Derivatives and Poly (Vinylpyrrolydone) K30: Evaluation of the Effect on Drug Bioavailability. Int. J. Pharm. 2010, 398, 61-72.
38. Süvegh, K. and Zelkó , R. Physical Aging of Poly (Vinylpyrrolidone) under Different Humidity Conditions. Macromolecules 2002, 35, 795-800.
39. Sinclair, W.; Leane, M.; Clarke, G.; Dennis, A.; Tobyn, M. and Timmins, P. Physical Stability and Recrystallization Kinetics of Amorphous Ibipinabant Drug Product by Fourier Transform Raman Spectroscopy. J. Pharm. Sci. 2011, 100, 4687-4699.
40. Ohta, M. and Buckton, G. A Study of the Differences between Two Amorphous Spray-Dried Samples of Cefditoren Pivoxil Which Exhibited Different Physical Stabilities. Int. J. Pharm. 2005, 289, 31-38.
41. Yamaguchi, T.; Nishimura, M.; Okamoto, R.; Takeuchi, T. and Yamamoto, K. Glass Formation of 4-O-(4-Methoxyphenyl) Acetyltylosin and Physicochemical Stability of the Amorphous Solid. Int. J. Pharm. 1992, 85, 87-96.
42. Wu, J.X.; Yang, M.; Berg, F.v.d.; Pajander, J.; Rades, T. and Rantanen, J. Influence of Solvent Evaporation Rate and Formulation Factors on Solid Dispersion Physical Stability. Eur. J. Pharm. Sci. 2011, 44, 610-620.
43. Available at http://www.aapsj.org/abstracts/AM_2009/AAPS2009-001712.PDF (accessed on 29/10/2012).
44. Alonzo, D.E.; Zhang, G.G.Z.; Zhou, D.; Gao, Y. and Taylor, L.S. Understanding the Behavior of Amorphous Pharmaceutical Systems During Dissolution. Pharm. Res. 2010, 27, 608-618.
45. Dahlberg, C.; Dvinskikh, S.V.; Schuleit, M. and Furo, I. Polymer Swelling, Drug Mobilization and Drug Recrystallization in Hydrating Solid Dispersion Tablets Studied by Multinuclear NMR Microimaging and Spectroscopy. Mol. Pharmaceutics 2011, 8, 1247-1256.

Chapter VII: General Discussion and Future Perspectives

VII.1 Evaluation of the Predictability of Drug-Polymer Miscibility by Existing Mixing Models

As a first step, we aimed to understand the binary phase behavior of the selected drug-polymer system which is very important for the subsequent studies. Naproxen was selected as a model drug and solid dispersions with several drug-polymer compositions were prepared with PVP K 12, K 25 and K 90 by spray drying using a set of process parameters. The chain length difference among these polymers is of several orders of magnitude. Despite the diverse phase behavior of solid dispersions prepared from different molecular weight PVP, the upper limits of miscibility were identical. More precisely, the SDD with ≥ 55% drug content underwent amorphous-amorphous/crystalline phase separation regardless of the PVP chain length. The T_g-composition profiles for all systems showed negative deviation from that predicted by the GT equation indicating the imbalance between homo- and heteromolecular interactions.

Next, we applied various methodologies that were based on the FH solution theory to extract the information on the nature of composition/ polymer chain length dependent miscibility and molecular interactions in solid dispersions. The first attempt was to estimate the equilibrium solid solubility of drug in the selected polymers by using their solubility parameters and by utilizing the measured solubility and hence thermodynamic activity of drug in a small molecular analogue of PVP (*n*-methyl pyrrolidone). In contrast to the diverse miscibility profiles observed by thermal analysis, the estimated solid solubility and FH interactions parameter (χ_{FH}) at room temperature were identical using the molecular properties of PVP of different sizes. Overall, the value of χ_{FH} obtained for all systems indicated the presence of favorable mixing interactions. Presumably, the observed discrepancy originates from the shortcomings inherent to the assumptions of the FH model applied for interacting systems. The FH mixing model assumes the random walk of polymer segment on the lattice and polymer molecules as freely joined chains[1, 2]. Another serious factor that this model lacks is the term attributable to directional interactions like H-bonding or other strong polar interactions. These interactions affect not only the enthalpy of mixing but can also significantly influence the entropy of mixing which is not explicitly accounted for by this theory. Such functional interactions can alter the molecular orientation of drug and/or polymer and hence lead to alteration in the entropy of mixing. This can result in poor miscibility predictions by this model for the interacting composites like the present drug-polymer system. Also, the solvate formation reported for some drugs during solubility studies

in a liquid analogue of the polymer signifies the practical problem regarding its universal applicability[3].

The treatment of melting point depression data with a FH based analytical expression (Nishi-Wang equation) provided the values of the composition dependent χ_{FH} and composition independent interaction energy density. These values were the most negative for the polymer with the medium chain length, PVP K 25. We hypothesized that the higher abundance of interacting groups strengthens the composition dependent saturable H-bonding interaction on increasing the polymer chain length and this trend continues up to a critical size beyond which further increase in the chain length propagates self-aggregation among polymer chains that pushes the drug molecules out. At present, we are not able to provide the experimental evidence of the same. Further studies including other intermediate chain lengths PVPs can interrogate this concept. However, a similar inconsistent trend of PVP K 30 exhibiting the strongest crystallization inhibition of sulfa drugs was reported among K 12, K 30 and K 90[4]. As drug-polymer physical mixtures were used in our study to generate these data, there is a chance of other kinetic factors such as polymer rheology contributing to the results. The moisture sorption data at high humidity was again analyzed using a FH based model for ternary systems (drug-polymer-water) and $\Delta\chi_{FH}$ effect. Although, it provided information on composition dependent molecular interaction in presence of water, the applied model could again be too simple in view of the complex moisture dependent molecular behavior of PVP. The PVP molecules are reported to exhibit anomalous H-bonding behavior with water as a function of moisture content and therefore its local structure is highly altered and that can have an effect on the mutual interaction with the drug[5].

Overall, the results from this study provided a thorough evaluation of existing thermodynamic models for solid solubility and miscibility estimation of drug in polymer which has direct relevance to the drug loading and physical stability of solid dispersions. In spite of various shortcomings, this multi-methodological approach can certainly present an efficient scientific benchmark on the drug-polymer interaction and miscibility.

VII.2 Relation of Feed Solvent Composition and Properties to the Solid-State Outcome of SDDs

The solvent(s) system is an important variable for pharmaceutical particle engineering by spray drying. A growing concern is observed towards the use of solvent blends for tailoring the particulate properties. For manufacturing SDD, cosolvent feed solution is getting more preference as it can be often tedious to find a single solvent solubilizing a

physicochemically diverse drug and polymer. Hence, this study was designed to get insight into the impact of spray drying from a solution containing binary blends of solvents of different polarity, proticity and volatility on the physical structure and stability of resulting SDDs. The solutions of naproxen and PVP K 25 of two compositions were prepared in binary combinations of methanol, DCM and acetone at three different levels. Naproxen has appreciable solubility in all selected solvents with the highest in acetone while PVP has poor solubility in acetone but good solubility in the rest of the solvents.

In acetone containing feed solutions, the increase of acetone, an anti-solvent for PVP, decreased the dispersivity of and solvency to the PVP molecules while the same trend was observed with the increase of methanol in DCM-methanol systems. This was revealed by the decrease in viscosity and increase in PVP globular size. The solvent evaporation rate profiles from different solvent compositions measured at ambient temperature showed the relative volatility effect of the solvents. However, the marked deviation of these profiles from that of pure solvent blends provided the clue of multiple molecular interactions among drug, polymer and solvents. This can further be confirmed by spectroscopic monitoring during evaporation.

All SDDs containing 30%w/w naproxen were X-ray amorphous and most of them with 55%w/w drug content were partially crystalline. The solvent composition in the spray drying feed solution showed a marked influence on the compositional heterogeneity of both amorphous and partially crystalline SDDs. The extent of amorphous homogeneity before and after exposure to elevated humidity was superior in the systems prepared from DCM-acetone. We proposed that the combined effect of higher DCM volatility and polymer anti-solvency of acetone contributed for the sudden vitrification of polymer before radial demixing during spray drying from DCM-acetone systems. The high volatility of DCM compared to that of methanol tends to the chaotic initial evaporation from the DCM-acetone system that helps in instantaneous redistribution of the drug molecules within the precipitated PVP matrix from the remaining acetone rich solution/suspension. This points to the importance of the relative volatility of the added anti-solvent. Additionally, the difference in solution properties such as viscosity, surface tension and vapor pressure of feeds prepared from different solvent composition can result into different droplet sizes and their density and distribution. Therefore, online droplet size measurement during spray drying can provide further support to the present data. Wulsten et al. monitored and correlated the solvent evaporation kinetics during the itraconazole-HPMC particle formation from the acoustically levitated droplet of solution in organic solvent blends to the surface properties of the resulting solid[6]. Likewise,

the particulate properties of SDDs might vary with solvent composition. Especially, the diversity in the porosity and internal holes within SDD particles can result into different extent of moisture-induced structural reorganization, molecular diffusion in amorphous SDDs and crystallization therefrom. Further temporal monitoring using powerful techniques to study the kinetics and routes of moisture induced phase separation for dispersions prepared from different solvent blends can provide additional information on the intermediate phases. Also, chemical analysis of the preferential retention of solvent(s) in SDDs prepared from cosolvents would be important.

The effects of solvent composition are different at different zones of miscibility (amorphous and partial crystalline). Similar effect of adding a bad solvent (for polymer) to the spray drying solution has been reported to yield SDD with better micromeritic properties and dissolution performance for different drug-PVP systems[7]. In contrast, inferior miscibility and physical stability of PVP based SDDs of a drug candidate prepared from acetone/water system has been shown as compared to that prepared from methanol alone. Induction of liquid-liquid phase separation of acetone/water by PVP is proposed as the root cause behind this deleterious effect. Therefore, while listing solvent/anti-solvent pairs for cosolvent spray drying, the effect of solutes, especially polymer, on the phase behavior of solvents should be critically considered and properly analyzed.

The overall results showed that all complex molecular interactions in solution-state are not innately transferred to the solid-state. Although, the solvent composition dependent molecular interactions in the feed should be duly considered, the effect of the solvent compositions on the solution properties influencing various kinetic processes during spray drying play a vital role for the molecular behavior of resulting SDD products. It is therefore important to elucidate the competition among various rate processes such as molecular diffusion, solvent recession, phase separation, vitrification, precipitation and crystallization as well as to consider the role of solvent composition in these processes and to relate them to the resulting physical structure. Hence, study of the influence of solvent compositions should be coupled with the process parameters to gain an optimum combination. This means that the metastable solution nearing to liquid-liquid or liquid-solid phase separation can result into an acceptable molecular structure of SDDs provided the right process parameter combinations are applied.

VII.3 Molecular Miscibility/Interactions in Dispersions Originated from Quasi-Equilibrium and Non-Equilibrium Process

We compared the thermal and spectroscopic data obtained from two types of solid dispersions namely solution cast (SC) films prepared by very slow solvent evaporation (quasi-equilibrium) from methanolic drug-polymer solution and quench-cooled (QC) films prepared by rapid cooling (non-equilibrium) of the SC samples heated beyond the melting temperature of the drug. The samples were prepared in DSC pans or pXRD sample holders to facilitate direct analysis.

The compelling difference in the miscibility-molecular interaction profiles were obtained for the dispersions prepared by two different methods. The macroscopically distinct SC films showed a single amorphous up to 20%, two amorphous phases up to 35%, two amorphous phases and a crystalline phase up to 60% and one amorphous phase and a crystalline phase at ≤ 65% drug content. On the other hand, QC films showed a single amorphous form without (<75% drug content) or with (≥80% drug content) a crystalline phase. Moreover, the composition-T_g width profile extracted from the cooling curve provided the homogeneity status across the resulting QC films. Analysis of the locality of intermolecular interactions in SC films using IR helped in identifying drug rich and polymer rich phases. The drug rich regions were expectedly rich in strongly H-bonded fractions of drug-polymer and polymer rich fractions were rich in the free carbonyl group of PVP. Despite two adjoining T_gs observed in thermal analysis the difference could not be detected by IR possibly due to either identical molecular interactions within these separated domains or due to the poor spatial resolution of IR for phase identification. The application of localized probe based techniques such as nano-thermal or AFM analysis worth the composition dependent phase mapping while solid state NMR spectroscopy can reveal the nature of H-bonding interactions that differ within the separated domains at molecular level. The QC films showed saturation of strongly H-bonding interaction from beyond 45% drug content which was related to the T_g width of the cooling curve. Furthermore, an additional vibration band within the carbonyl region was noticed for the compositions for which two crystallization exotherms were apparent in DSC.

The characteristics of the casting solution showed some relation with that of solid state structures of the resulting films. For example, IR analysis of solution revealed that the naproxen dimer fraction increases rapidly when changing the solution composition from that corresponding to amorphous to that corresponding to partially crystalline SC films. Also, two

populations of PVP globules were present across the compositions corresponding to heterogeneous solid-state.

In contrast to the first study, films were generated from the mixed states (solution or melts). Also, equilibrium melting points extrapolated to 0°C/min heating rate were employed for the estimation of thermodynamic activity of drug in polymer and χ_{FH} therefrom. The line fitted to the melting point depression profiles using FH activity model intersect the T_g-composition line at ca. 17-18% naproxen independent of the preparation methods. Further, an erratic quasi-binary phase behavior of naproxen-PVP SC films indicated partial kinetic control on the film formation process. The experimental T_g-composition profile of QC films was fitted with a novel expression, BCKV equation[8]. In comparison to the previously used models, the empirical fitting constants provided a better physical meaning in terms of the relative strength of homo-/hetero-molecular interactions. In spite of the successful application of this model to a wide diversity of pharmaceutical drug-polymer systems, the explanation of the fitting parameters is subject to further experimental validation and physical interpretation.

VII.4 Exploration of the Missing Link between Process Parameters-Phase Structures of SDDs

The final stage of research was deliberated to assess the effect of key spray drying process parameters that can impart the vital impact on the phase structure of SDDs. The Pro-C-epT micro-spray dryer was used for this study because process parameters could be precisely monitored and controlled with this system compared to the Buchi spray dryer. We preliminary investigated the effect of process parameters at various drug loadings for naproxen and PVP K 25 with methanol as spray drying solvent. Below 35% drug content, there was no substantial effect of processing conditions even using extreme settings on the amorphous solid dispersions. It is reasonable to state that the extent of change one can detect in physical structure depends upon the level of the investigation one can perform. For example, the detection of subtle amorphous phase separation depends upon the power of the analytical technique used. On the other hand, with drug loading ≥60%, partial crystallinity was observed in SDDs regardless of process parameters. This led our focus to the 40% drug containing systems. Moreover, this is also the borderline for the induction of crystallization for the same system under very slow solvent evaporation as mentioned in VII.3.

For the selected feed condition, variation of the drying airflow rate through the extreme values while keeping the rest of parameters constant at the medium setting led to no discernible effect on miscibility. The spray dryer used in this study provides a laminar flow of

the drying gas in the drying chamber. Therefore, we fixed the drying airflow rate to the medium value of the instrumental capacity. The lower value of atomization airflow rate was based on the range of expected droplet size. For this spray dryer and selected nozzle type, the droplet diameter is reported to range from 1-100μm. Hence, with 5L/min nozzle airflow rate, the estimated droplet diameter is already at the upper limit from the given setting. We observed profound effects of inlet temperature and atomization airflow rate that were discernable on the compositional homogeneity, drug-polymer interaction and crystallinity in SDDs. Moreover, the extent of moisture and compression induced destabilization of SDDs were remarkably dependent upon the process parameters applied to prepare them. In the context of solid oral dosage formulation of SDDs such as tablets, the stability data in humid environment has direct relevance to wet granulation and that under compression force to tableting. Adequate physical stability against humidity is also equally desired for the stability in course of storage/transport and during ingestion of the product. Hence, this implies that robust spray drying conditions are necessary for manufacturing SDDs that withstand the heat, mechanical and/or moisture imposed stress during subsequent downstream product development processes. Our results on the process effect still stand on the row of few that are focused on the molecular level manifestations in SDDs. There are several cases where particle engineering aspects of spray dried pharmaceuticals are covered. It is highly realized that the molecular level investigation of the process effect should be coupled with particle characterization. Especially, micromeritic and surface properties can markedly influence the physical stability of amorphous systems in humid environment.

The naproxen-PVP K 25 SDDs prepared using different process parameters also exhibited diverse *in vitro* dissolution behavior. More importantly, the effects of process dependent phase structure on the *in vitro* and/or *in vivo* performance of SDDs still remain a major concern. The current understanding about the complex dissolution behavior of supersaturating amorphous solid dispersions is very poor. Recently, some sound attempts have been made to deconvolute the concomitant physical processes governing the drug dissolution from amorphous systems using online monitoring and mathematical modeling[9, 10]. There is a lack of knowledge on the relation of the physical state of SDDs to the processes *viz.*, diffusion, nucleation/crystallization, polymer mobilization etc occurring during dissolution.

VII.5 Future Perspectives

This research project was able to identify key formulation and processing aspects in manufacturing amorphous solid dispersions by spray drying. It is generally acceptable that the complex thermodynamic and kinetic processes play a significant role in developing unique physical structures in SDDs and this has direct impact on the stability and pharmaceutical performance of the products. The results from this dissertation enable us to suggest the following research directions to improve our understanding on the spray dried amorphous systems:

VII.5.1 Modeling Miscibility

The increasing interest in the FH based model witnessed through recent literature on amorphous dispersions is indeed constructive[11]. Most of them focus on the modification of the classical analytical expressions such as breaking total ΔG_{mix} in form of mechanical changes, mixing and drug melting or complementing H-bonding contribution through Hansen's H-bonding solubility parameters[12, 13]. However, quantitative thermodynamic values of the strength of specific interactions such as H-bonding and the degree to which they influence thermodynamic properties still remain unaccounted in these miscibility models to apply for the interacting systems.

We advise the use of other modified forms of FH model that account for specific interactions between mixing components. One ubiquitously used methodology in polymer chemistry for the study of miscibility behavior of hydrogen bonding blends is the Painter and Coleman association model (PCAM)[14]. For the expression of ΔG_{mix}, this model includes a specific term of Gibbs free energy change due to H-bonding in addition to the combinatorial entropy and enthalpy of mixing terms. Its magnitude depends upon the relative strength of self-associating to inter-associating H-bonding and the density of specific interacting sites. These data can be obtained by measuring IR spectra of several compositions of drug-polymer or drug-liquid analogues of polymer[15]. Another useful model is Wertheim thermodynamic perturbation theory (WTPT) which accounts for the directional H-bonding interactions[16].

VII.5.2 Understanding the Solvent Evaporation Process

The physicochemical understanding of solvent evaporation is very important for the rational selection of spray drying solvents, feed concentration and composition. Rayleigh–Benard-Marangoni modeling for solvent convection through temperature and/or surface tension gradients can be applied to high quality data recorded during film formation from

solutions of several combinations of polymer and solvent(s) for a particular drug[17]. The snapshots of conformational alteration and molecular diffusion could be tracked by online spectroscopic or microscopic monitoring during evaporation. This can be extended to the different temperature and for varying solution concentration/composition. This could eventually provide a scientific guide for the selection of a right polymer-solvent combinations and appropriate concentration for obtaining the desired physical structure. Of course, this would be more relevant for the film and fiber based formulations that are getting importance for continuous manufacturing[18].

Techniques with acceptable throughput are desired for early screening and feasibility studies during SDD development. Recently, a smart disposable spray dryer built in a polymeric chip was used to prepare amorphous solid dispersions[19]. Provided the ease of economic fabrication such assembly can be certainly interesting for screening purposes. The acoustic levitator can be another interesting platform for multi-methodological monitoring of the events during containerless solvent evaporation from a suspended droplet, although the effect of molecular turbulence exerted during spray drying is excluded[6].

VII.5.3 Spray Drying Process Development for Manufacturing SDDs

The present paradigm of particle engineering based spray drying process development needs the shift towards consideration of the macroscopic as well as the molecular level quality attributes of the end product. We agree that the outcome of the process effect from the present study is far from conclusive without the data supporting the multifarious role of the particulate and surface properties of SDDs on their physical stability and dissolution behavior. Few studies reported on the influence of particle size, surface energetics and topography on molecular mobility, the phase separation and/or crystallization behavior of solid dispersion powders. More rigorous characterization of their relationship is necessary. It may be advantageous to scale down the experiment in an acoustic levitator to generate a single particle and the change in molecular and particulate characteristics under elevated humidity and/or temperature can be temporally monitored using online integrated analytical tools (Raman, NIR, AFM etc) for a SDD particle generated from different process parameter (s).

The current practice of pharmaceutical spray drying process development largely relies on statistically designed experiments (*"Design of Experiments"*, DoE). Different formulation and process parameters are the input variables for the designated powder characteristics as the responses. We applied a similar DoE approach to study the influence of these parameters designating the miscibility, drug-polymer interaction and crystallinity as the

response for the naproxen-PVP K 25 system. However, no conclusive trends were evident. Although, this approach is practically favorable, it lacks the mechanistic values on the effect due to the interactions of multiple parameters. Instead, the impact of process parameters or combinations thereof on the physicochemical process governing the particle formation during spray drying should be treated with molecular computations and first principles to understand the origin of a particular physical structure. The implementation of theoretical approaches has shown the success to an extent in relating spray drying process parameters on the quality attributes of spray dried food products[20]. In this sense, they have potential of utilization in process development and scale up for SDD manufacturing with the focus on molecular and particle characteristics together. The influence of scaling up on molecular miscibility of SDDs is rarely reported[21]. Upscaling of SDD manufacturing can be carried out among lab scale spray dryers of different drying capacities and hardware configurations (Buchi to Pro-C-epT) to pilot scale equipment by matching the operational parameters as much as possible. Interestingly, our group also noticed the variation in molecular miscibility and compositional homogeneity for SDDs collected from the different parts of spray dryer, *viz.*, conveyer, top and bottom of the cyclone. Detailed studies are ongoing to further address this issue.

VII.5.4 Deconvolution of Physicochemical Processes during Dissolution of Amorphous SDDs

The dissolution process from amorphous systems is extremely complex involving molecular, particle, surface and bulk level properties alongwith various solution mediated processes. The events occurring at the particle surface and in the static water layer surrounding the same have huge impact on the kinetics of dissolution and phase transformations. Unfortunately, there are not many tools available to study events in the static water layer. However, mimicking the static water layer in a macro system can possibly provide some insights. On the one hand, supersaturation generated in the static water layer/bulk solution and nucleation/crystallization driven by it needs to be monitored. On the other hand, some events occurring in the undissolved particle, especially at the particle surface, should be characterized too. Plasticization of the surface molecules of amorphous solid dispersion and devitrification on the surface can completely change the behavior. It is indeed challenging to mimic these conditions entirely and obtain deep insights. In situ monitoring of dissolution of amorphous systems using advanced spectroscopy, imaging or NMR relaxometry can potentially resolve some of the spatio-temporal events. It is a very interesting area definitely in need of aggressive scientific investigations.

VII.6 References

1. Flory, P.J. Thermodynamics of High Polymer Solutions. J. Chem. Phys. 1942, 10, 51.
2. Huggins, M.L. Thermodynamic Properties of Solutions of Long-Chain Compounds. Ann. N. Y. Acad. Sci. 1942, 43, 1-32.
3. Tao, J.; Sun, Y.; Zhang, G.G.Z. and Yu, L. Solubility of Small-Molecule Crystals in Polymers: D-Mannitol in Pvp, Indomethacin in PVP/VA, and Nifedipine in PVP/VA. Pharm. Res. 2009, 26, 855-864.
4. Sekikawa, H.; Nakano, M. and Arita, T. Inhibitory Effect of Polyvinylpyrrolidone on the Crystallization of Drugs. Chem. Pharm. Bull. 1978, 26, 118-126.
5. Suvegh, K. and Zelko, R. Physical Aging of Poly (Vinylpyrrolidone) under Different Humidity Conditions. Macromolecules 2002, 35, 795-800.
6. Wulsten, E.; Kiekens, F.; van Dycke, F.; Voorspoels, J. and Lee, G. Levitated Single-Droplet Drying: Case Study with Itraconazole Dried in Binary Organic Solvent Mixtures. Int. J. Pharm. 2009, 378, 116-121.
7. Brzeczko, A.W. and Doney, J.A. Formulation Process Method to Produce Spray Dried Products. US Patent Application 20080181962, 2008.
8. Kalogeras, I.M. A Novel Approach for Analyzing Glass-Transition Temperature Vs. Composition Patterns: Application to Pharmaceutical Compound+ Polymer Systems. Eur. J. Pharm. Sci. 2011, 42, 470-483.
9. Alonzo, D.E.; Zhang, G.G.Z.; Zhou, D.; Gao, Y. and Taylor, L.S. Understanding the Behavior of Amorphous Pharmaceutical Systems During Dissolution. Pharm. Res. 2010, 27, 608-618.
10. Langham, Z.A.; Booth, J.; Hughes, L.P.; Reynolds, G.K. and Wren, S.A.C. Mechanistic Insights into the Dissolution of Spray-Dried Amorphous Solid Dispersions. J. Pharm. Sci. 2012, 101, 2798-2810.
11. Tian, Y.; Booth, J.; Meehan, E.; Jones, D.S.; Li, S. and Andrews, G.P. Construction of Drug-Polymer Thermodynamic Phase Diagrams Using Flory-Huggins Interaction Theory: Identifying the Relevance of Temperature and Drug Weight Fraction to Phase Separation within Solid Dispersions. Molecular Pharmaceutics 2013, 10, 236-248.
12. Bellantone, R.A.; Patel, P.; Sandhu, H.; Choi, D.S.; Singhal, D.; Chokshi, H.; Malick, A.W. and Shah, N. A Method to Predict the Equilibrium Solubility of Drugs in Solid Polymers near Room Temperature Using Thermal Analysis. J. Pharm. Sci. 2012 101, 4549-4558.
13. Huang, J.; Li, Y.; Wigent, R.J.; Malick, W.A.; Sandhu, H.K.; Singhal, D. and Shah, N.H. Interplay of Formulation and Process Methodology on the Extent of Nifedipine Molecular Dispersion in Polymers. Int. J. Pharm. 2011, 420, 59-67.
14. Painter, P.C.; Graf, J.F. and Coleman, M.M. Effect of Hydrogen Bonding on the Enthalpy of Mixing and the Composition Dependence of the Glass Transition Temperature in Polymer Blends. Macromolecules 1991, 24, 5630-5638.
15. Coleman, M.M.; Guigley, K.S. and Painter, P.C. The Prediction of Hydrogen Bonded Polymer Blend Phase Behavior Using Equilibrium Constants Determined from Low Molar Mass Analogues. Macromol. Chem. Physic. 1999, 200, 1167-1173.
16. Wertheim, M.S. Fluids with Highly Directional Attractive Forces. I. Statistical Thermodynamics. J. Stat. Phys. 1984, 35, 19-34.
17. Bassou, N. and Rharbi, Y. Role of Benard-Marangoni Instabilities During Solvent Evaporation in Polymer Surface Corrugations. Langmuir 2008, 25, 624-632.
18. Brettmann, B.K.; Myerson, A.S. and Trout, B.L. Solid-State Nuclear Magnetic Resonance Study of the Physical Stability of Electrospun Drug and Polymer Solid Solutions. J. Pharm. Sci. 2012 101, 2185-2193.
19. Thiele, J.; Windbergs, M.; Abate, A.R.; Trebbin, M.; Shum, H.C.; Forster, S. and Weitz, D.A. Early Development Drug Formulation on a Chip: Fabrication of Nanoparticles Using a Microfluidic Spray Dryer. Lab Chip 2011, 11, 2362-2368.

20. Kuriakose, R. and Anandharamakrishnan, C. Computational Fluid Dynamics (CFD) Applications in Spray Drying of Food Products. Trends Food Sci. Tech. 2010, 21, 383-398.
21. Thybo, P.; Hovgaard, L.; Lindelov, J.S.; Brask, A. and Andersen, S.K. Scaling up the Spray Drying Process from Pilot to Production Scale Using an Atomized Droplet Size Criterion. Pharm. Res. 2008, 25, 1610-1620.

Chapter VIII: Summary/ Samenvatting

VIII.1 Summary

In *chapter I,* a literature survey on phase behavior, carriers, manufacturing and characterization techniques for amorphous solid dispersion is presented alongwith the fundamentals of spray drying and existing cases of the effect of formulation and/or process on the molecular characteristics of spray dried dispersions of poorly water soluble drugs. The objectives of this PhD dissertation was to fundamentally understand the influence of key formulation and process variables on the physical structure and stability of solid dispersions prepared by spray drying (*chapter II*). Naproxen (a BCS class 2 drug) was selected as model drug and PVP as model carrier.

Chapter III presents the study on the phase behavior and molecular interactions of naproxen and PVPs with three different chain lengths solid dispersions prepared by spray drying. Naproxen exhibited diverse phase behavior with PVPs of different chain lengths but identical kinetic miscibility. The multiple methodologies based on the Flory Huggins (FH) solution theory estimated similar solid solubility of naproxen in PVPs and drug-polymer interaction parameter independent of chain lengths. The solid solubility and the FH interaction parameter at room temperature was estimated using the drug solubility measured in a liquid analogue of the polymer. Moreover, the composition dependent interaction parameter and the interaction energy density for the system were obtained from melting point depression studies. The interaction parameter was also estimated in presence of sorbed moisture by drug-polymer physical mixtures. The drug-polymer interaction values obtained by different methods varied markedly. Comparison of theoretical and experimental results overall suggested the distinctly higher kinetic miscibility of naproxen in PVP as compared to the solid solubility and the existence of favorable mixing interaction between the drug and the polymer molecules. The inadequacy of the FH model for discriminating the drug-polymer interactions among the systems containing PVP with very different chain length points to the necessity of better miscibility models that account for directional H-bonding interactions.

The solvent is one of the important parameters for manufacturing solid dispersions by spray drying. However, the practical difficulty of finding a single solvent that is capable of solubilizing drugs and polymers with significantly different physicochemical properties is increasing. To understand the effect of solvent composition on the physical structure, solid dispersions of naproxen and PVP K 25 with 30 and 55 %w/w drug content were prepared by spray drying from feed solutions containing binary blends of methanol, DCM and acetone at different levels (*chapter IV*). The feed solution characteristics indicated poor dispersivity and

solvency of PVP with increase of acetone in solution or methanol (in DCM-methanol). The evaporation rate profiles expectedly dictated the relative volatilities of solvents in the blends. As compared to the profiles of evaporation rates from blank solvent blends, drastic alteration in the same was altered in presence of drug and polymer at different compositions. This indicated the existence of differential molecular interactions among drug-polymer-solvent(s) molecules in solution. Further, the solid state analysis of spray dried dispersions prepared from different solvent blends showed the impact of solvent composition on their physical structure. More precisely, the 30% naproxen containing dispersions generated from all solvent combinations were X-ray amorphous and the dispersions containing 55% naproxen showed partial crystallinity except those prepared from DCM- acetone (3:1). The initial compositional heterogeneity and crystallinity were the least for dispersions originating from DCM-acetone followed by methanol-acetone and DCM-methanol. Similar effects of solvent composition were apparent on the physical stability of dispersions during storage at elevated humidity. The results overall showed that the addition of an anti-solvent (for the polymer) possessing optimum volatility with respect to the good solvent generated dispersions with improved miscibility and physical stability.

Solid dispersions are often prepared by solution casting and quench cooling for preliminary assessment of their manufacturability by solvent and non-solvent methods, respectively. However, the phase behavior and molecular structure in these solid dispersions generated from different routes and rates are rarely accounted for. We therefore thoroughly investigated and compared the relationship of miscibility with the H-bonding interactions in naproxen-PVP K 25 films prepared by i) slow casting from methanolic solution (SC films) and by ii) quench cooling the SC films heated beyond the melting point of the drug (QC films) (*chapter V*). The thermal and spectroscopic analysis of the films revealed substantial dependence of the miscibility-intermolecular interaction profiles on the preparation methods. Evolution of the phase behavior dependent on the drug concentration in the films was observed from a single amorphous dispersion (≤20%naproxen) through a coexisting drug rich and polymer rich amorphous phase (≤35%naproxen) to partially crystalline states constituting a single (≤60%naproxen) or multiple coexisting amorphous phases (≥65 % naproxen). This trend is supported by the increase of a strongly H-bonded drug-polymer fraction in the amorphous phase separated region. The decreasing trend of the strongly H-bonded population in partially crystalline states is complemented by the appearance of the naproxen dimer at higher crystallinity. The origin of the composition dependent heterogeneity in miscibility and

H-bonding interactions was partially forecasted by increasing fractions of naproxen dimer and bimodal globular populations of PVP in corresponding casting solutions. The QC films, on the other hand, exhibited a single amorphous phase across a wide composition range (≤70%naproxen) which was accompanied by a coexisting crystalline state at higher naproxen content (≥75%naproxen). However, the T_g width in the cooling curves increased up to 45% naproxen and decreased thereafter. The infrared spectroscopic data of QC films revealed the presence of two H-bonded populations from 35%naproxen and the saturation of strongly bonded fractions at ≥45%naproxen. As function of naproxen content, the extrapolated lines through the equilibrium melting point intersected the T_g line at 17-18% naproxen content for both SC and QC films. The FH interaction parameters were negative and comparable. Overall, this study provided a miscibility window ranging from quasi-equilibrium miscibility obtained from SC films and the kinetic limit obtained from QC films for naproxen-PVP K 25 systems.

Following the insight into the phase behavior, intermolecular interactions, solvent effect and physical stability, an investigation was performed to assess the effect of key spray drying process parameters on the physical structure, stability and *in vitro* dissolution behavior of naproxen-PVP K 25 spray dried dispersions (*chapter VI*). The spray dried dispersions (SDD) containing 40%naproxen were prepared using three inlet temperatures (ITs) (40, 80 and 120°C) with the atomization airflow rate (AR) of 10 L/min and using three ARs (5, 10 and 15 L/min) with IT of 80°C while keeping the rest of the parameters fixed. Initially, all dispersions were X-ray amorphous except for the presence of trace crystallinity in the dispersion prepared using AR of 5L/min. The compositional heterogeneity was comparatively higher in amorphous SDDs originating from higher IT and /or AR. However, these heterogeneous dispersions comprised the higher fraction of the PVP carbonyl fractions that were strongly H-bonded with naproxen or free in contrast to the weakly H-bonded fraction prevalent in dispersions prepared at lower IT or AR. However, higher initial rate of dissolution and the extent of supersaturation were attained by the initially heterogeneous dispersions prepared at higher parameters. Also, these dispersions developed relatively lower crystallinity and also retained comparatively a higher fraction of drug rich amorphous domains upon exposure to 75%RH. In addition, the extent and kinetics of moisture-induced crystallization from dispersions prepared using higher IT and AR was lower when stored at 98%RH. Besides, compression-induced phase reorganization was also different in SDDs prepared from different process parameters. This indicated the sensitivity of the phase

structure, physical stability and pharmaceutical performance of SDDs towards the parameters employed to prepare them.

In *chapter VII*, the key accomplishments of the present dissertation are highlighted on the formulation and process considerations in manufacturing amorphous solid dispersions of a poorly water soluble drug. Based on the experience with this model system, guidance for the future research direction to advance the understanding of the physical chemistry of amorphous solid dispersions is provided.

VIII.2 Samenvatting (Summary in Dutch)

In hoofdstuk I wordt een overzicht gegeven van de literatuur betreffende fasegedrag, carriers, en bereidings- en karakterizeringstechnieken voor amorfe vaste dispersies. Daarnaast werden ook de fundamentele aspecten van sproeidrogen toegelicht. Enkele voorbeelden worden besproken die het belang aantonen van de formulering en het bereidingsproces op de moleculaire karakteristieken van gesproeidroogde vaste dispersies van slecht oplosbare geneesmiddelen.

De doelstelling van dit doctoraatsonderzoek wordt beschreven in hoofdstuk II. Essentieel is het begrijpen van de invloed van de relevante formulerings- en procesvariabelen op de fysische structuur en stabiliteit van gesproeidroogde vaste dispersies. In deze studie werden naproxen (BCS klasse 2) en polyvinylpyrrolidone (PVP) gebruikt als modelgeneesmiddel en modelcarrier, respectievelijk.

De studie over het fasegedrag en moleculaire interacties in vaste dispersies van naproxen en PVP met verschillende ketenlengtes wordt besproken in hoofdstuk III. Het fasegedrag van naproxen varieerde naargelang de ketenlengte van het polymeer, doch de kinetische mengbaarheid was vergelijkbaar. Verschillende benaderingen om de vaste oplosbaarheid en de interactieparameter te bepalen gebaseerd op de Flory Huggins (FH) theorie leidden tot vergelijkbare waarden, onafhankelijk van de polymeerketenlengte. De vaste oplosbaarheid van naproxen in het polymeer en de interactieparameter bij kamertemperatuur werden geschat op basis van de geneesmiddeloplosbaarhied in een vloeibaar monomeeranaloog van het polymeer. Smeltpuntsdaling werd eveneens gebruikt om de samenstellingsafhankelijke interactieparameter te schatten alsook de interactie-energiedensiteit. De interactieparameter werd verder ook geschat in binaire fysische mengsels in aanwezigheid van waterdamp. Verschillende methoden om de interacties te schatten gaven

verschillende waarden. Op basis van de vergelijking tussen theoretische en experimenteel bepaalde waarden kunnen we besluiten dat de kinetische mengbaarheid merkelijk hoger is dan de vaste toestand oplosbaarheid en dat interacties tussen naproxen en PVP aanwezig zijn. Het feit dat de FH theorie niet in staat is om onderscheid te maken in interacties tussen systemen met duidelijk verschillende ketenlengte wijst op de noodzaak om betere theoretische modellen ter beschikking te hebben.

Het solvent is een belangrijke formuleringsparameter van het sproeidroogproces. Er is een toenemende trend in de moeilijkheid om solventen te vinden die zowel het geneesmiddel als de carrier kunnen oplossen. In hoofdstuk IV wordt de invloed van de solventsamenstelling op de resulterende fysische structuur van naproxen-PVP vaste dispersies onderzocht. Systemen met 30 en 55% w/w naproxen op basis van binaire solventsystemen van methanol, aceton en dichloormethaan werden gekarakterizeerd. De dispergeerbaarheid en oplosbaarheid van PVP daalde met toenemende concentratie van aceton en van methanol (in dichloormethaan). De verdampingsnelheid was gekoppeld aan de vluchtigheid van de solventmengsels. De verdampingssnelheid van de solventmengsels werd beïnvloed door de aanwezigheid van naproxen en PVP wat duidt op interacties tussen naproxen, PVP en de solventmoleculen.Ook de fysische structuur van de vaste dispersies was duidelijk afhankelijk van de initiële solventeigenschappen. Zo waren alle 30%-ige vaste dispersies amorf na XRD analyse, terwijl alle 55%-ige naproxen dispersies partieel kristallijn waren met uitzonderning van deze bereid uit dichloormethaan-aceton(3:1). Initiële heterogeniteit en kristalliniteit waren het laagst voor vaste dispersies bereid uit dichloormethaan-aceton, gevolgd door deze uit methanol-aceton en dichloormethaan-methanol. Een gelijkaardige trend werd waargenomen voor de fysische stabiliteit in vochtige bewaarcondities. De belangrijkste conclusie van deze studie was dat toevoegen van een anti-solvent (voor het polymeer) met optimale vluchtigheid vaste dispersies oplevert met verhoogde mengbaarheid.

De mogelijkheid tot formulering van vaste dispersies wordt vaak in een preliminair ontwikkelingsstadium uitgevoerd via casting en/of quench cooling. De invloed van deze verschillende bereidingsmethodieken op het fasegedrag en moleculaire structuur wordt al te vaak verwaarloosd. In hoofdstuk V werd de relatie tussen waterstofbrugvorming en mengbaarheid onderzocht in films van naproxen en PVP K25. Deze films werden bereid via casting (trage solventverdamping, SC films) vanuit een methanoloplossing en via quench cooling van deze SC films die werden verwarmd tot boven het smeltpunt van naproxen en snel weer afgekoeld (QC films). De bereidingsmethode had een duidelijke invloed op de

mengbaarheid en intermoleculaire interacties. Een duidelijke evolutie van het fasegedrag afhankelijk van de concentratie van naproxen werd waargenomen: tot 20% naproxen bestond het systeem uit een enkele amorfe fase, boven deze concentratie en tot 35% waren er twee coëxisterende amorfe fasen (een naproxen-rijke en een PVP-rijke). Boven 35% naproxen was er een kristallijne fase in aanwezigheid van een (tot 60% naproxen) of meerdere (boven 65% naproxen) amorfe fasen. Analoog werd een toename van een amorfe sterk waterstofbrug gebonden geneesmiddel-polymer fractie waargenomen. Samen met een afname van de sterk waterstofbrug gebonden populatie in partieel kristallijne domeinen wordt het naproxen dimeer waargenomen bij hogere graad van kristalliniteit. De heterogeniteit met betrekking tot mengbaarheid en waterstofbruginteracties kon gedeeltelijk worden voorspeld op basis van toenemende aanwezigheid van naproxen als dimeer en bimodale deeltjesgroottepopulatie van het polymeer in de oplossingen. De QC films bestonden uit een enkele amorfe fase tot 70% naproxen, maar bij een hogere concentratie (vanaf 75%) was er een additionele kristallijne fase. De span van het glastransitiegebied in de koelingcurve nam toe tot een concentratie van 45% naproxen, om vanaf dan terug af te nemen. IR analyse leverde het bewijs van twee waterstofbrug gebonden populaties in de QC films tot 35% naproxen en verzadiging van de sterk waterstofbrug gebonden fracties vanaf 45% naproxen. Extrapolatie van smeltpuntsdalingsdata snijdt de glastransitie-compositie curve bij 17-18% naproxen zowel in de QC als in de SC films; de FH interactieparameters waren negatief. Deze studie heeft het domein van mengbaarheid van naproxen in PVP afgebakend, gaande van de quasi-equilibriumwaarde bepaald via de SC films tot die van de kinetische mengbaarheid, bepaald via de QC films.

In hoofdstuk VI werd de invloed van enkele belangrijke parameters van het sproeidroogproces bestudeerd op de fysische structuur, stabiliteit en *in vitro* dissolutiegedrag van vaste dispersies met 40% naproxen. De vaste dispersies werden enerzijds bereid bij drie verschillende waarden van de temperatuur van de inkomende lucht (IT) (40, 80 en 120°C) en een atomizatieluchtdebiet (AR) van 10 L/min en anderzijds bij drie AR (5, 10 en 15 L/min) en een IT van 80°C; de rest van parameters werd steeds constant gehouden. Alle dispersies waren amorf in X stralen diffractie behalve deze bereid bij een AR van 5 L/min vertoonde sporen van kristalliniteit. De heterogeniteit was meer uitgesproken bij hogere IT en/of AR. Deze dispersies vertoonden een hogere concentratie van sterk waterstofbrug gebonden carbonyl-naproxen of vrije carbonyl in tegenstelling tot dispersies bereid bij lagere IT of AR waar de zwak waterstofbrug gebonden fractie belangrijker was. Een hogere initiële

oplossnelheid en mate van supersaturatie werd bekomen bij heterogene dispersies bekomen via sproeidrogen bij hogere waarden van de procesparameters. Deze dispersies vertoonden weinig kristalliniteit en behielden een hoge graad van naproxen-rijke amorfe domeinen na bewaring bij 75% RH. De snelheid en de mate van kristallizatie van dispersies bereid bij hogere waarden van IT en AR was lager na bewaring bij 98% RH. Een interessante vaststelling was verder dat ook compressie geïnduceerde phase reorganisatie afhankelijk was van de gebruikte procesparameters. Dit wijst op de algemene gevoeligheid van de fysische structuur, stabiliteit en performantie van de vaste dispersies voor de condities van het bereidingsproces.

In het laatste hoofdstuk (VII) worden de belangrijkste bevindingen uit dit onderzoek kritisch belicht met betrekking tot formulerings- en procesaspecten. Bovendien worden mogelijke verdere onderzoekspistes naar voren gebracht om de onderliggende fysicochemie van amorfe vaste dispersies beter te begrijpen.

Appendix

Chapter III:

Theoretical and Experimental Investigation on the Solid Solubility and Miscibility of Naproxen in Poly(vinylpyrrolidone)

Figure III.A1. DSC thermogram of pure crystalline naproxen.

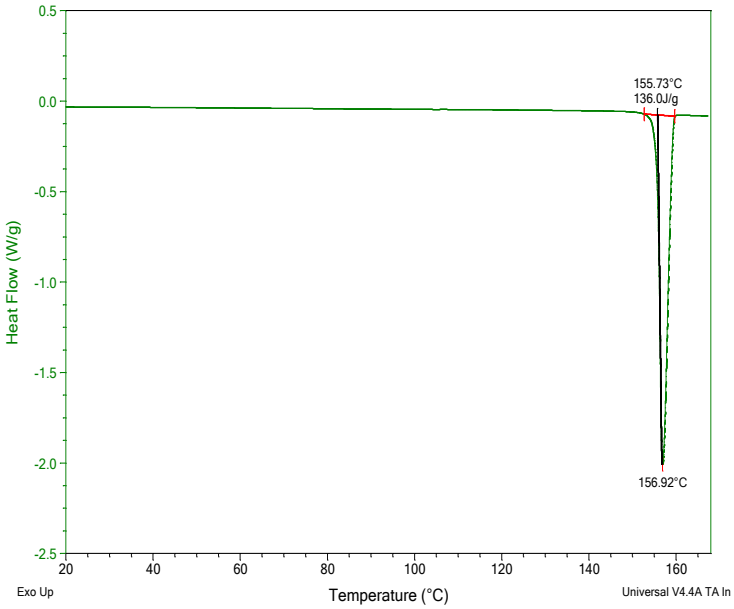

Figure III.A2. mDSC thermogram of ex situ quenched naproxen showing T_g and melting (in reversing heat flow curve) and crystallization (in non-reversing heat flow curve which also shows some degradation with melting).

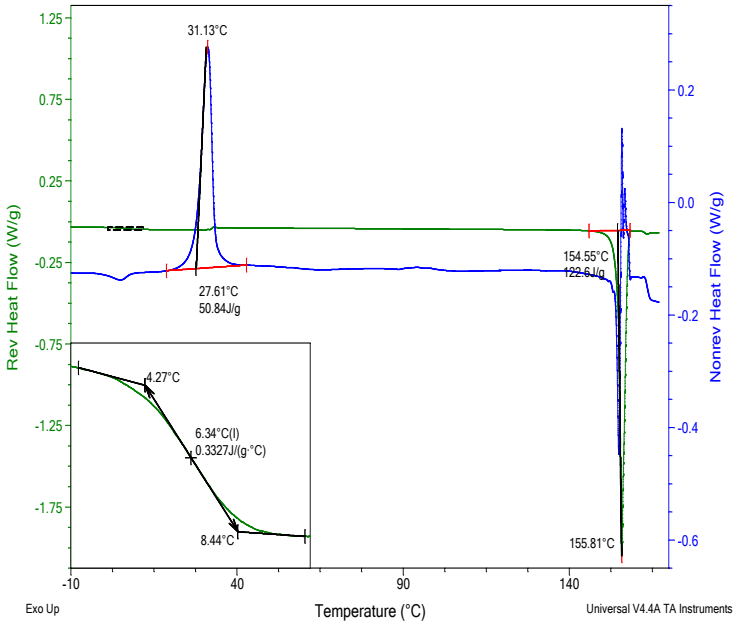

Figure III.A3. Reversing heat flow signals of PVP K 12, PVP K 25 and, PVP K 90 showing T_g and heat capacity change.

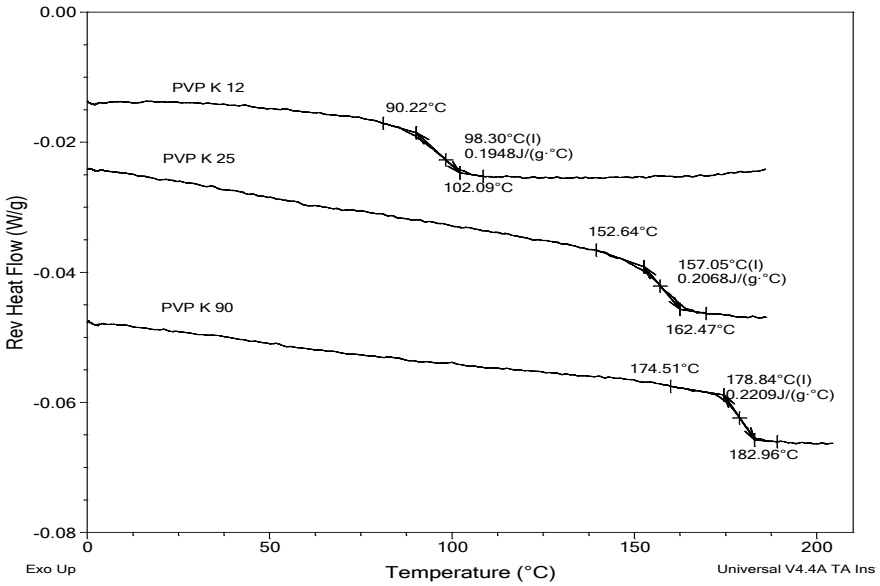

Figure III.A4. Overlays of reversing heat flow curves (first heating cycle) of spray dried composites of naproxen with PVP K 12 (from top to bottom: 5%, 10%, 15%, 20%, 30%, 40%, 50% and 75% naproxen containing samples).

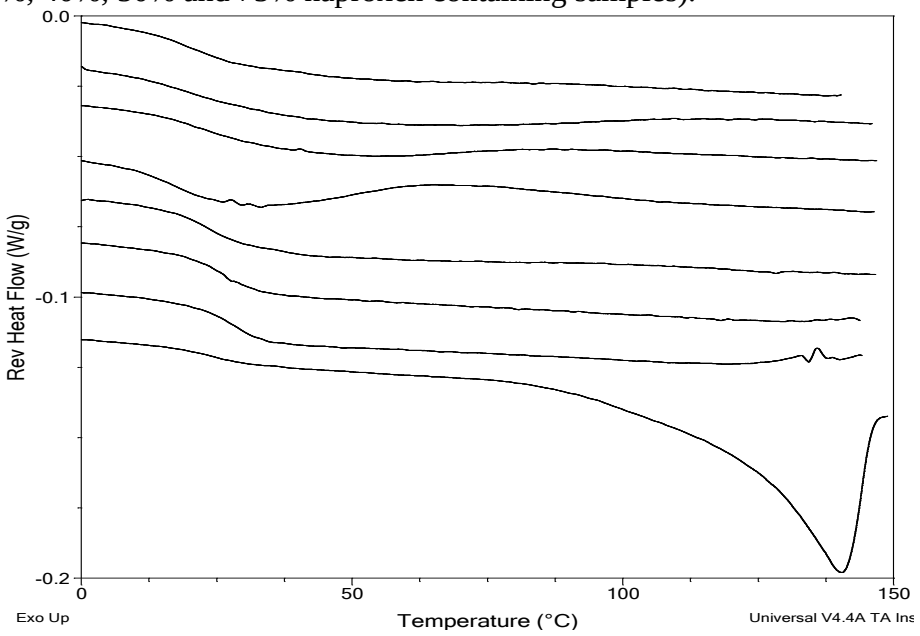

Figure III.A5. Overlays of reversing heat flow curves (first heating cycle) of spray dried composites of naproxen with PVP K 25 (from top to bottom: 5%, 10%, 15%, 20%, 25%, 30%, 40%, 50% and 75% naproxen containing samples).

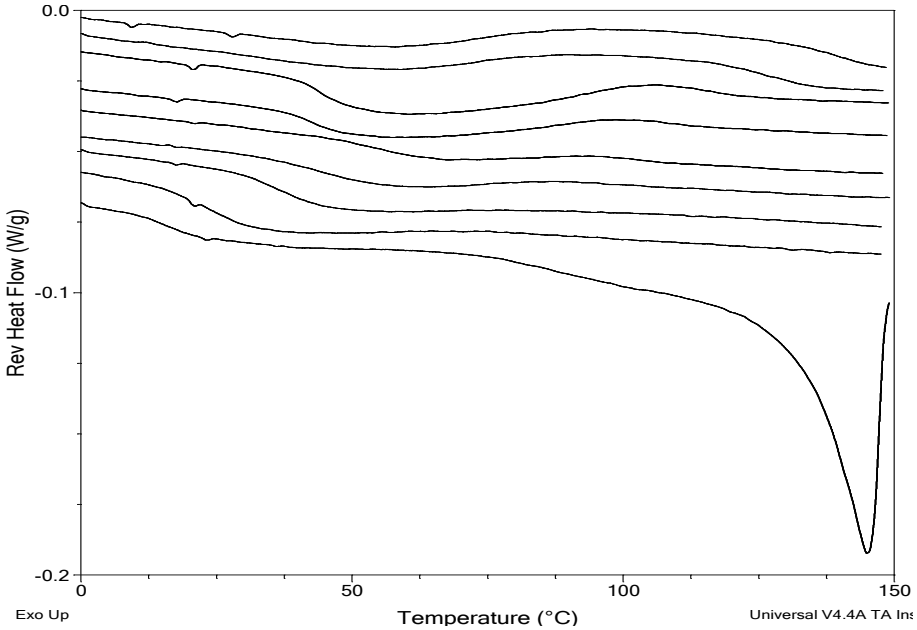

Figure III.A6. Overlays of reversing heat flow curves (first heating cycle) of spray dried composites of naproxen with PVP K 90 (from top to bottom: 5%, 10%, 15%, 20%, 30%, 40%, 50% and 75% naproxen containing samples).

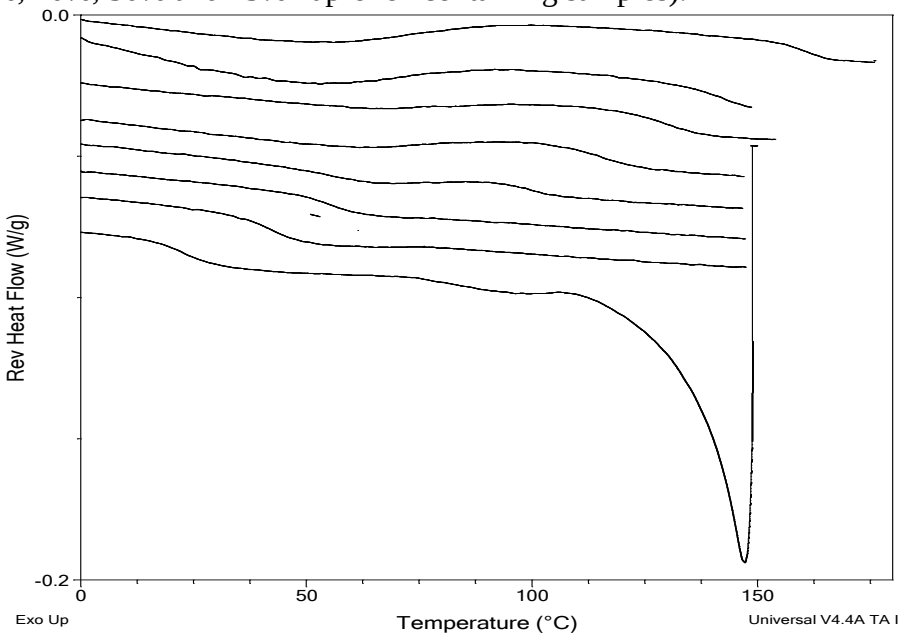

Figure III.A7. Overlays of reversing heat flow curves (second heating cycle) of spray dried composites of naproxen with PVP K 12 (from top to bottom: 5%, 10%, 15%, 20%, 30%, 40%, 50% and 75% naproxen containing samples).

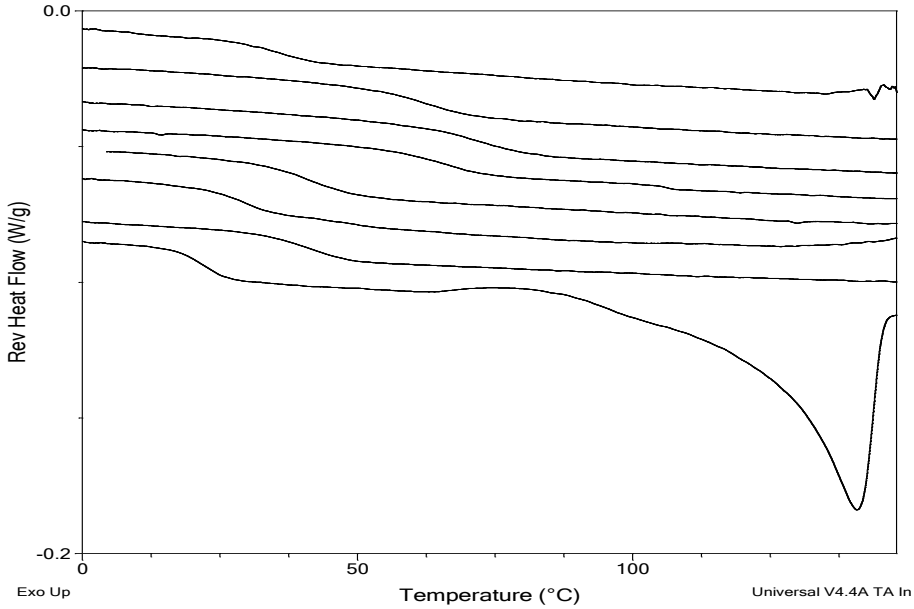

Figure III.A8. Overlays of reversing heat flow curves (second heating cycle) of spray dried composites of naproxen with PVP K 25 (from top to bottom: 5%, 10%, 15%, 20%, 25%, 30%, 40%, 50% and 75% naproxen containing samples).

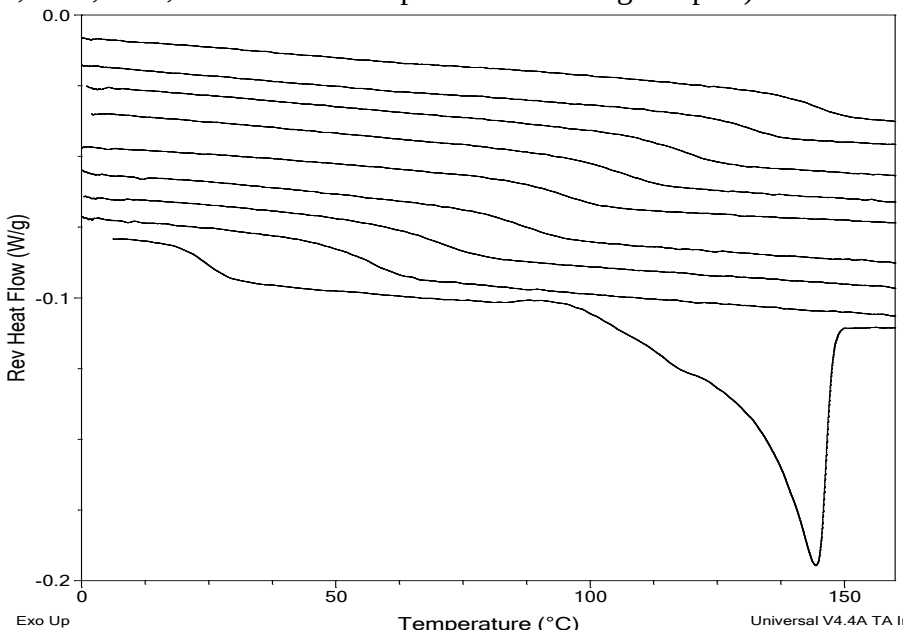

Figure III.A9. Overlays of reversing heat flow curves (second heating cycle) of spray dried composites of naproxen with PVP K 90 (from top to bottom: 5%, 10%, 15%, 20%, 30%, 40%, 50% and 75% naproxen containing samples).

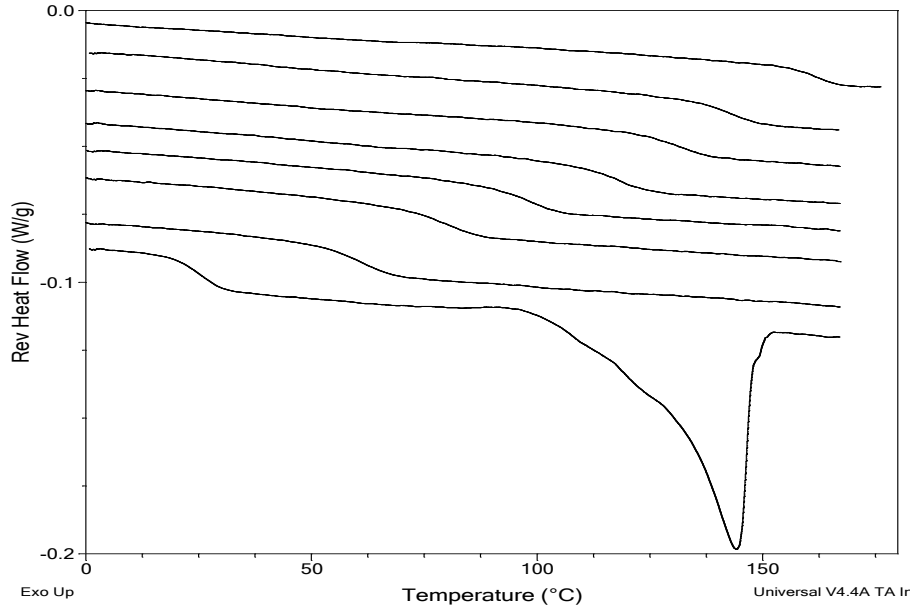

Figure III.A10. Melting point depression data for naproxen in PVP K 12 (figures in the parentheses represent corresponding %drug/%polymer in the mixture).

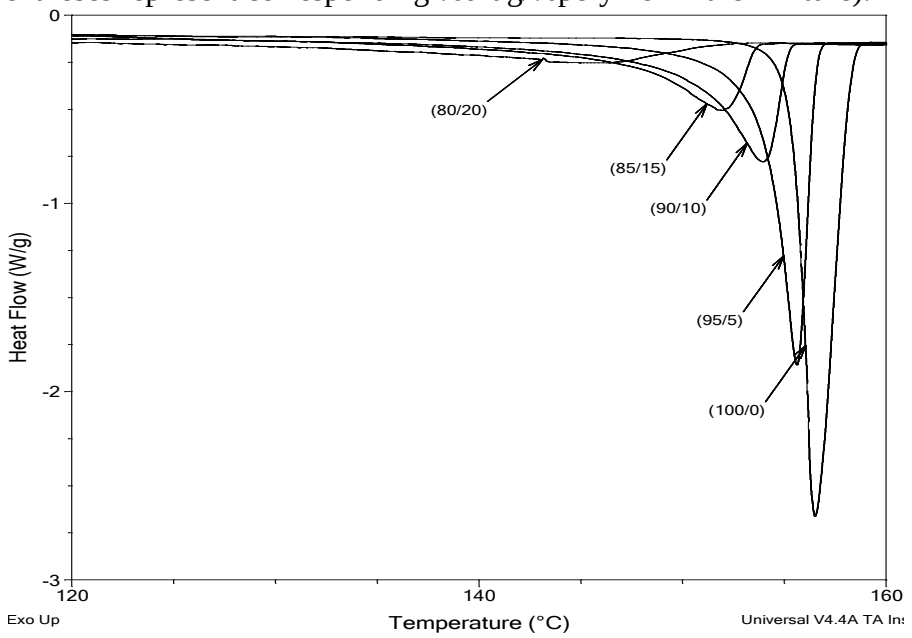

Figure III.A11. Melting point depression data for naproxen in PVP K 25 (figures in the parentheses represent corresponding %drug/%polymer in the mixture).

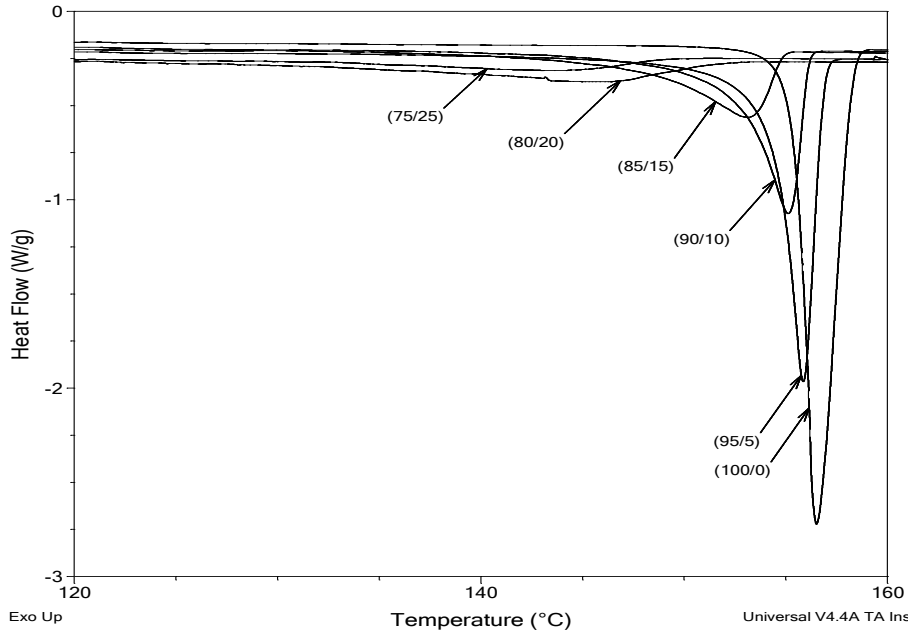

Figure III.A12. Melting point depression data for naproxen in PVP K 90 (figures in the parentheses represent corresponding %drug/%polymer in the mixture).

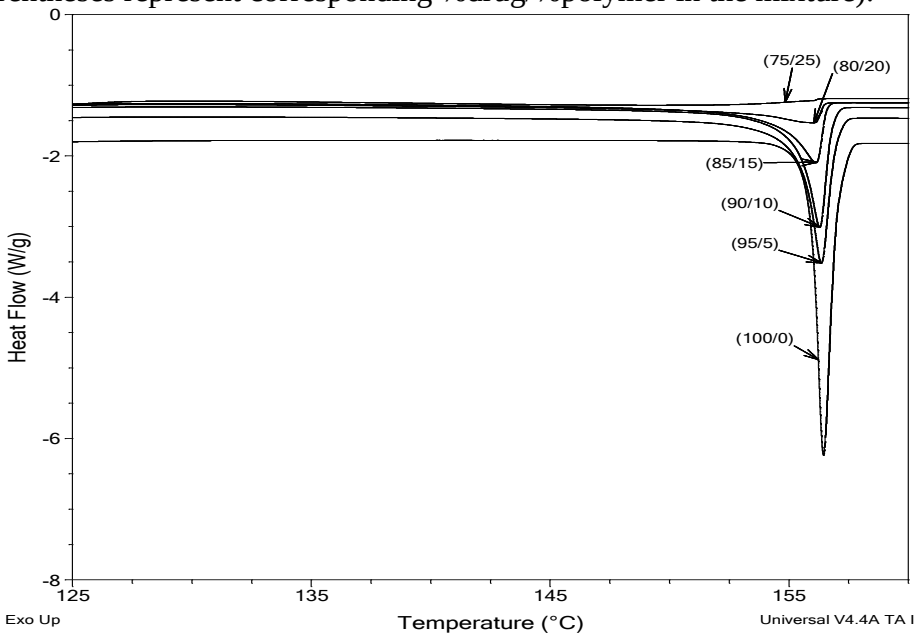

Chapter V:

Relating hydrogen-bonding interactions with the phase behavior of naproxen/PVP K 25 solid dispersions: Evaluation of solution-cast and quench-cooled films

Supplementary Figure: V.A1

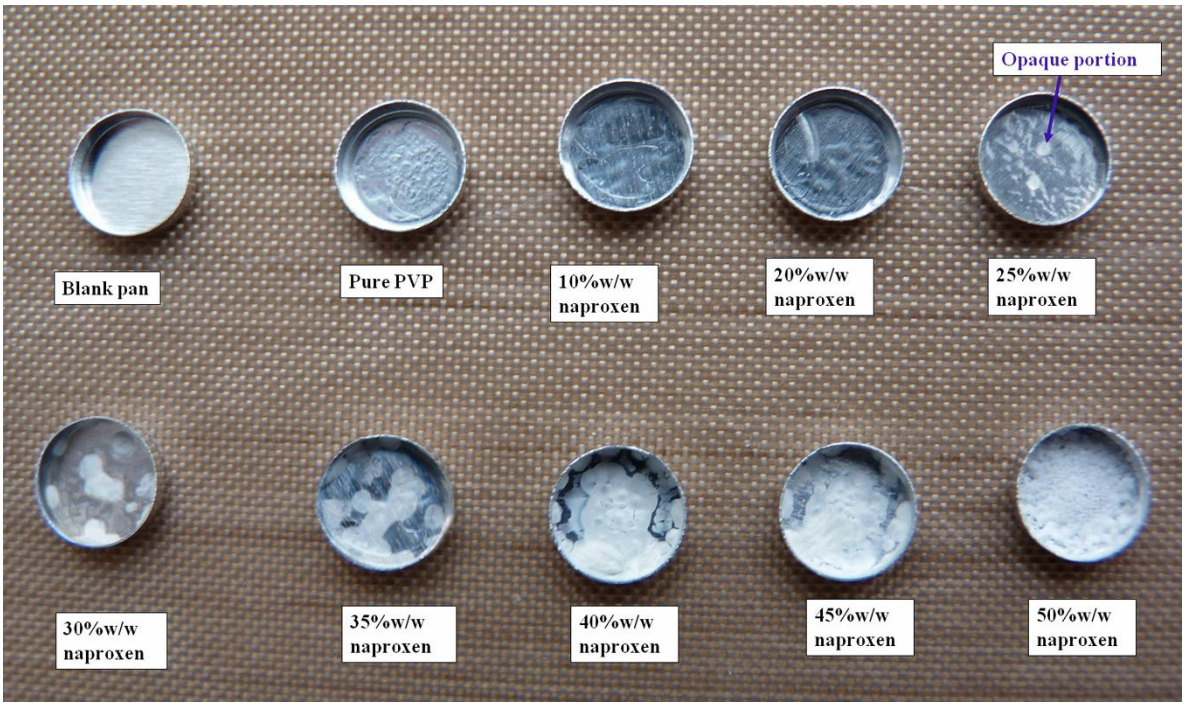

Figure V.A1: Photographs of solution casted films of naproxen-PVP developed in the pans as the function of composition from 0-50%w/w naproxen.

V.A2 Fitting procedure

Least square curve-fitting of spectral region comprising multiple shoulders peaks confronts with the low resolution of superimposing bands resulting into broadened experimental spectral profile. For such bands, seeking the fitting parameters for the best least square values (R^2 and $\varkappa$) can often result into a large number of deconvulated peaks which have less or no chemical and spectroscopic relevance. These problems can be addressed by taking care of following steps:

1. The automatic baseline corrections available in the fitting programs for the sloping baseline should not be executed. This may result into fitting aberrations. In the spectral region selected for fitting in the present study, this problem was not present as the baseline appeared straight. Hence, the straight baseline with the fixed experimental offset was used.
2. The prior information on the number of potential vibration bands superimposed within the particular experimental spectral profile and their positions/relative intensities is important for the correct initialization of the solution from the curve fitting leading to the meaningful convergence. As second order derivative method of peak searching proposed several peaks, the extra peaks appearing at the positions without the chemical and spectroscopic

identities were eliminated before starting the iteration as the composition dependent spectral evolution was known .

The spectral deconvolution was carried out using in-built hybrid Gaussian-Lorentzian (GL) function in Origin following the stepwise procedure as mentioned below:

1. The partial (1760-1560 cm^{-1}) IR absorption spectrum normalized to the most intense peak was plotted in Origin.
2. Then nonlinear curve fitting wizard was initialized wherein pseudoVoigt 2 (GL) function from the category 'spectroscopy' was selected.
3. In advanced setting, number of expected peaks upon deconvolution was defined based on the correspondence of the spectrum to the particular drug to polymer ratio. Under peak finding method, '2^{nd} derivative (search hidden peak)' option was selected for 'only positive peaks' with the '20 points Savitsky-Golay smoothing preference'.
4. Under the fitting parameter section, the auto parameter initialization was activated for the first iteration fixing the common offset, y_0. Subsequently, the position of peak maximum and peak intensity from the FTIR analysis were inserted as the initial values for peak amplitude, A and central frequency, x_c for each peak. This was followed by the execution of further iteration till the cumulative fitting profile converged to the experimental spectrum. This was further confirmed by the minimization of Levenberg-Markquardt reduced $\varkappa^2$ value with the highest possible value of coefficient of determination (COD), i.e. R^2.
5. The completion of fitting resulted into the values of x_c, w_L, w_G and A and from these values the algorithm calculated the area and full width at half maxima (FWHM).
6. The absolute area of peak ascribed to strongly H-bonded fraction in solid dispersions was corrected for the possible contribution from a small peak attributable to aromatic skeleton vibration of naproxen present at the same position. This was done by subtracting the area of deconvoluted aromatic vibration peak in the pure naproxen spectrum from that of the strongly H-bonded fraction peak area for each composition.
7. Finally, percentage area fractions of different vibration bands were calculated using the absolute normalized peak area obtained for each peak for different drug to polymer ratio.

Chapter VI:

An Investigation into the Effect of Spray-Drying Temperature and Atomizing Conditions on Miscibility, Physical Stability, and Performance of Naproxen–PVP K 25 Solid Dispersions

VI.A1: Derivation of eq VI.3

Eq V.3 can be derived by assuming that upon mixing atomization air and liquid feedstock flowing per unit time within a critical length of flow generates droplets of particular diameter or less. The critical length per unit time covered by the air flowing at the rate of AR while exiting between the nozzle cap and nozzle tip (L_A) is given by:

$$L_A = \frac{AR}{cross\ section\ area\ between\ cap\ and\ nozzle\ tip} = \frac{AR}{\pi d_{ic}^2 - \pi d_{on}^2} \quad \text{.....Equation (a)}$$

On the other hand, the length per unit time covered by feedstock passing at FR (L_F) is given by:

$$L_F = \frac{FR}{a\ single\ droplet\ volume\ with\ the\ diameter\ D} \times D = \frac{FR}{4/3 \times \pi \times D^3/8} \times D = \frac{6 \times FR}{\pi \times D^2} \quad \text{... Equation (b)}$$

At unit time, for the generation of droplets with diameter *D* by linear breakage of the feed thread by atomizing air, L_A should equals to L_F .therefore

$$\frac{AR}{\pi d_{ic}^2 - \pi d_{on}^2} = \frac{6 \times FR}{\pi \times D^2} \quad \text{..... Equation (c)}$$

Solving Equation (c) for *D* gives eq VI.3 [$D = \sqrt[1/2]{\frac{6 \times FR}{AR} \times (d_{ic}^2 - d_{on}^2)}$].

Figure VI.A1:
Pictorial illustration of humidity-pXRD (a) and humidity-IR measurement (b) at 98%RH.

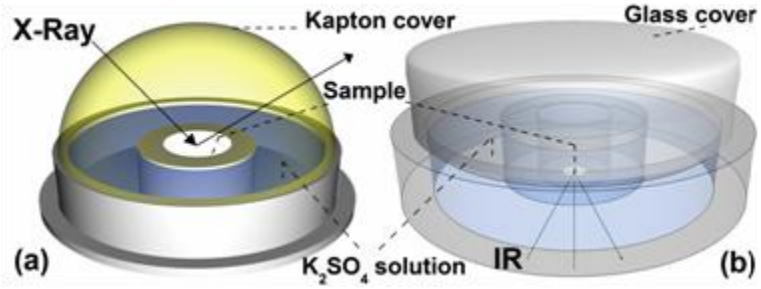

Figure VI.A2:
Polarized light micrographs taken at 98%RH, 6 h. $IT_{80}AR_{10}$ (a) and $IT_{80}AR_{15}$ (b)

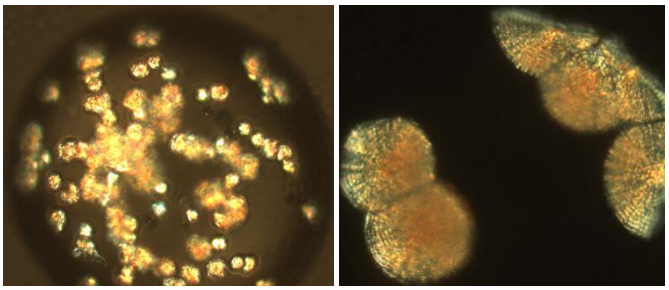

(a) **(b)**

Figure VI.A3:
Polarized light micrograph of dissolution system of $IT_{80}AR_{10}$ at 30 min

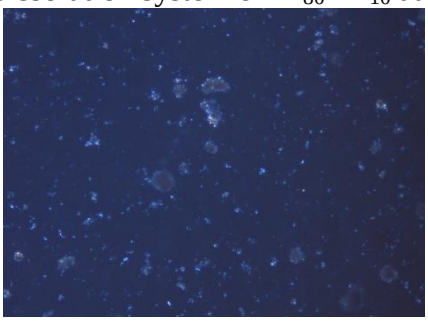

Amrit Paudel (28/07/1981, NEPAL)

Jan-Pieter Minckelersstraat-11, 3000 Leuven, Belgium

Tel.: +32 16 330 320 Mobile: +32 485 515 617

E-mail:amrit.paudel@hotmail.com

Education and training

2009 – April, 2013: PhD student in the pharmaceutical sciences, University of Leuven, Belgium

Dissertation title: **Formulation and Process Considerations in Manufacturing Amorphous Solid Dispersions**
Supervisor: *Prof Guy Van den Mooter*

2008–2009: Scientist, Pharmaceutics and Analytical R & D, Bristol-Myers Squibb, India

Key functions: **Preformulation, solid-state screening, physicochemical profiling, preclinical formulation development**

2006–2008: M. S. (Pharmaceutical Analysis), National Institute of Pharmaceutical Education and Research (NIPER), Punjab, India

Thesis title: **Degradation chemistry of carbapenem antibiotics**
Supervisor: *Prof Saranjit Singh*

2002–2006: Bachelor of Pharmacy, L.M. college of Pharmacy, Ahemadabad, India

Publications (http://scholar.google.com/citations?user=k7_oWsEAAAAJ&hl=en)

- **Paudel, A.**, Loyson, Y., Van den Mooter, G. *An investigation into the effect of spray drying temperature and atomizing conditions on miscibility, physical stability and performance of naproxen/PVP K 25 solid dispersions, J. Pharm. Sci. 2013*
- **Paudel, A.**, Nies, E., Van den Mooter, G. *Relating hydrogen-bonding interactions with the phase behavior of naproxen/PVP K 25 solid dispersions: Evaluation of solution-casted and quench-cooled films Mol. Pharmaceutics 2012*
- **Paudel, A.**, Worku, Z.A., Meeus, J., Guns, S., Van den Mooter, G. *Manufacturing of solid dispersions of poorly water soluble drugs by spray drying: Formulation and process considerations Int. J. Pharm. 2012*
- Ayenew, Z., **Paudel, A.**, Rombaut, P., Van den Mooter, G. *Effect of compression on non-isothermal crystallization behavior of amorphous indomethacin. Pharm. Res. 2012*
- *Ayenew, Z., ***Paudel, A.**, Van den Mooter, G. *Can compression induce demixing in amorphous solid dispersions? A case study of naproxen–PVP K 25. Eur. J. Pharm.Biopharm. 2012 (*contributed equally)*
- **Paudel, A.**, Van den Mooter, G. *Influence of solvent composition on the miscibility and physical stability of naproxen/PVP K 25 solid dispersions prepared by cosolvent spray-drying. Pharm. Res. 2012*
- **Paudel, A.**, Van Humbeeck, J., Van den Mooter, G. *Theoretical and experimental investigation on the solid solubility and miscibility of naproxen in poly (N vinyl pyrrolidone). Mol. Pharm. 2010*

- Janssens, S., De Zeure, A., **Paudel, A.**, Van Humbeeck, J., Rombaut, P., Van den Mooter, G. *Influence of preparation methods on solid state supersaturation of amorphous solid dispersions: a case study with itraconazole and eudragit E100. Pharm. Res. 2010*
- Raijada, D.K., Prasad, B., **Paudel, A.**, Shah, R.P., Singh, S. *Characterization of degradation products of amorphous and polymorphic forms of clopidogrel bisulphate under solid state stress conditions. J. Pharm. Biomed. Anal. 2010*
- Singh, S., **Paudel, A.**, Bedse, G., Thakare, R., Kumar, V. *The Challenge of Diverse Climates: Adequate stability testing conditions for India. Chapter 6, Pharmaceutical Stability Testing to Support Global Markets 2010 (Springer New York)*

Presentations

- Relating hydrogen-bonding interactions with the phase behavior of naproxen/PVP K 25 solid dispersions: Evaluation of solution-casted and quench-cooled films [**Oral presentation at the 6th Annual Pharmaceutical solid-state research cluster (PSSRC) Symposium, University of Lisbon, Portugal, 2012**]
- Towards understanding the processing parameters-physical structure relationship for spray dried naproxen/PVP K 25 solid dispersions: exploring the missing link [**Oral presentation at the 16th Forum of Belgian Society of Pharmaceutical Sciences, Blankenberge, Belgium, 2012**]
- Influence of solvent composition on the miscibility and physical stability of naproxen/PVP K 25 solid dispersions prepared by cosolvent spray-drying [**Poster presentation at the 25th conference of AAPS annual meeting and exposition, Washington, DC, USA and ULLA Summer School 2011 Parma, Italy, 2011**]
- Theoretical and experimental investigation on the solid solubility and miscibility of naproxen in poly (N vinyl pyrrolidone) [**Poster presentation at the 24th conference of AAPS annual meeting and exposition, New Orleans, USA, 2010**]
- Solid state characterization of a new polymorphic modification of naproxen [**Poster presentation at the 10th European Symposium on Thermal Analysis and Calorimetry, Rotterdam, The Netherlands, 2010**]
- Application of LC-NMR and LC-MS for the structural characterization of epimeric degradation products of faropenem generated under alkaline media [**Poster presentation at International NMR Symposium, IISC, Bangalore, India, 2008**]
- Identification of hydrolytic degradation products of imipenem using LC-MS-TOF [**Poster presentation at 2nd Chandigarh Scientific Conference, Panjab University, Chandigarh, India, 2008**]
- Identification of degradation and interaction products formed during compatibility studies between atenolol and aspirin [**Poster presentation at 59th Indian Pharmaceutical Congress, Varanasi, India, 2007**]